Numerical study of vortex and force characteristics of inclined offshore cylindrical structures

Jitendra Thapa

A thesis submitted for the Degree of Doctor of Philosophy in Civil Engineering at Western Sydney University

Supervisory panel

Associate Professor Ming Zhao

Associate Professor Tongming Zhou

School of Computing, Engineering and Mathematics

Western Sydney University, Sydney, Australia

November 2015

ABSTRACT

Investigating vortex shedding flow in the wake of circular cylinders is of importance in order to understand the hydrodynamics around offshore cylindrical structures. In this thesis, three-dimensional numerical simulations of steady flow past inclined circular cylinders have been performed for various Reynolds numbers. The incompressible Navier-Stokes (NS) equations are solved to simulate the vortex shedding flows using the Petrov-Galerkin finite element method (PG-FEM) developed by Zhao *et al*. (2009). The so-called periodic boundary condition was applied at the two end boundaries of the cylinder(s) to eliminate any end effects. The effects of the cylinder inclination angle on the flow and the forces of single and double cylinders are the focus of this study. In the present thesis, the cylinder inclination angle, based on which, 0° corresponds to the case where cylinder is perpendicular to the flow direction and 90° corresponds to the case where cylinder is parallel to the flow direction and the applicability of the independence principle is examined.

At first, vortex shedding flows around a circular cylinder at two different inclination angles, namely 0° and 45°, and Reynolds numbers between 100 and 1000 were simulated to examine the effects of the inclination angle on the transition from two-dimensional (2D) to three-dimensional (3D) wake flows. It was found that the transition from 2D to 3D at α = 45° was distinctively different from that at α = 0°. The vortex dislocation in Mode A, which is characterised by the inception of vortex loops and the formation of vortex pairs due to the deformation of primary vortices as they shed from the cylinder, transition for α = 0° was not observed at α = 45°. Then flow past an inclined circular cylinder close to a plane boundary, which is relevant to the pipeline industry, was studied at Re = 500 for gap-to-diameter ratios (e/D) of 0.4 and 0.8, where e and D are the gap between the cylinder surface and the solid boundary and the diameter of the cylinder, respectively. It was found that the independence principle is better satisfied at e/D = 0.8 than that at e/D = 0.4 due to the more apparent influence of the plane boundary in the latter case.

To broaden our knowledge of flow past multiple inclined cylindrical structures, three-dimensional flow past two identical cylinders in side-by-side and tandem arrangements at oblique attacks were simulated. In the first case, it was found that the normal Reynolds number, which is based on the velocity component perpendicular to the cylinder, should be used in the implementation of the independence principle. The well-defined biased flow observed at 0° is also identified at 45°. When two inclined cylinders are arranged in tandem

at *Re* = 500, it was found that the influence of the gap between the two cylinders is similar to that when the flow passes the cylinders at a right attack angle.

Finally, flow past two cylinders of different diameters, which resembles the piggyback pipelines in offshore oil and gas engineering, was studied using 3D model at a constant diameter ratio of 0.45 and gap ratio of 0.0625. The main focus is to identify the effects of the position angle of the small cylinder relative to the large cylinder on the forces of the cylinders. The reduction of the oscillatory forces on the large cylinder by placing a small cylinder close to it was successfully predicted by the 3D numerical model, which cannot be predicted by two-dimensional models.

PREFACE

This thesis consists of a number of peer-reviewed international journal and conference publications listed below and is submitted for fulfilment for the degree of Doctor of Philosophy (PhD) at Western Sydney University, Australia. It describes the entire work of the candidate during his study in School of Computing, Engineering and Mathematics at Western Sydney University under the supervision of **Associate Professor Ming Zhao** and **Associate Professor Tongming Zhou**.

LIST OF PUBLICATIONS

Refereed journal papers

Zhao, M., Thapa, J., Cheng, L., Zhou, T., 2013. Three-dimensional transition of vortex shedding flow around a circular cylinder at right and oblique attacks. Physics of fluids 25, 014105.

Thapa, J., Zhao, M., Zhou, T., Cheng, L., 2014. Three-dimensional simulations of vortex shedding flow in the wake of a yawed circular cylinder near a plane boundary at a Reynolds number of 500. Ocean Engineering 87, 25-39.

Thapa, J., Zhao, M., Cheng, L., Zhou, T., 2015. Three-dimensional simulations of flow past two circular cylinders in side- by-side arrangements at right and oblique attacks. Journal of Fluids and Structures 55, 64–83.

Thapa, J., Zhao, M., Cheng, L., Zhou, T., 2015. Three-dimensional flow around two circular cylinders of different diameters in a close proximity. Physics of Fluids 27, 085106.

Refereed conference papers

Thapa, J., Zhao, M., Cheng, L., Zhou, T., 2014. Three-dimensional simulations of flow Past two circular cylinders in a side-by-side arrangement. In Proceedings of twenty-fourth International Ocean and Polar Engineering Conference Busan, Korea.

Thapa, J., Zhao, M., Cheng, L., Zhou, T., 2014. Three-dimensional simulation of flow past two circular cylinders of different diameters. In Proceedings of 19th Australasian Fluid Mechanics Conference, Melbourne, Australia.

Zhao, M., Vaidya, S., Kaja, K., Thapa, J., 2014. Local scour around two pipelines in tandem in steady current. 7th International Conference on Scour and Erosion, Perth, Australia.

STATEMENT OF AUTHENTICATION

‘I hereby certify that the work presented in this thesis is my own creation and is original to the best of my knowledge, and any work adopted from other authors is indicated by references and also none of the part of this thesis has been submitted for any award or degree in other university.’

Signed

Jitendra Thapa

ACKNOWLEDGMENTS

I would like to express my sincere gratitude to my supervisor, **Associate Professor Ming Zhao** for his tremendous support on my PhD study and research, for his patience, motivation, enthusiasm, and immense knowledge.

I would like to thank Associate Professor Tongming Zhou and Professor Liang Cheng from University of Western Australia, and Associate Professor Surendra Shrestha from Western Sydney University for their encouragement, insightful comments, and suggestions.

I am very grateful to the **School of Computing, Engineering and Mathematics** at **Western Sydney University** for continuous support to carry out this research and also to my fellow researchers for the stimulating discussions and for all the fun we have had in the last three and half years. I would like to acknowledge the support of the PhD scholarship provided by **Australian Research Council** (ARC) through the ARC discovery project (DP110105171). All the calculations for this research were carried out on two Supercomputer facilities in Australia (Intersect NSW and iVEC in WA).

Last but not least, I would like to thank my parents, **Mr. Hari Bahadur Thapa** and **Mrs. Krishna Kumari Thapa**, for their patience in nurturing and supporting me all the way through and my sisters for their prayers. A special thanks to my wife **Shobha Parajuli** and my son **Kabir Thapa** for their endless support and understanding throughout my study.

TABLE OF CONTENTS

LIST OF FIGURES

LIST OF TABLES

LIST OF SYMBOLS

C_D	Drag coefficient
C'_D	Root mean square drag coefficient
C_{Dn}	Normal drag coefficient
C_{Ln}	Normal lift coefficient
C_L	Lift coefficient
C'_L	Root mean square lift coefficient
$\overline{C}_L(z)$	Time-averaged lift coefficient
$C_{L,rms}(z)$	Sectional root mean square lift coefficient
C_p	Pressure coefficient
D	Diameter of the cylinder
d	Diameter of small cylinder
e	Gap between the cylinder and the plane boundary
f	Vortex shedding frequency
$F_D(z)$	Sectional drag force
$F_L(z)$	Sectional lift force
G	Gap between two circular cylinders
k	Karman's constant
L	Distance between two centre of two circular cylinders
Re	Reynolds number
Re_N	Normal Reynolds number
Re_T	Total Reynolds number

U	Free stream velocity
u_f	Maximum friction velocity
u_i	Velocity component in the x_i-direction
Ut/D	Non-dimensional time
x_i	Cartesian coordinate
P	Pressure
p_0	Pressure at the inlet boundary
St	Strouhal number
St_n	Normal Strouhal number
t	Time
y^+	Near wall mesh density
z	Spanwise direction
Δz	Mesh size in the spanwise direction
Δr	Mesh size in the radial direction on the cylinder surfaces

GREEK SYMBOLS

α	Flow attacking angle
Δ	Distance from the wall
v	Kinematic viscosity of fluid
Ψ	Symmetric eigenvalue of the tensor
Ω	Anti-**s**ymmetric eigenvalue of the tensor
λ_1	The intrinsic wavelength of the vortex pair
λ_2	The distance between adjacent pairs
ω_x	Vorticity component in *x*- direction
ω_y	Vorticity component in *y*- direction
ω_z	Vorticity component in *z*- direction

LIST OF ABBREVIATIONS

2D	Two-dimension
3D	Three-dimension
NS	Navier-Stokes
PG-FEM	Petrov-Galerkin Finite Element Method
DNS	Direct Numerical Simulation
CFD	Computational Fluid Dynamics
FEM	Finite element method
CPU	Central processing unit
RMS	Root mean square
IP	Independence Principle
NW	Narrow wake
WW	Wide wake
FFT	Fast Fourier Transform
Eq	Equation
Fig	Figure
PIV	Particle Image Velocimetry
RANS	Renolds-Averaged Navier-Stokes
SG	Symmetric in the Gap
AG	Alternating in the Gap
WG	Wake in the Gap
VIV	Vortex-induced Vibration

CHAPTER 1

INTRODUCTION

1.1 GENERAL

This thesis investigates the flow past cylindrical structures at oblique attacks, in other words, flow past inclined cylindrical structures. In this thesis, zero attack angle of the flow (or zero inclination angle of the cylinder) corresponds to the case where the flow is perpendicular to the cylinder span. The study is conducted using computational fluid dynamics (CFD) and it focuses on the effects of the flow attack angle on the vortex shedding flow and force characteristics at Reynolds numbers near the lower boundary of the sub-critical regime. Both flow past a single cylinder and two cylinders in different arrangements at oblique attack angles are studied. The popularly used Independence Principle assumes that the hydrodynamics force coefficients based on the velocity component normal to the cylinder span are independent on the flow attack angle. The accuracy of the Independence Principle for flow past inclined cylinders in various conditions is discussed through extensive numerical simulations.

1.2 BACKGROUND

Flow over cylindrical structures has attracted much attention of many engineers and scientists due to its engineering applications such as sub-sea pipelines, mooring lines or risers in offshore oil and gas industry. The interaction between fluid and structures can be studied either experimentally or numerically. Early studies of flow past the cylindrical structures were mainly conducted through laboratory experiments. Recently, computational fluid dynamics (CFD) also plays an important role to predict the hydrodynamics of cylinders because of its efficiency and the rapid development of the computer technique. The non-dimensional quantities describing the flow around a circular cylinder depend on the cylinder Reynolds number defined as $Re = DU/\upsilon$ where D is the diameter of the cylinder, U is the flow velocity and υ is the kinematic viscosity.

It is well-known that when a circular cylinder is placed in a fluid flow, the wake flow pattern depends on the Reynolds number. The separation of the flow starts to occur when the Reynolds number (Re) exceeds 5, but below this Reynolds number separation of the flow does not exist. A fixed pair of vortices forms in the wake of the cylinder for Reynolds

numbers in between 5 and 40. The unsteady vortex shedding happens when the Reynolds number is above 40. Vortex shedding is the phenomenon that the vortices are formed and separated alternately at either side of the cylinder at a certain frequency. For the range of Reynolds numbers $40 < Re < 200$, the vortex flow is laminar and the vortex shedding flow is essentially two-dimensional (Williamson, 1989). Observations show that the two-dimensional feature of the vortex shedding was observed in the range $40 < Re < 200$ and the flow starts to transition to three-dimensional flow as Reynolds number exceeds 200 (Gerrard, 1978 and Williamson, 1988). The flow transition to turbulence starts in the wake and the turbulent flow region moves towards the cylinder as Reynolds number increases from 200 to 300 (Bloor, 1964). For $300 < Re < 3\times10^5$, the wake is completely turbulent and the boundary layer over the cylinder surface remains laminar throughout the perimeter of the cylinder until separation. The flow for $300 < Re < 3\times10^5$ is classified as in the sub-critical regime (Sumer and Fredsøe, 2006).

Sumer and Fredsøe (2006) investigated the transition of the boundary layer flow over the cylinder surface to turbulence. When the Reynolds number exceeds 3×10^5, transition to turbulence occurs in the boundary layer itself. The transition first takes place at the point where the boundary layer separates and the region of transition to turbulence moves upstream over the cylinder surface towards the stagnation point as the Reynolds number is increased. For the range of $3\times10^5 < Re < 3.5\times10^5$, the boundary layer becomes turbulent at the separation point, but only on one side of the cylinder. The boundary layer separation is turbulent on one side and laminar on the other side of the cylinder. In the regime of $3.5\times10^5 < Re < 1.5\times10^6$, the boundary layer separation is turbulent on both sides of the cylinder. However, transition to turbulence in the boundary layer has not been completed yet. The region of transition to turbulence is located somewhere between the stagnation point and separation point. In the Reynolds number regime of $1.5\times10^6 < Re < 4\times10^6$, the boundary layer is completely turbulent on one side of the cylinder and partly laminar and partly turbulent on the other side. Further increasing the *Re*, the boundary layer over the whole cylinder surface is virtually turbulent and this regime is called trans-critical flow regime.

The important feature of the flow in the wake of a cylinder is the vortex shedding phenomenon and is common for all the flow as $Re > 40$. For those values of *Re*, boundary layer over the cylinder surface will separate due to adverse pressure gradient imposed by the divergent geometry of the flow environment at the rear side of the cylinder. The separated free shear layer formed downstream the separation point on each side of the cylinder, which

contains a significant amount of vorticity rolling up into a vortex with a sign identical to that of incoming vorticity.

At *Re* > 40, the pair of vortices formed in the wake of the cylinder is actually unstable. A small disturbance will cause one vortex growing larger than the other. The larger vortex becomes strong enough to draw the opposite vortex across the wake. In Fig. 1.1 (a), the larger vortex is in the clockwise direction while the smaller vortex is in the anticlockwise direction. The approaching of vortex B will then cut off further supply of vorticity to vortex A from its boundary layer, leading to the shedding of vortex A from the cylinder surface. The free vortex A is then convected downstream by the flow. Following the shedding of vortex A, a new vortex will be formed on the top side of the cylinder named as vortex C in Fig. 1.1 (b). Vortex B will now play the same role as vortex A and will be shed from the cylinder due to vortex C. The vortex shedding will continue to occur in an alternate manner between the two sides of the cylinder Sumer and Fredsøe (2006).

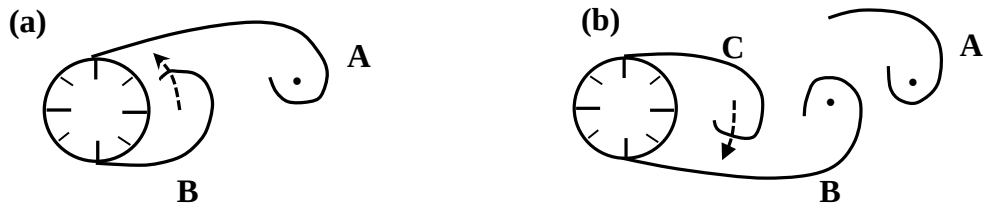

Fig. 1.1 Vortex shedding process reproduced based on Sumer and Fredsøe (2006). Prior to shedding of vortex A, vortex B is being drawn across the wake (b): Prior to shedding of vortex B, vortex C is being drawn across the wake.

The critical Reynolds numbers for vortex shedding found by different researchers are slightly different. It was reported to be from 40 to 47 (Norberg, 2003). As Vortex shedding occurs, the wake is characterized by alternative vortex shedding at a frequency f . The non-dimensional vortex shedding frequency is defined as the Strouhal number (S_t) as

$$S_t = \frac{fD}{U}, \tag{1.1}$$

Vortex shedding causes oscillatory forces on the cylinder. The force components in the in-line and the cross-flow directions are defined as the drag and the lift forces, respectively. The oscillation frequency of the lift force is the same as the vortex shedding frequency and that of the drag force is twice the vortex shedding frequency (Faltinsen, 1990). The lift and

drag forces can be non-dimensionalised as the lift coefficient (C_L) and the drag coefficient (C_D), respectively:

$$C_L = \frac{F_L}{\frac{1}{2}\rho U^2 DL}, \tag{1.2}$$

$$C_D = \frac{F_D}{\frac{1}{2}\rho U^2 DL} \tag{1.3}$$

where L is the length of the cylinder, F_L and F_D are the lift and drag forces, respectively, which can be obtained by integrating the pressure and the shear stress over the cylinder surface.

In coastal and offshore engineering applications, such as subsea pipelines in the near shore region, tethered marine structures and raked piles on deep-water oil terminals, and catenary risers, which are effectively curved riser pipes, etc. It is very common that the ocean flow approaches these structures with an oblique attack. In these cases, the fluid velocity in the axial direction of the structures will have effects on the vortex instability, the vortex regime classifications and the force characteristics. The commonly used independence principle (IP) assumes that the hydrodynamic forces on a cylinder only depend on the velocity components perpendicular to the cylinder span and are independent on the flow in the axial direction.

The understanding of the force characteristics, the vortex structures and the vortex shedding is important in the calculation of the dynamic loads on bluff structures such as subsea pipelines and risers. However, in many situations, multiple subsea structures encounter flows that approach them at an oblique angle. The force characteristics, the vortex instability and the vortex shedding regime classifications for flow past multiple inclined cylinders have not been studied systematically. In fact, the correct evaluation of the hydrodynamic forces on the structures in flow requires a clear understanding of the flow characteristics.

1.3 SIGNICANCE OF THIS STUDY

The significance of this study mainly lies in Australia's offshore oil and gas industry and its intrinsic interest in the fundamental of fluid dynamics research. The multi-billion dollars per annum offshore oil and gas industry is one of the key components of the Australian economy. As the extraction activities extend towards deep down the ocean, the pipelines, risers, and mooring lines are being installed and planned in Australian waters increases exponentially. For example, the total length of large diameter trunkline (42 inch) that is being designed for the Ichthys project is approximately 880 km. The typical per kilometre cost of a large diameter pipeline on the North West Shelf (NWS) of Australia is approximately $ 4.5 million. Large diameter pipelines are used as gas export trunklines that transport gas products to onshore processing facilities. The pipelines are normally stabilized by its self-weight in relatively deep water (>80m) and by its self-weight combined with secondary stabilization in medium to shallow water depth (20m-80m). Typical costs for secondary stabilization of large diameter pipelines in the NWS are approximately between $300 million and $500 million, depending on the magnitude of the project. A recent review of metocean, conditions for a number of projects on the NWS by a joint-industrial project STABLE pipe JIP has identified that most of the pipelines on the NWS are subject to the most onerous wave or current loads at highly oblique angles of attack (i.e. >45°) in water depths between 80m and 20m where secondary stabilization is anticipated to be required. Secondary stabilizations can be demonstrated to be redundant if hydrodynamic forces due to oblique waves are quantified confidently. So, accurate evaluation of the hydrodynamic loads and their frequencies are important to minimise the chance for structural failures of the cylindrical structures in offshore engineering that can be translated to significant cost saving and prevent from the possible environmental hazard for future oil and gas projects in Australian waters.

Due to the increased installation activities of pipe lines, mooring lines, risers in order to explore the oil and gas in Australian ocean, the chance of brittle failure of pipelines also increases equally leading to the huge possible economic and environmental losses. In order to prevent subsea structures from that possible failure, a systematic study is needed that can predict the force and the vortex shedding behaviour on these structures accurately.

1.4 RESEARCH OBJECTIVES

This research mainly focuses on the effect of cylinder inclination angle on the inception of vortex instability and force characteristics. The investigation will cover the flow around single and double cylinders at different arrangements such as side-by-side, tandem and piggyback pipelines. The main part of this study is to explore the accuracy of the IP at various cylinder inclination angles by analysing the velocity, vorticity fields and vortex structures at various Reynolds numbers, and to explore the methods to predict the hydrodynamic loads and their frequencies reliably at cylinder inclination angles. Direct numerical simulation (DNS) is performed to carry out the calculations for vortex shedding flow around a circular cylinder at right and oblique attacks, flow in the wake of a yawed cylinder near a plane boundary at two gap ratios (e/D = 0.4 and 0.8), flow past two circular cylinders in side-by-side arrangements at right and oblique attacks at four gap ratios (G/D = 0.5, 1, 3 and 5), flow past two circular cylinders in tandem arrangements at different inclination angles and flow around two circular cylinders of different diameters where Navier-Stokes equations are solved using the Petrov-Galerkin finite element method developed by Zhao *et al*. (2009). In addition to its efficiency, the advantage of the numerical methods over the experiments is their capability to provide detailed vortex structures and force characteristics that are sometimes difficult to be obtained from experiments. The numerical parameters of this study are considered to be the domain size, grid geometry, element size, element spacing and time step and are described in each chapter from chapter 3 to chapter 7. This research covers three-dimensional numerical simulation study only.

1.5 ORGANIZATION OF THIS THESIS

This thesis includes 8 Chapters and they are arranged as follows:

- Chapter 1 discusses the flow patterns due to the variation of Reynolds numbers and the generation of vortices in the wake of the cylinder and is referred as the backbone of this study which is included in the background section. Due to the generated vortex shedding in the wake of the cylindrical structures, the chances of brittle failure of pipelines cannot be neglected and is described in the significance of the study section and the research objectives describes the establishment of IP at different cylinder inclination angles by direct numerical simulation.

- In Chapter 2, a detailed literature review for flow past cylindrical structures is presented.
- In Chapter 3, a systematic study of flow past a cylinder at an oblique attack is performed. The onset of the three-dimensionality of the flow and its dependence on the Reynolds number are examined, and the accuracy of IP in various Reynolds numbers is discussed.
- In Chapter 4, steady flow over a circular cylinder near a plane boundary is simulated at two gap-to-diameter ratios (e/D = 0.4 and e/D = 0.8) and yaw angles ranging from 0°–60° to investigate the influences the plane boundary on the flow.
- In Chapter 5, the study is further extended to the case of flow over two identical circular cylinders in side-by-side arrangements for four gap-to-diameter ratios (G/D = 0.5, 1, 3 and 5). The effects of the flow attack angle on the interference between the vortex shedding from the two cylinders on the hydrodynamics are discussed. Normal and total Reynolds numbers of 500 are examined to implement the Independence Principle.
- In Chapter 6, the two circular cylinders are in tandem arrangements in fluid flow. Eight gap-to-diameter ratios (G/D= 0.5, 1.0, 1.5, 2.0, 2.5, 3.0, 3.5 and 5.0) at right attack and four gap-to-diameter ratios (G/D= 0.5, 1.0, 3.0 and 5.0) at oblique attack are considered.
- In Chapter 7, flow past two cylinders of different diameters are studied at a constant gap-to-diameter ratio (G/D = 0.0625) and various positions (0°–180°) of small cylinder relative to large (main) cylinder. In this chapter, only right attack angle case is considered and the focus of the study is on the effects of the position of the small cylinder on the hydrodynamics.
- In Chapter 8, the conclusions of this thesis with future works that would refine the present study are recommended.

CHAPTER 2

LITERATURE REVIEW

The interaction between fluid flow and cylindrical structures is of engineering significance because of its relevance to the engineering applications. The examples of cylindrical structures in the offshore oil and gas engineering include subsea pipelines, offshore riser pipes, mooring cables, etc. The so-called vortex shedding phenomenon happens when a bluff body is placed in a fluid flow, leaving a vortex street in the wake of the body. The alternate vortex shedding is the result of the interaction between two free shear layers that are separated from the two sides of a cylindrical structure. The dynamic oscillatory forces on structures due to vortex shedding have to be predicted accurately to ensure the structural stability. This chapter describes the comprehensive literature review on flow past an isolated circular cylinder with and without the influence of a plane boundary and flow over two circular cylinders in different arrangements.

2.1 FLOW OVER AN ISOLATED CIRCULAR CYLINDER

When a cylinder is exposed to a steady uniform approaching flow, the wake structure downstream the cylinder is three- dimensional (3-D) as long as the Reynolds number (*Re*) is greater than about 170, even before it becomes turbulent (Roshko, 1954; Bloor, 1964; Williamson, 1988; Norberg, 2001). The wake flow is in the transitional regime when the Reynolds number is between 170 and 300 and becomes fully turbulent as the Reynolds number is greater than about 400. In most of civil and mechanical engineering applications, the Reynolds number is usually much greater than 400. Therefore, the wake flow is normally turbulent.

Extensive studies on turbulent wake flows past a circular cylinder have been conducted using both experimental and numerical methods. Williamson (1988, 1991, and 1992) investigated the three-dimensional transition of the flow behind a circular cylinder from laminar to turbulent flow. It was found that the three-dimensionality and turbulence in the wake are triggered by instabilities within the vortex formation region. The instabilities include the generation of the small-scale streamwise vortices, large- scale vortex dislocations and small-scale shear-layer instability vortices. When the Reynolds number is in the turbulent flow regime, the hydrodynamic forces on the circular cylinder fluctuate with time due to the

vortex shedding. Karniadakis and Triantafyaaou (1992); Zhang and Dalton (1998) simulated 3-D flow past a circular cylinder using a three-dimensional model for Reynolds numbers in the range of 100–500. Their findings about the transition of the flow to turbulence agreed well with the experiments (Williamson, 1992).

Previous investigations have shown that there are mainly three types of vortical structures in the near wake, namely, the Karman alternating vortices with predominantly spanwise vorticity (Roshko, 1961), the longitudinal smaller-scale rib-like vortices wrapping around and connecting the consecutive spanwise structures (Williamson, 1992) and the Kelvin-Helmholtz vortices in the shear layer (Bloor, 1964). Williamson (1989) found that two discontinuities exist in the S_t – *Re* relationship in the laminar-to-turbulence transitional regime. The first discontinuity occurs at *Re* between 170 and 180, and corresponds to the secondary flow that takes the form of vortex loops. This discontinuity shifts vortex shedding toward the lower frequency. Williamson's flow visualization shows that the spanwise wavelength is slightly smaller than three diameters of the cylinder. At the second discontinuity, which occurs at *Re* between 230 and 260, finer scales develop in the streamwise vortex structure, and vortex shedding is shifted to a higher frequency. The spanwise wavelength after this discontinuity is about one diameter. Vortex dislocation is an important phenomenon for the three-dimensionality in the wake of a circular cylinder. In the region of dislocation, the variation in vorticity is more irregular than at other places. The stronger tilting and stretching of vortices in these regions can promote the transition to turbulence. Vortex dislocation has been studied by many researchers, among which are Williamson (1989), Lewis and Gharib (1992), Williamson (1992), and Yang *et al*. (1993). The end effects on the vortex shedding mode, including parallel vortex shedding, oblique vortex shedding, and vortex dislocations, is clearly shown in the study by Hammache and Gharib (1989). It was found that oblique vortex shedding can be avoided if special care is given to the end conditions. Enforcement of parallel shedding by reducing end effects also delays the transition to turbulence through reduction of the number of vortex dislocations. Varshney (2012) studied the vortex structures in the wake of inclined cylinders and reported that the stability of the vortices are depend on the angle of attack and vortex shedding frequency remained nearly constant to the change of Reynolds number.

In reality, it is very often that the flow approaching a cylinder at an inclined attack angle. Flow past a yawed circular cylinder has been studied by a number of investigators both

experimentally (King, 1977; Kozakiewicz *et al*., 1995; Ramberg, 1983; Thakur *et al*., 2004) and numerically (Chiba and Horikawa, 1987; Lucor and Karniadakis, 2003; Marshall, 2003). For the convenience of discussion, a flow approaching angle (or the inclination angle of the cylinder), α, is defined as the angle between the flow direction and a plane that is perpendicular to the cylinder span. The zero-flow-approaching angle corresponds to the case where the flow is perpendicular to the cylinder. Experimental results showed that the force coefficients and the Strouhal number, which are normalized by the velocity component perpendicular to the cylinder, are approximately independent on the yaw angle if the flow approaching angle is small. This is often called the independence principle or the cosine law in the literature. Kozakiewicz *et al*. (1995) found that the independence principle can be applied to stationary cylinders in the vicinity of a plane boundary for a yawed angle between 0° and 45°. In case of flow past a yawed cylinder of finite length, it was shown that the wake vortices far from the upstream end of the cylinder are approximately parallel to the cylinder. The vortices near the upstream end of the cylinder are aligned at an angle larger than the cylinder's yaw angle. Lucor and Karniadakis (2003), Ramberg (1983) and Thakur *et al*. (2004) conducted numerical simulations of flow past a yawed cylinder of infinite length at two large yaw angles, namely 60° and 70°. They reported that the vortex shedding angles of the vortices in the wake of a yawed cylinder are somewhat less than the cylinder's yaw angle. Zhao *et al*. (2009) studied flow past an infinitely long stationary circular cylinder at yawed angles in the range of 0° – 60° and reported that the Strouhal number and mean drag coefficients at different yaw angles follows the independence principle well as the yaw angle is less than 45°.

The validity of independence principle (IP) in predicting the fluid forces for steady current past an inclined cylinder was studied by a number of investigators both experimentally (e.g. Van Atta, 1968; Ramberg, 1983; Kozakiewicz *et al*., 1995; Zhou *et al*., 2009, 2010) and numerically (e.g. Chiba and Horikawa, 1987; Marshall 2003; Lucor and Karniadakis 2003; Zhao *et al*., 2009). The IP states that the force coefficients and the vortex shedding frequency, normalized by the velocity component perpendicular the cylinder, are independent on the inclination angle of the cylinder. Most of the studies confirmed the validity of IP when the cylinder inclination angle α is small. Van Atta (1968) showed that the IP is approximately valid for $\alpha \leq 35°$, whereas for larger α, the decrease of the vortex shedding frequency with the increase of α is slower than that predicted by the IP. Surry and Surry (1967) found that the Strouhal number based on the normal velocity component is

approximately constant for Re = 4000 ~ 63000 up to α = 40° ~ 50°. Ramberg (1983) studied the effect of the inclination angle (α = 0° ~ 60°) and the end conditions on vortex shedding for stationary and forced vibrating circular cylinders with aspect ratios of 20 ~ 90 at Re = 160 ~ 1100. It was shown that slantwise vortex shedding at angles other than the cylinder inclination angles is intrinsic to stationary inclined cylinders in the absence of end effects. As a result, the IP is not valid in the case of stationary inclined cylinders. Zhou *et al*. (2009) showed that the IP is valid up to α = 40°. For larger inclination angles (e.g. at α = 45°), the maximum concentrations of the coherent transverse and spanwise vorticity components decrease by about 50%, while that of the streamwise vorticity increases by about 70%, suggesting that the strength of the Karman vortex shedding from a yawed cylinder decreases and the three-dimensionality of the flow is enhanced (Zhou *et al*., 2010). Their results indicated the generation of the secondary axial vortices in yawed cylinder wakes when α is larger than 15°.

The studies of IP in oscillatory flows are not as many as those in steady flows. By measuring the lift and drag forces of an inclined cylinder in steady current and oscillatory flow, Kozakiewicz *et al*. (1995) showed that the IP can be applied in both steady current and waves to stationary cylinders in the vicinity of a plane wall in the subcritical regime for α = 0° ~ 45°. They found that the wake flow characteristics began to change at α = 55°, and for α = 70°, the water particles moved predominantly along the cylinder axis rather than perpendicular to the cylinder axis. Sarpkaya *et al*. (1982) measured forces on smooth and rough cylinders in a uniform oscillatory flow for angles of attack α = 0°, 30° and 45°. The values of the hydrodynamic force coefficients were calculated based on the component of flow normal to the cylinder axis. These results, after the correction by Garrison (1986) for the inappropriate experimental procedures in Sarpkaya *et al*. (1982), revealed that the IP works well for the force in the in-line direction. In the latter case the inertia coefficient was significantly larger than the drag coefficient.

From the above review, it is clear that there are still many uncertainties regarding the flow past circular cylinder at an inclined angle in the sense of vortex dislocation and the application of independence principle and the investigation of three-dimensional transition of flow around a circular cylinder at different flow attacking angles will be studied as a part of my research.

2.2 CYLINDER NEAR PLANE BOUNDARY

In the offshore pipeline engineering, flow around and the forces on a subsea pipeline are affected by the pipeline's proximity to the seabed. When flow past a horizontal pipeline is studied, the flow can be modelled by considering the seabed to be a flat rigid wall. The flow around a circular cylinder in the proximity of a plane boundary has been investigated by several researchers. This flow configuration is of academic interest and has many practical engineering applications.

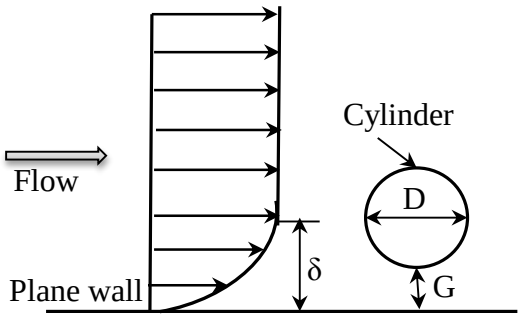

Fig. 2.1 Sketch of the flow past a circular cylinder near a plane boundary

The cylinder and the plane boundary are separated by a gap G and generally, a boundary layer forms on the plane boundary as shown in Fig. 2.1. According to the review by Zdravkovich (2003), the influence of the plane boundary is primarily dependent on the following parameters in addition to the Reynolds number Re: gap-to-diameter ratio G/D, the relative boundary layer thickness δ/D, and the flow characteristics of the boundary layer, i.e. whether the boundary layer is laminar, transitional or turbulent. The turbulence in the boundary layer affects the hydrodynamic forces on the cylinder (Zdravkovich, 2003).

When a circular cylinder is located near a plane boundary, vortex shedding flow is dependent not only on the Reynolds number but also the gap-to-diameter ratio G/D. Due to its engineering relevance, flow around a cylinder close to a plane boundary has been well studied over the past few decades (Taneda, 1965; Bearman and Zdravkovich, 1978; Grass *et al*., 1984; Taniguchi and Miyakoshi, 1990; Lei *et al*., 1999). Most of the existing studies are based on experimental measurements at Reynolds numbers in the sub-critical regime. The sub-critical flow regime was selected in experiments because the vortex shedding is relatively insensitive to the Reynolds number in this regime. Therefore, the wall effect can be

thoroughly investigated without involvement of the effect of the Reynolds number. Bearman and Zdravkovich (1978), Grass *et al*. (1984) and Lei *et al*. (1999) reported that the vortex shedding in the wake of a cylinder close to a plane boundary was suppressed as G/D is less than 0.3. Lei *et al*. (2000) solved the two-dimensional time-dependent Navier-stokes equations and the pressure Poisson equation for viscous flow using finite difference method for Re = 80 to 1000. The numerical results showed that the amplitude of the fluctuating lift force decreases with a decrease in the gap-to-diameter ratio or the Reynolds number. For Reynolds numbers above 600 in their study, the critical gap-to-diameter ratio approached a value $(G/D)_{cr}$=0.2.

Early experiments of flow past a cylinder close to a plane boundary at low Reynolds numbers were performed by Taneda (1965) with a towed cylinder at Re = 170 and different gap-to-diameter ratios G/D. Because the cylinder was towed in the still water, no boundary layer formed near the wall. At G/D = 0.1, one single row of vortices was observed while at G/D = 0.6, a double row of vortices was observed. To the best knowledge of the author, this is the only published experimental study of flow past a yawed cylinder near a plane boundary at low Reynolds numbers in the laminar flow regime. Most of the published experimental and numerical studies were carried out at Reynolds numbers in the order of 10^3-10^5. The suppression of vortex shedding observed mainly in the range of G/D =0.2-0.4 (Bearman and Zdravkovich, 1978; Grass *et al*., 1984; Buresti and Lanciotti, 1992; Lei *et al*., 1999; Wang and Tan 2008). The boundary layer thickness δ/D in these experiments ranged from 0.1 to 0.9. However, larger values of the critical gap for vortex shedding suppression are reported at thicker boundary layers (Taniguchi and Miyakoshi, 1990; Grass *et al*., 1984). Grass *et al*. (1984) suggest that this increase in critical gap could be due to the large velocity differential Δu across the cylinder, advocating the importance of velocity gradient in the approaching flow. Taniguchi and Miyakoshi (1990) reported that the critical value of G/D for vortex shedding suppression corresponds to the point where the wall side of the cylinder comes in contact with the outer part of the turbulent boundary layer forming near the wall. Buresti and Lanciotti (1992) also reported that the critical gap for vortex shedding decreases with the thickness of the boundary layer.

Generally, the drag coefficient decreases with a decrease in the gap-to-diameter ratio (Lei *et al*., 2000; Zdravkovich, 1985). At small gap-to-diameter ratios, a steady mean lift force in the direction away from the wall is observed (Bearman and Zdravkovich, 1978; Lei

et al., 1999), although it is dependent on the boundary layer some incidents of lift in the opposite direction (towards the wall) are reported by Lei *et al*. (1999) and Zdravkovich (1985). At *Re* in the range of 10^3-10^4, separation regions are observed both upstream and downstream of the cylinder at small gap-to-diameter ratios (Bearman and Zdravkovich, 1978; Grass *et al*., 1984; Lin *et al*., 2009). The upstream separation region is reported to form an obstacle to the approaching flow and its presence reduces the flow velocity through the gap and deflects upstream fluid over the top of the cylinder. The downstream separation region is reported to deflect the jet flow originating from the gap away from the wall to form a free jet (Grass *et al*., 1984).

Taniguchi and Miyakoshi (1990) suggested that the vortex street was formed by the concentration of vorticity by roll-up of separated shear layers originating from both sides of the cylinder. The free-stream side shear layer containing clockwise vorticity whereas the wall side shear layer containing counter clockwise vorticity and the boundary layer formed on the wall contains clockwise vorticity. Grass *et al*. (1984) suggested that the free jet inhibits large-scale vortex roll-up in the wall side wake region. Furthermore, cancellation of opposite signed vorticity in the wall boundary layer and the wall side shear layer is suggested as the cause of vortex shedding suppression (Lei *et al*., 2000; Taniguchi and Miyakoshi, 1990; Grass *et al*., 1984). When the gap is smaller than the critical gap for vortex suppression, flow separation of the wall boundary layer is observed to coincide with the outward deflection of the wall side shear layer. Observations clearly indicated interaction between the wall side shear layer and the wall boundary layer: each (counter clockwise) vortex shed from the wall side of the cylinder is accompanied by a clockwise vortex in the near-wall region (Lei *et al*., 2001). As a result the wall boundary layer is destabilized and the flow detaches from the wall and ejects upwards (Wang and Tang 2008; Price *et al*., 2002).

Lin *et al*. (2009) presents a summary of previous experimental studies of flow past a circular cylinder near a plane boundary and suggested that the flow phenomena in the wake of the cylinder can be roughly classified into three regions depend on the gap-to-diameter ratios: (1) the characteristics of vortex shedding is similar to that of an isolated cylinder at large gap-to-diameter ratios, (2) the plane boundary influence the vortex shedding and the periodic shedding from the upper shear layer is evident at intermediate gap-to-diameter ratios, (3) periodic vortex shedding is suppressed at small gap-to-diameter ratios.

Unlike the case of uniform flow, flow past a circular cylinder close to plane boundary at an inclined angle has not been studied. It is expected that, when a cylinder is placed close to a plane boundary, the inclination of the cylinder affects not only the vortex shedding frequency and the forces on the cylinder, but also the critical gap for vortex shedding suppression. In this thesis, flow past an inclined circular cylinder close to a plane boundary will be studied.

2.3 TWO CYLINDERS IN SIDE-BY-SIDE ARRANGEMENTS

Two circular cylinders placed side-by-side in a fluid flow has drawn much attention from many researchers in fluid mechanics because of its importance in many engineering applications such as offshore oil and gas engineering, bridge pilings and heat exchanger's bundles etc. (Alam *et al*., 2003; Liu *et al*., 2001; Zdravkovich and Pridden 1977; Zhou *et al*., 2001). When two circular cylinders are arranged side-by-side to the fluid flow, the wake of the two cylinders interacts with one another on either side of the gap between the two cylinders. If the gap between the two cylinders is in a very close proximity, they may behave as a single bluff body. If the gap between the cylinders is sufficiently large, they may behave as two independent bluff bodies, although the synchronization between the adjacent vortex streets may occur. Complex wake and vortex-street interactions occur when the two cylinders are spaced between the intermediate regimes, in particular an asymmetric or biased flow pattern that may be bi-stable in nature. Because the jet flow biased towards the two cylinders intermittently, the bi-stable biased flow is also called the flip-flopping regime. Two parallel vortex streets are formed either as an in-phase or an anti-phase pattern in flow visualization for laminar wake of two side-by-side circular cylinders and two distinct vortex streets lead to a single and large scale wake when they are in in-phase and two distinct vortex streets are formed when they are in anti-phase (Williamson, 1985).

In this study, the gap ratio is defined as the ratio of the gap between the two cylinders to the diameter of the cylinders, i.e., G/D. The spacing ratio $L/D = G/D + 1$ was also used regularly to represent the gap between the two cylinders, with L being the distance between the two cylinder centres. It should be noted that the gap and spacing between two cylinders refer to the surface-to-surface and the centre-to-centre distances between two cylinders, respectively. Kim and Durbin (1988) performed an experimental study on the flow between a pair of circular cylinders in the flip-flopping regime and revealed that the flip-flopping occurred randomly with time at Reynolds numbers in the subcritical regime. Alam *et al*. (2003) performed experiments of uniform flow past two side-by-side circular cylinders at a

Reynolds number of 5.5×10^4. When the gap ratio (G/D) is less than 1.2, the wake flow was found to bias towards one of the cylinders, leading to a narrow wake (NW) behind one cylinder and a wide wake (WW) behind the other. Hesam and Navid (2011) studied the flow around two side-by-side cylinders for different gap ratios using the Cartesian-staggered grid finite volume method in laminar and turbulent regimes. They predicted that biased flow pattern with the wide and narrow wakes behind the two cylinders occurred when $G/D < 1.5$ in the laminar flow regime. Afgan *et al*. (2011) simulated flow past two side-by-side circular cylinders at $Re = 3000$ by using the large eddy simulation method and revealed the detection of shedding frequencies with a biased wake flow deflection for the intermediate gap ratios $0.25 \leq G/D \leq 0.75$ in their study and also addressed the formation of the bi-stable (switching) phenomenon behind the wake of the cylinders. However, the study on flow past two circular cylinders at oblique attack case cannot be neglected in offshore oil and gas industry and hence effort has been put to discuss the effect of attack angle, the Reynolds number and gap between the two cylinders.

2.4 TWO CYLINDERS IN TANDEM ARRANGEMENTS

When two cylindrical structures are placed in a fluid flow at tandem arrangement, the behaviour of the flow can be completely different from any other arrangements and hence has attracted attention from many researchers due to its importance in engineering applications either on land or in the ocean. Two circular cylinders in a tandem arrangement are commonly used to evaluate the interaction of multiple structures in a fluid flow where one cylinder is located upstream of another cylinder.

When two identical cylinders are arranged in a tandem configuration, the flow patterns can be classified into different flow regimes according to the spacing ratios between the cylinders (Zdravkovich, 1987; Ljungkrona and Sunden 1993; Mittal *et al*., 1997; Meneghini *et al*., 2001; Lin *et al*., 2002; Alam *et al*., 2003; Xu and Zhou 2004). Zdravkovich and Pridden (1977) reported the discontinuous jump of the base pressure of the downstream cylinder at the critical spacing (G/D>2.5) between the two cylinders. The flow around two circular cylinders in a tandem arrangement in subcritical Reynolds numbers 3.3×10^3 <Re<12×10^3 at various spacing has been visualized by using smoke-wire technique (Ljungkrona and Sunden, 1993). It was reported that the change in the flow mode due to the change in the spacing between the cylinders has significant effect on the Strouhal number. Alam *et al*. (2003) carried out an experimental study on aerodynamics characteristics of two

circular cylinders in a tandem arrangement at $Re = 6.5\times10^4$ and reported the bistable flow at G/D=3 (critical spacing), the reattachment of shear layer occurred intermittently at $G/D< 2$. Xu and Zhou (2004) conducted an experimental study on the wake of two tandem cylinders based on hot-wire measurement and LIF flow visualisation for Reynolds numbers between 800 and 4.2×10^4 and various spacing ratios (L/D = 1 – 15) and reported that the critical spacing ratio (L_{cr}/D) decreases with increasing Reynolds numbers (L_{cr}/D = 4.5 for Re = 1400, L_{cr}/D = 4 for Re = 8500 and L_{cr}/D = 3 for Re = 42000).

Extensive numerical studies on flow past two circular cylinders in tandem arrangements have also been reported in literature. Meneghini *et al*. (2001) studied the shedding of vortices and flow interference between two circular cylinders in tandem and side-by-side arrangements for Reynolds numbers from 100 to 200 by using the two-dimensional fractional step finite element method and their numerical results of the interference regimes agree with the experimental results. Liu *et al*. (2014) simulated 2D flow past two circular cylinders in tandem arrangements at various spacing ratios ($0.1 \leq G/D \leq 6.0$) at a Reynolds number of 200 by solving the Navier-Stokes equations using the upwind finite element method and reported the hydrodynamic jump at G/D = 0.9 and 2.6. Efforts have also been made to understand the 3D turbulent flow past the multiple bodies. Carmo and Meneghini (2006) employed spectral finite element method to simulate 2D and 3D flow for various centre-to-centre spacing ratios from 1.5 to 8 at Reynolds numbers 160 – 320. It was found that the 3D vortical structures have significant effects on the fluid loads and 2D simulations are not able to accurately determine the interference regime in the vicinity of critical spacing. Papaioannou *et al*. (2006) studied flow around two tandem cylinders at centre-to-centre spacing ratios ranging from 1.1 to 5.0 and Reynolds numbers from 100 to 1000 and revealed the 3D effects on critical spacing at various Reynolds numbers. Carmo *et al*. (2010) studied flow past two circular cylinders in tandem arrangements by linear stability analysis and 3D direct numerical simulations at various centre-to-centre spacing ratios from 1.2 to 10 and identified three different vortex shedding regimes (SG: symmetric in the gap, AG: alternating in the gap and WG: wake in the gap). Tong *et al*. (2015) performed 3D simulations on two identical circular cylinders at tandem, side-by-side and staggered arrangements at Reynolds number of 1000 and the spacing ratios (L/D) from 1.5 to 4.0. For a tandem arrangement, the small drag coefficients is reported due to complete or partial immerse of downstream cylinder in between the two shear layer from upstream cylinder.

Most of previous studies on flow past two tandem cylinders focused on the cases where the flow direction is perpendicular to the cylinders. In many engineering applications, the flow may approach the cylinder at an oblique attack angle. It is expected that the inclination angle of the flow has influences on the vortex shedding flow patterns (Gregory *et al*., 2009; Thapa *et al*., 2015).

2.5 TWO CYLINDERS OF DIFFERENT DIAMETERS

Offshore pipelines of different diameters are sometimes bundled together. The simplest configuration is two pipelines of different diameters, forming the so-called piggyback pipeline in the oil and gas industry. Sometimes, a small cylinder is also used to control the flow around a large cylinder. Strykowski and Sreenivasan (1990) studied the vortex shedding behind a circular cylinder at low Reynolds numbers by placing a smaller cylinder in the near wake of larger cylinder and claimed the significant role of small cylinder in the wake from their experimental study such as the change in local stability, minimizes the growth rate of disturbances and also controls the vortex shedding due to the reduced drag. Lee *et al*. (2004) demonstrated that a control rod makes possible to control hydrodynamic actions on a circular cylinder. The vortex shedding behind a cylinder could be varied and suppressed over a limited range of Reynolds numbers by placing a small secondary control rod (Strykowski and Sreenivasan, 1990). The uniform flow past two circular cylinders of different diameters was studied by Zhao *et al*. (2005, 2007a) and found that the hydrodynamic forces on the cylinders and the vortex shedding frequency depend on the arrangements of the cylinders. Also the vortex shedding flow past a piggyback pipeline studied by Zhao *et al*. (2007b) and their study focused on the gap effect between the small and large pipelines on the vortex shedding flow.

Tsutsui *et al*. (1997) investigated the behaviour of an interactive flow around two circular cylinders of different diameters at close proximity using both experimental and numerical methods. The shear layer separated from the main cylinder was found re-attached and adhered to the rear surface of the main cylinder. The effect of a small cylinder on the main cylinder studied by using 2-D Large Eddy Simulation as CFD study and flow-visualisation technique for Reynolds numbers of 100, 1000 and 3000 by Dalton *et al.* (2001) and indicated the noticeable influence on the drag and lift on the main cylinder due to the presence of a small cylinder. In order to control the flow around the cylinder, Tsutsui and Igarashi (2002) carried out an experimental study on the reduction of bluff body drag by the use of rod set upstream of a circular cylinder and claimed the 63% of reduced drag compared to an isolated

cylinder. Vortex shedding behind a cylinder can be controlled by placing another small cylinder behind it and studied excessively by Dipankar *et al.* (2007) by using over-set grid method for low Reynolds numbers (63, 79 and 150) and reported the reduction of drag and decreased shedding frequency. Moreover, numerical calculations of the intermittent re-attachment and time-averaged fluid forces agreed well with those of previous experiments, and the qualitative characteristics of calculated Strouhal numbers coincided with those of experiments. The influence of the position angle of small pipeline on vortex shedding flow around a sub-sea piggyback pipeline was studied by Zhao (2012) by solving two-dimensional Reynolds-averaged Navier-Stokes equations using finite element method and reported that the critical gap ratio, below which the vortex shedding is suppressed, depend on the position angle of small pipeline.

CHAPTER 3

THREE-DIMENSIONAL TRANSITION OF VORTEX SHEDDING FLOW AROUND A CIRCULAR CYLINDER AT RIGHT AND OBLIQUE ATTACKS

Vortex shedding from an inclined circular cylinder at low values of Reynolds number (*Re*) is investigated numerically. The aim of the study is to investigate the effect of cylinder oblique angle on the transition from two-dimensionality (2D) to three-dimensionality (3D) of the wake flow. The Navier-Stokes equations are solved by the Petrov-Galerkin finite element method for Reynolds numbers ranging from 100 to 1000 and the flow attack angles of α = 0° and 45°. For the right attack angle case (α = 0°), the predicted wavy spanwise vortices in the early stage of the transition mode A, the vortex dislocation in the late stage of the transition mode A and the streamwise-vortex dominant wake flow structure in the transition mode B are found to agree well with independent experimental observations and measurements. The transition from 2D to 3D at α = 45° was found distinctively different from that at α = 0°. For α = 45°, no clear-cut transition modes are observed. The wake is characterized by wavy spanwise vortices close to the lower boundary of the transition Reynolds number regime, which are similar to those in the early stage of the transition mode A at α =0°. The vortex-dislocation in the transition mode A was not observed at α =45°. It appears that the fluid flow in the spanwise direction in the primary vortices at α = 45° does not allow the instability to sustain at a specific spanwise location and trigger the vortex dislocation. Although the wake flow structure is different, the variation of the normal Strouhal number with the normal Reynolds number (both based on the velocity component perpendicular to the cylinder span) at α = 45° is close to that at α = 0° in the transitional Reynolds number regime. The root mean square of the lift coefficient normalized by the velocity component perpendicular to the axial direction of the cylinder at α = 45° is about 20% to 25% larger than that at α = 0° in the Reynolds number regime between 250 and 500.

3.1 INTRODUCTION

The focus of this chapter is to study the transition of the flow from laminar to turbulence in the transition Reynolds number regime. For a circular cylinder in a steady flow, vortex shedding starts to occur if Reynolds number exceeds about 40. The Reynolds number is defined as $Re = UD/v$, with U, D and v being the free-stream velocity, the diameter of the cylinder and the kinematic viscosity of the fluid respectively. The wake vortex flow remains two-dimensional (2D) until Reynolds number is about 140-190, beyond which the wake flow becomes unstable and transits to three-dimensional (3D) flow. The critical Reynolds numbers for transition obtained by different researchers are slightly different from each other (Williamson, 1996). It was found to be Re = 150 by Roshko (1954) and Tritton (1959), 160 by Zhang *et al*. (1995), 165 by Eisenlohr and Eckelmann (1989) and Norberg (1994) and 178 by Williamson (1988 and 1989). Miller and Williamson (1994) found that the laminar regime for parallel shedding can be extended up to Re = 194 and even beyond 200 for short period of time if there is not effect from the end condition. The Floquet stability analysis by Barkley and Henderson (1996) showed that the 3D instability starts at a Reynolds number of about 188.5.

Two wake flow modes (modes A and B) have been identified to be the dominant flow features in the transition regime (Williamson, 1988). The earliest 3D transition, denoted as mode A, is characterized by the inception of vortex loops and the formation of streamwise vortex pairs due to the deformation of primary vortices as they are shed from the cylinder. The wavelength of the spanwise feature was found to be 3 to 4 diameters (Zhang *et al*., 1995; Barkley and Henderson 1996). The wavelength in mode A can only be measured in the early stage of the instability before the so-called vortex dislocations appear (Williamson, 1995). In the transition regime, vortex dislocations are generated between spanwise cells of different frequency when the primary vortices move out of phase with each other. The critical Reynolds number for wake transition is very sensitive to the end condition of the cylinder (Hammache and Gharib 1989). By using suction tubes downstream of the cylinder to achieve "clean" end conditions, Miller and Williamson (1994) found that the laminar regime can be extended up to 194 and even beyond 200.

As Reynolds number is increased to 250, the flow is in mode B, where the wake pattern is dominated by the streamwise vortex pairs spaced by a distance of about one cylinder diameter. The dislocations that are observed in mode A do not exist in mode B, unless they

are artificially introduced (Prasad and Williamson 1997). With regard to the variation of Strouhal number S_t ($\equiv fD/U$, where f is the vortex shedding frequency) with Reynolds number; two discontinuities occur when the flow changes from 2D laminar flow to mode A and from mode A to mode B, respectively (Tritton, 1959; Williamson, 1988).

Flow around an inclined circular cylinder has also been investigated extensively both experimentally (King, 1977; Ramberg, 1983; Kozakiewicz *et al*., 1995; Thakur *et al*., 2004; Zhou *et al*., 2009, 2010) and numerically (Chiba and Horikawa, 1987; Marshall, 2003; Lucor and Karniadakis, 2003; Zhao *et al*., 2009) in the past few decades. In engineering practice, the Independence Principle (or the cosine law) is commonly employed to predict the hydrodynamic forces and vortex shedding frequency of an inclined circular cylinder. The inclination angle α is defined as the angle between the incoming flow and the plane normal to the cylinder axis. The Independence Principle assumes that if the force coefficients and the Strouhal number are normalized by the velocity component perpendicular to the cylinder, they are approximately independent of α. The validity of the Independence Principle has been checked by a number of researchers. Kozakiewicz *et al*. (1995) found that the Independence Principle can be applied to stationary cylinders in the vicinity of a plane wall for α between 0° and 45°. In case of flow past a yawed cylinder of finite length, it was found that the wake vortices far from the upstream end of the cylinder are approximately parallel to the cylinder and the vortices near the upstream end of the cylinder are aligned at an angle larger than the cylinder yaw angle (Ramberg, 1983; Thakur *et al*., 2004). Lucor and Karniadakis (2003) simulated flow past a yawed cylinder of infinite length at two large yaw angles, namely 60° and 70°. They found that the angles of the vortices in the wake are somewhat less than the cylinder's yaw angle. The numerical study by Zhao *et al*. (2009) showed that the error of the Independence Principle increases with the increasing inclined angle. The experimental study of Zhou *et al*. (2009) also showed that the Independence Principle is valid up to α of about 45°.

It is noted that most previous studies of flow past an inclined circular cylinder have been focused on the applicability of the independence principle at high Reynolds numbers in the subcritical regime, while the study on flow transition from 2D to 3D has been rare. The critical Reynolds number for flow transition and the vortex characteristics in the wake of an inclined cylinder have not been studied systematically. In this study, flow past an inclined circular cylinder at low Reynolds numbers is simulated numerically. This study is focused on

the wake transition from 2D to 3D at low Reynolds numbers. The incompressible Navier-Stokes equations are solved using a Petrov-Galerkin finite element method developed by Zhao *et al*. (2009). The simulations are carried out for α = 0° and 45° over a range of Reynolds numbers between 100 and 1000. The effects of α on the wake transition are studied by analysing the wake vortex flow structure and the hydrodynamic forces on the cylinder. In the case of flow past an inclined circular cylinder, two Reynolds numbers are defined, one of which is defined based on the incoming velocity of the flow and the other is based on the velocity component perpendicular to the cylinder span. The effects of the two Reynolds numbers on the wake transition are also studied.

3.2 NUMERICAL METHOD

The governing equations for simulating the flow are the incompressible Navier-Stokes (NS) equations. The non-dimensional form of the NS equations are expressed as

$$\frac{\partial u_i}{\partial t} + u_j \frac{\partial u_i}{\partial x_j} + \frac{\partial p}{\partial x_i} - \frac{1}{\mathrm{Re}} \frac{\partial^2 u_i}{\partial x_j^2} = 0, \tag{3.1}$$

$$\frac{\partial u_i}{\partial x_i} = 0, \tag{3.2}$$

where $(x_1, x_2, x_3) = (x, y, z)$ are the Cartesian coordinates, u_i is the fluid velocity component in the x_i-direction, p is the pressure. The governing equations are solved by a Petrov-Galerkin finite element model developed by Zhao *et al*. (2009). Fig. 3.1 Non-dimensional computational domain for flow past a circular cylinder at oblique attack shows the non-dimensional computational domain for simulating the flow past a circular cylinder at an oblique angle of attack. A 40 by 60 by 19.2 rectangular computational domain is used. It has been shown that the computational domain size in the *z*-direction (refer to Fig. 3.1) must be greater than 4 in order to predict the hydrodynamic forces on the cylinder accurately (Lei *et al*., 2001). In the study by Zhao *et al*. (2009) of flow around a yawed circular cylinder at *Re* = 1000, the computational domain size in the *z*-direction was set at 9.6. The computational domain size in the *z*-direction in this study is extended to 19.2 in order to clearly identify the variation of the flow in the axial direction of the cylinder. The initial values of the velocity and the pressure in the whole domain are set to zero while the non-dimensional velocity at the inlet boundary is given by

$$(u_1,\ u_2,\ u_3) = (\cos\alpha,\ 0,\ \sin\alpha) \tag{3.3}$$

At the two side boundaries that are parallel to the $x-z$ plane, a free-slip boundary condition is employed, namely, the velocity component and the pressure gradient perpendicular to the boundary are zero. When the flow approaches the cylinder at an inclined angle, the velocity in the axial direction of the cylinder can be significant. A periodic condition was imposed by setting velocity and pressure gradients (in all three directions) at the top boundaries to be equal to their counterparts at the bottom boundary (Zhao *et al*. 2009 and 2012). At the cylinder surface the no-slip boundary condition is applied.

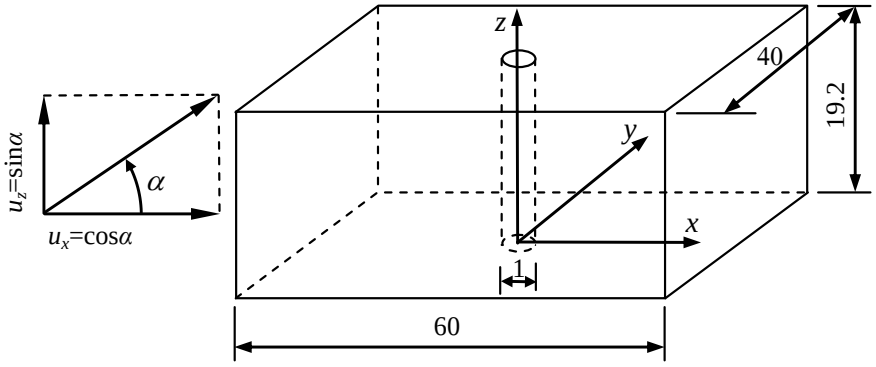

Fig. 3.1 Non-dimensional computational domain for flow past a circular cylinder at oblique attack

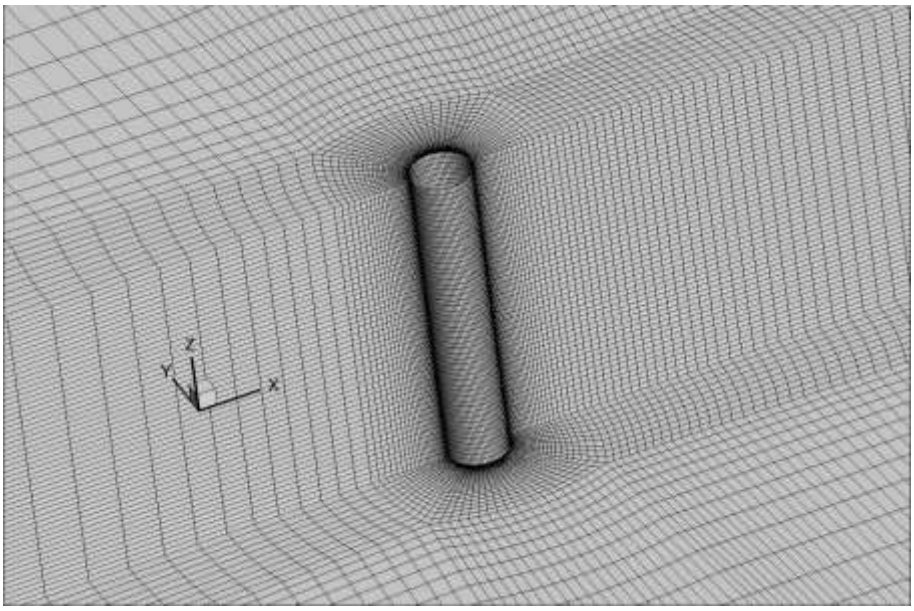

Fig. 3.2 Computational mesh around the cylinder (only ¼ of the cylinder length is presented).

Fig.3.2 shows the computational mesh near the cylinder. The cylinder surface is divided into 80 elements and the minimum mesh size in the radial direction is 0.001. The length of the cylinder (19.2) is divided into 192 layers of hexahedral 8-node linear finite element elements in the axial direction. For each case of the simulations, 64 CPUs are used and three layers of mesh are allocated to each CPU. The near wall mesh density can be evaluated by the non-dimensional distance of a nodal point to the wall: $y^+ = u_f \Delta / \nu$, where Δ is the distance from the wall and u_f is the maximum friction velocity. The non-dimensional distance between the nodes next to the wall y^+ is less than 1 for the highest Reynolds number simulated in this study.

3.3 MESH DEPENDENCE STUDY

Zhao *et al*. (2009) demonstrated that the numerical results at *Re*=1000 and α=0° converge if the minimum mesh size in the radial direction is less than 0.001. The mesh density used in this study is very similar to that used by Zhao *et al*. (2009). The effect of the mesh density on the numerical results at *Re*=1000 and α=45° is tested by performing the simulations at three meshes of different densities. The mesh size in the spanwise direction is defined as Δz. The mesh in the *xy*-plane used in this study is defined as the normal mesh. Another mesh (defined as the dense mesh) that is denser than the normal mesh is used in the mesh dependence study. In the dense mesh the minimum mesh size in the radial direction is 0.0006 and the cylinder circumference is divided into 120 nodes.

Fig. 3.3 shows the time histories of the sectional drag and lift coefficients at the mid-span of the cylinder (z=9.6) calculated from three meshes at *Re*=1000 and α=45°. The drag and the lift coefficients are defined as $C_D(z) = F_D(z)/(\rho DU^2/2)$ and $C_L(z) = F_L(z)/(\rho DU^2/2)$, where ρ is the fluid density, $F_D(z)$ and $F_L(z)$ are the sectional drag and lift force at the location of z, respectively. Since the wake flow at *Re*=1000 is turbulent, the forces from three meshes are not identical to each other. Although the time histories of the forces are very irregular, the mean value and the amplitude of the forces from the three meshes are close to each other. Table 3.1 shows the comparison of the statistic values of the force coefficients from different meshes. The Strouhal number is obtained based on the oscillatory lift coefficient. The agreement between the results from the three meshes shows that the results converge at the normal mesh and Δz=0.1. The maximum difference between the results from any two meshes is less than 2.5%. Because the highest Reynolds number was chosen for the mesh dependence

study, the normal mesh and Δz = 0.1 should be dense enough for other lower Reynolds numbers.

Table 3.1 Comparison of the force coefficients and the Strouhal numbers from different meshes (*Re* =1000, α = 45°)

Mesh	Strouhal number	Mean C_D	RMS C_D	RMS C_L
Δz=0.1, normal mesh	0.143	0.584	0.041	0.177
Δz=0.05, normal mesh	0.145	0.587	0.040	0.177
Δz=0.05, dense mesh	0.145	0.580	0.041	0.174

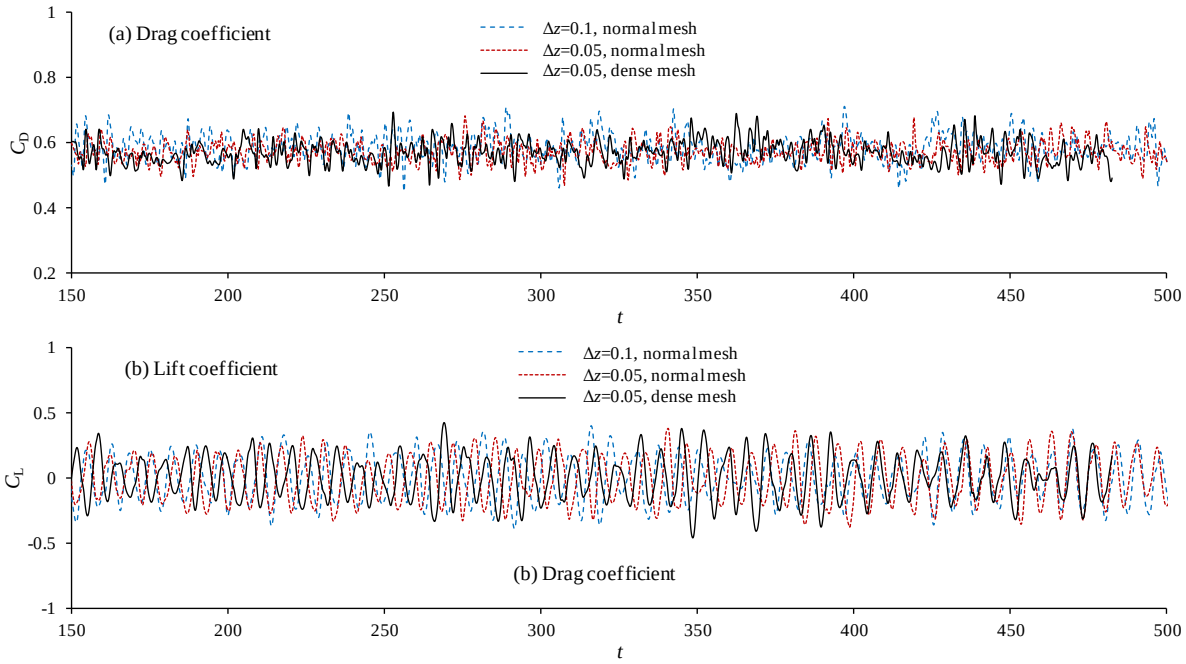

Fig. 3.3 Comparison of the sectional force coefficients at the mid-span of the cylinder (z=9.6) from three difference meshes at *Re* = 1000 and α = 45°

3.4 α = 0°

Vortex shedding from a circular cylinder at α=0° is simulated in order to validate the numerical model and provide a benchmark against which the comparisons can be made. Simulations are carried out for Reynolds numbers ranging from 100 to 700 with an interval of 50. Three-dimensionality is observed when Reynolds number is increased up to 250. Fig. 3.4 shows the variation of the pressure coefficient along the line of θ=45° on the cylinder surface with time at α=0° and *Re*=250. The pressure coefficient C_p is defined as $C_p = (p - p_0)/(\rho U^2/2)$, with p_0 being the pressure at the inlet boundary. The position angle θ is defined as the angle from the downstream edge of the cylinder in the anti-clockwise

direction (measured from the *x*-axis). Zhao *et al*. (2009) showed numerically that the flow is initially 2D and transits from 2D to 3D gradually. The fluctuation of the pressure in time is due to the periodic vortex shedding. The contours of the pressure coefficient before *t*=250 are parallel to the *z*-direction, indicating that the flow is still two-dimensional. Starting from *t*=260, the variation of the pressure in the *z*-direction becomes more and more obvious. The regular periodic variation of pressure in the *z*-direction from *t*=260 to 350 corresponds to the wavy vortex tubes in the spanwise direction as shown in Fig. 3.5 (b). It can be seen that two very small disturbances start developing at about *z*=2.5 and 16 respectively at *t*=625. These disturbances become stronger and stronger and finally make the variation of the pressure in the *z*-direction irregular. Between *t*=700 and 720, the variation of the pressure contours at *z*=0 with time has about 180° phase difference with that at *z*=7.5. The phase difference in the pressure corresponds to the phase difference in the vortex shedding.

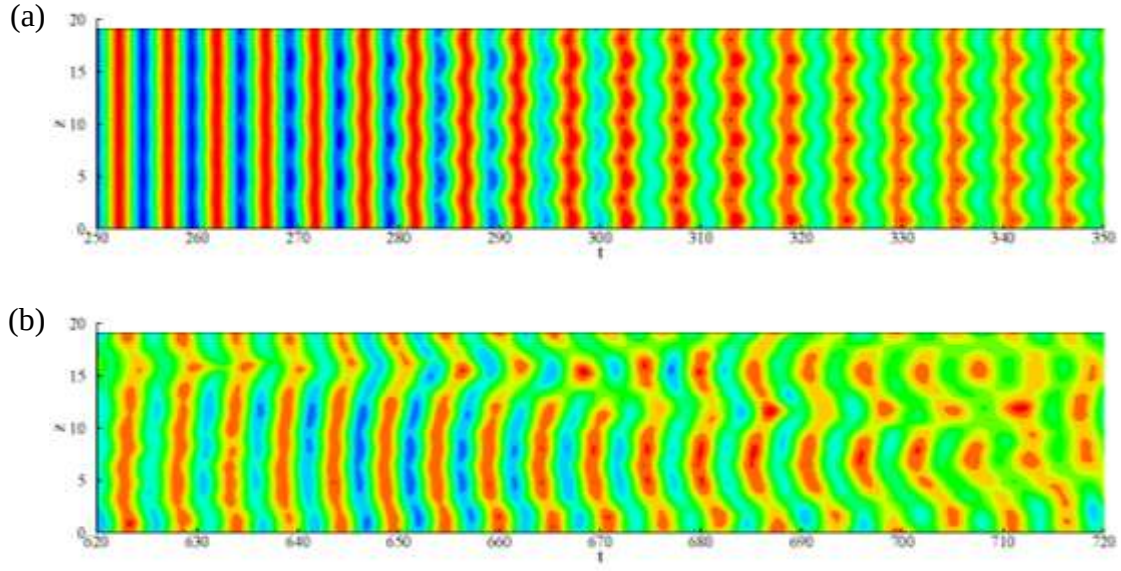

Fig. 3.4 Variation of the pressure coefficient distribution along the line of θ=45° on the cylinder surface with time at α=0° and *Re*=250. (a) Transition from 2D to 3D flow; (b) Transition from periodic variation in the *z*-direction to irregular variation

The vortex flow structure can be identified by the iso-surface of the second negative eigenvalue of the tensor $\mathbf{\Psi}^2 + \mathbf{\Omega}^2$, where $\mathbf{\Psi}$ and $\mathbf{\Omega}$ are the symmetric and the anti-symmetric parts of the velocity-gradient tensor, respectively. This second eigenvalue, say e_2, represents the location of the vortex core (Jeong and Hussain, 1995). Fig. 3.5 shows the iso-surfaces of $e_2 = -0.25$ for α=0° and *Re*=250. In the early stage of the simulation (*t*<250), the flow is two-

dimensional and all the vortices in the wake are aligned in the spanwise direction. The vortex structures in Fig. 3.5 (b) are the same as the mode A vortex wake shown in Figure 13 in Williamson (1996). The wavy primary vortices in mode A that has been observed in the experiments are clearly observed in Fig. 3.5 (b). The wavy spanwise vortices result in the formation of axial vortices that are in pairs (Williamson, 1996). The streamwise vortex pairs are weaker than the axial vortices. The wavelength of the wavy vortices in the axial direction of the cylinder is found to be between 3 and 4 by both experimental studies and 3D direct numerical simulations (Zhang *et al*., 1995; Williamson, 1995; Braza *et al*., 2001). In Fig. 3.5 (b), it appears that there are about 5 waves in each axial primary wavy vortex tube. Since the length of the cylinder is 19.2, the 5 waves correspond to a wavelength of about 3.84, which is close to 4.27 reported in Braza *et* al. (2001). The regular wavy variation of the vortices in mode A can only be observed in the early stage of the transition, after which the dislocations occur along the axial direction of the cylinder (Williamson, 1995). It is found in this study that the wavy primary vortices are parallel to the axis of the cylinder in the early stage of the transition. As shown in Fig. 3.5 (b) and (c) the vortices are no longer parallel to the axis of the cylinder after t=650. Obvious dislocations can be seen in Fig.3.5 (c), where the wavelength in the axial direction is difficult to identify.

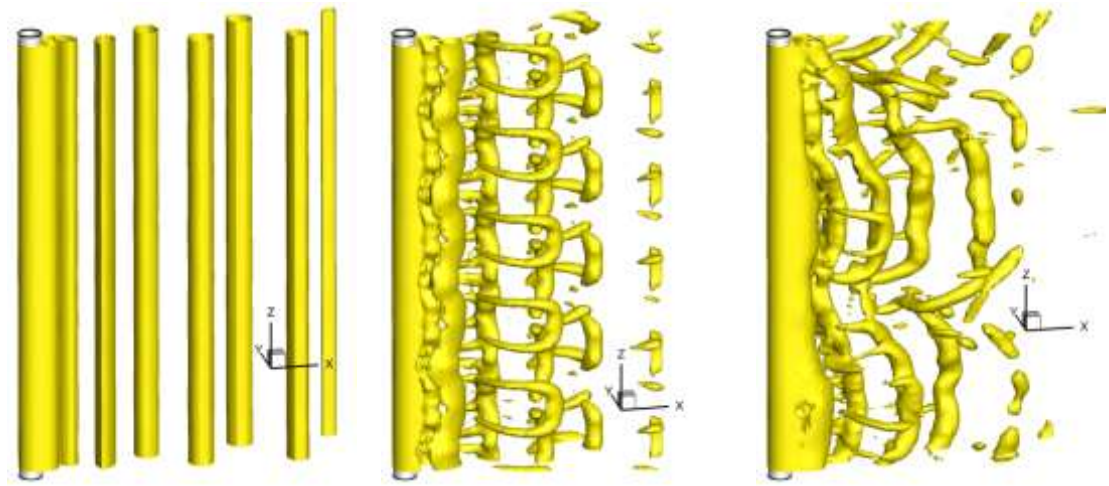

(a) Re=250, t=237 (b) Re=250, t=365 (c) Re=250, t=740

Fig. 3.5 Iso-surface of $e_2 = -0.25$ at α=0° and Re=250

Fig. 3.6 shows the contours of the axial vorticity at different cross sections along the axial direction of the cylinder at *Re* = 250, α=0° and *t*=740. Dislocations of the vortices found at *z*=0 (Fig. 3.6 (c)) are also apparent in Fig. 3.6 (a). The two main vortices from the two sides of the cylinder in Fig. 3.6 (a), which corresponds to the location of dislocation, are similar to each other and the vortices behind them are very weak. It can be seen that there are significant phase differences among the vortex shedding processes at different axial locations. For example, at *z*=6.4 and 9.6, the positive vortex from the top side of the cylinder has been separated from the cylinder and the negative vortices from the bottom side are still developing. However, the vortex shedding at *z*=16, where the vortex from the bottom side of the cylinder has been shed and that from the top side is growing, is almost in anti-phase with those at *z*=6.4 and 9.6. The phase difference of the vortex shedding along the axial direction of the cylinder, which is the direct result of the vortex dislocation as shown in Fig. 3.5 (c), leads to the total lift coefficient on the cylinder obtained by integration over the whole cylinder surface less than the sectional lift coefficient. At *Re* = 300, the vortex flow pattern is very similar to that at *Re*=250 and the vortex structure is not shown here.

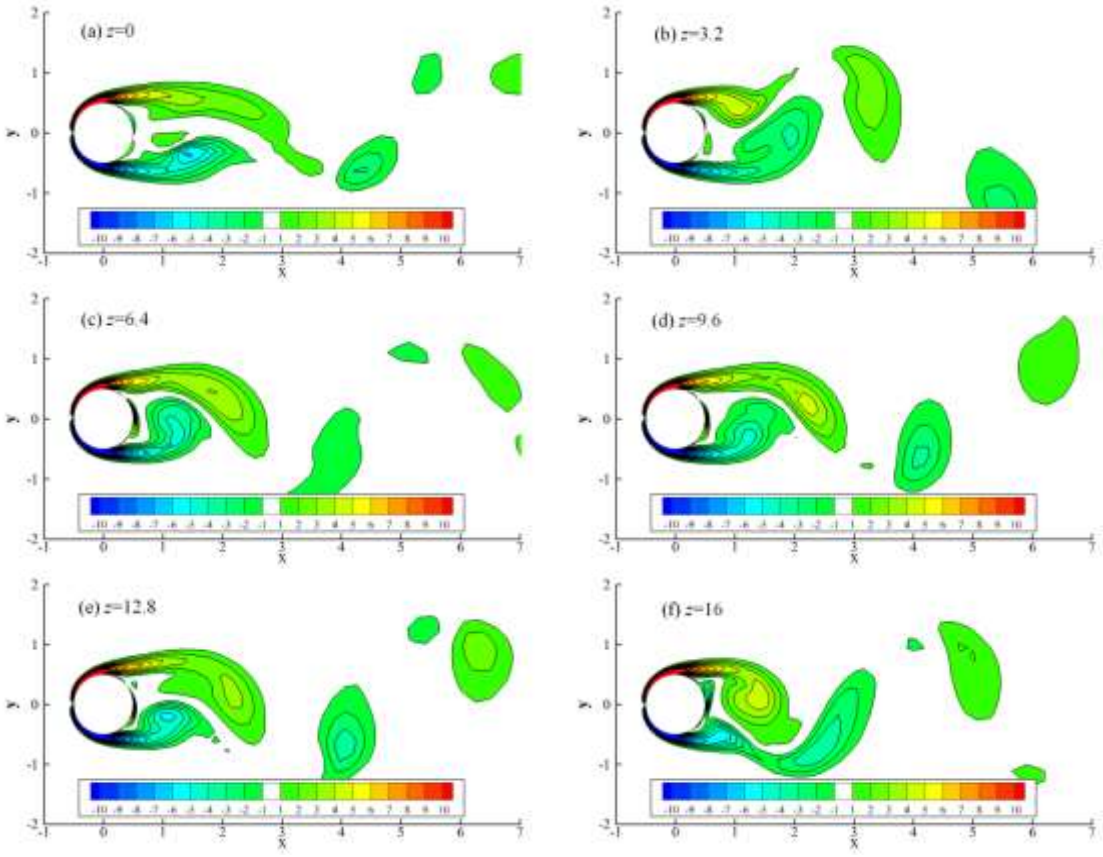

Fig. 3.6 Contours of axial vorticity at different cross sections (α=0°, *Re*=250, *t*=740)

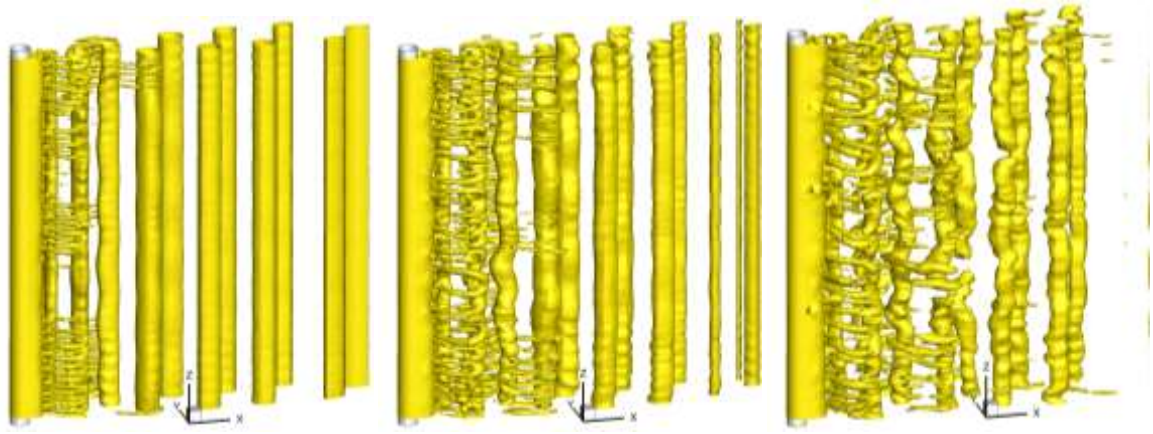

(a) t=85 (b) t=90 (c) t=95

Fig. 3.7 Iso-surface of $e_2 = -0.25$ at α=0°, *Re*=700 at three instants for α=0°

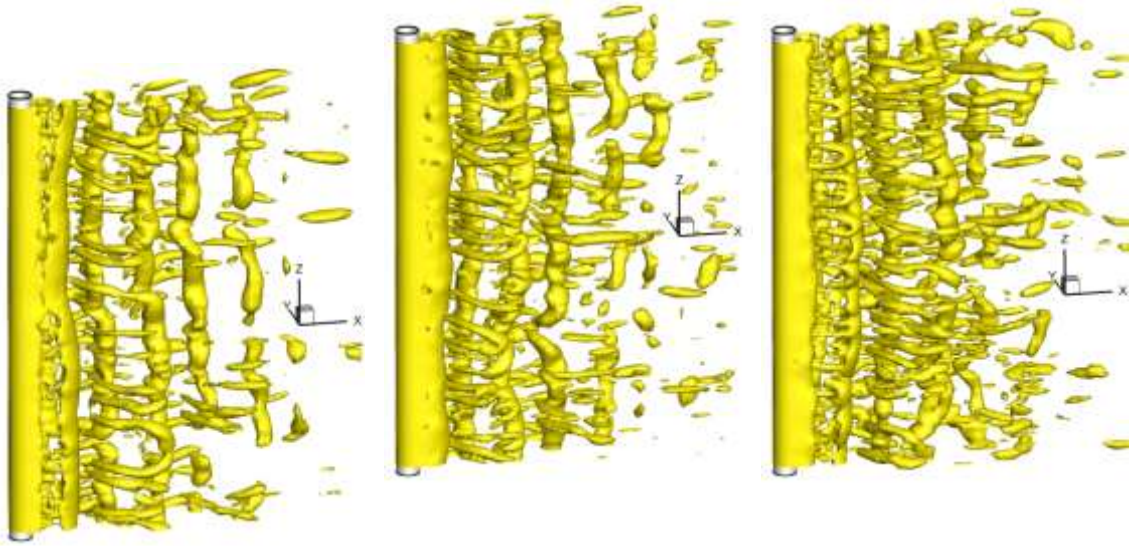

(a) α=0°, Re=350, t=557 (b) Re=500, t=555 (c) Re=700, t=435

Fig. 3.8 Iso-surface of $e_2 = -0.25$ at α=0° and different Reynolds numbers for α=0°

Fig. 3.7 shows the iso-surfaces of e_2=-0.25 at three instants during the transition of the flow. Fig. 3.8 show the iso-surface of e_2=-0.25 at α=0° and *Re*=350, 500 and 700 in the fully developed 3D flow condition. Transition of the flow from 2D to 3D at *Re*=700 is characterized by the occurrence of the streamwise vortices in the early stage and the gradual increase in the streamwise vortices until the flow becomes fully developed. In Fig. 3.7 (a) the streamwise vortices occurs at the two ends and the centre of the cylinder. The streamwise vortices become stronger and stronger and the wake flow has been dominated by the streamwise vortices in Fig. 3.7 (c). After t=95, the strength of the streamwise vortices continues increasing. The fully developed flow in Fig. 3.8 (c) is different from that in Fig. 3.7

in two ways. Firstly, the strength of the streamwise vortices is stronger than those in Fig. 3.7 Secondly, because the energy is transferred from the spanwise vortices to the streamwise vortices, the spanwise vortices in Fig. 3.8 (c) dissipate faster than those in Fig. 3.7. The streamwise vortices that are relatively weak at *Re*=250 and 300 have been the dominant flow feature as Reynolds number exceeds 350. The wake flow pattern featured by counter-rotating vortex pairs in the perpendicular direction of the cylinder as shown in Fig. 3.8 was referred to as model B (Williamson, 1996; Barkley and Henderson 1996; Scarano and Poelma 2009). Mode B is reported to persist typically up to about *Re*=1000. Williamson (1996) reported that the wavelength of the axial vortex feature in mode B is about one cylinder diameter. Scarano and Poelma (2009) defined two different axial wave lengths: λ_1 as the intrinsic wavelength of the vortex pair and λ_2 corresponding to the distance between adjacent pairs. They found that λ_1 is less than one diameter (λ_1/D~0.6) and λ_2 is larger than twice the inter-axial distance (λ_2/D=1.2) at *Re*=360. In this study, the vortex pairs are not regularly distributed along the axial direction of the cylinder. In order to clearly identify the distance between two adjacent pairs, the contours of streamwise vorticity in the *x*=2.5 plane at *Re*=400 is shown in Fig. 3.9. By observing the vortex contours, the maximum distance between two neighbour pairs is found to be about 2.0 and the minimum is about 1.0. The distance between the two vortices in a pair is found to be less than 1. Much less axial vortex dislocations are found at *Re*=350 and 400 than at *Re*=250 and 300 at the dislocations disappears at *Re*=500. The dominance of the streamwise vortices shown in Fig. 3.9 has significant effects on the hydrodynamic forces on the cylinder. Energy transfer from the axial vortices to the streamwise vortices appears to weaken the fluctuation of the lift which will be discussed later on.

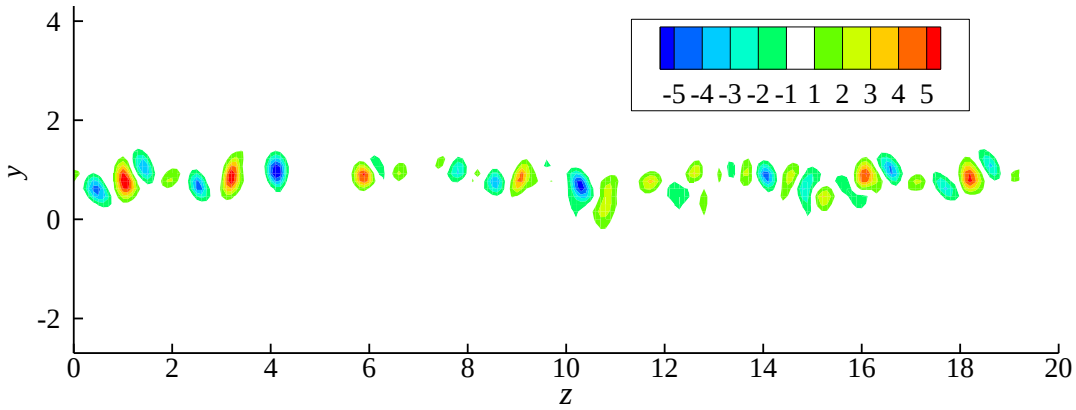

Fig. 3.9 Contours of streamwise vorticity in the *x*=2.5 plane at *Re* = 400

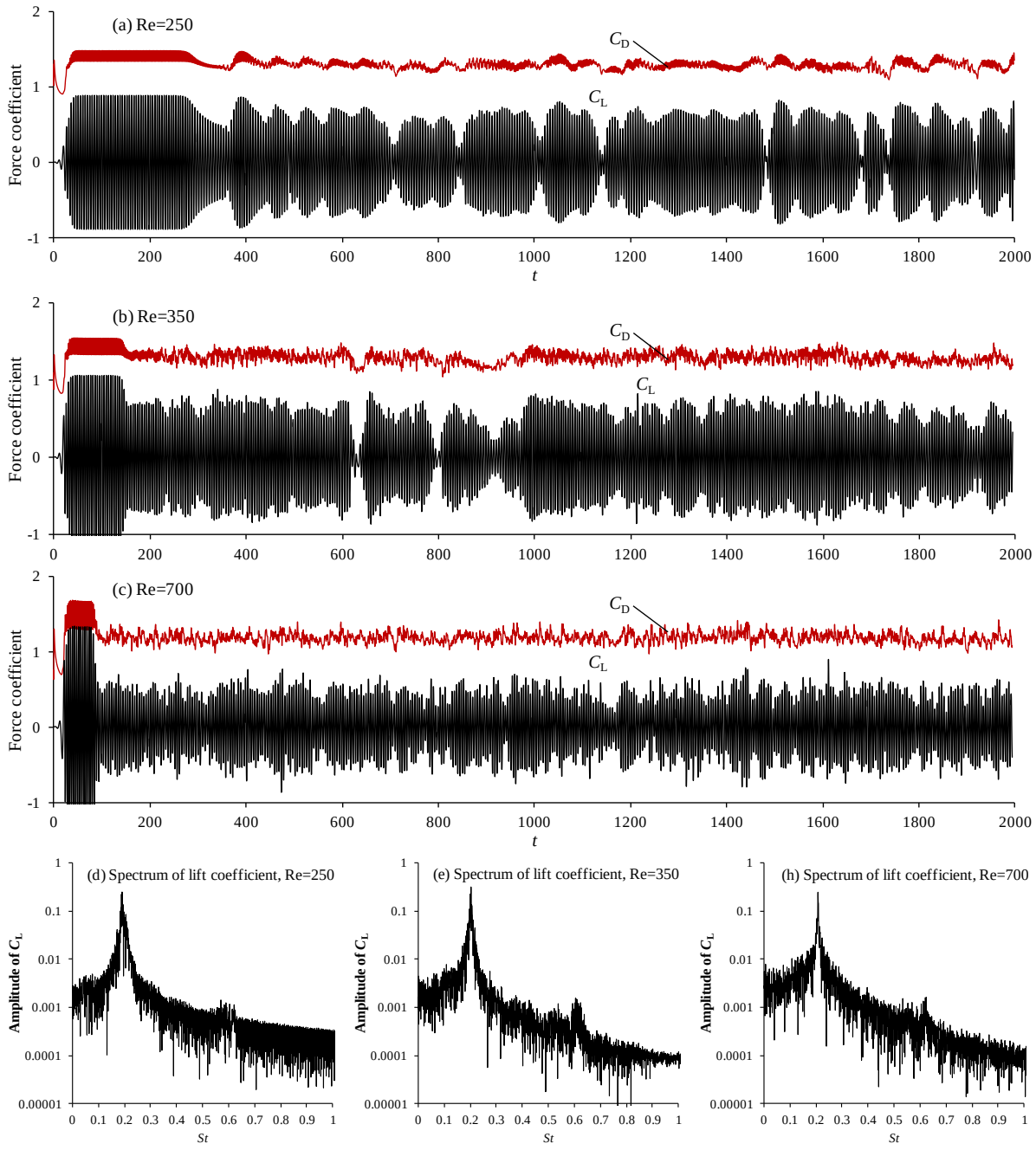

Fig. 3.10 Time histories and the spectra of sectional force coefficient at the mid-span of the cylinder for α=0º

Fig. 3.10 (a) – (c) shows the time histories of the sectional force coefficients at the mid-span (z=9.6) of the cylinder at α=0° and three Reynolds numbers. Fig. 3.10 (d) – (e) shows the corresponding amplitude spectra of the lift coefficient. In the early stage of the simulation, where the flow is still two-dimensional, the force coefficients are very regular and have high amplitudes. Once the flow becomes three-dimensional, both drag and lift coefficients are reduced significantly. The force coefficient decreases as the flow transits from 2D to 3D is partially caused by the energy transfer from axial vortices to the streamwise

vortices. By comparing the force coefficients at the three Reynolds numbers in Fig. 3.10, it can be seen that the 3D flow occurs earlier as *Re* increases. Sometimes the instantaneous amplitude of the lift coefficient is almost zero at *Re*=250 and 350. It has been shown in Fig. 3.6 that the spanwise vortices are very weak at the dislocation location. The amplitude of the sectional lift coefficient becomes very small due to the weakened vortices at the locations where the dislocation occurs. For example, the dislocation is found at the mid span of the cylinder at *t*=740 at *Re*=250 (see Fig. 3.5 (e)) and correspondingly the amplitude of the lift coefficient is found to be close to zero at *t*=740 in Fig. 3.10 (a). By observing Fig. 3.10 (a) and (b), it can been seen that the dislocation at *Re* = 250 occurs more frequently than it does at *Re* = 350. At *Re* = 700, the amplitude of the lift coefficient is overall smaller than those at *Re* = 250 and 300. It is believed the energy transfer from the spanwise vortices to the streamwise vortices leads to a reduction in the lift coefficient. The dislocations do not affect the vibration frequency. Each of the spectra in Fig. 3.10 (d) – (e) is dominated by single frequency, which is close to 0.2.

The wavelength of the vortex feature in the spanwise direction are analysed in detail by performing the spectral analysis along the spanwise direction. Fig. 3.11 shows the variation of the spanwise velocity components (*w*) along three lines parallel to the cylinder at *Re* = 250. At *t*=365, when the flow is in mode A without dislocation, the variation of *w* in the spanwise direction are periodic along all the three lines. However, the variations contain multiple wavelengths. The variation of *w* in the spanwise direction at *t*=740 become irregular and waves with very long wave length occurs. The variation of the velocity *w* in the spanwise direction comprises short waves riding on very long waves. It appears that the longest wavelength corresponds to the distance between two dislocation locations.

Fourier transform is use to analyse the variation of the velocity component *w* along the spanwise direction of the cylinder. Fig. 3.12 shows the special amplitude spectra of *w* along two lines of *x*=1.55 and 2.05 in the *xz*-plane in about one vortex shedding period. Each spectrum in Fig. 3.12 is presented in the time-wave-number-domain, which is generated using a series of spectra with a time interval of 0.25. The wave number is defined as $k = 1/\lambda$, with λ being the wavelength of the vortex feature in the spanwise direction. At *t*=365, three distinct peak wave numbers are identified in Fig. 3.12 (a), (b). The wave number of 0.25 (wavelength of about 4) corresponds to the distance between two neighbour vortex pairs shown in Fig. 3.5 (b), while the wave number of 0.53 (wavelength of about 1.9) corresponds

to the distance between the two vortices in a vortex pair. At *t*=740, one of the peak wave number is about 0.2. Another peak wave number of about 0.4-0.5 is not very clear. In Fig.3.12 (c) there is a peak wave number of about 0.125, corresponding to a very long wavelength of about 8. This wave number occurs because of the dislocation as shown in Fig.3.5 (c). It can be seen in Fig.3.12 that sometimes the spanwise waves are obvious and sometimes they are weak. The waves become stronger when the main vortex is passing the interested location.

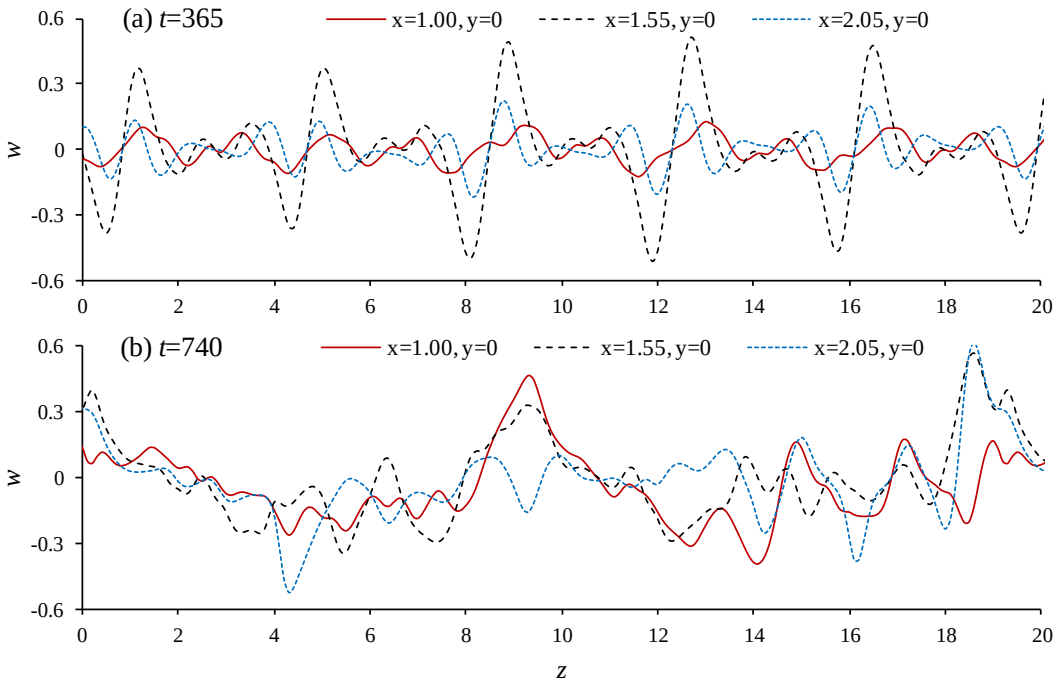

Fig. 3.11 Variation of the spanwise velocity component *w* along three lines parallel to the cylinder at *Re*=250

Fig. 3.13 shows the spatial amplitude spectra of the spanwise velocity along two lines parallel to the cylinder in the frequency-time domain at *Re* = 700. At *Re* = 700, where the flow has been fully turbulent, it appears that no distinct peak wave numbers can be identified in Fig. 3.13. The wave number at *Re* = 700 varies from 0.25 to 1.0, corresponding to wave lengths from 1 to 4. Within one vortex shedding period (about 5), the peak wave number of about 0.625 occurs more frequently than others.

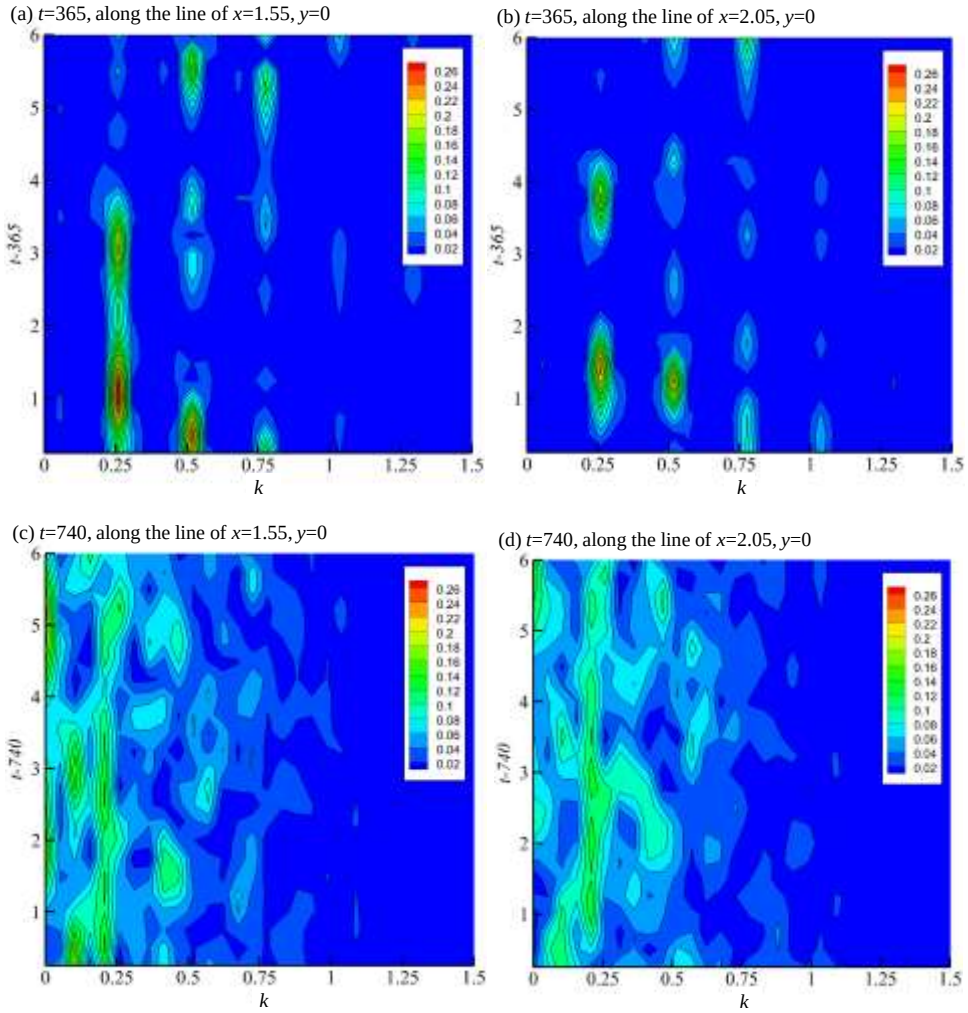

Fig. 3.12 Amplitude spectra of the spanwise velocity along two lines parallel to the cylinder in the wave-number-time domain at Re = 350 and α = 0°

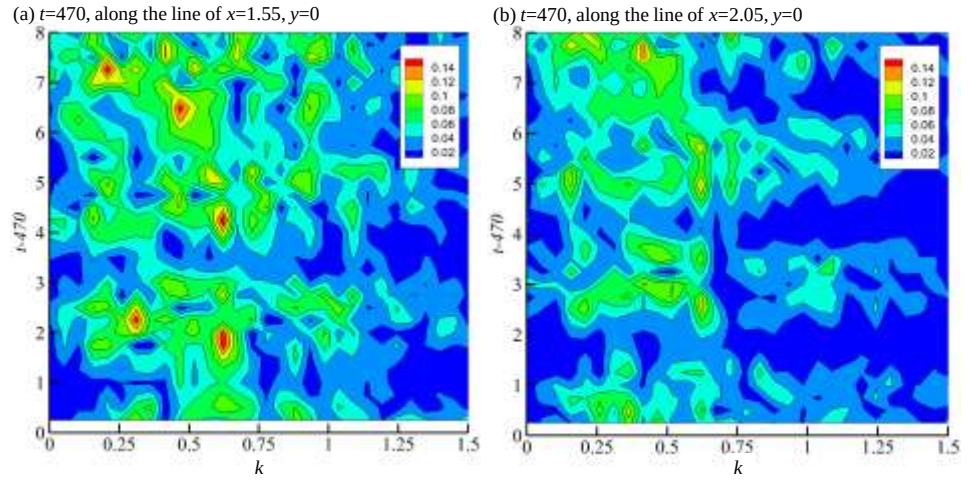

Fig. 3.13 Amplitude spectra of the spanwise velocity along the lines parallel to the cylinder in the wave-number-time domain at Re = 700

The transition of the flow to 3D has significant influences on vortex shedding frequency. In this study, the vortex shedding frequency is determined based on the oscillatory sectional lift force at the mid-section (z=9.6) of the cylinder. Fig. 3.14 shows the variation of the Strouhal number with the Reynolds number at α = 0°. Two discontinuities were observed in the Strouhal number in the experimental data. The dislocation of the vortices leads to one discontinuity as the flow changes from 2D to mode A.

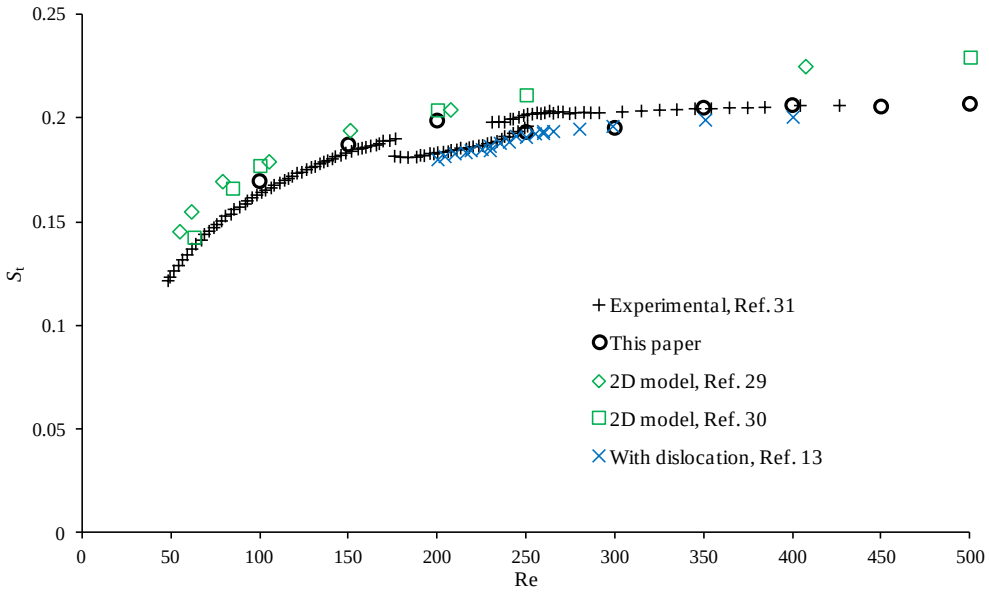

Fig. 3.14 Variation of the Strouhal number with the Reynolds number at α = 0°

Another discontinuity occurs as the flow transits from mode A to mode B, where the vortex dislocation does not exist. The 2D numerical model results by Lei *et al*. (2000) and Zhao *et al*. (2005) obviously over-predict the Strouhal number, especially at the high Reynolds number regime. Because the 2D model cannot predict the change in the vortex shedding mode, the Strouhal number from the 2D model varies with *Re* Smoothly. By artificially producing dislocations through end control, Prasad and Williamson (1997) found that the Strouhal number with dislocations was lower than that without dislocations. The calculated Strouhal number agrees well with the experimental data except at around *Re* = 200. The simulated Strouhal number at *Re* = 200 is greater than the experimental data because the simulated wake flow is found to be 2D. Miller and Williamson (1994) found that the end condition has significant effect on the critical Reynolds number for transition and the laminar regime can be extended up to 194 and even beyond 200. The critical Reynolds number found in present study is greater than 200 because the configuration is exactly

symmetric and no end effect exists due to the periodic boundary conditions at the two ends of the cylinder. At *Re* = 300, the Strouhal number agrees with Prasad and Williamson (1997) because vortex dislocations are observed in the numerical simulation. When $Re \geq 350$, vortex dislocations disappear and the Strouhal number agrees very well with that measured by Williamson (1992).

The variation of the sectional lift coefficient in the axial direction is examined by the correlation factor defined as $R(z_1, z_2) = C_L'(z_1)C_L'(z_2)/[C_{L,\mathrm{rms}}(z_1)C_{L,\mathrm{rms}}(z_2)]$, where $C_L'(z) = C_L(z) - \overline{C}_L(z)$ is the fluctuating lift coefficient, $\overline{C}_L(z)$ is the time-averaged lift coefficient, $C_{L,\mathrm{rms}}(z)$ is the root-mean-square (RMS) of the lift coefficient. The correlation factor is obtained based on the lift forces in the last 20 vortex shedding periods of the simulation. Fig.3.15 shows the variation of the correlation factor *R*(0, *z*) along the cylinder span at α =0° and different Reynolds numbers. Fig.3.15 (b) is the same as Fig.3.15 (a) but with a zoomed-in view of the *y*-axis. When *Re* = 200, *R* (0, z) is 1 along the whole cylinder because the flow is 2D. The correlation factor *R* (0, 19.2) is 1 for all the Reynolds numbers because the periodic boundary condition is used at the two ends of the cylinder. The negative correlation factors are found at *Re* = 250 and 350 because the vortex shedding at one axial location is in anti-phase with that at *z*=0 due to vortex dislocations. Based on the zoom-in view of the R-axis in Fig.3.15 (b), it appears that the decrease rate of *R* with increasing *z* increases with *Re*, except at *Re* = 250 and 300. At *Re* = 700, the correlation factor *R* (0, 9.6) at the mid-span of the cylinder is about 0.61. The small wavelength in the *z*-direction is observed in the curves of *R*(0,z) at *Re* = 350 and 400, indicating that the wavy vortex structures still exist in the low Reynolds number regime of transition mode B.

3.5 α = 45°

When the flow past an inclined circular cylinder is studied, apart from the Reynolds number that is defined as $\mathrm{Re} = UD/\nu$, another Reynolds number $\mathrm{Re_n}$ is defined based on the velocity component normal to the cylinder as $\mathrm{Re_n} = UD\cos\alpha/\upsilon$. $\mathrm{Re_n}$ is named as the normal Reynolds number in this study. Fig. 3.16 shows the iso-surface of the eigenvalue e_2 = -0.25 at α=45° and a number of Reynolds numbers. The flow at α=45° is different from that at α=0° in the following aspects.

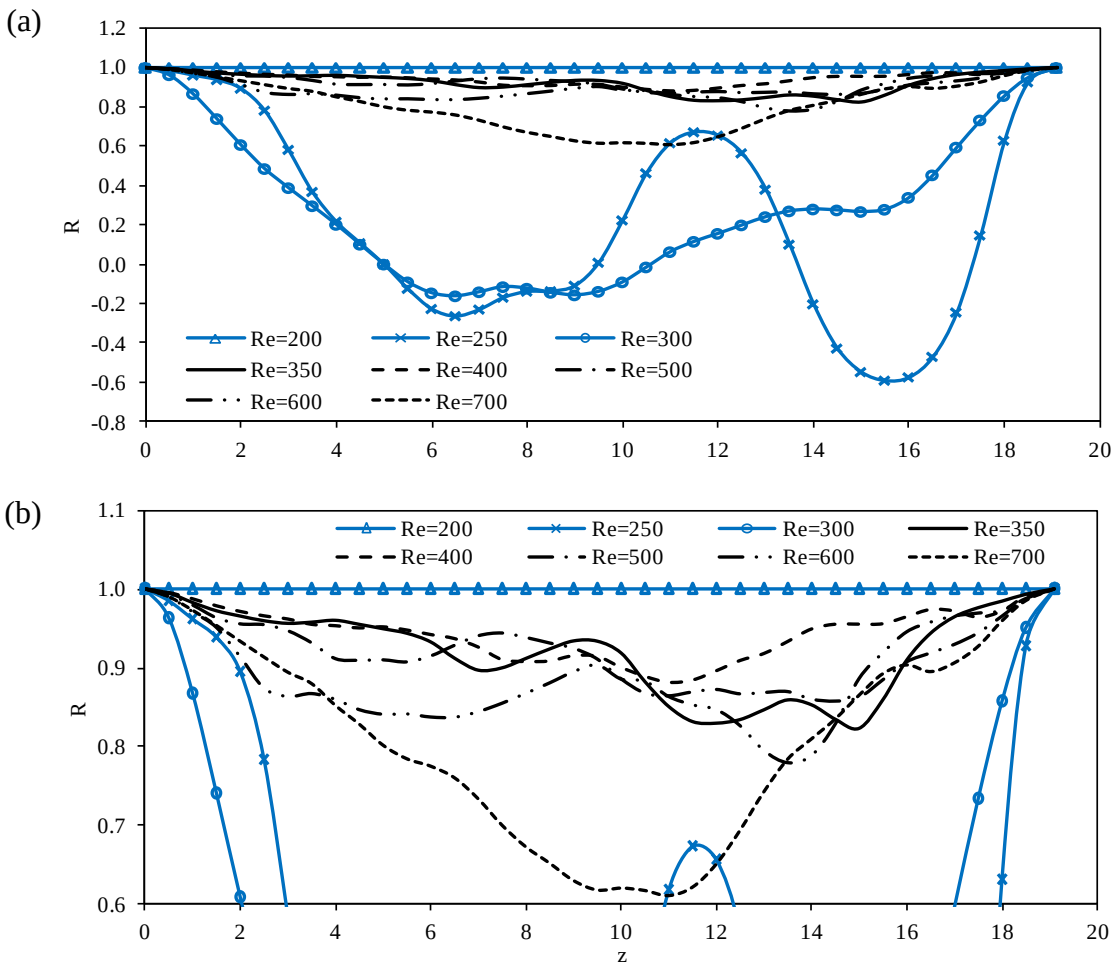

Fig. 3.15 Variation of the correlation factor $R(0,z)$ along the cylinder span at α=0°. (b) zoom-in view of (a).

Firstly, the critical Reynolds number for flow transition from 2D to 3D at α=45° is greater than that at α=0°. The flow is found to be two-dimensional at Re=250 as α=45° (Fig. 3.16 (a)). At Re=300, although the axial vortices become wavy in the axial direction of the cylinder, the vortices that are perpendicular to the cylinder axis are too weak to be identified in Fig. 3.16 (b). Along the total length (19.2) of the cylinder, there are 6 waves in each of the axial vortex tubes shown in Fig. 3.16 (b), corresponding to a wavelength of 3.2. This axial wavelength at α=45° is slightly (about 20%) smaller than that at α=0°. The axial wavelength at Re=400 can still be identified from the vortex structure shown in Fig. 3.16 (c) and it is found to be about 4.0, which is larger than that at Re=300. At Re=500 and 600, the wavelength of the axial variation of the vortices cannot be identified clearly from the vortex structures. It appears that if it is evaluated based on the normal Reynolds number Re_n, the 3D flow for α=45° occurs at Re_n=212 (Re=300), which is close to that for α=0°. However, it can be seen in the following discussion that the wake vortex flow structure at α=45° is not quite the same as that at α=0°.

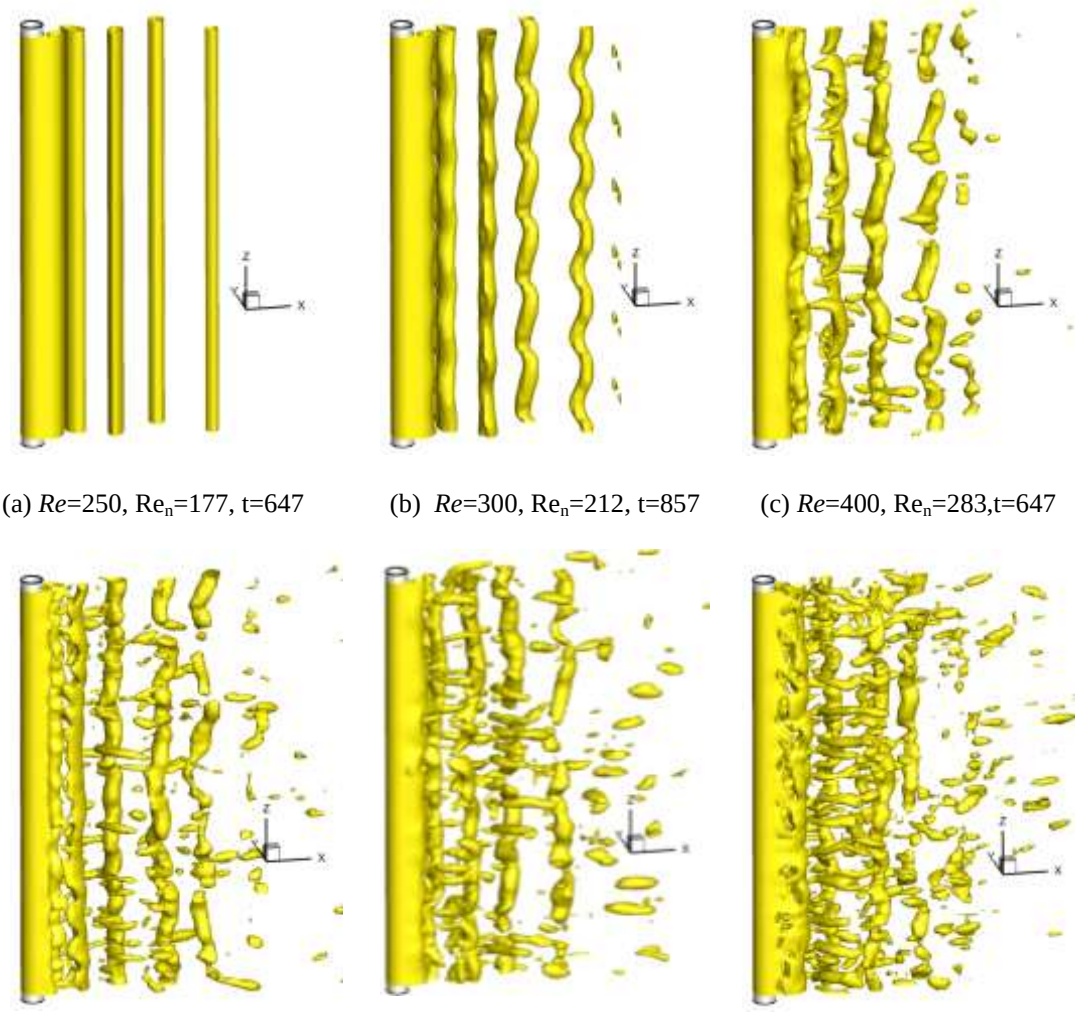

(a) *Re*=250, Re_n=177, t=647 (b) *Re*=300, Re_n=212, t=857 (c) *Re*=400, Re_n=283,t=647

(d) *Re*=500, Re_n=354,t=660 (e) *Re*=600, Re_n=424, t=430 (f) *Re*=1000, Re_n=707, t=595

Fig. 3.16 Iso-surface of $e_2 = -0.25$ at α=45° and different Reynolds numbers

The second difference between the wake flow at α=45° and that at α=0° is that the streamwise vortices at α=45° occur at higher Reynolds numbers than the case with α=0° (even based on the normal Reynolds number). The streamwise vortices almost do not exist at $Re \leq 350$ (Re_n=248) and only occur sporadically as $400 \leq Re \leq 600$ ($283 \leq Re_n \leq 424$). At *Re*>700 (Re_n=495 and 566), the streamwise vortices can be clearly identified (Fig.3.16 (f)). Thirdly, the dislocation observed in mode A is not obvious at α=45° for all the calculated Reynolds numbers. After the wake flow becomes 3D at *Re*=300, the axial vortices become stronger and stronger gradually with the increasing Reynolds number.

Fig. 3.17 shows the contours of the pressure coefficient at θ=45° in the *z*-*t* plane. The pressure contours in Fig. 3.17 (a) is very regular and the wavelength in the *z*-direction can be

clearly identified. Although they are some spanwise features of long wavelength, the pressure contours are overall parallel to the *z*-axis in Fig. 3.17 (b), indicating that dislocations are very weak. Fig. 3.18 shows the streamlines around the primary axial vortex in the wake of the circular cylinder at *Re*=500 and the two different flow approaching angles. The variation of the streamlines in the axial direction shows the three-dimensionality of the flow. At α=0°, an axial flow inside the primary vortex can be identified in Fig. 3.18 (a). This axial flow does not sustain and will vanish after certain distance in the axial direction. However, it can be seen in Fig. 3.18 (b) that axial streamlines in the main vortex are throughout the whole length of the cylinder. The plane view of the streamlines shows that these axial streamlines are mainly located at the core of the primary vortex. The helical streamlines observed at α=45° are very similar to Kozakiewicz *et al*. (1995) at *Re*=1700 and Zhao *et al*. (2009) at *Re*=1000. Braza *et al*. (2001) found that dislocations occur where the braid configuration of the streamwise vortex pair occurs initially, which progressively ejects fluid from the first violet main eddy. At α=45°, because the fluid inside the primary vortices behind the cylinder flows in the axial direction helically, any disturbance that may trigger the dislocation of the axial vortex is suppressed at the location where it is generated. This might be the reason that inhibits the dislocation of the vortices. It can be seen in Fig. 3.18 (b) that although some discontinuities of the pressure contour occur, the axial flow tends to smooth out these discontinuities.

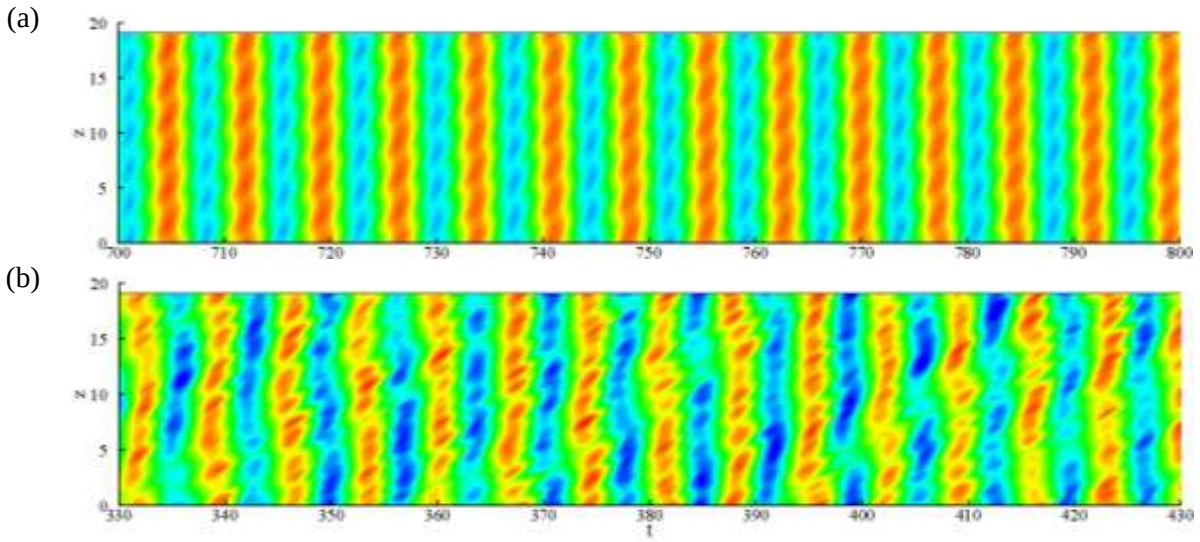

Fig. 3.17 Contours of the pressure coefficient along the line of θ=45° in the *z*-*t* domain. (a) *Re* = 300, Re_n = 212; (b) *Re* = 600, Re_n = 424

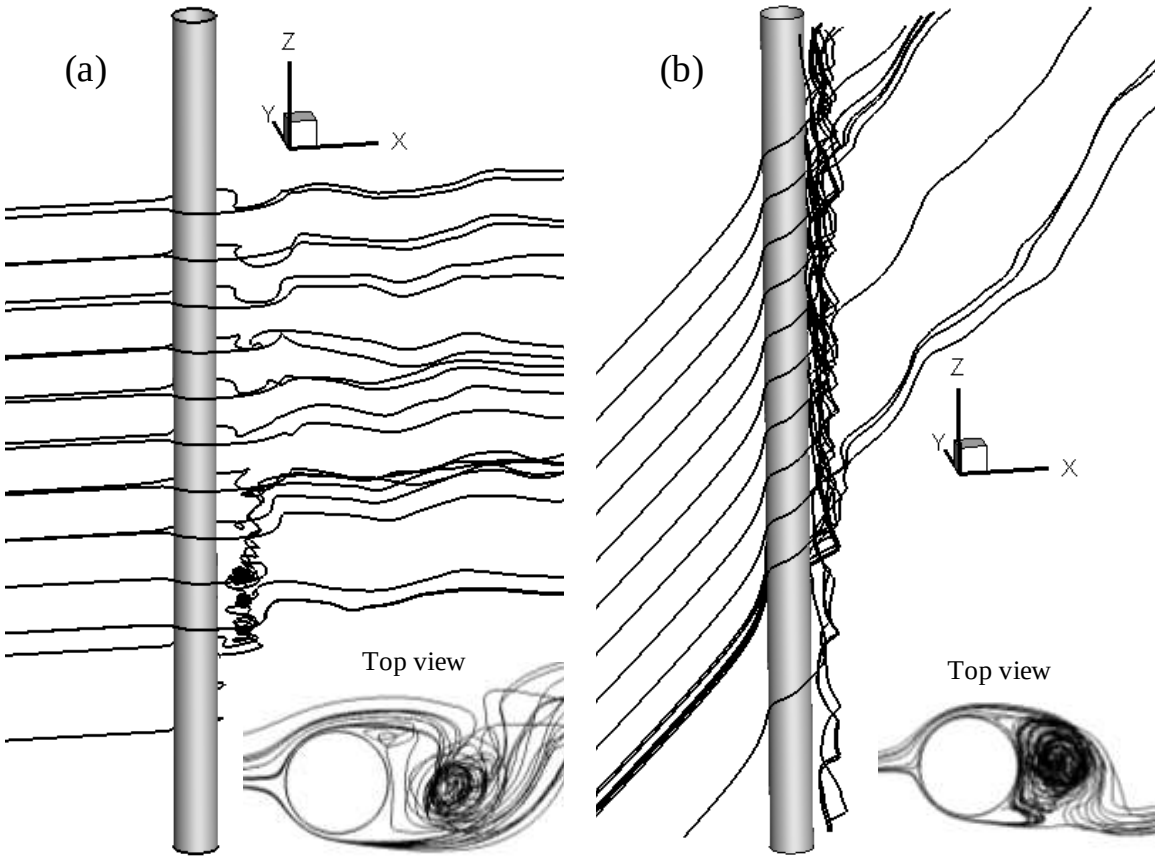

Fig. 3.18 Streamlines around the circular cylinder at *Re* = 500. (a) α = 0°, (b) α = 45°

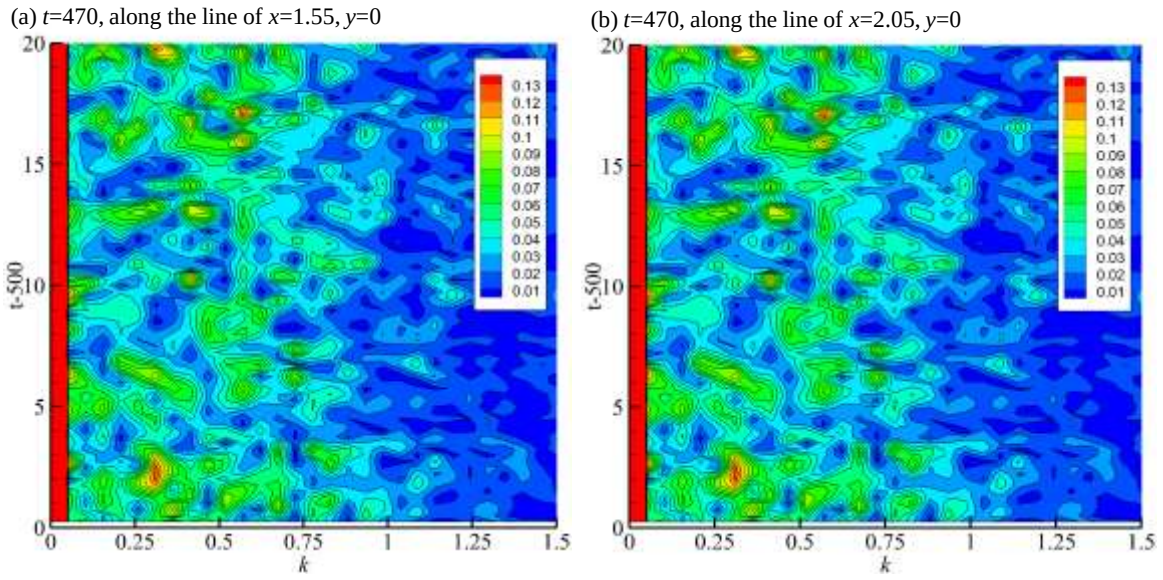

Fig. 3.19 Amplitude spectra of the spanwise velocity along two lines parallel to the cylinder in the wave-number-time domain at *Re* =1000 and α = 45°

Fig. 3.19 shows the amplitude spectra of the spanwise velocity along two lines parallel to the cylinder in the wave-number-time domain at *Re*=1000 and α=45°. Because the incoming velocity has a component in the spanwise direction, the zero wave number component of the spanwise velocity, which corresponds to the mean value of *w*, in the spectra is significantly large. Peak wave number varies with time and the highest wave number is 1. The component of $k>1$ has been very weak. Similar to those in Fig. 3.13, the high amplitude mainly located between $0.25 \le k \le 0.75$.

Fig. 3.20 shows the comparison of the Strouhal number at α=45° with that at α=0°. The normal Strouhal number S_{tn} is defined as $S_{tn} = fD/(U\cos\alpha) = S_t/\cos\alpha$. It can be seen that if the Strouhal number at α=45° is defined based on the incoming velocity ($S_t=fD/U$), it is much smaller than that at α=0° and does not change much as Re is larger than 600. However, the variation of the normal Strouhal number with the normal Reynolds number at α=45° is close to that at α=0°. Because the dislocation of the vortices is not observed at α=45°, the sudden decrease in Strouhal number at the boundary Reynolds number between the 2D flow and Mode A, which is observed at α=0°, is very weak at α=45°. In the laminar flow zone, i.e. $Re_n \le 200$, the normal Strouhal number from α=45° is very close to that for α=0°. As $Re_n>300$, the normal Strouhal number at α=45° is slightly smaller than that at α=0°. As $Re_n>500$, the normal Strouhal number becomes almost independent on Re_n at both inclined angles of the cylinder.

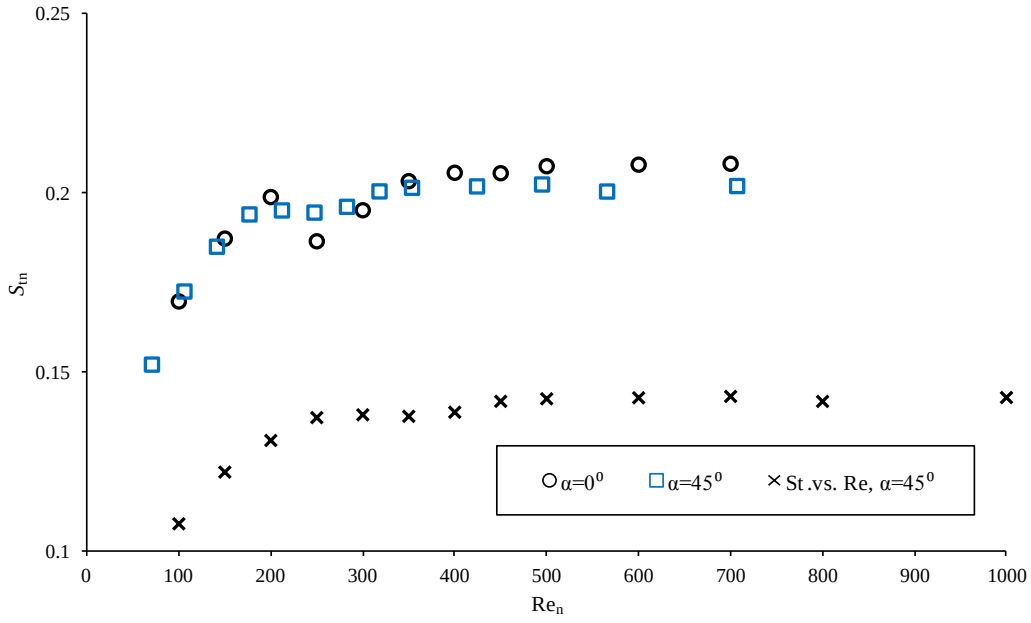

Fig. 3.20 Comparison of Strouhal number between α = 0° and α = 45°

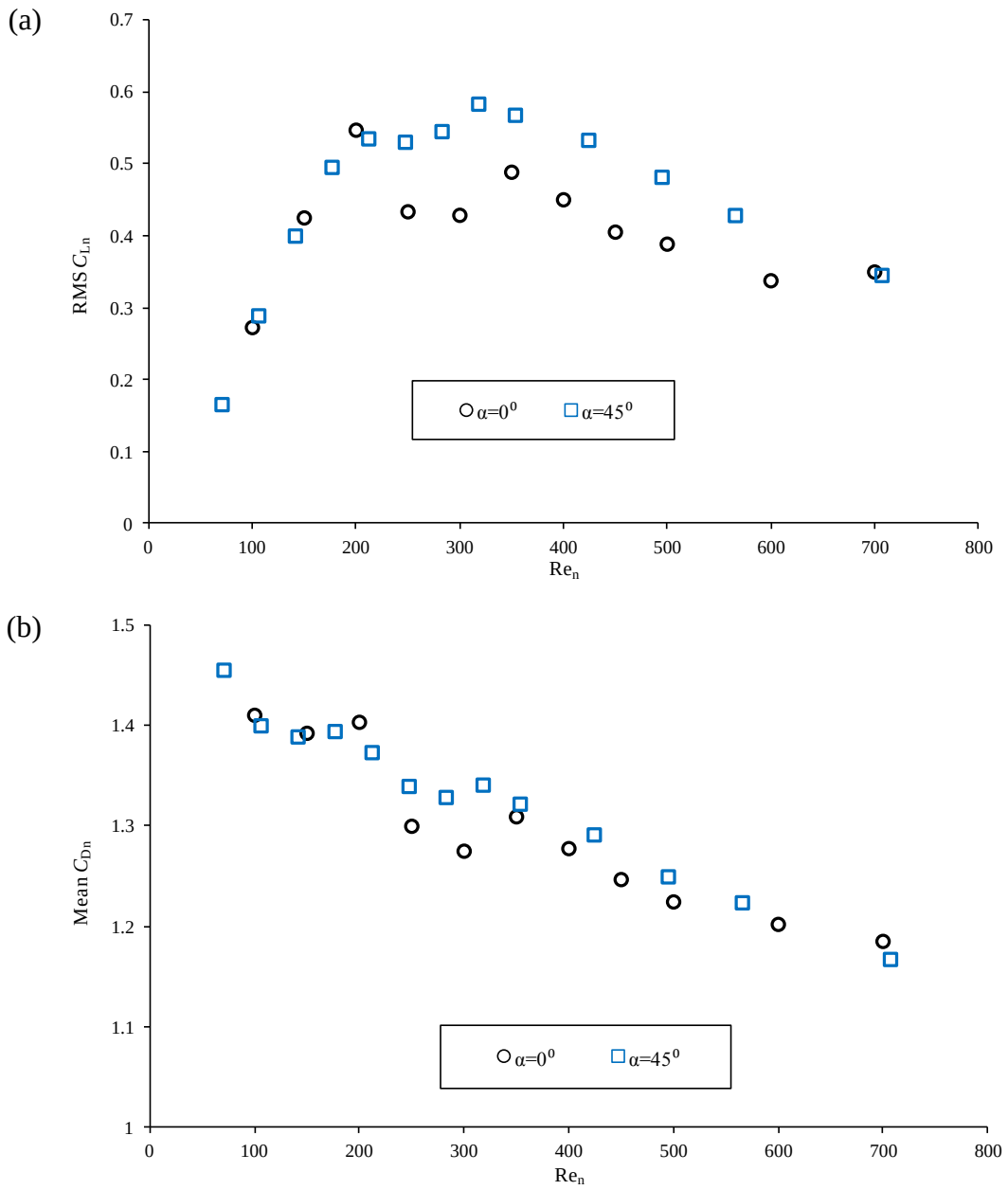

Fig. 3.21 Variation of mean drag and RMS lift force coefficients with Reynolds number. (a) RMS lift coefficient; (b) Mean drag coefficient

Fig. 3.21 shows the variation of the mean sectional drag and the root-mean-square (RMS) sectional lift coefficients with the Reynolds number. The normal drag coefficient C_{Dn} and the normal lift coefficient C_{Ln} are defined based on the velocity component perpendicular to the cylinder, i.e. $C_{Dn}(z) = F_D(z)/\left(\rho DU^2 \cos^2 \alpha / 2\right)$ and $C_{Ln}(z) = F_L(z)/\left(\rho DU^2 \cos^2 \alpha / 2\right)$. The statistic values of the force coefficients are obtained based on the sectional force coefficients at the middle of the cylinder span (z=9.6) in at least 80 vortex shedding periods. In the laminar flow regime, the RMS normal lift coefficient at α=45° are almost the same as

that at α=0°. Big difference in RMS normal lift coefficient occurs over $250 \leq Re_n \leq 550$, where the flow is transiting from laminar flow regime to fully turbulent flow regime. As discussed above, the streamwise vortices in the wake of the cylinder at α=45° occurs later than those at α=0°. The weaker streamwise vortices makes the RMS normal lift coefficient at α = 45° larger than that at α = 0° over $250 \leq Re_n \leq 550$. The difference in the RMS normal lift coefficient between α = 0° and 45° in the Reynolds number range of $250 \leq Re_n \leq 550$ is about 20 to 28%. At Re_n= 700, the RMS lift coefficients from the two inclined angles of the cylinder are quite close. Zhao *et al*. (2009) studied flow past an inclined circular cylinder at Re_n=1000 and also found that the RMS lift coefficient at α = 0° is almost the same as that at α=45°. The biggest difference in mean C_{Dn} between the two inclined angles also occurs at Re_n = 250 and 300, where the dislocation occurs at α = 0° and does not at α = 45°. Apart from these two Reynolds numbers, the difference in the mean C_{Dn} between the two inclined angles is less than 10%.

Fig. 3.22 shows the variation of the correlation factor $R(0,z)$ of the sectional lift coefficient along the cylinder span at α = 45°. At *Re* =300 (Re_n=212), weak oscillation of the correlation factor R (0, z) in the z-direction has been seen, indicating the occurrence of the three-dimensionality of the flow. Although the dislocation is not observed, the correlation factor at the middle of the cylinder at *Re* =350 (Re_n = 248) is greater than those at *Re* = 300 and *Re* = 400. The variations of the correlation factor at *Re*=400, 450, 500, 600 are generally close to each other, with that at *Re* = 400 retaining the small-wavelength component. The minimum correlation factor at the middle section occurs at *Re* = 1000 (Re_n = 707). It seems that the variation of the correlation factor R in the z-direction at *Re* = 800 and 1000 (Re_n = 566 and 707) for α = 45° are similar to those at *Re* = 600 and 700 for α = 0°, respectively.

3.6 CONCLUSIONS

Numerical simulations have been carried out to examine flow transition in the wake of a circular cylinder at two inclination angles (i.e. 0° and 45°) over the Reynolds number range of 100 ~ 1000. The Navier-Stokes equations are solved by the Petrov-Galerkin finite element method It is found that flow in the transition regime at α = 45° is different from that at α=0°. The conclusions are summarized as follows.

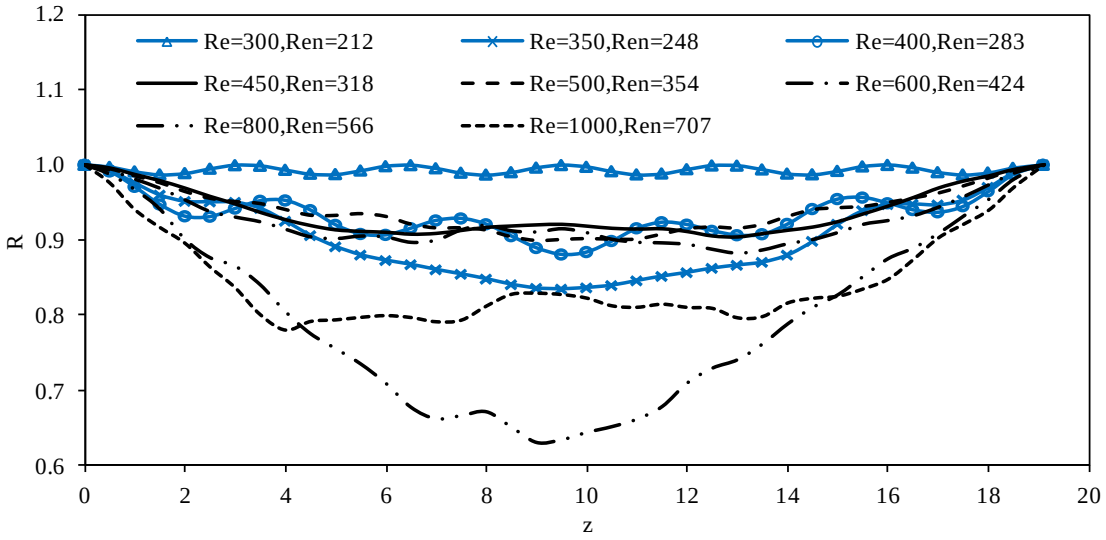

Fig. 3.22 Distribution of the correlation factor of the sectional lift coefficient along the cylinder span at α = 45°

At α = 0°, the typical wake flow structures that were observed in the laboratory tests such as the wavy axial vortices in the early stage of mode A, the vortex dislocation in the late stage of mode A and the streamwise vortex dominant wake vortex flow structure in mode B, dimensions of the vortex structures, force coefficients and Strouhal number are well predicted by the numerical model. At α = 45° the wake flow is characterized by wavy axial vortices at low Reynolds numbers in the 3D flow regime, which are similar to those in the early stage of mode A at α = 0°. The wavelength in the axial direction is slightly smaller than that at α = 0° and decreases with the increase of Reynolds number. The wavy axial vortices in the wake of the cylinder gradually become irregular as *Re* increases to 600 (Re_n = 425). The strengths of the axial vortices are observed to increase with the increase of Reynolds number in the oblique attack angle case of α = 45°.

If the normal Reynolds number is defined based on the velocity component perpendicular to the cylinder span, the critical normal Reynolds number for transition at α = 45° is close to that at α = 0°. The fact that the vortex-dislocation in mode A is not observed at α = 45° makes the normal force coefficients and the normal Strouhal number at α = 45° different from those at α = 0° in the Mode A Reynolds number regime. In the Reynolds number regime for Mode A, the normal Strouhal number, the RMS normal lift coefficient and the mean normal drag coefficient at α = 45° are larger than their counterparts at α = 0°. It appears that the fluid flow in the spanwise direction in the primary vortices at α = 45° smooths out the instability and inhibits the vortex dislocation.

At α = 45°, the Strouhal number varies with the Reynolds number smoothly and the obvious discontinuity in Strouhal number due to the flow changing from one mode to another was not observed at α = 45°. The RMS normal lift coefficient at α = 45° is consistently larger than that at α = 0° throughout the transition regime ($250 \leq Re_n \leq 550$) because the streamwise vortices are weaker. At Re_n = 700, the RMS normal lift coefficient at α = 45° is close to that at α = 0°.

CHAPTER 4

THREE-DIMENSIONAL SIMULATION OF VORTEX SHEDDING FLOW IN THE WAKE OF A YAWED CIRCULAR CYLINDER NEAR PLANE BOUNDARY AT A REYNOLDS NUMBER OF 500

Flow past a yawed circular cylinder in the vicinity of a plane boundary is investigated numerically by solving the three-dimensional Navier-Stokes equations using the Petrov-Galerkin finite element method. Simulations are carried out at a constant Reynolds number of 500, two gap ratios of 0.4 and 0.8 and six cylinder yaw angles (α) ranging from 0° to 60° with an increment of 15°. The gap ratio is defined as the ratio of the gap between the cylinder and the plane boundary to the cylinder diameter. The focus of the study is on the effects of α and the gap ratio on the vortex shedding flow and the hydrodynamic forces of the cylinder. It is found that increasing the cylinder yaw angle weakens the three-dimensionality of the flow. The root mean square lift coefficient decreases at α = 60°, indicating that the vortex shedding is suppressed more than that at small yaw angles. The independence principle, which states that the drag and lift coefficients based on the velocity component perpendicular to the cylinder axis are independent on the yawed angle of the cylinder, applies to the flow at the gap ratio of 0.8 better than that at the gap ratio of 0.4. Because of the strong influence from the plane boundary on the flow, the force coefficients for a gap ratio of 0.4 do not follow the independence principle if the yaw angle is greater than α >30°.

4.1 INTRODUCTION

Flow around cylinders has been studied extensively both experimentally and numerically due to its engineering importance. It has been well known that vortex shedding starts to appear when the Reynolds number is approximately above 40. The flow starts to transit from two-dimensional (2D) laminar flow to three-dimensional (3D) turbulent flow at a Reynolds number of about 140-190 (Roshko, 1954; Tritton, 1959; Zhang *et al*., 1995; Eisenlhr and Eckelmann1989; Williamson, 1988, 1989). Miller and Williamson (1994) found that the laminar regime for parallel vortex shedding can be extended up to *Re* = 194 and even beyond 200 for a short period of time if there is no effect from the end condition. The vortex shedding modes in the transition regime of the Reynolds number are classified into mode A and mode B. Mode A is characterized by the inception of vortex loops and the formation of streamwise vortex pairs due the deformation of the primary vortices in the wake of the

cylinder and mode B is characterized by the dominance of the streamwise vortex pairs spaced by a distance of about one cylinder diameter. Barkley and Henderson (1996) and Robichaux *et al*. (1999) used the Floquet stability analysis method to study the transition modes of the flow. Scarano and Poelma (2009) measured the wake flow field using PIV and presented the transition flow using the three-dimensional iso-surfaces of the vorticity. The flow transition was also successfully predicted by three-dimensional numerical simulations (Karniadakis and Triantafyllou 1992, Zhang and Dalton 1998, Zhao *et al*. 2013). The hydrodynamic forces on the circular cylinder oscillate with time due to the vortex shedding. Schewe (1983) presented experimental results of the drag and lift coefficients over a wide range of Reynolds numbers. It was reported that the force coefficients and vortex shedding frequency are not sensitive to Reynolds number if the Reynolds number is in the subcritical regime ($300<Re<3\times10^5$).

In offshore oil and gas engineering, cylinder structures such as subsea pipelines are generally laid on the seabed surface. Due to the unevenness of the seabed surface or the erosion of the sediment, a gap between a subsea pipeline and the seabed surface occurs. Flow around a subsea pipeline can be modelled by flow past a circular near a plane boundary in research. When a circular cylinder is located near a plane boundary, vortex shedding flow is dependent on not only the Reynolds number, but also the gap ratio e/D, with e being the gap between the bottom surface of the cylinder and the plane boundary and D being the cylinder diameter as shown in Fig. 4.1. Due to its engineering relevance, flow around a cylinder close to a plane boundary has been well studied over the past few decades (Taneda, 1965; Bearman and Zdravkovich, 1978; Grass *et al*., 1984; Taniguchi and Miyakoshi, 1990; Lei *et al*., 1999). Many of the existing studies are based on experimental measurements at Reynolds numbers in the sub-critical regime. The experiments were mostly conducted in the sub-critical Reynolds number regime where the vortex shedding is relatively insensitive to the Reynolds number in this regime (Schewe, 1983). When flow passes a circular cylinder close to a plane boundary, the flow is affected more by the gap between the cylinder and the plane boundary than the Reynolds number if the Reynolds number is in the sub-critical regime. Bearman and Zdravkovich (1978), Grass *et al*. (1984), Lei *et al*. (1999) and Cheng and Su (2012) reported that the vortex shedding from both top and bottom sides of the cylinder close to a plane boundary was fully suppressed as e/D is less than 0.3. The experimental study by Wang and Tan (2008) demonstrated that the effects of the plane boundary on the flow were weak if e/D exceeds 0.8. When the vortex shedding is fully suppressed, the flow becomes static and the oscillation of the flow-induced force disappears. Akoz *et al*. (2010), Lin *et al*. (2009) and

Zang *et al*. (2013) studied flow characteristic of circular cylinders close to a plane boundary using the particle image velocimetry technique. Lin *et al*. (2009) found the occurrence of a recirculating eddy formed on the plane boundary upstream of the circular cylinder for the gap ratio less than 0.5. Zang *et al*. (2013) found that, by the swirling strength analysis, that the lee-wake patterns for flow past two cylinders of different diameters are affected by the arrangement of the two cylinders.

Numerical method is also popularly used to predict flow past a cylinder near a plane boundary. Lei *et al*. (2000) studied flow past a circular cylinder by solving the 2D Navier-Stokes equations for Reynolds numbers up to 1000 and found that the critical gap ratio decreased with an increase in Reynolds number. By conducting 2D numerical simulation, Bimbato *et al*. (2013) found that the fluid viscosity and Venturi effect were responsible for the increase in the lift force and the decrease in the drag force on a cylinder close to a plane boundary. Ong *et al*. (2010, 2012) investigated flow past a marine pipeline using two-dimensional k-epsilon turbulence model and obtained good prediction of flow, although there were some difference between the model results of the forces and the experimental data. Jiang and Lin (2012) and Lin *et al*. (2013) investigated flow and flow-induced vibrations of two tandem cylinders between two plane walls and found that the distance between the two walls affected the critical spacing between the cylinders for vortex shedding from the upstream cylinder. Camarri and Giannetti (2010) investigated the three-dimensional stability of the wake behind a cylinder confined in two lateral walls with a blockage ratio of 1/5 and found that the transition to a three-dimensional state has the same space-time symmetries of the unconfined case.

When the cylinder is placed in the fluid at an inclined angle to the flow, the independence principle (or the cosine law) is commonly used in practical applications to approximately estimate the vortex shedding frequency and hydrodynamics forces on the cylinder. The independence principle states that the force coefficients and the Strouhal number, which are normalized by the velocity component perpendicular to the cylinder, are approximately independent on the inclination angle of the cylinder, with the zero-degree angle corresponding to the case where the cylinder is perpendicular to the flow direction. In case of flow past an inclined cylinder of finite length, it was found that the wake vortices far from the upstream end of the cylinder are approximately parallel to the cylinder and the vortices near the upstream end of the cylinder are aligned at an angle larger than the cylinder yaw angle (Ramberg, 1983; Thakur *et al*., 2004). The numerical study by Zhao *et al*. (2009)

showed that the error of independence principle increases with the increasing yaw angle. The experimental study of Zhou *et al*. (2010) also showed that the independence principle is valid up to about the yaw angle of 40°. Lam *et al*. (2010) reported that the flow past the yawed circular cylinder followed the independence principle for yawed angles up to 45°. The numerical simulation of flow past a yawed cylinder at large yaw angles of 60° and 70° by Lucor and Karniadakis (2003) showed that the vortices in the wake of the cylinder were not exactly parallel to the cylinder. By conducting three-dimensional numerical simulations of flow past an inclined square cylinder at low Reynolds numbers, Yoon *et al*. (2012) found that the effects of the Reynolds number are weak on the mean flow and the Strouhal number and strong on the lift coefficient.

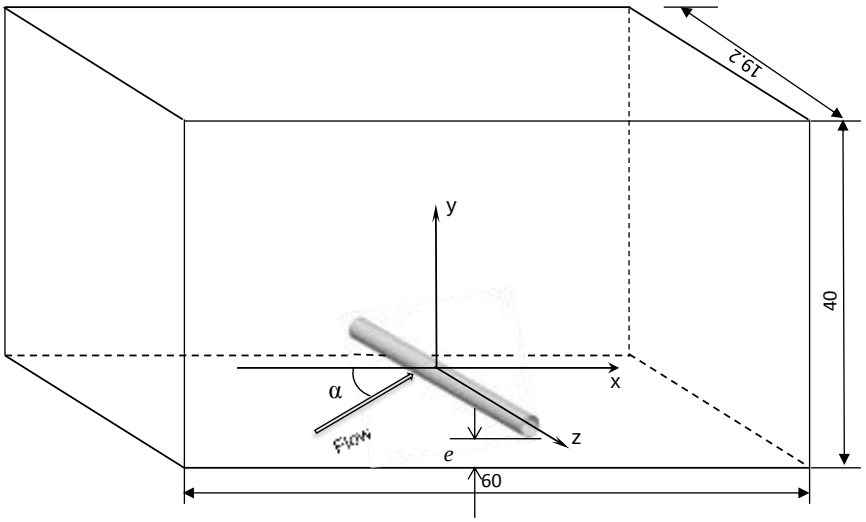

Fig. 4.1 Sketch of flow past a circular cylinder at oblique attack

The study of flow past a yawed circular cylinder close to plane boundary is relatively rare. Kozakiewicz *et al*. (1995) found that the Independence Principle can be applied to stationary cylinders in the vicinity of a plane boundary for a yaw angle between 0° and 45°. It is expected that both the yaw angle and the gap ratio affect the transition of the flow in the low Reynolds number regime. In the present study, flow past a yawed circular cylinder at yaw angles in the range of 0°- 60° was investigated numerically at a Reynolds number of 500. The focus of this study is to examine the influence of the yaw angle on the vortex shedding flow at a relatively low Reynolds number. The yaw angle (defined by α) of 0° corresponds to the case where the cylinder is perpendicular to the flow direction as shown in Fig. 4.1. A relatively low Reynolds number in the turbulent flow regime is chosen based on

the following considerations. First, the wake flow at *Re*=500 is in the turbulent flow regime based on previous studies (Williamson, 1988, 1989). Three-dimensional vortex shedding flow occurs at *Re*=500 for an isolated cylinder with zero yaw angle. Second, effect of yaw angle on vortex suppression is the aim of this study, which is stronger at this relative low Reynolds number than higher Reynolds numbers. Finally, a relatively low Reynolds number allows the direct numerical simulations (DNS) to be conducted at affordable computational time.

4.2 NUMERICAL METHOD

The incompressible Navier-Stokes (NS) equations are solved for simulating the flow. The non-dimensional NS equations are written as

$$\frac{\partial u_i}{\partial t} + u_j \frac{\partial u_i}{\partial x_j} + \frac{\partial p}{\partial x_i} - \frac{1}{\mathrm{Re}} \frac{\partial^2 u_i}{\partial x_j^2} = 0, \tag{4.1}$$

$$\frac{\partial u_i}{\partial x_i} = 0, \tag{4.2}$$

where $(x_1, x_2, x_3) = (x, y, z)$ are the Cartesian coordinates, u_i is the fluid velocity component in the x_i direction and p is the pressure. The Reynolds number is defined as $\mathrm{Re} = UD/\nu$ with U being the velocity at one cylinder diameter above the plane boundary and ν being the kinematic viscosity of the fluid. In a fully developed boundary layer flow, the flow velocity varies in the vertical direction. In this study, the velocity at one-diameter above the cylinder surface is used for the normalization of the NS equations and the force coefficients.

Fig.4.1 shows the non-dimensional computational domain for simulating the flow past a yawed circular cylinder. The non-dimensional computational domain is 60 in length, 19.2 in width and 40 in height. Lei *et al*. (2001) reported that the length of the cylinder should be no less than 2 diameter for obtaining accurate results of the force coefficient for flow past a cylinder at *Re*=1000. Gioria *et al*. (2011) found that the three-dimensional flow could be reasonably represented if the cylinder length exceeds 6 diameters.

Table 4.1 Mesh dependency check for *Re* = 500 and *e*/*D* = 0.8

Mesh	Density	α(degree)	Δz	Length	$\overline{C}_D$	$\overline{C}_L$	C'_D	C'_L	S_t
1	Normal	0	0.1	19.2	1.129	-0.079	0.041	0.308	0.227
2	Denser	0	0.1	19.2	1.138	-0.081	0.041	0.300	0.229
3	Densest	0	0.05	9.6	1.140	-0.07	0.040	0.301	0.225
4	Normal	60	0.1	19.2	1.096	-0.113	0.052	0.332	0.204
5	Normal	60	0.05	9.6	1.100	-0.109	0.048	0.340	0.198

In the studies of uniform flow past a yawed cylinder by Zhao *et al*. (2009) and Zhao *et al*. (2013), the lengths of the cylinder were 9.6 and 19.2 diameter, respectively. Based on the previous experiences, the cylinder length of 19.2 diameters should be enough for presenting the variation of the flow along the cylinder span. The NS equations are solved by the Petrov-Galerkin finite element method and parallel computation code developed by Zhao *et al*. (2009). Parallel computations are performed on the iVEC supercomputer facility in Western Australia. The pressure Poisson's equation is solved by the Conjugate gradient method and the momentum equations are solved by the successive over-relaxation method. For solving the linear equation systems from the finite element discretization, the iteration is performed until the maximum error between the two successive iteration steps is less than 10^{-6} for all the finite element nodes. The initial values of the velocity and the pressure in the whole domain are set to zero. The boundary layer thickness at the inlet boundary is the same as the height of the computational domain in the *y*-direction. The non-dimensional velocity at the inlet boundary is given by

$$(u_1,\ u_2,\ u_3) = (V(y)\cos\alpha,\ 0,\ V(y)\sin\alpha), \tag{4.3}$$

where the magnitude of the velocity $V(y)$ at the level y is calculated based on the velocity profile of the fully developed boundary layer, i.e.

$$\frac{V(y)}{u_*} = \begin{cases} \dfrac{yu_*}{\nu}, & \dfrac{yu_*}{\nu} \le 11.63 \\ \dfrac{1}{k}\ln\left(9.0\dfrac{yu_*}{\nu}\right), & \dfrac{yu_*}{\nu} > 11.63 \end{cases}, \tag{4.4}$$

where k= 0.4 is the von Karman's constant. Eq. (4.4) assumes that the boundary layer is divided into the viscous and the log layers. For Re=500, the thickness of the viscous layer is about 0.334 cylinder diameter based on Eq. (4.4). The incoming turbulence intensity varied significantly in experimental tests because it depends on the test condition. Because the

viscous layer is very thick (about one third of the cylinder diameter) for *Re*=500, it is expected the intensity of the turbulence near the top of the viscous layer is very weak. In this study, the constant value of velocity without turbulence component based on Eq. (4.4) is given. On the top boundary that are parallel to the $x-z$ plane, a free-slip boundary condition is employed, namely, the velocity component and the pressure gradient perpendicular to the boundary are zero. When the flow approaches the cylinder at an inclined angle, the velocity in the axial direction of the cylinder is significant and the fluid should be allowed to flow through the two side boundaries (the two boundaries that are perpendicular to the cylinder axis). A periodic boundary condition is imposed by setting velocity and pressure gradients (in all three directions) on one side boundary to be equal to their counterparts on another side boundary. Periodic boundary condition is an approximation because the flow at one end of the cylinder is the same as that at another end only when the flow is perfectly two dimensional. However, it is expected that the influence of the periodic boundary condition on the results will only be limited to the small area near the cylinder ends. The periodic boundary condition on the two side boundaries allow the fluid flowing through the boundary. On the cylinder surface and the plane boundary the no-slip condition is applied. On the outflow boundary, the pressure is set to zero and the gradient of the velocity in the direction normal to the boundary is zero.

Hydrodynamic forces on the cylinder and the vortex shedding frequency are studied extensively. The sectional force coefficients are examined. The sectional drag and the sectional lift coefficients are defined as $C_D(z) = F_D(z)/\left(\rho D U_n^2/2\right)$ and $C_L(z) = F_L(z)/\left(\rho D U_n^2/2\right)$, where $F_D(z)$ and $F_L(z)$ are the sectional drag and lift forces per unit length of the cylinder at the *z*-location, respectively and U_n ($\equiv U\cos\alpha$) is the velocity component normal to the cylinder. The sectional forces are obtained by integrating the pressure and the shear stress along a circumference of a cross-section of the cylinder. The Strouhal number is defined as $S_t = fD/U_n$ with *f* being the frequency of the fluctuating lift force.

4.3 RESULTS AND DISCUSSIONS

Numerical simulations were carried out at a constant Reynolds number of *Re* = 500 with cylinder yaw angles (defined in Fig.4.1) of 0°, 15°, 30°, 45° and 60° and gap ratios of *e*/*D* = 0.4 and 0.8. The flow becomes fully turbulent as the Reynolds number exceeds 300. The

Reynolds number of 500 used in this study is slightly greater than the critical Reynolds number of Re = 300 for turbulent flow. The critical gap ratio for vortex shedding flow is found to be about 0.3 for Reynolds numbers much greater than 500 (Bearman and Zdravkovich, 1978; Grass *et al*., 1984; Lei *et al*., 1999). It is expected that the critical Reynolds number for such a small Reynolds number of 500 may be slightly greater than 0.3 because it decreases with an increase in Reynolds number (Lei *et al*., 2000).

Because the focus of this study is to find out the influence of the gap ratio on the vortex shedding flow, instead of finding out the critical gap ratio, the two gap ratios used are greater than the critical gap ratio for vortex shedding. The gap ratio of e/D = 0.4, which is close to the critical gap ratio for vortex shedding is chosen, in order to see the effects of the yawed angle on the suppression of the vortex shedding. It is anticipated that the vortex shedding would be more sensitive to the change of yaw angle at this gap ratio than at larger gap ratios. The gap ratio of e/D = 0.8 is chosen because the vortex shedding is expected to be fully developed in the wake of the cylinder at this gap ratio. All simulations were performed on two Australian supercomputer facilities, Intersect in NSW and iVEC in WA. Sixty-four processors were used for each of the simulations. Each simulation was conducted up to the non-dimensional time of Ut/D = 1350 to ensure that vortex shedding has been fully developed.

4.3.1 MESH DEPENDENCE STUDY

Fig. 4.2 shows a typical computational mesh used for the simulations in the present study. 192 layers of elements are distributed along the cylinder span. For each case, simulation is conducted by the parallel calculation using 64 computer CPUs. The whole computational domain is divided into about 2.1 million 8-node hexahedral tri-linear finite elements. The cylinder circumference is divided into 72 elements. The minimum mesh size next to the cylinder surface (in the radial direction) and that next to plane boundary (in the direction perpendicular to the plane boundary) is 0.0072. The mesh size in the spanwise direction of the cylinder Δz is 0.1. A mesh dependency study was carried out at first and the results are listed in Table 4.1. The mesh shown in Fig. 4.2 is referred to be mesh 1. The major difference among meshes 1, 2 lies in the density on the xy-plane and mesh 3, whose node number is about 5.7 million, is denser than mesh 2 both on xy-plane and in the z-direction. Mesh 4 is the same as mesh 1 but with different yaw angle. Mesh 5 has the same density on the xy-plane as Mesh 4 but with smaller mesh size in the z-direction. The statistical values

shown in Table 4.1 are based on the data within 60 periods of vortex shedding. The density of the mesh in Table 4.1 referred to the mesh density in the *xy*-plane. In the denser mesh, the radial mesh size next to the wall (cylinder surface and the plane boundary) is 0.0062 and the cylinder circumference is divided into 85 elements in each layer of the mesh. In the densest mesh 3, the radial mesh size on the cylinder surface and the axial mesh size are 0.002 and 0.05, respectively, and the cylinder circumference is divided into 144 elements. Fig. 4.3 shows the comparison of the time history of the sectional lift coefficient from the all the meshes. At α=0°, the flow is 3D and the lift coefficient is no perfectly periodic. It has been seen that the lift coefficients in both cases are basically the same as in Fig. 4.3 (a). Mesh 3 and 4 are of the same density in the *xy*-plane, but different Δz, i.e. 0.1 and 0.05 respectively.

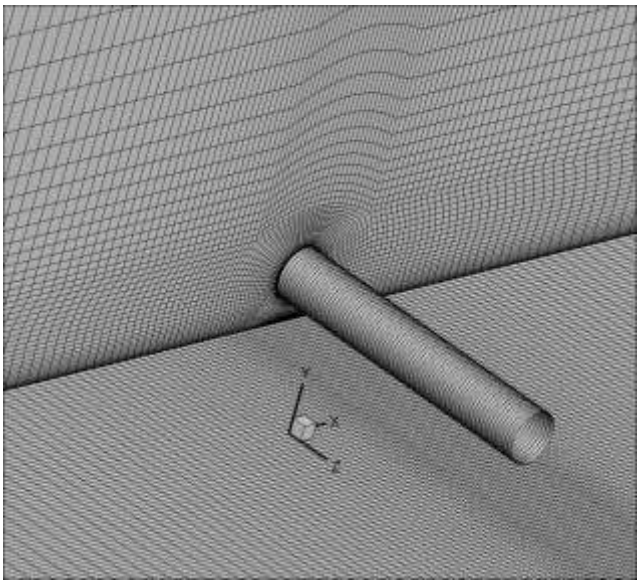

Fig. 4.2 Computational mesh around the cylinder (one quarter length of cylinder is presented)

The results from the very dense Mesh 3 have little difference from those from Meshes 1 and 2. At α = 60°, the three-dimensionality of the flow is very weak and the numerical results from Meshes 4 and 5 in Fig. 4.3 (b) are almost identical, except the phase difference. The difference in phase occurs because the onset of the vortex shedding happens at a random time in the numerical simulation. At α = 60°, the velocity components perpendicular to the cylinder surface has been half the incoming velocity. If the Reynolds number is defined by the velocity component perpendicular to the cylinder, it would be 250, where the three-dimensionality is much weaker than that at *Re* = 500.

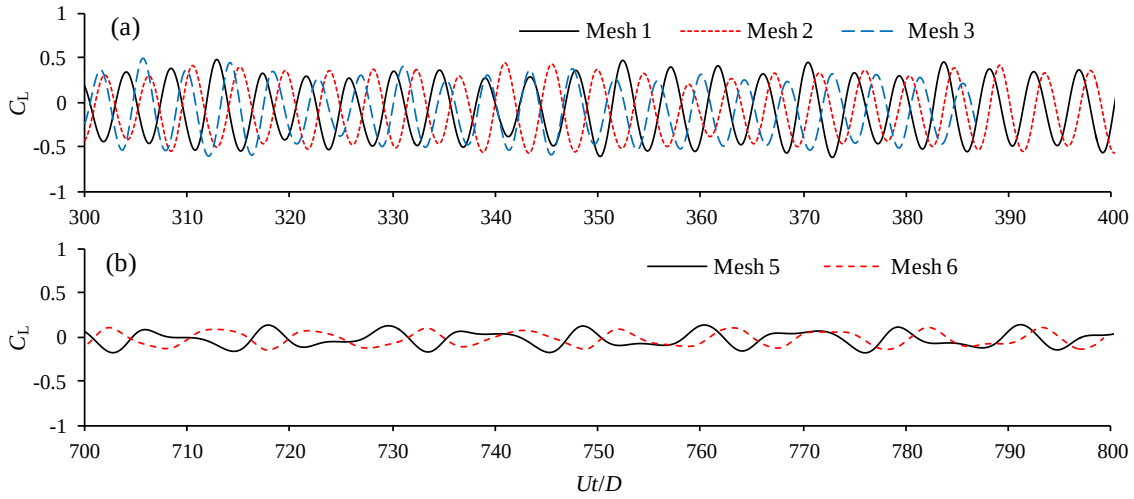

Fig. 4.3 Time history of the sectional force coefficient at mid span and e/D = 0.8: (a) The normal, denser and densest meshes at α=0°; (b) The normal meshes at Δz=0.1 and 0.05; α=60°

Wang and Tan (2008) demonstrated that the effects of the plane boundary on the flow were weak if e/D is exceeds 0.8. The mean drag coefficient $\overline{C}_D$ at α = 0° from the normal mesh at e/D = 0.8 is 1.129 which is in the range of the measured results from 1.0 to 1.2 (Braza *et al*., 1986; Niemann and Hölscher, 1990). The Strouhal number at α = 0° from the normal mesh is about 0.227 and agrees well with the experimental result between 0.207 and 0.22 (Roshko, 1954). The differences in the mean drag coefficient, the RMS lift coefficient and the Strouhal number from the normal mesh and those from the densest mesh are less than 3%. The agreement between the results from meshes 1, 2 and 3 demonstrates that the mesh density of mesh 1 in the *xy*-plane has been enough to provide accurate solutions. The agreement between the results at α = 60° from meshes 4 and 5 demonstrates that the mesh size in the spanwise direction (Δz) has been small enough to ensure that the results is mesh-independent at the largest yaw angle simulated in this study.

4.3.2 VORTEX SHEDDING FLOW

The vortex shedding flow is discussed by examining the time histories of the force coefficients and vortex shedding flow structures, which are visualized through vorticity contours and the iso-surface of the second negative eigenvalue of the tensor $\mathbf{\Psi}^2 + \mathbf{\Omega}^2$, where $\mathbf{\Psi}$ and $\mathbf{\Omega}$ are the symmetric and the anti-symmetric parts of the velocity-gradient tensor respectively. The vorticity components in the *x*-, *y*- and *z*-directions are defined as $\omega_x = \partial w/\partial y - \partial v/\partial z$, $\omega_y = \partial u/\partial z - \partial w/\partial x$ and $\omega_z = \partial v/\partial x - \partial u/\partial y$ respectively with *u*, *v* and *w* being velocity components in the *x*-, *y*- and *z*-directions respectively. Vorticity

component ω_z and ω_x are often referred to as spanwise vorticity and streamwise vorticity respectively. The second eigenvalue, defined by e_2, represents the location of the vortex core (Jeong and Hussain 1995). Fig. 4.4 shows the iso-surface of e_2 = -0.25 for e/D=0.8 at two instants at all the yaw angles. Of the two instants of each yaw angle shown in Fig. 4.4, one is at the early stage where the flow transits from 2D to 3D and another is the fully developed 3D flow.

For α = 0°, central part of the downstream wake is still two-dimensional at Ut/D = 95 and thereafter it becomes three-dimensional quickly. The onset of three-dimensionality is evidenced by the occurrence of the streamwise vortices near to the two ends of the cylinder in Fig. 4.4 (a). In Fig. 4.4 (b), the flow has become fully 3D at Ut/D = 450. Although the wakes shown in Fig. 4.4 are three-dimensional, they appear to be dominated by the spanwise vortices. Fig. 4.5 shows the contours of the vortices in the x-direction ω_x for e/D=0.8. The ω_x contours for an isolated cylinder at Re = 500 are shown in Fig. 4.5 (f) for comparison. For an isolated cylinder, the wake flow structure at Reynolds number (Re) of 500 is in mode B, where the streamwise vortices dominate (Williamson 1988). The flow at the early stage of the transition is characterized by regular rib-shaped streamwise vortices at different yaw angles except at α=60°. The streamwise vortices at α=0° appear to be similar to those in the wake of an isolated cylinder at the same Reynolds number. With an increase in the yawed angle, the strength of ω_x decreases. At α=60°, ω_x has been very weak and cannot be identified based on the ω_x contours. Because the vorticity in the boundary layer has components in the x-direction if the yaw angle is greater than 0°, some vorticity contours are seen on top of the plane boundary in Fig. 4.5 (c), (d) and (e), but they are not due to the vortex shedding from the cylinder. The decrease in the streamwise vortices with the increasing yaw angle can also be seen in Fig. 4.4.

The vortex shedding patterns shown in the left column of Fig. 4.4 (a), (c), (e) and (g) are very similar to that observed in transition mode A of uniform steady flow past an isolated circular cylinder (as shown in Fig. 5 in Zhao *et al*. 2013), which is characterized by the wavy spanwise vortices and the inception of the streamwise vortices. The vortex shedding regimes around an isolated circular cylinder transit from mode A to mode B at about Re = 250 and mode B persists up to Reynolds number of 1000 at uniform flow. The wake behind an isolated circular cylinder in mode B is dominated by streamwise vortices.

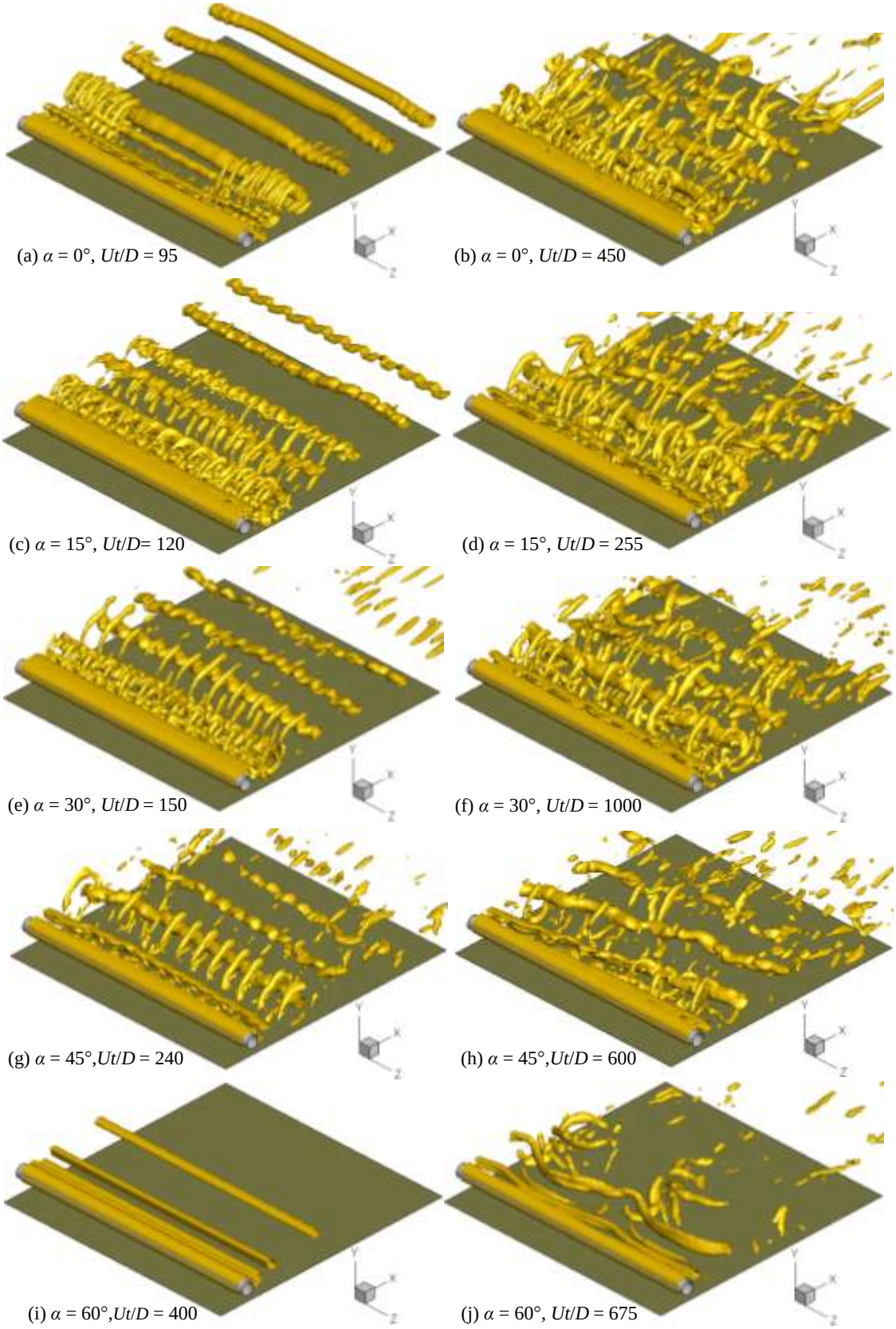

Fig. 4.4 Iso-surface of e_2 = -0.25, e/D = 0.8 and Re = 500

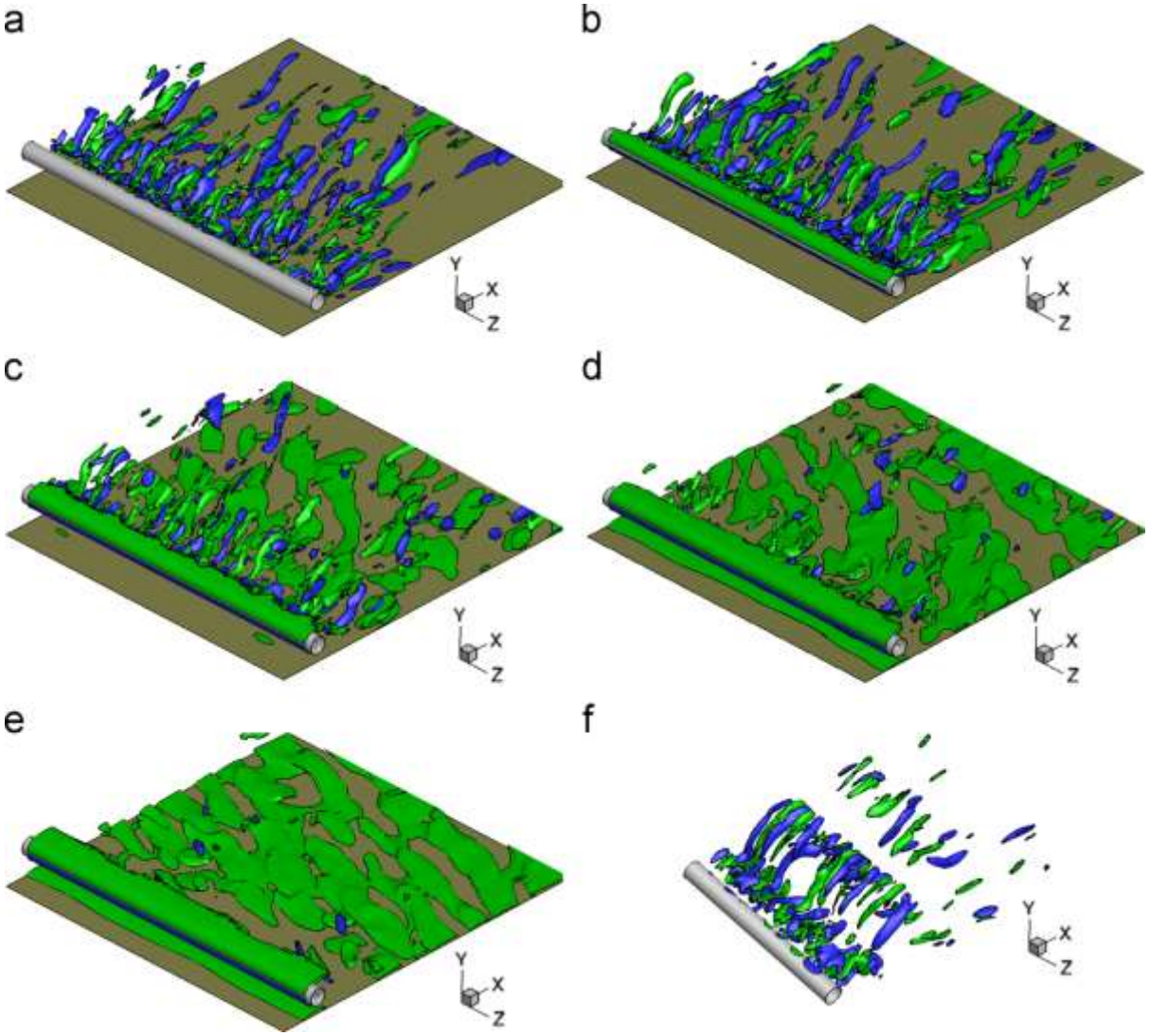

Fig. 4.5 Iso-surfaces of the vorticity $\omega_x = \pm 1$ for the fully developed flow at e/D = 0.8. (a) Ut/D=450, α=0°, (b) Ut/D=255, α=15°, (c) Ut/D=1000, α=30°, (d) Ut/D=900, α=45°, (e) Ut/D=1000, α=60°, (f) Ut/D=500, isolated cylinder.

At α = 0° and e/D=0.8, the dominance of the streamwise vortices is as strong as that in mode B of uniform flow past an isolated circular cylinder (as shown in Fig. 8 in Zhao *et al*. 2013). Wavy spanwise vortex structures are observed at the early stage of the transition (Fig. 4.4(a)) and the wavelength of the spanwise vortex structures is about 1.5 to 1.6 (about 12 or 13 waves along the 19.2 long cylinder). Williamson (1992) found similar type of rib-shaped streamwise vortices and reported that the spanwise wavelength is about 3 diameters at *Re* = 180 and about 1 diameters at *Re* = 230. Once the flow becomes fully three-dimensional (Fig. 4.4 (b), (d), (f) and (h)), the wake flow is very chaotic and it is difficult to identify the wavelength of the spanwise features based on the vortex shedding structure. At α = 60°, the

flow is totally two-dimensional up to Ut/D = 550 and slowly becoming three-dimensional but very weak based on the vortex structures shown in Fig. 4.4 (i) and (j). It appears that the yaw angle affects the development of three-dimensionality of the flow significantly. The vortex shedding for yawed angle $\alpha \geq 45°$ has been much different from the mode B vortex shedding from an isolated cylinder at Re = 500.

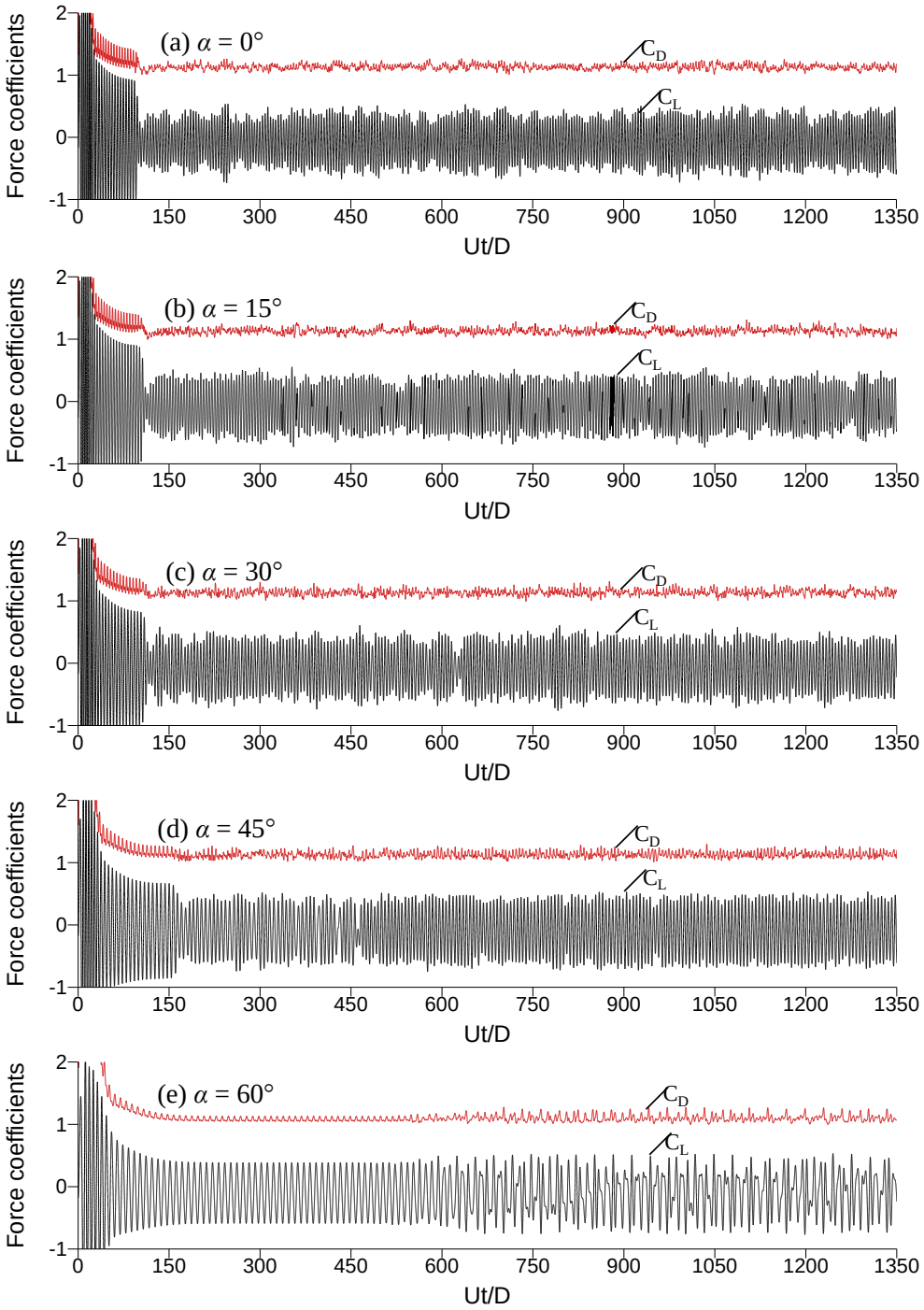

Fig. 4.6 Time history of sectional force coefficient at the mid-section of the cylinder at e/D = 0.8, Re = 500

Fig. 4.6 shows the time histories of sectional force coefficients on the mid-section of the cylinder (z=0) at e/D = 0.8 and different yaw angles. The fluctuating amplitudes of drag and lift coefficients decrease suddenly after the flow transits from 2D to 3D. The drag and lift coefficients decreases because part of the energy of the spanwise vortices is transferred to that of streamwise vortices and near wake structures are less synchronised in the spanwise direction. For α = 60°, the sudden reduction in the force coefficients is not observed and the fluctuation of the force coefficients is quite regular until Ut/D = 550, indicating that the flow is completely 2D. Beyond Ut/D = 550 fluctuating lift coefficient is getting irregular, revealing the three-dimensionality of the flow. The three-dimensionality is quite weak. The dislocation that was observed in the studies of uniform flow past an isolated cylinder is not observed in this study. Fig. 4.7 shows the contours of spanwise vorticity at different cross sections at the instant of Ut/D = 467.5 for α = 0° and e/D = 0.8. The variation of the spanwise vortices in the z-direction is weak, indicating that there is no dislocation of the spanwise vortices. If the dislocation of vortices occurs, the vortex shedding at one location may be in different phase from that at another location (Zhao *et al*., 2013). The vortex shedding at different locations shown in Fig. 4.7 is approximately in phase, although there is slightly variation in the strength of the vortices along the cylinder span.

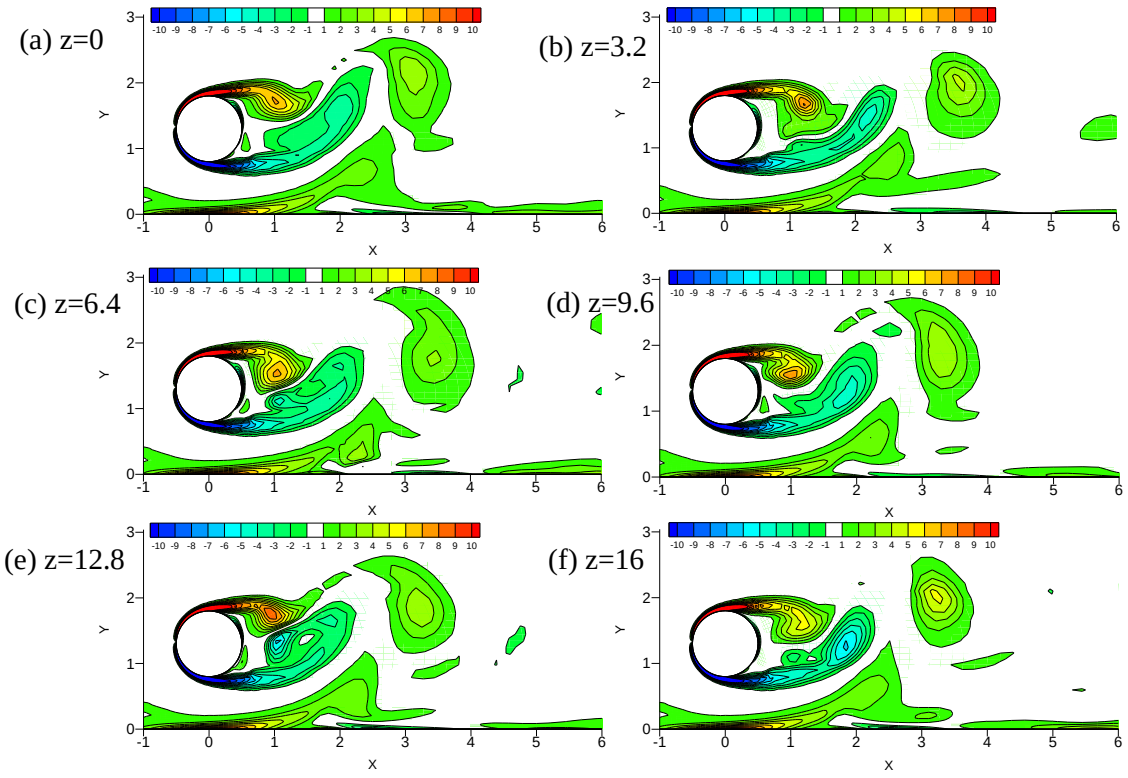

Fig. 4.7 Contours of spanwise vorticity at different cross section (α = 0°, Re = 500, Ut/D = 467.5, e/D = 0.8)

Fig. 4.8 shows the iso-surface of e_2= -0.25 at e/D = 0.4 and Re = 500. It is understood that the vortex shedding becomes weaker as the gap ratio is reduced and is fully suppressed if e/D<0.3 at high Reynolds numbers in the sub-critical regime (Bearman and Zdravkovich, 1978; Grass *et al*., 1984; Lei *et al*., 1999). The 2D numerical simulation by Lei *et al*. (2000) indicated that the critical gap ratio for full vortex shedding suppression reduced with an increase in the Reynolds number. The reduction of vortex shedding strength with the reducing gap ratio is also anticipated in this study. Judging by the very small amplitude of the lift coefficient in Fig. 4.9 (a), the gap ratio of e/D = 0.4 is expected to be a gap that is very close to the critical gap for full vortex suppression. The three-dimensionality observed in Fig. 4.8 with e/D=0.4 appear to be much weaker than that at e/D=0.8 shown in Fig. 4.6.

The suppression of flow three-dimensionality appears to occur at a smaller flow yaw angle at e/D = 0.4 than that at e/D = 0.8. The three-dimensionality of the flow is very weak at α=60° due to the combined influences from the large yaw angle and plane boundary. The large yaw angle makes the velocity component perpendicular to the cylinder small. The vortex shedding is weakened because the shear layer form the plane boundary attracts the shear layer from the bottom surface of the cylinder and weakens the interaction between the shear layers from the top and bottom of the cylinders. The streamwise vortices at α = 0° in Fig. 4.8 (b) are very weak and hardly to be seen near the cylinder and they become even weaker as the yaw angle α increases. The three-dimensionality at e/D=0.4 is weaker than that at e/D = 0.8 at all the calculated yaw angles. In Fig. 4.7 (j), where the yaw angle is 60º, it appears that the vortices are not parallel to the cylinder and this phenomenon is not observed at e/D = 0.8. The smaller vortex shedding angle than the yawed angle of the cylinder at a high yaw angle of α=70º was also reported by Lucor and Karniadakis (2003). Fig. 4.9 shows the time histories of the sectional force coefficient at the mid-section of the cylinder at e/D = 0.4 and Re = 500. At α = 0°, the sudden decrease in the drag and lift coefficients at Ut/D = 70 (Fig. 4.8 (a)), indicates the flow transition from 2D to 3D quickly. The sudden decreases in the force coefficients in Fig. 4.8 (b) to (d) are not as obvious as that shown in Fig. 4.8 (a) because the three-dimensionality of the flow is very weak. At α = 60°, the amplitude of the lift coefficient has been almost zero, indicating that vortex shedding has been almost fully suppressed. Fig. 4.10 shows the contours of the spanwise vorticity at different cross-sections at Ut/D = 222.5 for e/D = 0.4, α=0° and Re = 500. Compared with those at e/D = 0.8 (Fig. 4.6), the negative vortices from the bottom side of the cylinder at e/D = 0.4 appear to be weakened by the shear layer from the plane boundary. The interaction of the vortices shed

from the top and bottom sides of the cylinder are significantly weaker than those shown in Fig. 4.7, resulting in weaker lift oscillations.

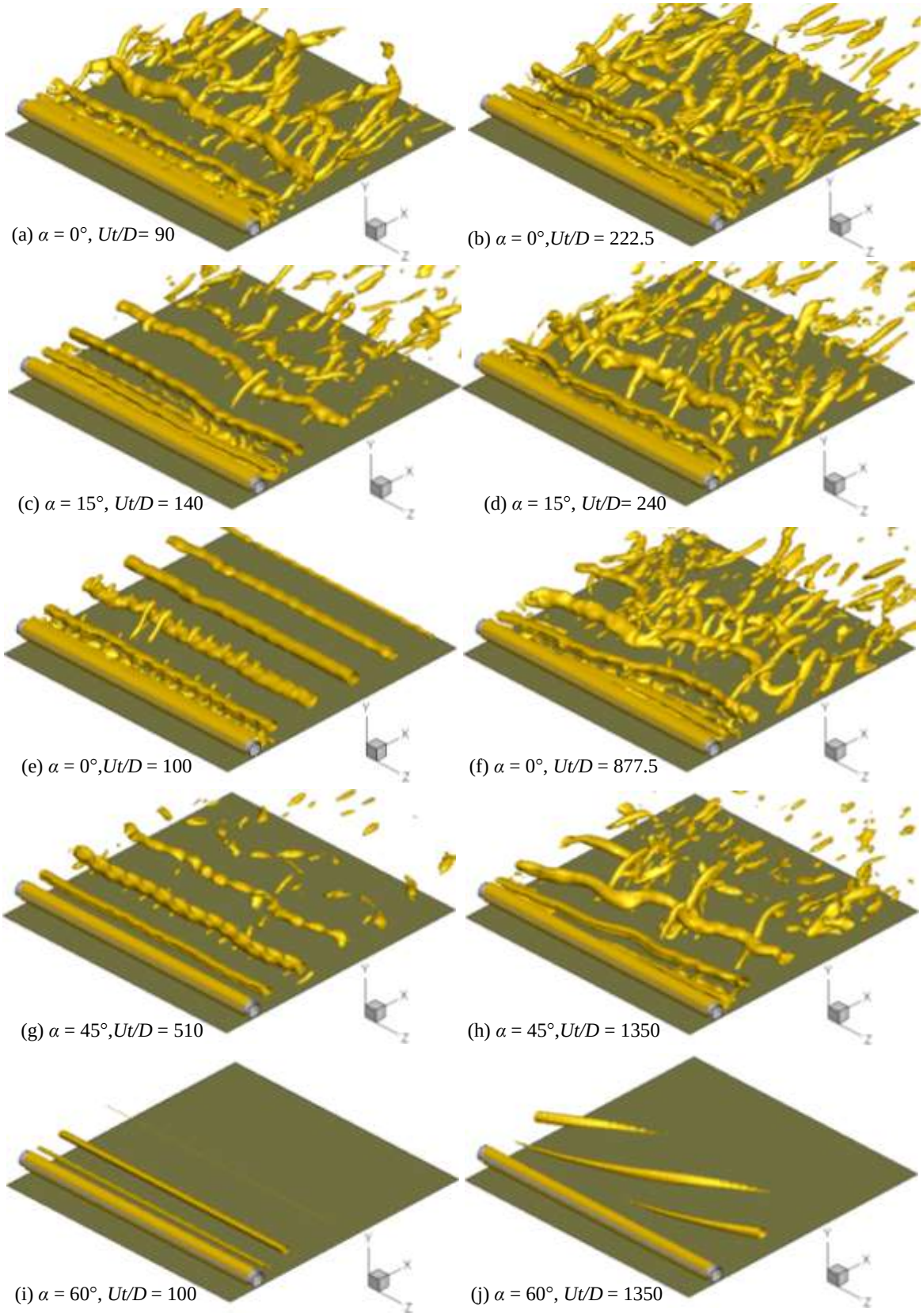

Fig. 4.8 iso-surface of e_2= -0.25, e/D = 0.4 and Re = 500

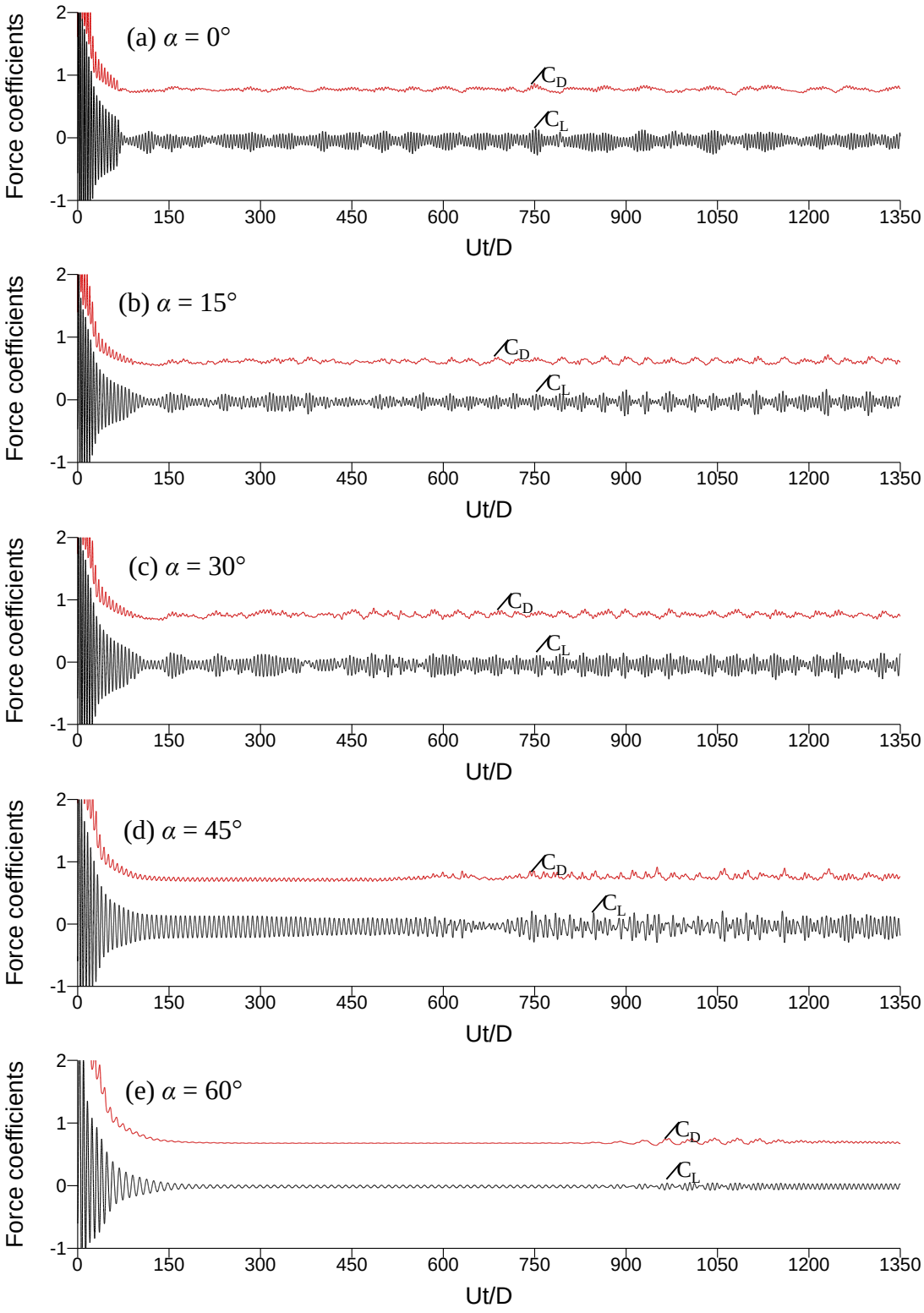

Fig. 4.9 Time history of sectional force coefficient at the mid-section of the cylinder at e/D = 0.4 and Re = 500

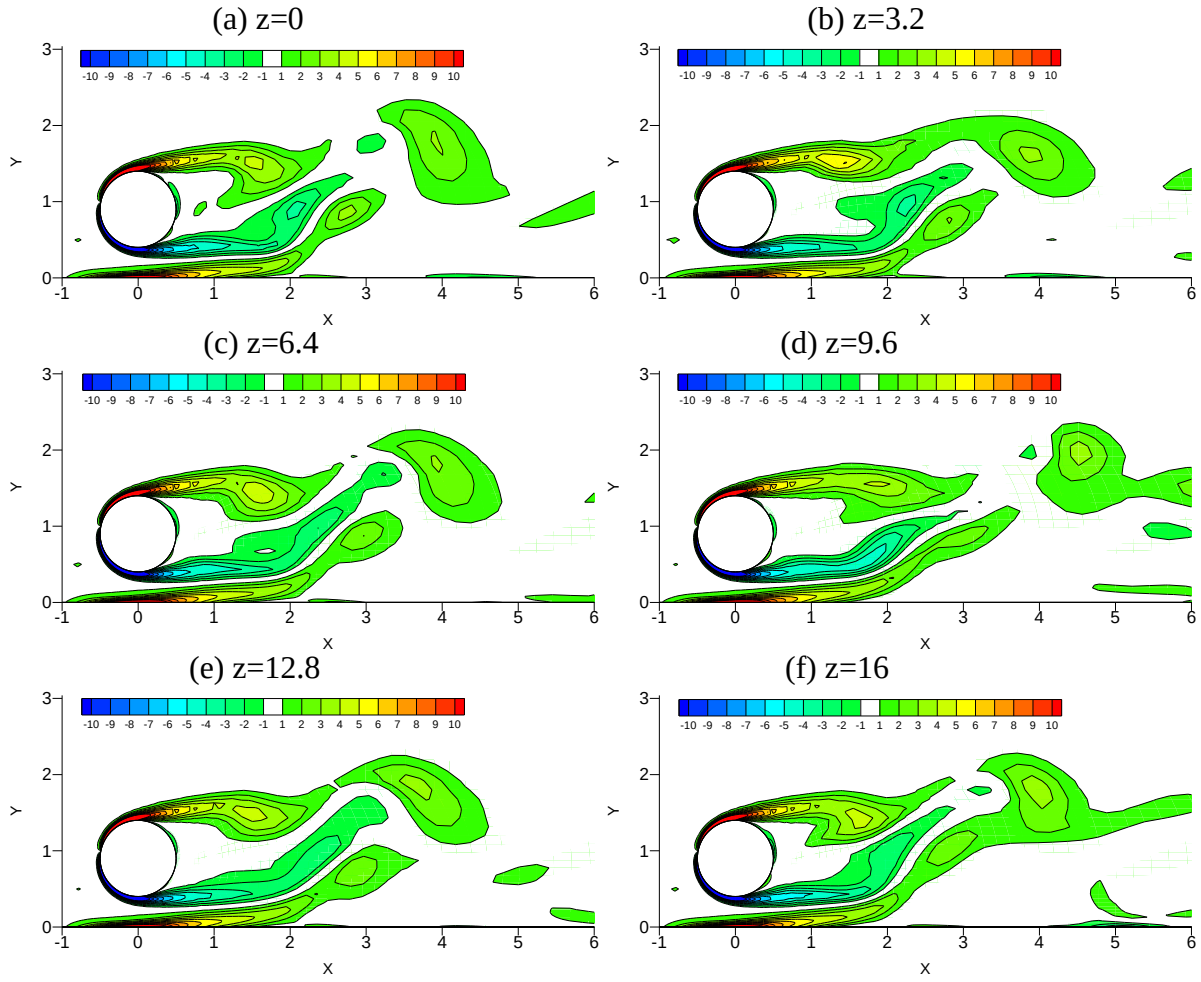

Fig. 4.10 Contours of spanwise vorticity at different cross section (α=0°, *Re*=500, Ut/D = 222.5 and e/D = 0.4)

It has been shown in Fig. 4.4 (h) and Fig. 4.8 (h) and (j) that there is an angle between the cylinder and the main vortices in the wake. Lucor and Karnidakis (2003) showed that for uniform flow past a cylinder, the alignment of the vortices in the wake is not parallel to the cylinder at large yaw angle of 60° and 70°. It is found that, with the effect of the plane boundary, the inclination of the wake vortices occurs at α = 45°. The inclination of the wake vortices affects the hydrodynamic lift force on the cylinder. Fig. 4.11 shows the comparison of lift coefficients at different cross sections at α = 45°, e/D = 0.8 and 0.4 respectively. It can be clearly seen in Fig. 4.11 (a) that the amplitudes of the lift coefficient at different locations are almost the same. However, the phase of the lift coefficient varies along the cylinder's axial direction. The phase difference between z = 2.4 and 9.6 is about 90°. The variation of the phase of the lift coefficient in the cylinder's axial direction is due to the inclination of the wake vortices. For e/D = 0.4 and α = 45°, the phase difference among the z-locations can also be clearly seen.

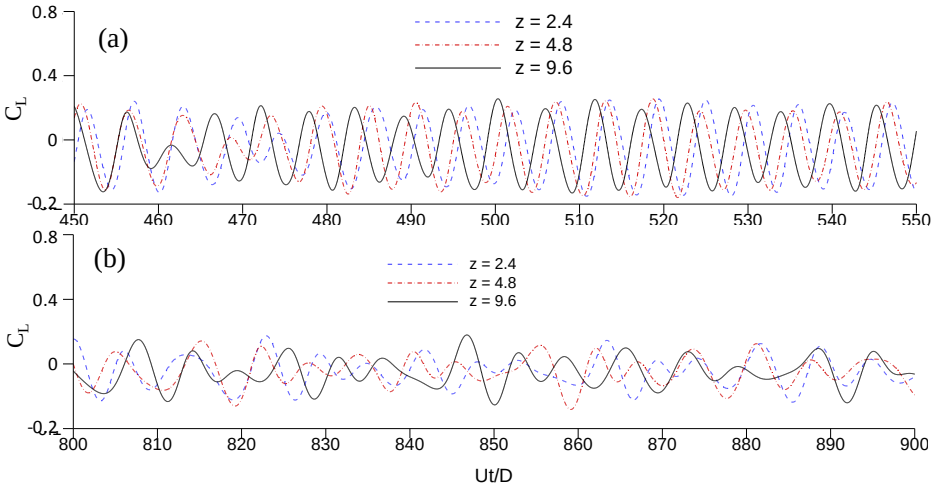

Fig. 4.11 Lift coefficient at different sections of a cylinder; (a) e/D = 0.8, α = 45° and (b) e/D = 0.4, α = 45°

Fig. 4.12 (a) and (b) shows the contours of pressure coefficient along the line of θ = 45° on the cylinder surface on the z–t plane at α = 0^0, e/D = 0.8 and α = 45^0, e/D = 0.4 respectively. The pressure coefficient C_p is defined as $C_p = (p - p_0)/(\rho U_n^2/2)$, with p_0 being the pressure at the inlet boundary and θ being the angle from the downstream edge of the cylinder in anticlockwise direction (measured from x-axis). The pressure coefficient contours before Ut/D = 80 in Fig. 4.12 (a) are generally parallel to z-direction, revealing that the flow is two-dimensional and after that, the variation of pressure along the z-direction gradually becomes clear, revealing the three-dimensionality of the flow. But the contours of the pressure coefficient before Ut/D = 480 in Fig. 12 (b) are still parallel to z-direction showing the two-dimensionality of the flow and beyond this point wavy vortex tubes in the spanwise direction start to appear indicating the three-dimensionality of the flow but obvious phase difference was not observed in both cases.

Fig. 4.13 shows the streamlines around the circular cylinder at α = 0° and 45°; e/D = 0.8 and Re = 500. The three-dimensionality of the flow is evidenced by the variation of the streamlines in the axial direction of the circular cylinder. In Fig. 4.13 (a), the very weak axial flow inside the primary vortex at α = 0^0 can be seen and this axial flow disappeared after certain distance in the axial direction. In Fig. 4.13 (b), the axial streamlines in the main wake vortex appear throughout the whole length of the circular cylinder. The helical streamlines observed at α = 45^0 are quite similar to those by Zhao *et al*. (2009) at Re = 1000.

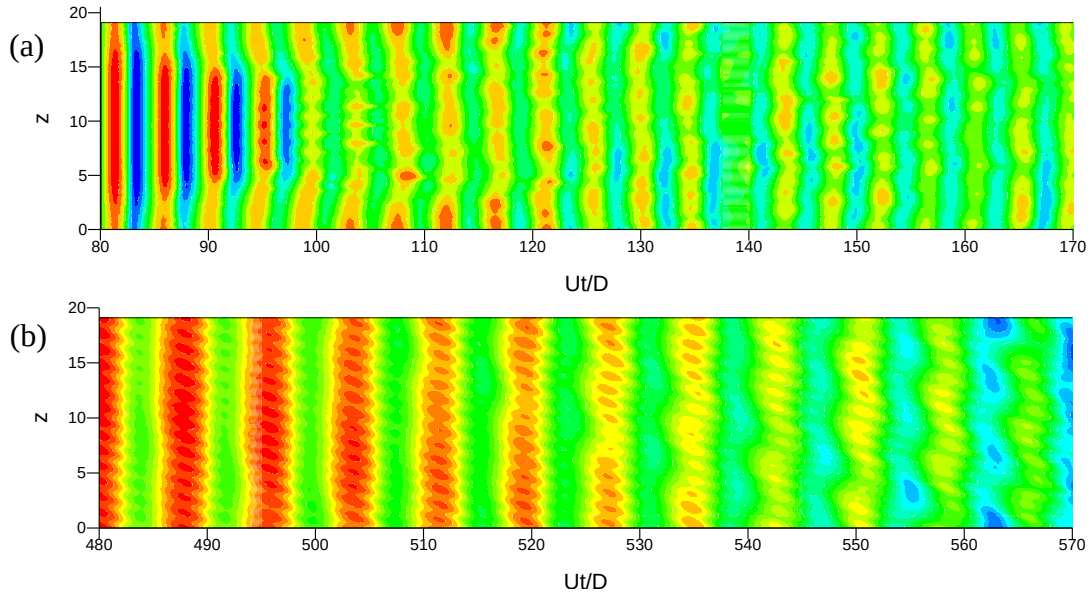

Fig. 4.12 Variation of pressure coefficient distribution along the line of Θ = 45° on the cylinder surface with time and *Re* = 500; (a) α = 0°, *e*/*D* = 0.8 (b) α = 45°, *e*/*D* = 0.4; transition of flow from 2D to 3D

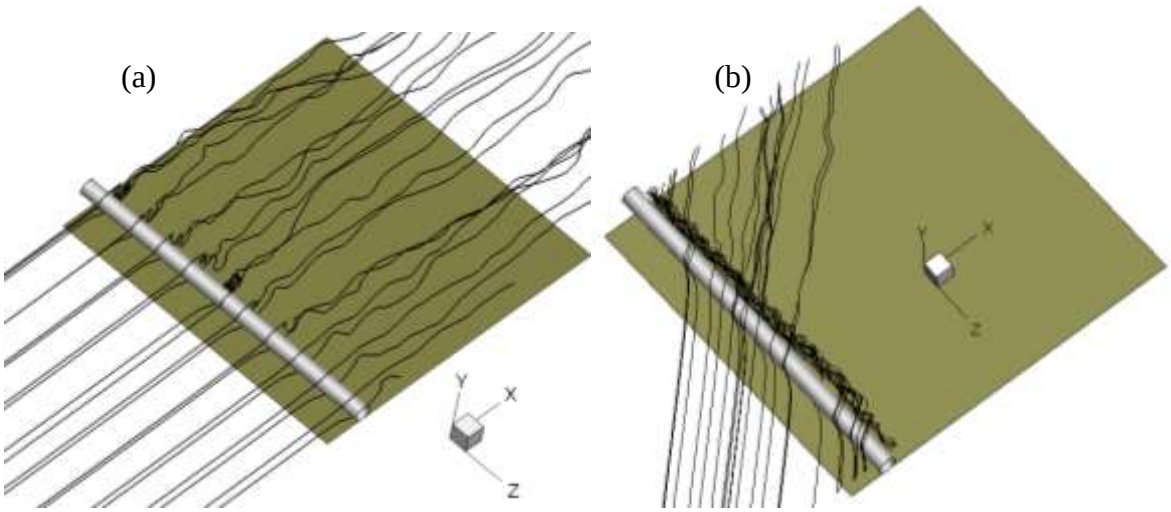

Fig. 4.13 Streamlines around the circular cylinder at *Re* = 500 (a) α = 0° (b) α = 45° for *e*/*D* = 0.8

4.3.3 FORCE COEFFICIENTS

By comparing Fig. 4.9 with Fig. 4.6, it is clearly seen that the amplitude of lift coefficient decreases with the decreasing gap ratio. The change in the amplitude of the fluctuating lift shows the strong influence of the gap ratio on the vortex shedding when it is

close to the critical gap for full vortex shedding suppression. The calculated mean values and root mean square (RMS) values of the force coefficients and the Strouhal numbers at α = 0° are compared with the experimental data by Jensen *et al*. (1990) and Roshko *et al*. (1975) and 2D numerical results by Lei *et al*., (2000) in Fig. 4.14.

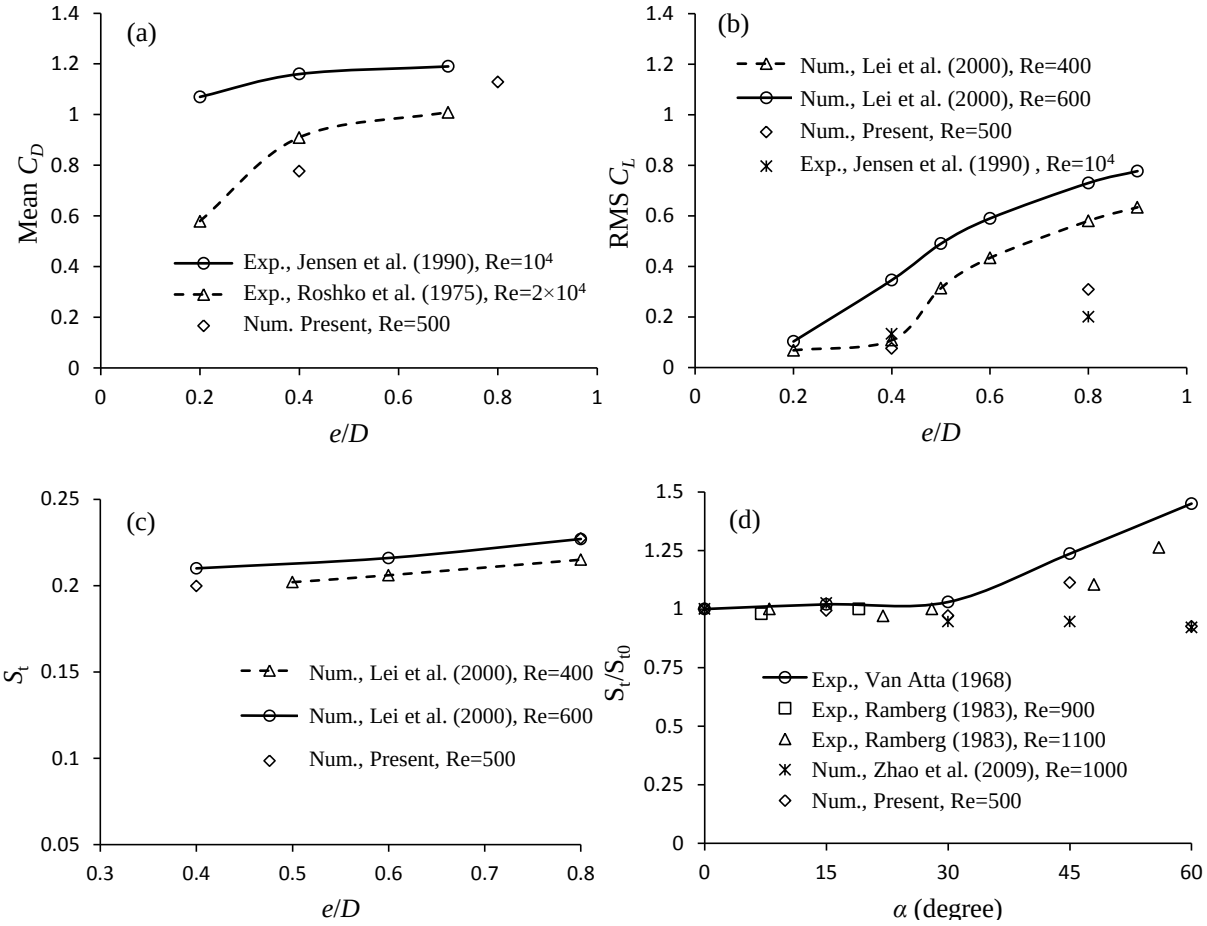

Fig. 4.14 Comparison of (a) mean sectional C_D (b) RMS C_L (c) S_t and (d) normalized S_t with previous data

The mean drag coefficient increases with the increasing *e*/*D* and RMS lift coefficient. The trend of the variation of force coefficients with *e*/*D* obtained in this study agrees with other data in general. However, the values of the force coefficients in different studies are scattered, probably because the difference in the boundary layer thickness. The mean drag coefficient in this study is close to the experimental result by Roshko *et al*. (1975) at *e*/*D* = 0.4 and between two experimental results at *e*/*D* = 0.8. The RMS lift coefficient of this study is closer to the experimental results by Jensen *et al*. (1990) than the 2D numerical results by Lei *et al*. (2000). It appears that the influence of *e*/*D* on S_t is weaker than that on the force coefficients. Yoon *et al*. (2012) also found that the effects of the Reynolds number are weak on the mean flow and the Strouhal number and strong on the lift coefficient. The calculated

Strouhal number is very close to the 2D numerical results by Lei *et al*. (2000) and it increases slowly with the increasing *e*/*D*. The variation of the Strouhal number normalized by the Strouhal number at α=0° (S_{t0}) with the yaw angle are compared with the experimental data and other numerical results in the uniform flow condition without the plane boundary in Fig. 4.13 (d). All the results agree well with each other as $\alpha \leq 30°$. The difference among different sets of results starts to increase as α exceeds 30°. The perfect periodic condition at the two ends of the cylinder in the numerical simulation may contribute the difference between the numerical results and the experimental data.

Fig. 4.15 shows the variations of mean drag and lift coefficients, RMS drag and lift coefficients and Strouhal number with α. The force coefficients and the Strouhal numbers are measured at the mid-section of the cylinder (*z*=0). In Fig. 4.15 (a), it is clearly observed that mean drag coefficient follows the independence principle pretty well for large gap ratio of *e*/*D*=0.8. The RMS drag coefficient increases slowly with the yaw angle for both gap ratios except for *e*/*D* = 0.4, α = 60°. For *e*/*D* = 0.4, the sudden reduction in the RMS drag and lift coefficient as α is increased from 45° to 60° is due to the suppression of vortex shedding. At *e*/*D* = 0.8, the magnitude of the negative $\overline{C}_L$ increases with the increasing α. Unlike that at *e*/*D* = 0.8, the magnitude of the negative $\overline{C}_L$ at *e*/*D* = 0.4 decreases with the increasing α. The root mean square lift coefficient (C_L') generally increases as α increases from 0° to 60° except at *e*/*D* = 0.4 and α = 60°, where the vortex shedding is almost fully suppressed. The RMS lift coefficient increases with the increasing α because the three-dimensionality of the flow is weakened. As discussed above, the weakness of the three-dimensionality corresponds to the strong spanwise vortices and the weak streamwise vortices and the increase in the lift fluctuation, which is directly linked to the spanwise vortices. At *e*/*D* = 0.8, Strouhal number decreases slightly with α except at α = 45° and is increased by 9.9% than at α = 0° and its value at α = 60° is around 7% less than that at α=0°. S_t is found to be decreased at α = 15° but gradually increased at $\alpha \geq$ 15° and the decrease is around 5% less than at α = 0° at *e*/*D*=0.4. The out-of-trend force coefficients and the Strouhal number at α=15° is due to the fact that the flow is 3D at α<15° and three-dimensionality is getting to weaker for α>15°.

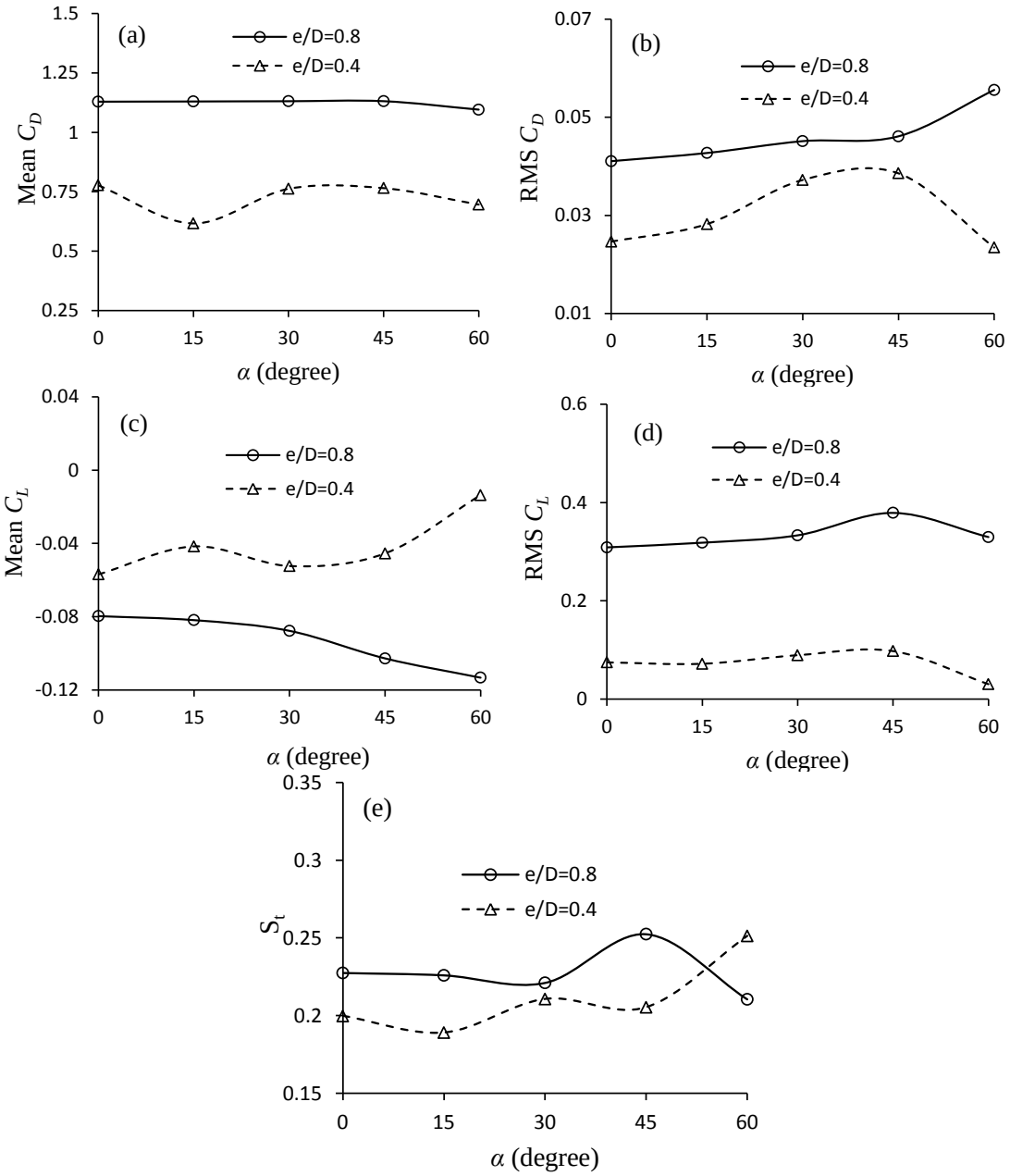

Fig. 4.15 Variation of (a) mean C_D (b) RMS C_D (c) mean C_L (d) RMS C_L and (e) S_t with α

4.4 CONCLUSIONS

Flow past a yawed circular cylinder near a plane boundary at yaw angles in the range of 0°– 60° was investigated numerically at two gap ratios (i.e. e/D = 0.4 and e/D = 0.8) and a constant Reynolds number of 500. Three-dimensional Navier-Stokes equations are solved by the finite element method. The focus of this study is to examine the effect of the yaw angle of the cylinder and the gap ratio on the transition of the flow from 2D to 3D. The effect of the

gap ratio on the vortex shedding flow regime and the force coefficients on the cylinder are summarized below.

The three-dimensionality of the flow decreases as the gap ratio is reduced from e/D = 0.8 to 0.4. The vortex shedding in the wake of an isolated circular cylinder at Re = 500 is in the streamwise vortex dominated mode B. However, the spanwise vortices dominate the wake flow at both e/D = 0.4 and 0.8, although streamwise vortices are observed. The spanwise vortices becomes strong and streamwise vortices becomes weak with increasing α, resulting in an increase in the RMS lift coefficient. The wake flow structure at e/D = 0.4 is characterized by wavy spanwise vortices with much weaker streamwise vortices. Increase in the yaw angle α leads to the suppression of vortex shedding at larger gap ratios. For example, the vortex shedding is fully suppressed at e/D = 0.4 and α = 60°, while it still exist at the same gap and α = 0°. The spanwise vortex dislocation that had been found in the case of uniform flow pass an isolated circular cylinder is not observed in this study, mainly due to the influence of plane boundary.

The independence principle is well followed by mean drag coefficient at e/D = 0.8. The mean drag coefficient reaches its minimum value at α = 15° for e/D = 0.4, which is 19% less than that at α = 0°. The RMS lift coefficient is found to increase with α at e/D = 0.8. Its value at α = 60° and e/D = 0.8 is about 6% larger than that at α = 0°. The independence principle law applies to the RMS lift coefficient up to α = 45° with a maximum error of up to 23.5%, which occurs at α = 45° and e/D = 0.4. The study has been focused on the transition of flow from 2D to 3D at relatively low Reynolds numbers. All the conclusions are based on the results of a relatively low Reynolds number in the turbulent flow regime and may not apply to the flow at high Reynolds numbers.

CHAPTER 5

THREE-DIMENSIONAL SIMULATIONS OF FLOW PAST TWO CIRCULAR CYLINDERS IN SIDE-BY-SIDE ARRANGEMENTS AT RIGHT AND OBLIQUE ATTACKS

The flow past two identical circular cylinders in side-by-side arrangements at right and oblique attack angles is numerically investigated by solving the three-dimensional Navier-Stokes equations using the Petrov-Galerkin finite element method. The study is focused on the effect of flow attack angle and gap ratios between the two cylinders on the vortex shedding flow and the hydrodynamic forces of the cylinders. For an oblique flow attack angle, the Reynolds number based on the velocity component perpendicular to the cylinder span is defined as the normal Reynolds number (Re_N) and that based on the total velocity is defined as the total Reynolds number (Re_T). Simulations are conducted for two Reynolds numbers of Re_N=500 and Re_T=500, two flow attack angles of α=0° and 45° and four gap ratios of G/D = 0.5, 1, 3 and 5. The biased gap flow for G/D=0.5 and 1 and the flip-flopping bistable gap flow for G/D=1 are observed for both α=0° and 45°. For a constant normal Reynolds number of Re_N=500, the mean drag and lift coefficients at α=0° are very close to those at α=45°. The difference between the root mean square (RMS) lift coefficient at α=0° and that at α=45° is about 20% for large gap ratios of 3 and 5. From small gap ratios of 0.5 and 1, the RMS lift coefficients at α=0° and 45° are similar to each other. The present simulations show that the agreement in the force coefficients between the 0° and 45° flow attacking angles for a constant normal Reynolds number is better than that for a constant total Reynolds number. This indicates that the normal Reynolds number should be used in the implementation of the independence principle (i.e., the independence of the force coefficients on the flow attacking angles). The effect of Reynolds number on the bistable gap flow is added to investigate by simulating the flow for Re_N=100 to 600, α=0° and 45° and G/D=1. Flow for G/D=1 is found to be two-dimensional at Re_N=100 and weak three-dimensional at Re_N=200. While well-defined biased flow can be identified for Re_N=300 to 600, the gap flow for Re_N=100 and 200 changes its biased direction too frequently to allow stable biased flow to develop.

5.1 INTRODUCTION

Vortex shedding patterns for flow around multiple cylinders have attracted much attention because of its importance in many engineering applications such as risers in offshore oil and gas engineering, bridge piers and tube heat exchangers etc. (Zdravkovich, 1977; Liu *et al*., 2001; Zhou *et al*., 2001; Alam *et al*., 2003). Flow past two cylinders in a side-by-side arrangement has been studied from different points of view, including the pressure distribution about the cylinder, the predominant vortex formation frequency and the flow-induced forces on the cylinders (Zdravkovich, 1977; Zdravkovich and Pridden, 1977). Williamson (1985) found two parallel vortex streets either as an in-phase or an anti-phase system in the wake of two side-by-side cylinders with a sufficient gap between them. The two distinct vortex streets were found to form a single and large scale wake when they are in in-phase and two distinct vortex streets when they are in anti-phase with each other. The gap ratio (G/D), as defined in Fig. 5.1 with G being the gap between the two cylinders and D being the cylinder diameter, plays an important role in determining the wake flow pattern. A number of studies on the classification of flow regime in the wake of two side-by-side cylinders have been reported previously. One single vortex street is formed for small gap ratios ($G/D<0.1$). For intermediate gap ratios of $0.1<G/D<1.2$, the flow through the gap between two side-by-side cylinders was found to act biased towards one cylinder, forming a narrow wake behind one cylinder and a wide wake behind the other (Zdravkovich 1977, Williamson 1985). The direction of the biased gap flow was found to change intermittently, resulting in a bistable flow regime (or the flip-flopping regime). Kim and Durbin (1988) performed an experimental study on flow past a pair of circular cylinders in the flip-flopping regime and revealed that the direction of the biased flow changes randomly with time in subcritical Reynolds number regime. Zhou *et al*. (2002) studied the turbulent wake of two side-by-side circular cylinders experimentally at a Reynolds number of 5800 and found one single vortex street for $G/D<0.1$ and two vortex streets in anti-phase with each other for $G/D=2$. Alam *et al*. (2003) conducted an experimental study on uniform flow past two side-by-side cylinders at a Reynolds number of 5.5×10^4 and the gap ratios less than $1.2D$. The vortex wake behind the cylinder where the gap flow is biased towards is found to be narrower than that behind the other cylinder.

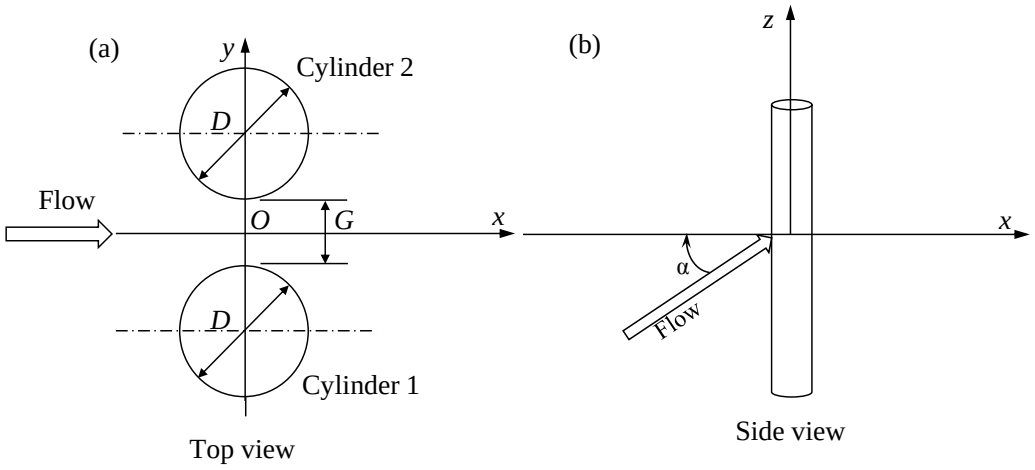

Fig. 5.1 Sketch for flow past two cylinders in a side-by-side arrangement with a flow approaching angle α

Many numerical studies on flow around two side-by-side circular cylinders have also been performed in the last few decades. Meneghini *et al*. (2001) studied the vortex shedding and wake interference between tandem and side-by-side circular cylinders at Reynolds numbers of 100 to 200 and various spacing ratios using the finite element method. They identified the flip-flopping flow pattern for $G/D \leq 1$ and synchronized anti-phase vortex shedding for $G/D>1.5$. Liu *et al*. (2001) simulated flow around two side-by-side circular cylinders at Reynolds number of 200 and identified the dependency of wake pattern on space between the cylinders. Kondo and Matsukuma (2005) studied the flow around two circular cylinders in side-by-side arrangement by three-dimensional simulations using a third-order upwind finite element method at Re = 1000 and the gap ratios of $1 \leq G/D \leq 4$ and successfully predicted the phenomena of the biased gap flow behind the two circular cylinders. By using the large eddy simulations, Afgan *et al*. (2011) simulated flow past two side-by-side circular cylinders at a Reynolds number of 3000 and predicted the three-dimensional biased wake flow for the intermediate gap ratios of $0.25 \leq G/D \leq 0.75$ and also the flip-flopping phenomena. Hesam and Navid (2011) studied the bistable flow around two side-by-side cylinders in both laminar and turbulent flow regimes using finite volume method.

In practical applications, flow often approaches cylindrical structures at an oblique attack. The so-called independence principle (IP) is commonly used to predict flow-induced force on a circular cylinder at an oblique attack angle. The independence principle states that the force coefficients that are normalized by the velocity component normal to the cylinder are independent on the flow attack angle. Many studies have proved that the independence principle is valid to predict flow-induced forces on a cylinder for flow attack angles up to 45°

(Kozakiewicz *et al*., 1995; Zhao *et al*., 2009, 2013; Zhou *et al*., 2009). When a flow past a circular cylinder of a finite length, the wake vortices far from the upstream end of the cylinder were found approximately parallel to the cylinder (Ramberg, 1983; Thakur *et al*., 2004). Lucor and Karniadakis (2003) found that wake vortices for flow past a yawed cylinder at large yaw angles of 60° and 70° were not exactly parallel to the cylinder.

So far, little attention has been paid on flow past two cylinders at an oblique attack and cannot be ignored while judging the hydrodynamics around the cylindrical structures. The objective of the present study is to numerically predict the wake characteristics and the hydrodynamic forces for two cylinders in a fluid flow in a side-by-side arrangement at a right attack angle of α=0° and oblique attack angles. The effects of the attack angle, the Reynolds number and the gap between the two cylinders are discussed.

5.2 NUMERICAL METHOD

The three-dimensional incompressible Navier-Stokes (NS) equations are solved for simulating the flow past two side-by-side cylinders as shown in Fig. 5.1. The length, time, velocity and pressure are non-dimensionalized as $x_i = x_i'/D$, $t = U_N t'/D$, $u_i = u_i'/U_N$ and $p = p'/\rho U_N^2$, respectively, where the prime stands for the dimensional values, x_1, x_2 and x_3 represent the coordinates x, y and z, respectively, t is the time, u_i is the velocity component in the x_i-direction, ρ is the density of the fluid and U_{N} is the velocity component perpendicular to the cylinder. The non-dimensional NS equations are written as

$$\frac{\partial u_i}{\partial t} + u_j \frac{\partial u_i}{\partial x_j} + \frac{\partial p}{\partial x_i} - \frac{1}{\mathrm{Re}_N} \frac{\partial^2 u_i}{\partial x_j^2} = 0, \tag{5.1}$$

$$\frac{\partial u_i}{\partial x_i} = 0, \tag{5.2}$$

where Re_N is the Reynolds number based on the velocity component normal to the cylinder span. The governing equations are solved by the Petrov-Galerkin finite element model (PG-FEM) developed by Zhao *et al*. (2009). The PG-FEM was successfully used to simulate the flow past a single cylinder at oblique attacks for Reynolds numbers in a wide range between 100 and 1000 (Zhao *et al*., 2013). The size of the rectangular non-dimensional computational domain is 50 in the flow direction, 9.6 in the spanwise direction of the cylinder and 40 in the

cross-flow direction. The non-dimensional distance between the cylinder centres and the inlet boundary is 20. The initial values of the velocity and the pressure in the whole domain are set as zero. The non-dimensional velocity at the inlet boundary is given by

$$(u_1,\ u_2,\ u_3) = (1,\ 0,\ \tan\alpha). \tag{5.3}$$

The free-slip boundary condition is employed at the two side boundaries that are parallel to the $x-z$ plane, namely, the velocity component and the pressure gradient perpendicular to the boundary are zero. When the flow approaches the cylinder at an inclined angle, fluid mass needs to be allowed to pass through the two end boundaries (the boundaries perpendicular to the cylinder axis). To allow the flow to pass the end boundaries, the periodic boundary condition is imposed by setting velocity and pressure gradients (in all three directions) on one of end boundary to be equal to their counterparts on another end boundary. The periodic boundary condition at the two end boundaries allow the fluid flowing through the boundary. On the cylinder surface, no-slip condition is applied.

Fig. 5.2 shows a typical computational mesh near the cylinders for G/D=1. The computational domain is divided into 192 layers of hexahedral 8-node linear finite elements in the axial direction. The non-dimensional mesh size Δz in the spanwise direction of the cylinder is 0.05. The surface of each cylinder is divided into 84 elements in the circumferential direction. The normalized distance is defined as $y^+ = u_f \Delta / \nu$, where Δ is the distance from the wall and u_f is the friction velocity is used to evaluate the near wall mesh density. The maximum y^+ along the cylinder surfaces is less than 0.5. For each case, parallel simulations are conducted using 64 CPUs (Central processing units) on the iVEC supercomputer facility in Western Australia.

After the NS equations are solved, the drag and lift coefficient on each cylinder are calculated as $C_D = 2F_D / \rho DLU_N^2$, $C_L = 2F_L / \rho DLU_N^2$, respectively, where F_D and F_L are the drag and lift forces on the whole cylinder in the x- and y- direction, respectively, L is the length of the cylinder. The drag and lift forces (F_D and F_L) are calculated by integrating the pressure and shear stress along the whole cylinder surface.

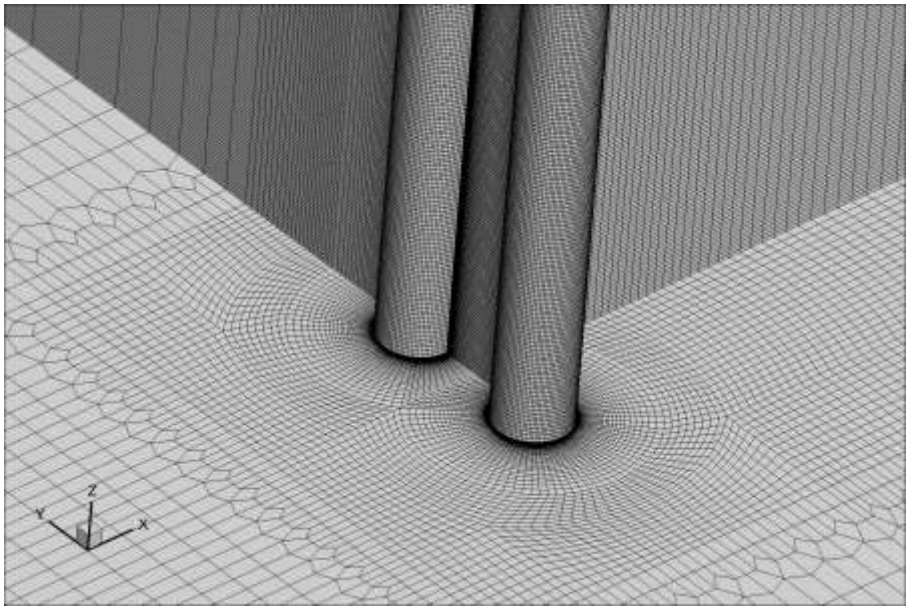

Fig. 5.2 Computational mesh near the cylinders for G/D=1

Two Reynolds numbers are defined for the convenience of the discussion in this study. The Reynolds number based on the velocity component normal to the cylinder span is defined as the normal Reynolds number $\mathrm{Re_N}$ and the Reynolds number based on the total velocity is defined as the total Reynolds number $\mathrm{Re_T}$. Specifically, $\mathrm{Re}_N = U_N D/\nu$ and $\mathrm{Re}_T = UD/\nu$, where U is the free stream velocity, U_N is the component of U in the perpendicular direction of the cylinder, ν is the kinematic viscosity of the fluid and D is the diameter of the cylinder. The velocity U and U_N are related by $U_N = U\cos\alpha$. If the flow direction is perpendicular to the cylinder span, $\mathrm{Re_N}$=$\mathrm{Re_T}$. Simulations are carried out for Reynolds number of $\mathrm{Re_N}$=500 and $\mathrm{Re_T}$=500. Four gap ratios of G/D=0.5, 1, 3 and 5 are considered, with G being the gap between the two cylinders as shown in Fig. 5.1. Also, the simulations are carried out to examine the Reynolds number ($\mathrm{Re_N}$ = 100-600) effect in bistable flow regime gap ratio. These gap ratios cover the bistable flow regime and also the regime where the interaction between the two wakes is very weak. The Reynolds number of 500 in the turbulent flow regime is chosen considering the affordability in terms of the computational time for the direct numerical simulation at low Reynolds numbers. Each simulation was conducted for at least the non-dimensional time of $U_N t/D = 600$ to ensure that vortex shedding has been fully developed. For small gap ratios of 0.5 and 1, where the flow changes between two patterns intermittently, simulations were conducted up to $U_N t/D = 800$ to ensure the changes in the flow pattern can be identified if they exist.

5.3 RESULTS AND DISCUSSIONS

Simulations for a constant Reynolds number of Re_N=500 and four gap ratios of G/D=0.5, 1, 3 and 5 are firstly conducted to examine the effects of the gap ratio on the flow. These gap ratios cover the bistable flow regime and also the regime where the interaction between the two wakes is very weak. Then simulations for G/D=1 and Re_N=100 to 600 are performed to examine the effects of the Reynolds number on forces and flow structures on the bistable gap flow. Finally, the effects of the flow approaching angle on the force coefficients are studied by simulating the flow for G/D=1, Re_N=500 and flow approaching angles of 0°, 15°, 30° and 45°.

5.3.1 MESH DEPENDENCY STUDY

The mesh dependency study is carried out before the effect of α on the flow characteristics is investigated. Simulations for flow past a single cylinder at Re_T=Re_N=500 and α=0° are conducted using two meshes of different densities on the xy-plane. The mesh with the density that is used in all simulations of flow past two side-by-side cylinders is defined as the normal mesh. In the normal mesh, the non-dimensional finite element size in the radial direction at the cylinder surface is 0.002. In the dense mesh, the circumference of each cylinder is divided into 128 elements and the minimum mesh size in radial direction is 0.0005. Fig. 5.3 shows the time histories of lift and drag coefficients calculated from two meshes (normal and dense) at Re_N=Re_T= 500 and α=0°. The forces from the two meshes as shown in Fig. 5.3 are not perfectly identical to each other because of the strong turbulence of the wake flow. However, the amplitudes of the drag and lift coefficients from the two meshes are similar to each other in Fig. 5.3. The quantitative comparison between the results from the normal and dense meshes are made in Table 5.1, where the mean drag coefficient ($\overline{C}_D$), root mean square (RMS) drag and lift coefficients (C'_D and C'_L) and the Strouhal numbers are listed. The agreements of the Strouhal number and the mean drag coefficient between the normal and dense meshes are excellent. The difference in C'_D and C'_L are found to be 2.5% and 2.35%, respectively. The variations of the force coefficient with time from the two meshes, especially the drag coefficient, are very irregular. It is difficult to have two statistic values of the force coefficient exactly the same, unless the simulations are conducted for an extremely long time. The very little difference between the results from the normal and dense meshes shows that the normal mesh has been dense enough to ensure the accuracy of the results.

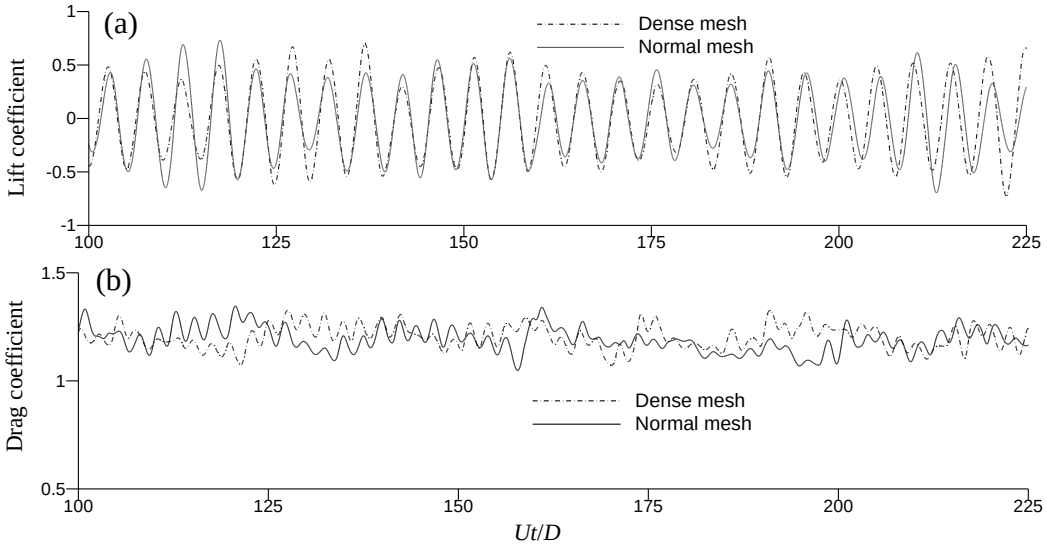

Fig. 5.3 Comparison in force coefficients between normal and dense meshes for Re_N=Re_T=500 and α=0°

The mesh dependency study for two cylinders is also carried out for G/D=1. Fig. 5.4 (a) and (b) show the time histories of the drag and lift coefficients calculated from the dense mesh for α=0°, G/D=1 and Re_N=500. The node number for the normal and dense meshes are 2.2 million and 5.5 million, respectively. Alam *et al*. (2003) found that, as the spacing between two side-by-side circular cylinders (G) is less than 1.2D, the gap flow was biased toward one side, resulting in the formulation of a narrow wake (NW) behind one cylinder and a wide wake (WW) behind the other. The cylinder with WW has much stronger oscillation of the lift force than the one with NW. The biased gap flow is bistable and switches from one side to the other at irregular intervals of time. This flow regime is therefore known as the flip-flopping regime or bistable flow regime (Bearman and Wadcock, 1973; Zdravkovich and Pridden, 1977; Kim and Durbin, 1988). The simulated biased flow for α=0°, G/D=1 and Re_N=500 was also found to be bistable, i.e. the biased direction of the flow switches from one side to the other intermittently. This can be evidenced by the intermittent changes in the oscillation amplitude of the lift coefficient. The flow structures for bistable flows will be discussed in Section 5.3.2. The force coefficients from the normal and dense meshes in three time periods, where the flow for both dense and normal meshes are in relatively stable biased flow mode, are compared in Fig. 5.4 (c). Because the biased direction of the gap flow in the calculation of dense mesh is found opposite to that of the normal mesh, the negative values of the lift coefficients from the dense mesh are shown in Fig. 5.4 (c). It can be seen that C_{L1} from the normal mesh and $-C_{L2}$ in the dense mesh are in WW mode when

$440 < U_N t / D < 510$, while they are in NW mode when $354 < U_N t / D < 394$ and $540 < U_N t / D < 580$.

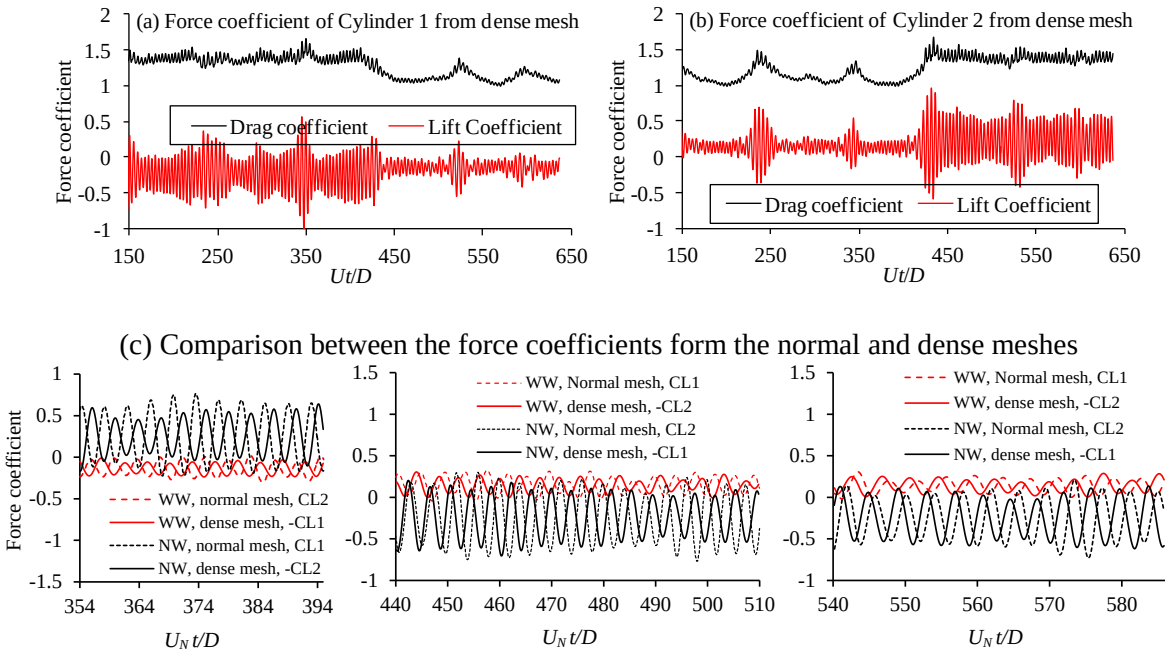

Fig. 5.4 Comparison between the time histories of the lift coefficient calculated from the normal and dense meshes for α=0°, G/D=1 and Re_N=500.

A further comparison between the mean and RMS values of the force coefficients from the normal and dense meshes is made in Table 5.2. These values are obtained from the time histories of the force coefficients in the three time periods with stable flow modes before U_N t/D=650 as shown in Fig. 5.4 (c). Because the simulations for the dense mesh is very time consuming (30 days were needed for up to U_N t/D=650), the comparison is only based on the data over the time periods shown in Fig. 5.4 (c). Much longer samples are preferred to obtain an ideal comparison between the results from the two meshes. It can be seen that the Strouhal number and the mean drag coefficient from the two meshes agree with each other excellently with a discrepancy of 1.5% and 2%, respectively. The difference in the mean lift coefficient is about 6% because the very small mean values of the lift coefficients signify the relative difference. The differences between the RMS drag coefficients from the two meshes are larger than that of the mean values because of the very strong variation of the flow with the time by using the small sample number and the very small values of RMS drag coefficients. Even in the stable biased flow regime, the mean direction of the gap flow was found changing from period to period as shown in Fig. 5.4 (c).

Table 5.1 Comparison of the results between the normal and dense meshes at Re_N=Re_T=500 and α=0°

Mesh	S_t	$\overline{C}_D$	C'_D	C'_L
Normal(Δz=0.05)	0.2032	1.2017	0.0322	0.3575
Dense(Δz=0.025)	0.2003	1.2046	0.0314	0.3491

Table 5.2 Comparison of the results between the dense and normal meshes for Re_N=500 and α=0°

Mesh and wake	$\overline{C}_D$	$\overline{C}_L$	C'_L	C'_D	S_t
WW normal mesh	1.060	-0.078	0.087	0.036	0.254
WW dense mesh	1.059	0.079	0.079	0.033	0.258
NW normal mesh	1.411	0.049	0.285	0.063	0.255
NW dense mesh	1.384	-0.046	0.260	0.059	0.259

5.3.2 EFFECTS OF THE GAP RATIOS ON WAKE FLOW PATTERN

The wake flow patterns for (Re_N, α) = (500, 0°) and (500, 45°) are presented in this section. For a fixed flow attack angle of 45°, the wake flow patterns at Re_T=500 are found similar to that for Re_N=500 for the simulated gap ratios and will not be presented here. The difference in the force coefficients for Re_T=500 and Re_N=500 will be discussed in Sections 5.3.3. Fig. 5.5 shows the three-dimensional iso-surfaces of the vorticity component in the axial direction of the cylinders (*z*-direction) for the four gap ratios and two flow approaching angles of 0° and 45°. The non-dimensional vorticity components in the *x*-, *y*- and *z*-directions are defined as $\omega_x = \partial w/\partial y - \partial v/\partial z$, $\omega_y = \partial u/\partial z - \partial w/\partial x$ and $\omega_z = \partial v/\partial x - \partial u/\partial y$, respectively. The spanwise vortices can be identified behind the cylinders in all cases. For gap ratios greater than 1, the shear layers separated from the cylinders form vortices over the region of *x/d* = 1- 3. It is interesting to see that for *G*/*D*=0.5, the shear layers from the two cylinders extend farther downstream of the cylinders before they form vortices. The delay in the formation of the vortices at this gap ratio leads to very weak oscillation of the lift coefficient, which will be discussed later on. It appears that more small scale vortices present for α=45° than for α=0°, indicating the decay of the spanwise vorticies as the attack angle increases. For the same Re_N, the free stream velocity at α=45° is $\sqrt{2}$ times that at α=0°. This is probably the reason why the turbulence in the wake flow for α=45° appears stronger than that for α=0°. When the Reynolds number is in the earliest transition regime A (*Re*<250), the flow is characterized by the inception of the vortex loops and the formation of the streamwise vortex pairs due to the deformation of primary spanwise vortices, and the non-dimensional

wavelength of the spanwise structure was found to be about 3~4D (Barkley and Henderson, 1996; Zhang *et al*., 1995).

It has been known that at the Reynolds number of 500, flow past a single cylinder is in mode B regime characterized by the dominance of the streamwise vortices (Williamson, 1996). Fig. 5.6 shows the three-dimensional iso-surfaces of the streamwise vorticity component for α = 0° and 45° and Re_N=500. The iso-surfaces shown in Fig. 5.6 are at the instants when the three-dimensional wake flows have been fully developed. At α=45°, the streamwise vorticity is also seen on the upstream surfaces of the cylinders because the vorticity in the boundary layer flow on the upstream surfaces has strong component in the *x*-direction. It can be seen that the streamwise vortices are distributed very irregularly. Scarano and Poelma (2009) found that the streamwise vortices in the wake of a single cylinder for a Reynolds number of 360 are in pairs and the distance between two neighbour pairs is about 1.2 diameters. Each pair comprises two vortices of opposite directions. Zhao *et al*. (2013) found that identifying the vorticity pairs is more difficult at high Reynolds numbers than at low Reynolds numbers due to the strong irregularity of the flow. The streamwise vorticity at α = 0° for all gaps studied are observed weaker than that at α = 45° that might be the possible reason of the reduction of the spanwise vorticity, which results in the increase of streamwise vorticity.

In order to see the detailed vortex shedding flow in a cross section of the cylinders, the vortex shedding flow at the mid-section of the cylinder on the *xy*-plane are presented in Fig. 5.7 using the contours of the vorticity in the axial direction of the cylinders (ω_z). The biased flow for *G*/*D*=0.5 and 1 can be clearly identified for both α=0° and 45° as shown in Fig. 5.7 (a) – (d). The flow through the gap biases towards the bottom cylinder (cylinder 1) for *G*/*D*=0.5 and α=0° and towards the top cylinder (cylinder 2) for *G*/*D*=0.5 and α=45°. The narrow wake (NW) is observed behind the cylinder towards which the gap flow biases and the wider wake (WW) occurs behind the other cylinder, which is similar to the observation by Alam *et al*. (2003).

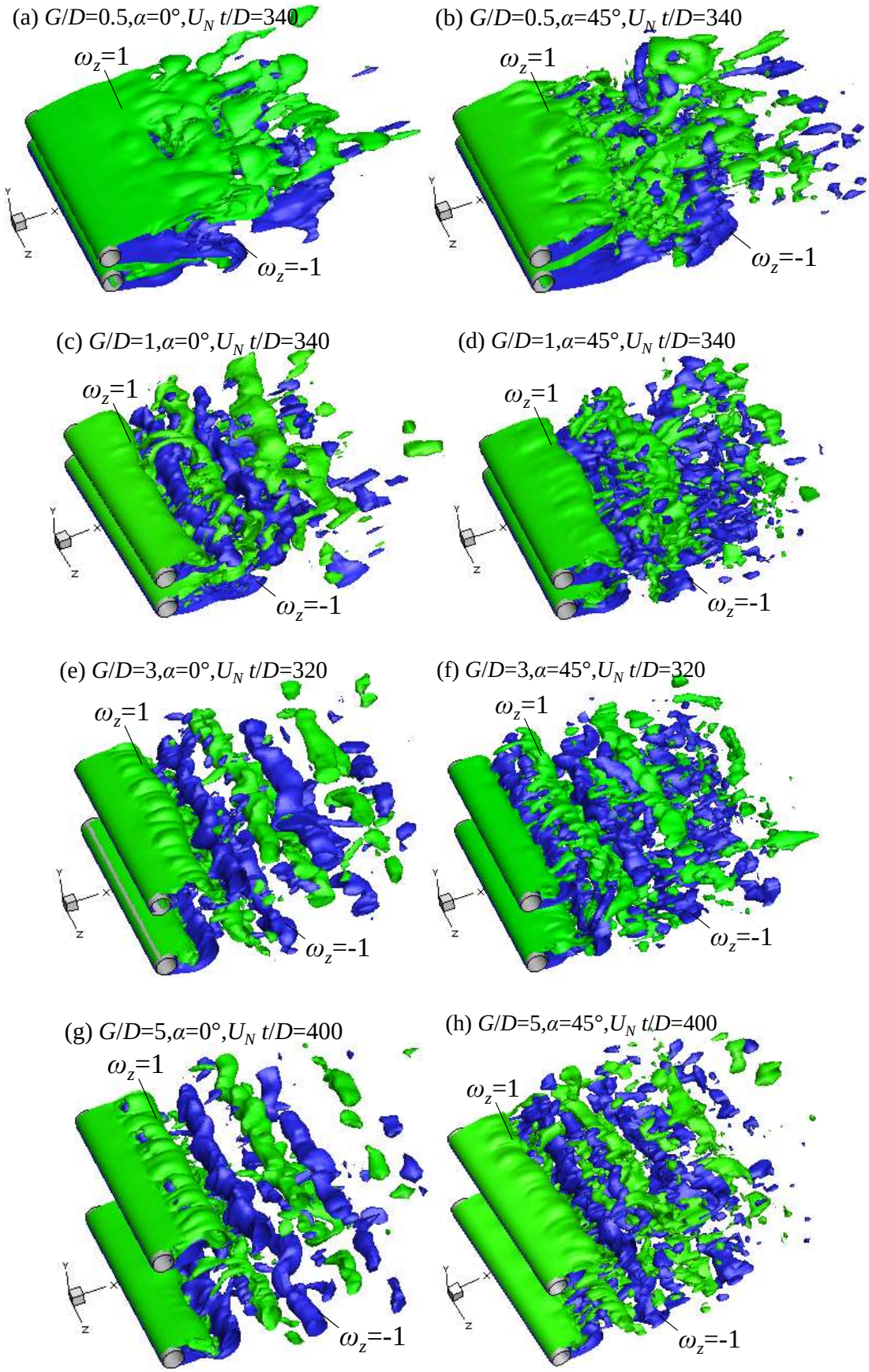

Fig. 5.5 Vorticity iso-surfaces of $|\omega_z|=1$ at Re_N=500 for α=0° and 45°

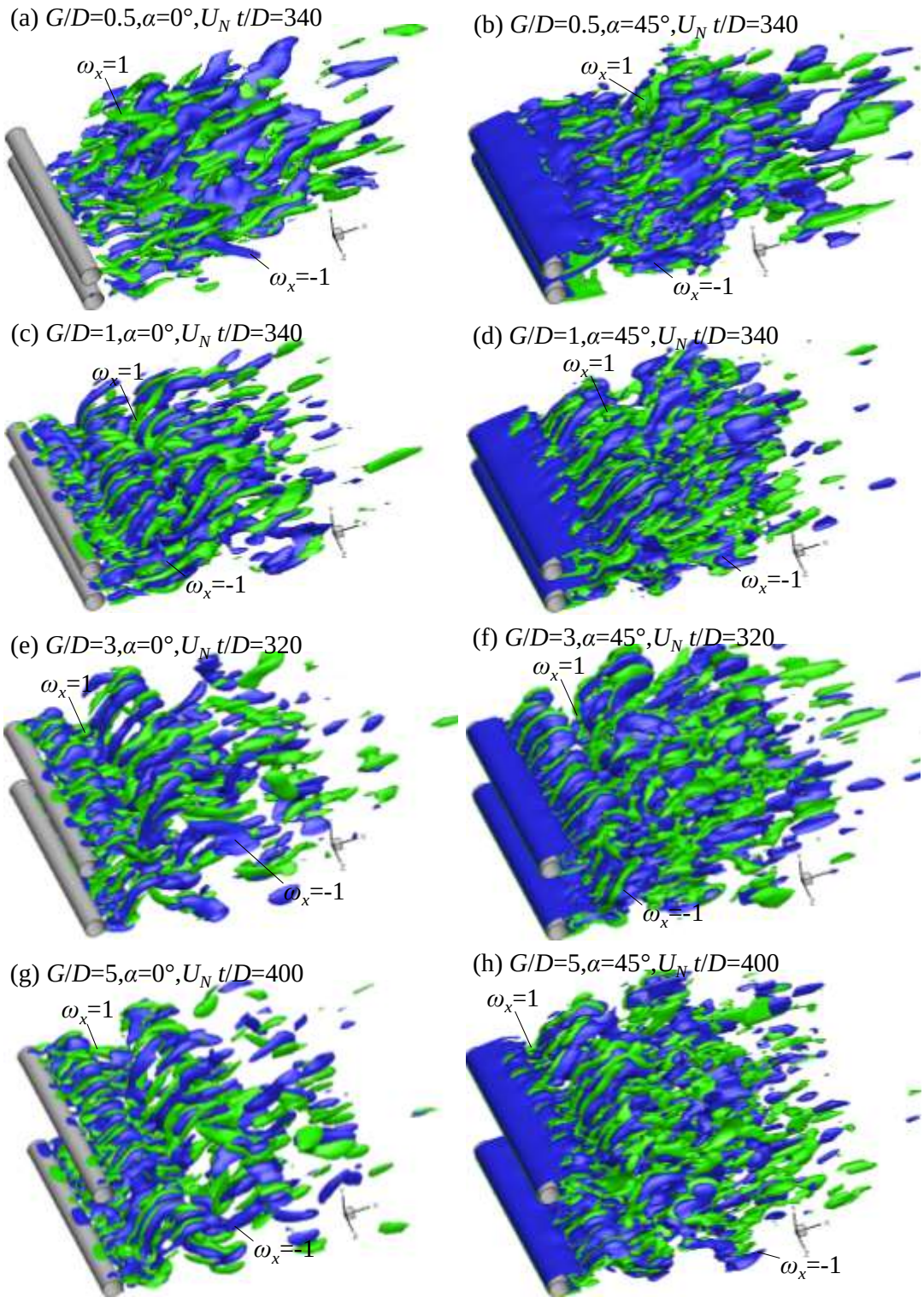

Fig. 5.6 Vorticity iso-surfaces of $|\omega_x|=1$ at Re_N=500 for α=0° and 45°

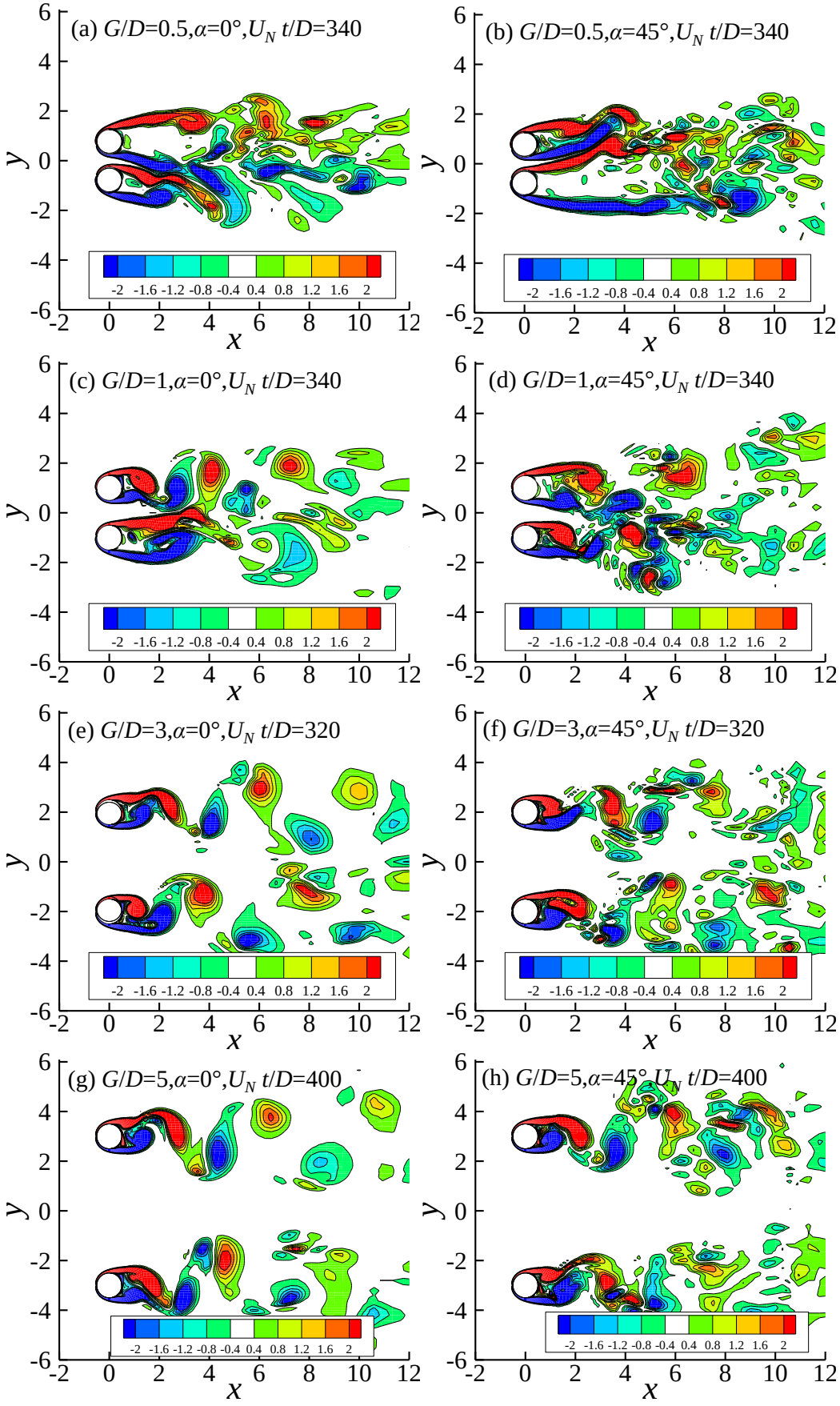

Fig. 5.7 Contour of axial vorticity at mid-section (z=4.8) and different instants for Re_N=500

Fig. 5.8 shows the time histories of the drag and lift coefficient of the cylinders for biased flows at G/D=0.5 and 1. When the flow is transiting from 2D to 3D, the drag and lift coefficients decrease dramatically because part of the energy in the spanwise vortices, which is responsible for the oscillation of the force coefficients, is transferred to streamwise vortices (Mansy *et al*., 1994). The dissipation of the spanwise vortices ω_z can be clearly seen in Fig. 5.7. For G/D=0.5, the flow is two-dimensional at early stage of the numerical simulation until $U_N t/D \leq 95$ and gradually changes to three-dimensional with the increase of non-dimensional time (Fig. 5.8). Based on the time histories of the force coefficients, the wake flow remains two-dimensional longer time at G/D = 1 than at G/D = 0.5 for α = 0°. But the formation of the three-dimensional flow is much quicker in α = 45° at G/D=1. For G/D=0.5, the gap flow always biases towards one cylinder and does not change its biased direction until $U_N t/D$=800 for both α=0° and 45°. The fixed biased direction of the gap flow during long time at G/D=0.5 is evidenced by the time histories of the force coefficients shown in Fig. 5.8 (a) and (b), where both the drag and lift coefficients oscillate regularly and no sudden changes are observed.

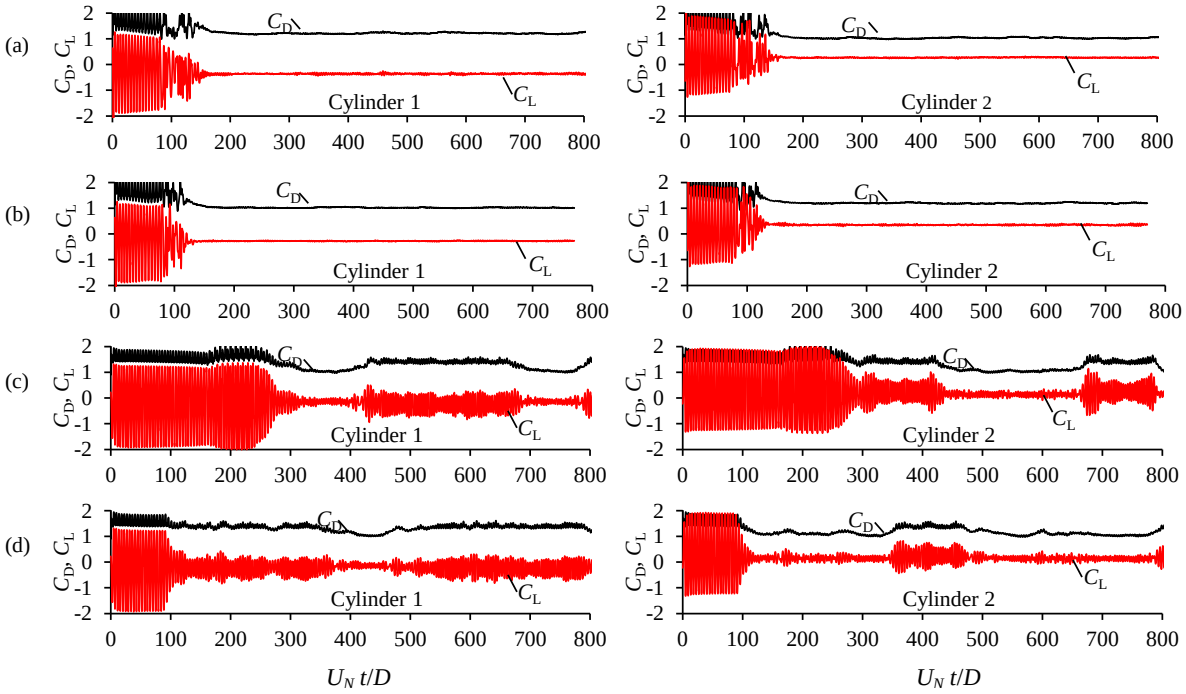

Fig. 5.8 Time histories of the force coefficients for Re_N=500 and small gaps of G/D=0.5 and 1. (a) G/D=0.5, α=0°; (b) G/D=0.5, α=45°; (c) G/D=1, α=0°; (d) G/D=1, α=45°.

As G/D = 1, the direction of biased gap flow switches from one side to the other intermittently for both flow approaching angles. The bistable and switching phenomenon of the biased flow occurs at irregular time interval and is known as flip-flopping regime or bistable flow regime (Bearman and Wadcock 1973, Kim and Durbin 1988). The occurrence of the switching phenomenon in bistable flow regime is further evidenced in Fig. 5.9 by the contours of the axial vorticity at the mid-section of the cylinder for G/D=1 at two instants for each flow attack angle. For α=0°, the gap flow biases towards the top cylinder at $U_N\ t/D$=360 as in Fig. 5.9 (a) and towards the bottom cylinder at $U_N\ t/D$=520 as in Fig. 5.9 (b). The corresponding force coefficients at $U_N\ t/D$=360 are very different from those at $U_N\ t/D$=520 as shown in Fig. 5.8. When G/D=1, the biased flows for α=0° and 45° are similar to each other. The switching behaviour of two modes is found to be consistent with that reported by Zdrakovich (1977) and Afgan *et al*. (2011).

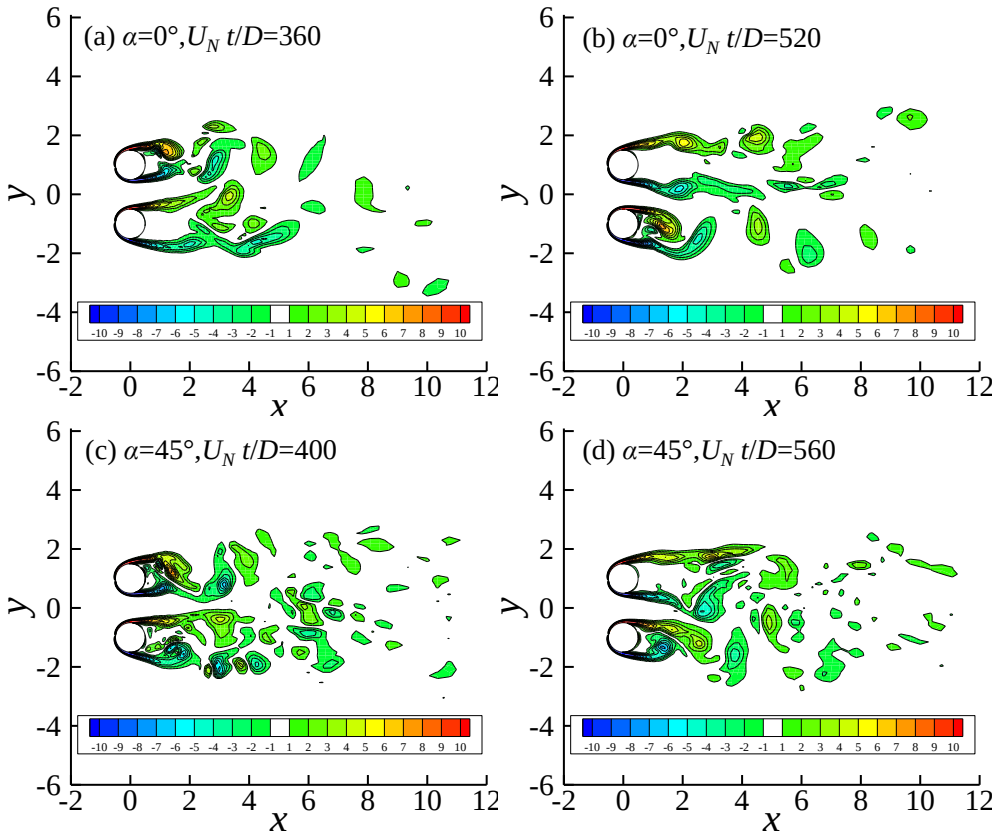

Fig. 5.9 Switching of the gap flow direction for Re_N=500 and G/D=1, shown by the contour of axial vorticity at the mid-section (z=4.8)

For G/D = 1 (Fig. 5.8 (c) and (d)), it can be seen that at a specific instant, the force coefficients on one of the cylinders are very different from those on the other. This phenomenon is related to the biased vortex flow patterns in the wake. For example, at

$U_N t/D$=340 for α=0°, the gap flow biases towards cylinder 2 (top cylinder) as shown in Fig. 5.7 (c), leading to a NW and a greater drag coefficient behind cylinder 2 than behind cylinder 1 (Fig. 5.8 (c)). It has been reported previously that the NW causes a greater drag and the WW causes a lower drag on the respective cylinders (Bearman and Wadcock, 1973). The timing when the biased flow changes from one direction to the other can be clearly identified by the variations of the drag and lift coefficients with time shown in Fig. 5.8. As shown in Fig. 5.8 (c), for G/D=1 and α=0°, the flow becomes three-dimensional as $U_N\ t/D$>280. The sudden changes in the force coefficients can be clearly identified at three instants of $U_N t / D \approx 430$, 670 and 780. These sudden changes are due to the changes in the biased gap flow direction. The gap flow is biased towards the top cylinder during 300<$U_N\ t/D$<420 and 670<$U_N\ t/D$<780 and towards to the bottom cylinder during 430<$U_N\ t/D$<670 and 790<$U_N\ t/D$<810. The intermittent changes in the biased gap flow direction is also observed at G/D=1 and α=45°. The cylinder that the gap flow is biased towards has lower amplitude of the oscillatory lift coefficient than the other cylinder. The correlation between the force coefficients and the biased flow direction is consistent with that observed in previous study as in Alam *et al*. 2003.

In order to check if the gap flow may bias towards one cylinder in some parts of the cylinder span and towards another cylinder in other parts, the contours of the lift coefficient on the *t-z* plane are shown in Fig. 5.10. It is observed that the lift coefficient along the whole span of the cylinder reduces and increases almost at the same time, indicating weak variation of the flow in the spanwise direction. For instance, the lift coefficient along the whole span of cylinder 1 reduces during 270<$U_N\ t/D$<300 and increases during 410<$U_N\ t/D$<450. No significant variation of the lift coefficient in the spanwise direction of the cylinder is observed for either α=0° or 45°, except during the very short period when the gap flow changes its biased direction.

The vortex shedding flows behind the two cylinders were found to be predominantly in an anti-phase pattern for large gap ratios (G/D = 3 and 5). Chen *et al*. (2003) reported the similar predominance of anti-phase vortex shedding pattern at G/D = 2 in their simulations for Re = 750. When the gap ratio G/D is further increased to 3 and 5, the vortex shedding flow behind each of the two side-by-side circular cylinders is very similar to that in the wake of a single cylinder and biasness of the flow disappears for both flow approaching angles of α=0° and 45°. For the gap ratio G/D=3 and 5, the interference between the wake flow from

the two cylinders becomes weak. The two wakes of the cylinders in large gap ratios (G/D = 3 and 5) are found either out of phase or in-phase (Sumner, 2010) with each other and the wakes from both cylinders are found to be very similar. Fig. 5.11 shows the time histories of the lift coefficient for large gap ratios of G/D = 3 and 5 at α = 0° and 45°. Because no biased flow is observed as shown in Fig. 5.7 (e - h), the lift coefficients of both cylinders are very similar to each other, and hence the lift coefficient of each cylinder is close to that of a single cylinder. It can be seen in Fig. 5.11 that the lift coefficients of the two cylinders are out of phase with each other most of the time, indicating that the vortex shedding flow from the two cylinders are in antiphase. The lift coefficient from one of the cylinders is neither in-phase nor out of phase with that from another cylinder occasionally. For instance, during 340<U_N t/D<480, the phase between the lift coefficients of the two cylinders change. In this study, the perfect in-phase between the vortex shedding flows from the two cylinders is not observed for G/D=3 and 5.

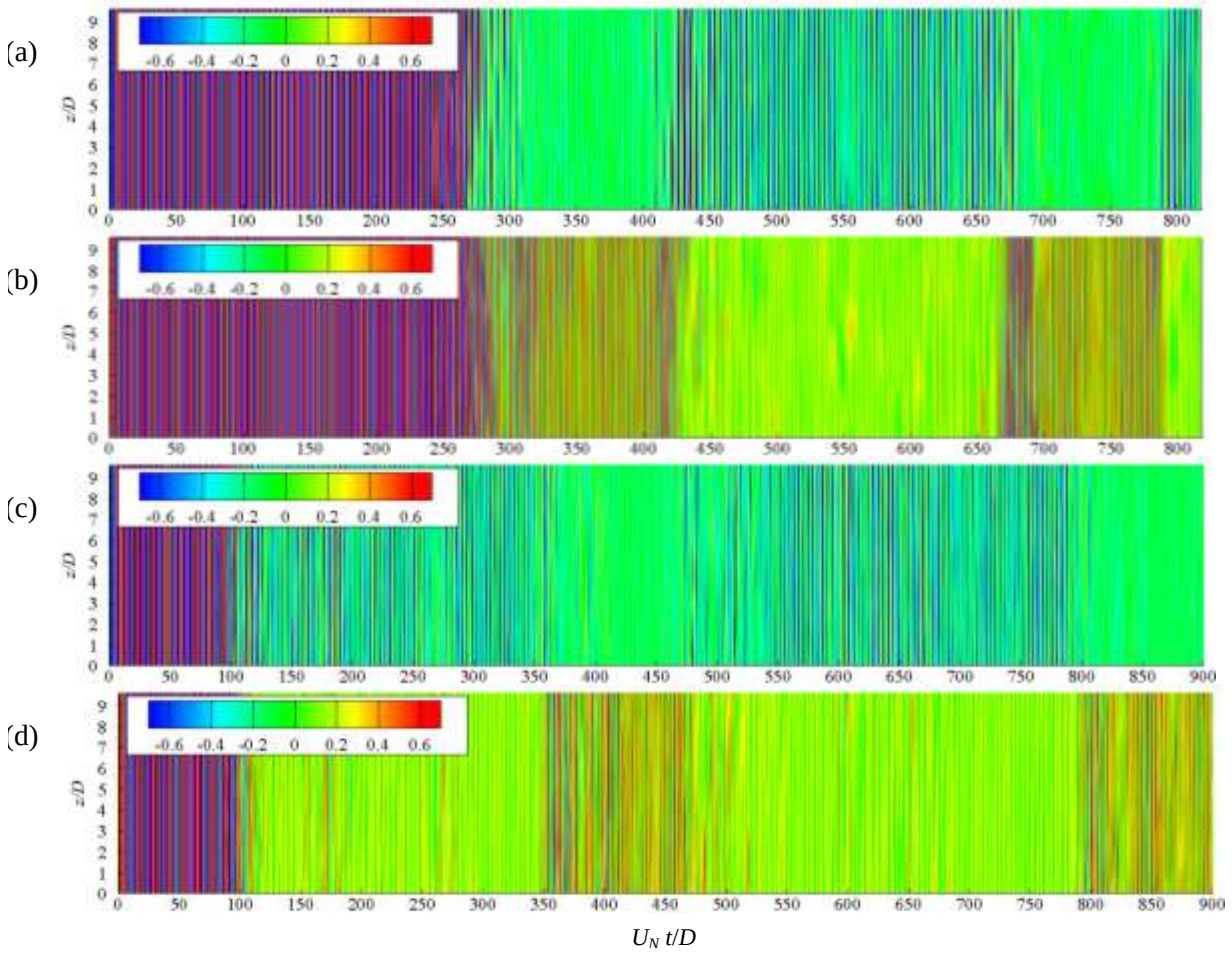

Fig. 5.10 Contours of the sectional lift coefficient on the z-t plane for G/D=1 and Re_N=500. (a) α=0°, Cylinder 1; (b) α=0°, Cylinder 2; (c) α=45°, Cylinder 1; (d) α=45°, Cylinder 2.

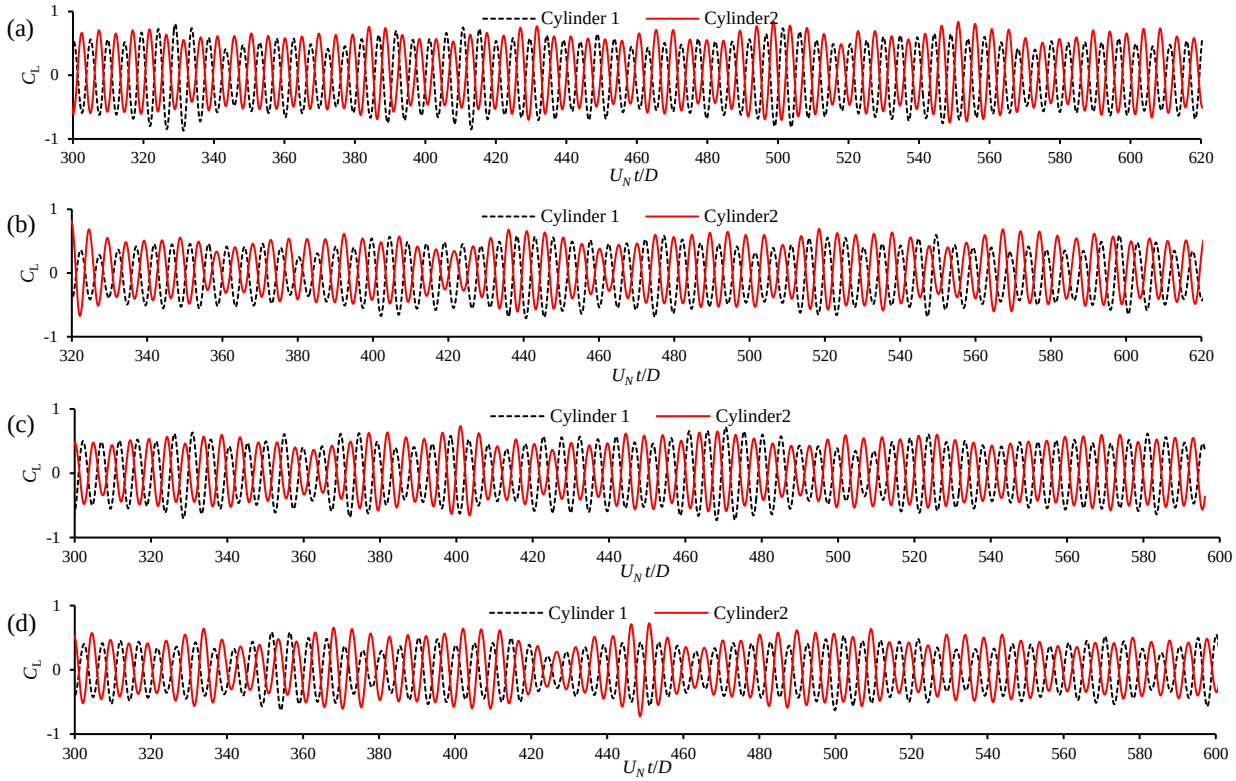

Fig. 5.11 Time histories of the lift coefficient for Re_N=500 and G/D=3 and 5. (a) G/D=3, α=0°; (b) G/D=3, α=45°; (c) G/D=5, α=0°; (d) G/D=5, α=45°

5.3.3 EFFECTS OF THE GAP RATIOS ON FORCE COEFFICIENTS

The above discussion demonstrates that the predicted flow patterns agree with the flow visualization in previous studies (Alam *et al.*, 2003; Chen *et al.*, 2003; Kondo and Matsukuma, 2005; Sumner, 2010; Afgan *et al.*, 2011) and the vortex shedding flow for α=45° does not have obvious difference from that for α=0°. The calculated mean force coefficients for α=0° are quantitatively compared with the experimental data in Fig. 5.12. For G/D=0.5 and 1, because the forces on the two cylinders are different from each other due to biased vortex shedding, the recorded force coefficients for the WW and that for the NW are separated from each other before they are averaged over time to get the mean force coefficients. A repulsive (downwards for the bottom cylinder and upwards for the top cylinder) mean lift coefficient is defined as positive and an attractive mean lift coefficient is defined as negative. For G/D=0.5 and 1, two force coefficients are presented in Fig. 5.12, the higher one is for NW and the lower one is for WW. For G/D=3 and 5, the force coefficients on the two cylinders are almost the same (less than 3% difference from each other) and the averaged value of the mean force coefficients between cylinders 1 and 2 are shown in Fig. 5.12. The variations of the mean drag and lift coefficients in this study are very close to the experimental and numerical results in Fig. 5.12. The mean drag and lift coefficients of a

single cylinder are 1.2 and 0, respectively. It can be seen in Fig. 5.12 that the mean lift coefficients for both cylinders show an asymptotic behaviour towards zero with increasing gap ratio and eventually become close to zero at $G/D>3$. The mean drag coefficients for G/D = 0.5 and 1 show a considerable difference in magnitude between NW and WW, which is also reported by Afgan *et al*. (2011). When the gap ratio exceeds 3, two mean drag coefficients for NW and WW approach the value of a single cylinder. The mean drag coefficient for $G/D=5$ is greater than the experimental data but in similar trend with Kondo and Matsukuma (2005). The slightly higher (by 6%) drag coefficient at $G/D=5$ than that of a single cylinder indicates that there is still slight influence from the gap to the flow. For small gap ratios (G/D = 0.5 and 1), the higher drag coefficient for the NW is associated with the flow deflection separating the shear layer from upper and lower cylinders are directed towards the narrow wake. This causes the increase of drag force by decreasing the wake width (Roshko, 1954). The mean lift coefficient decreases with increasing gap ratio because of the weakening repulsive force between the two cylinders (Sumner *et al*., 2005).

The calculated root mean square (RMS) values of the force coefficients at $\alpha = 0°$ are compared with experimental data by Alam *et al*. (2003) and numerical results by Kondo & Matsukuma (2005) and Afgan *et al*. (2011) in Fig. 5.13. The agreement in the RMS force coefficients with the experimental data is not as good as that in the mean force coefficients, especially for C_D'. Both the numerical results of C_D' in this study and those in Afgan *et al*. (2011) are much smaller than the experimental data by Alam *et al*. (2003) but follow a similar trend with the numerical results by Kondo and Matsukuma (2005). It appears that the RMS lift coefficients obtained in this study are closer to the experimental data than those by Kondo and Matsukuma (2005) and Afgan *et al*. (2011). The RMS drag coefficient for $G/D=5$ is close to the value for a single cylinder at $Re_N=500$ and $\alpha=0°$ predicted in this study (about 0.032). The RMS lift coefficient at $G/D=5$ predicted in this study is also very close to that of a single isolated cylinder predicted in this study (about 0.35). Similar to that in Afgan *et al*. (2011), the root mean square lift coefficients are very small at small gap ratio of $G/D=0.5$.

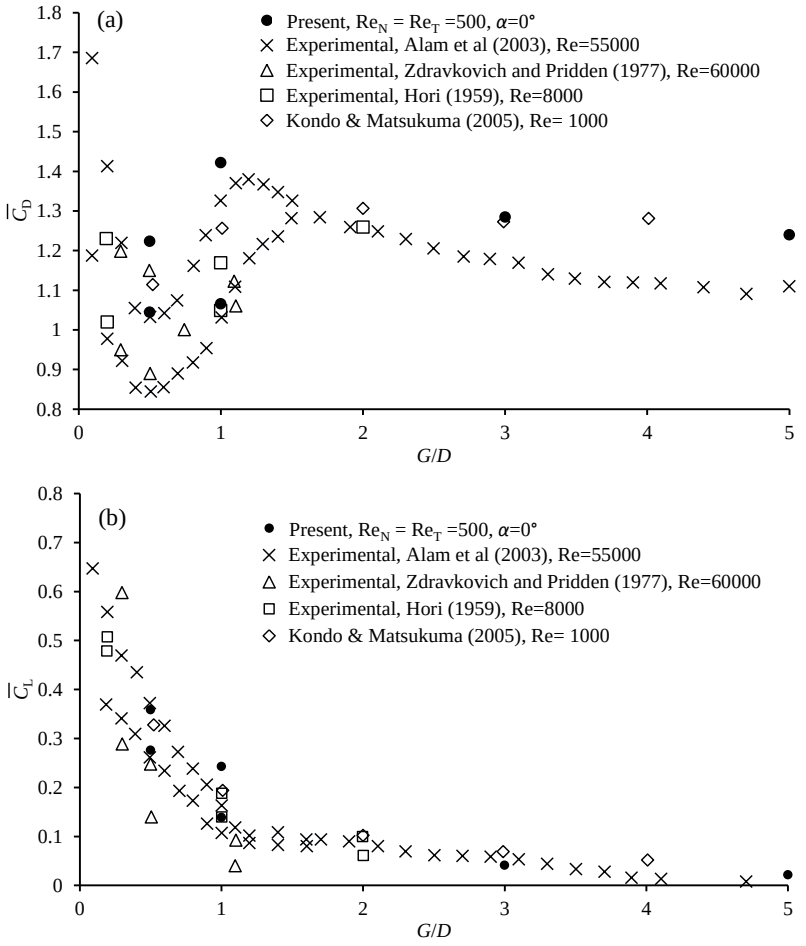

Fig. 5.12 Comparison between the calculated mean force coefficients with the experimental data for Re_N=500 and α=0°. (a) Mean drag coefficient; (b) Mean lift coefficient.

The variations of the mean and RMS force coefficient with the gap ratio for α=0° and 45° are shown in Figs.5.14 and 5.15, respectively. The Reynolds number of Re_T=500 at α = 45° is equivalent to the normal Reynolds number of Re_N=354. The results for Re_T=500 are presented in order to demonstrate which Reynolds number should be used in evaluating the independence principle. We did not present vortex shedding flow patterns for Re_T=500 because they exhibit almost similar patterns to that at Re_N=500. It can be seen in Fig. 5.14 that the mean drag and lift coefficients for (Re_N, α) = (500, 45°) are very close to their counterparts at (Re_N, α) = (500, 0°). However, the difference in the mean force coefficients between (Re_T, α) = (500, 45°) and (Re_N, α) = (500, 0°) is obvious. For instance, when G/D=1, the difference between the mean drag coefficients of NW and WW is for (Re_T, α) = (500, 45°) much smaller than that for (Re_N, α) = (500, 0°). The effect of Reynolds number on the RMS force coefficients in Fig. 5.15 is stronger than that on the mean force coefficient. For G/D=0.5 and 1, the RMS lift coefficient at (Re_N, α) = (500, 45°) is close to those at (Re_N, α) = (500, 0°). However, for G/D=3 and 5, the RMS lifts at (Re_N, α) = (500, 45°) are about 20%

greater than that for (Re_N, α) = (500, 0°). The difference between the RMS lift coefficients at (Re_T, α) = (500, 45°) and those when (Re_N, α) = (500, 0°) is bigger. These results demonstrate that the Reynolds number based on the velocity component perpendicular to the cylinder should be used instead the one based on the total velocity when the independence principle is employed.

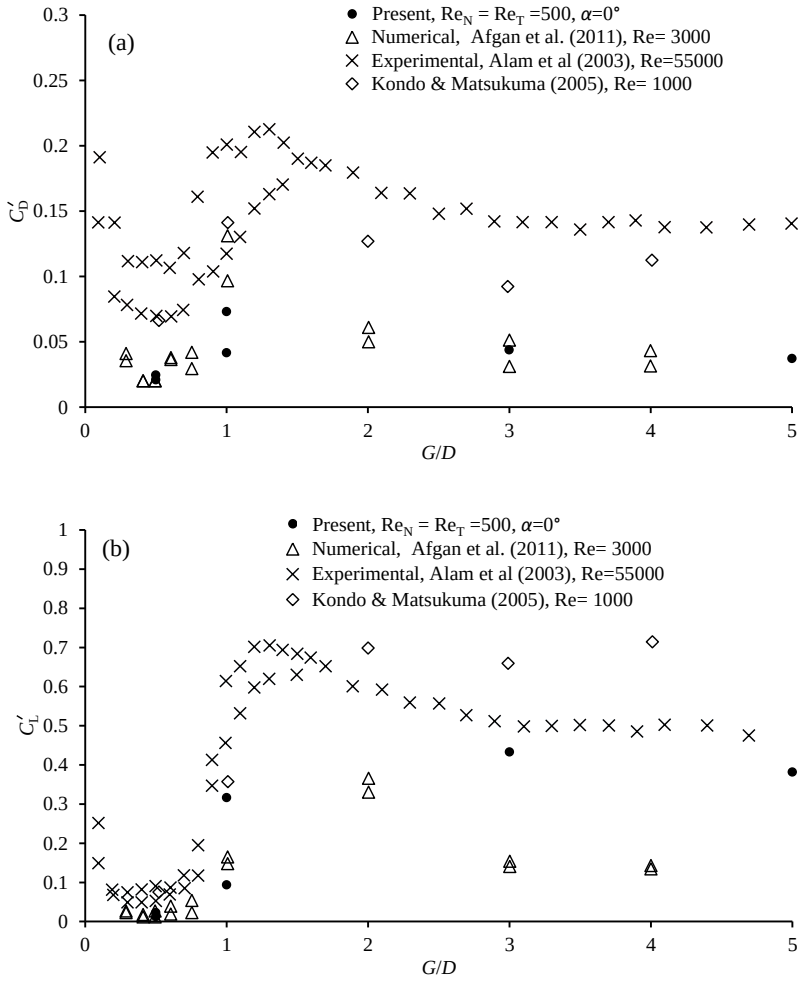

Fig. 5.13 Comparison between the calculated and measured RMS force coefficients for Re_N=500 and α=0°: (a) RMS drag coefficient; (b) RMS lift coefficient.

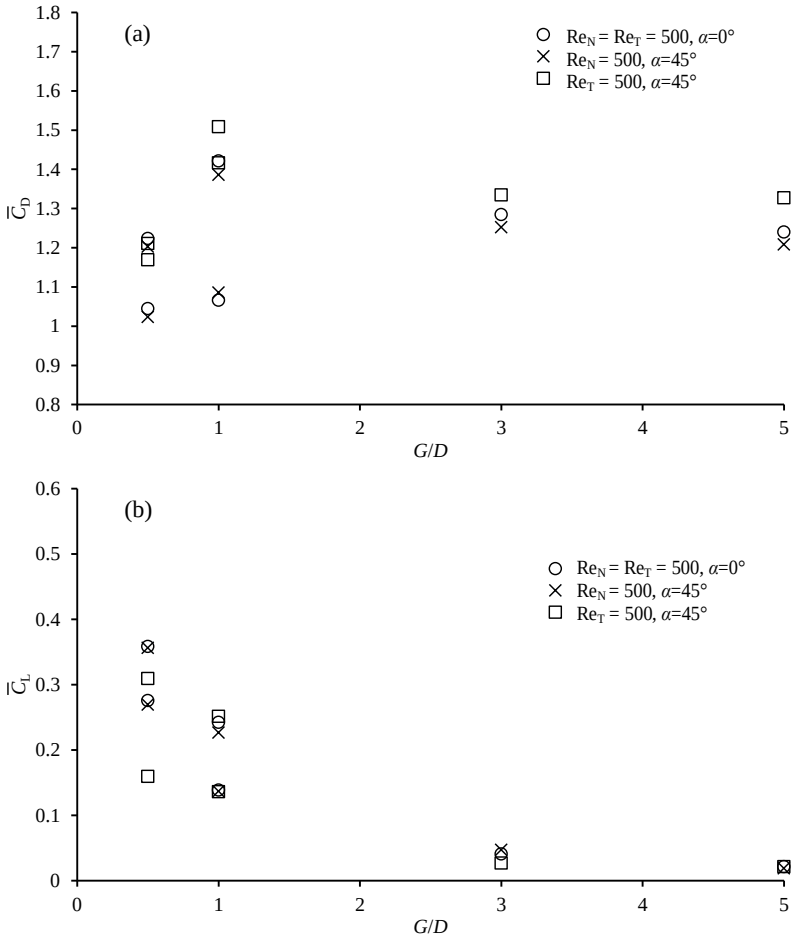

Fig. 5.14 Comparison among the results of the force coefficient: (a) Mean drag coefficient; (b) Mean lift coefficient

Fast Fourier Transform (FFT) is used to analyse the lift coefficient and the non-dimensional peak frequency of a FFT spectrum of the lift coefficient is defined as the Strouhal number (S_t), i.e. $S_t = fD/U_N$, where f is the frequency of the oscillatory lift force. The variations of the Strouhal number with the gap ratio for three Reynolds numbers are shown in Fig. 5.16. The agreement between the Strouhal number at (Re_N, α) = (500, 45°) and that at (Re_N, α) = (500, 0°) is very good, indicating the validity of IP on the Strouhal number. In the comparison, the Strouhal numbers at (Re_T, α) = (500, 45°) are different from that at (Re_N, α) = (500, 0°) for gap ratio G/D = 0.5.

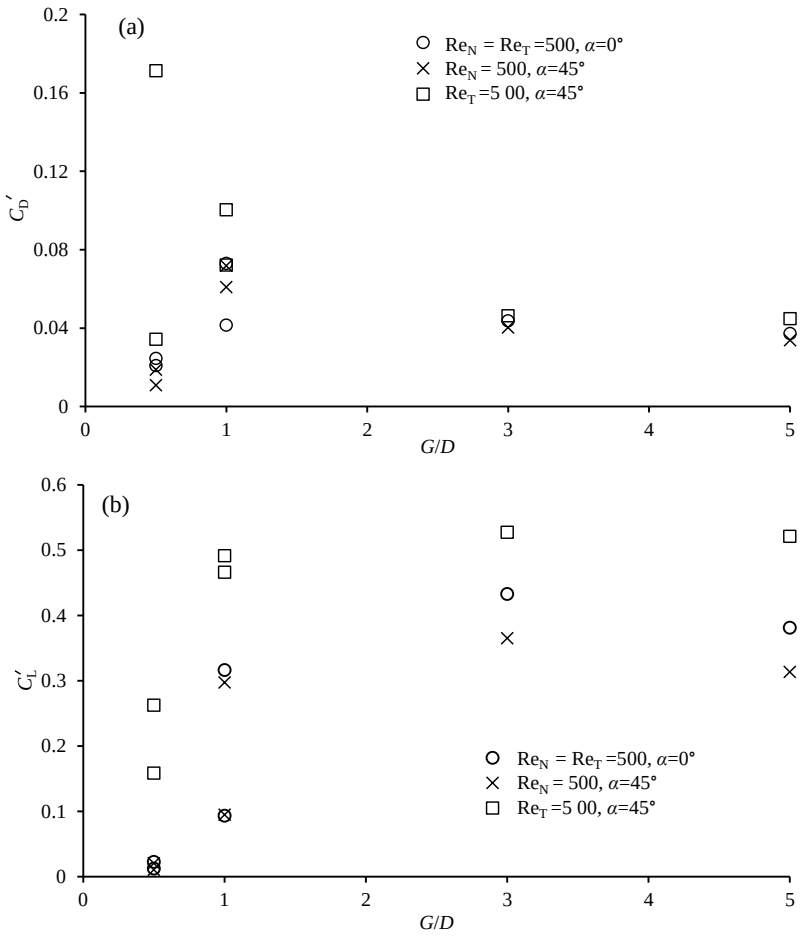

Fig. 5.15 Comparison among the results of the force coefficient: (a) RMS drag coefficient; (b) RMS lift coefficient

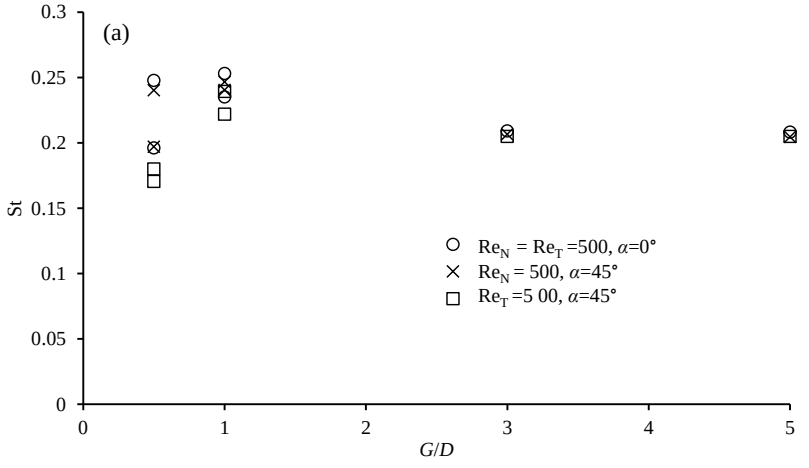

Fig. 5.16 Comparison of Strouhal number for the different flow approaching angles

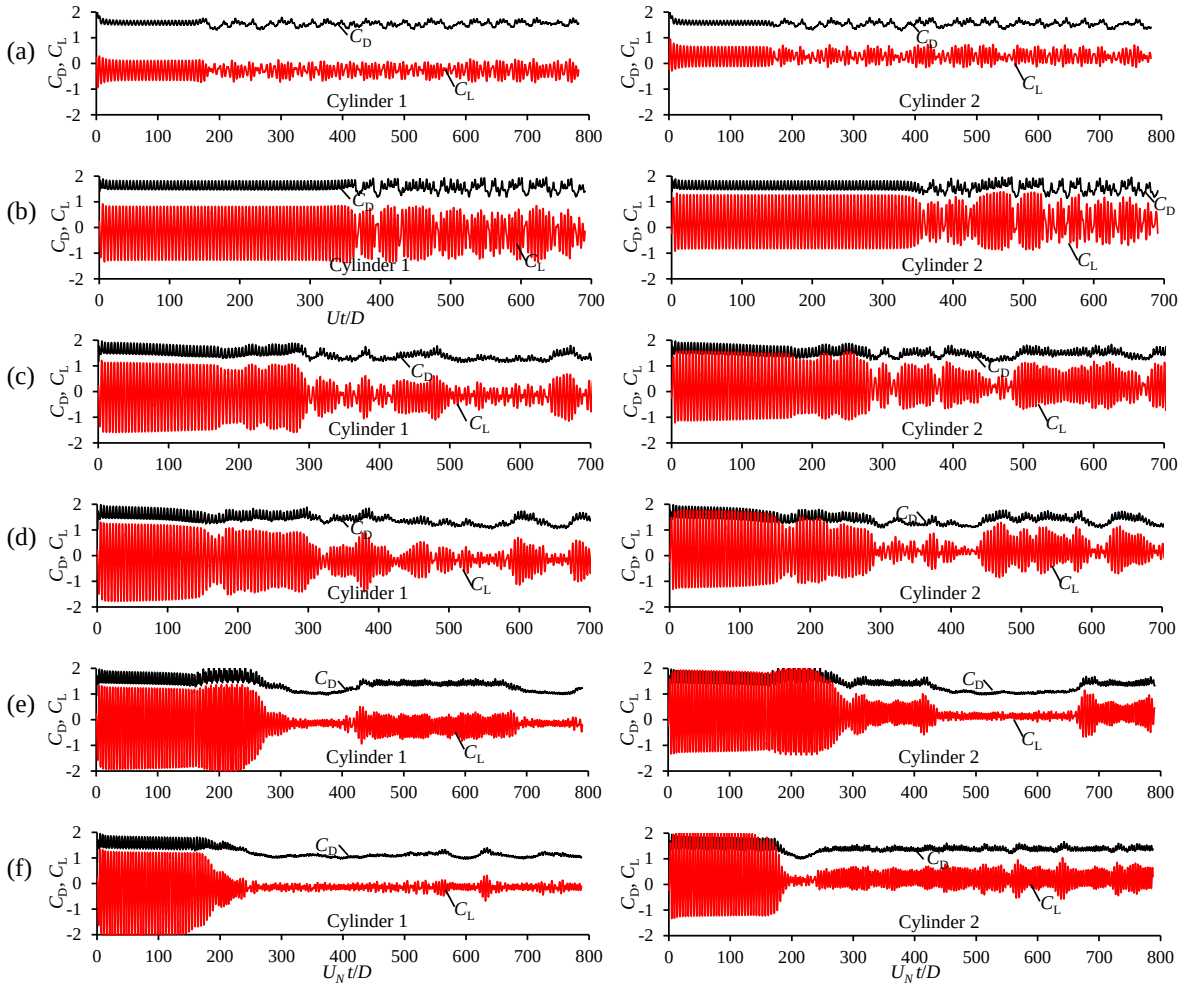

Fig. 5.17 Time histories of the force coefficients for G/D=1 and α=0°: (a) Re=100 (b) Re=200; (c) Re=300; (d) Re=400; (e) Re=500; (f) Re=600

5.3.4 EFFECTS OF REYNOLDS NUMBER AND FLOW APPROACHING ANGLES

In order to examine the effects of Reynolds number on the flow, simulations are carried out for various Reynolds numbers (Re_N=100 to 600 with an interval of 100) at G/D =1 and two flow approaching angles of α=0° and 45°. The time histories of the force coefficients for α=0° and α=45° are shown in Fig. 5.17 and 5.18, respectively. The flow is found to be bistable for all the simulated Reynolds numbers, reflected by the time histories of the force coefficients. However, for Re_N = 100 and 200, the biased flow switches its direction so frequently that stable biased flow cannot be identified. Stable long-duration biased flow can be identified as the normal Reynolds number exceeds 300. The flow is found to be totally two-dimensional at Re_N = 100 for α=0°, which is evidenced by the iso-surface of the axial vortices shown in Fig. 5.19 (a). For Re_N = 200, three-dimensionality of the flow appears but is very weak as shown in Fig. 5.19 (b). There are three waves along the axial direction of the cylinders in the flow feature, resulting a non-dimensional axial wavelength of the 3D feature

of 5.3.2. The wavelength in Fig. 5.19 (b) agrees well with the wavelength in transition mode A for a single cylinder (Zhang *et al.*, 1995). It is difficult to identify the biased flow in Fig. 5.19 (c) and (d). The wake in Fig. 5.19 (c) of the top cylinder is slightly wider than that of the bottom one and the gap flow biases slightly towards downwards. Because the degree of the biased direction of the flow is very small, the biased direction changes to upwards very quickly. The frequent change of the biased flow direction makes it difficult to separate the force coefficients for the WW from those for the NW in Fig. 5.17 (a) and (b) and Fig. 5.18 (a) and (b).

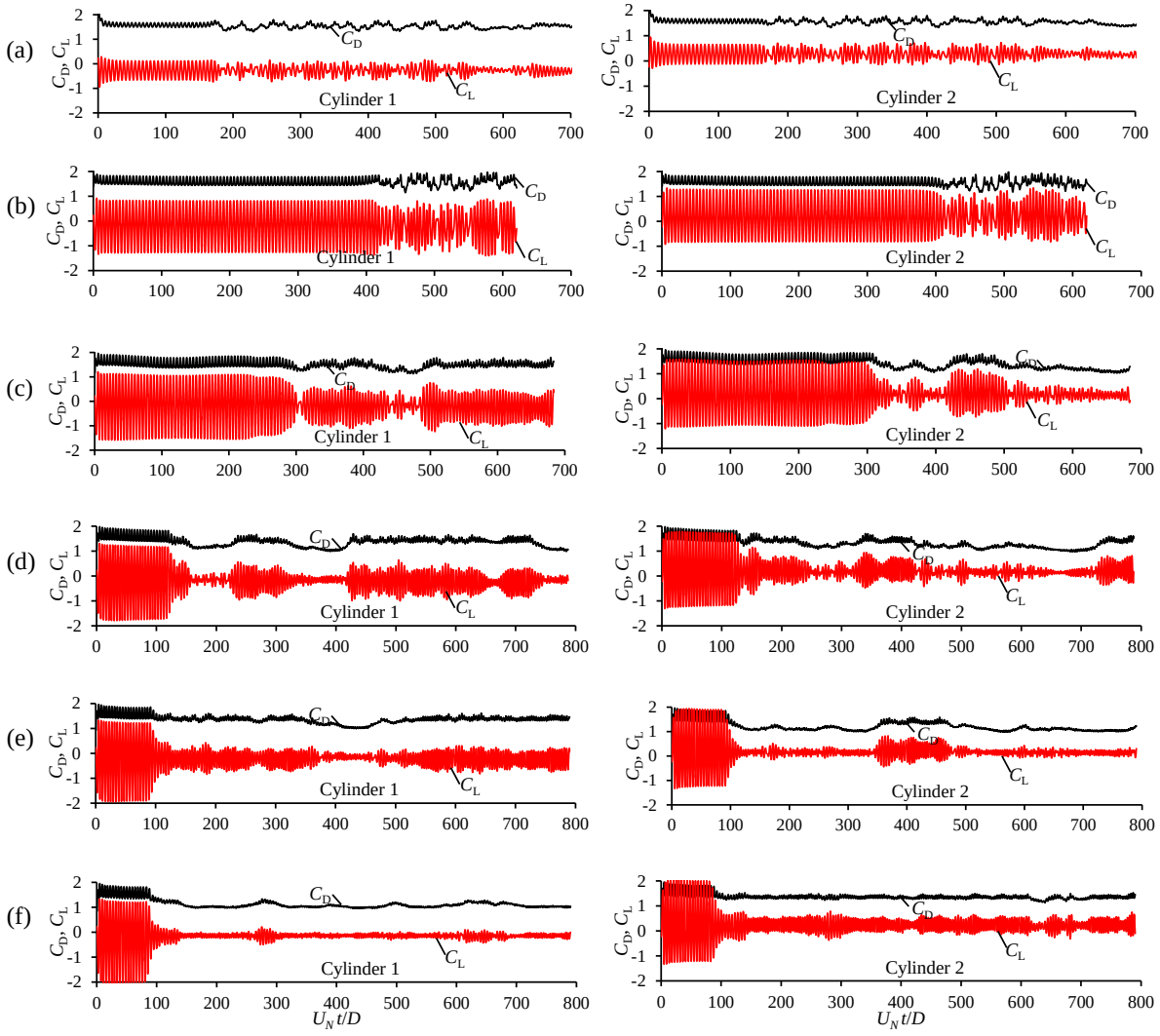

Fig. 5.18 Time histories of the force coefficients for G/D=1 and α=45°: (a) Re=100 (b) Re=200; (c) Re=300; (d) Re=400; (e) Re=500; (f) Re=600.

(a) Iso-surfaces of $|\omega_z|$=1 for Re_N=100, $U_N\,t/D$=600

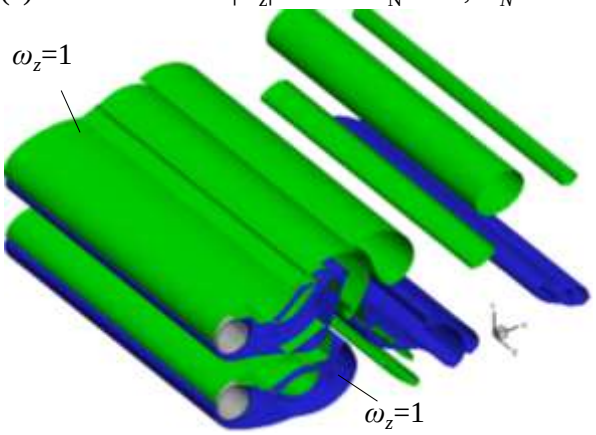

(b) Iso-surfaces of $|\omega_z|$=1 for Re_N=200, $U_N\,t/D$=640

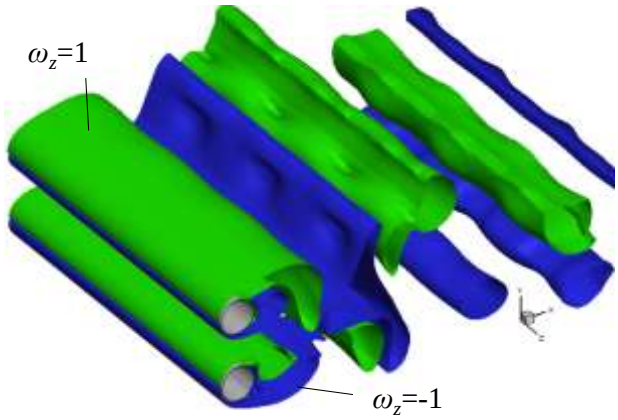

(c) Contours of $|\omega_z|$=1 for z=4.8, Re_N=100, $U_N\,t/D$=600

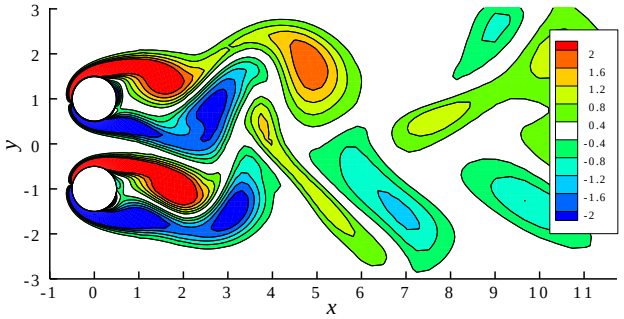

(d) Contours of $|\omega_z|$=1 for z=4.8, Re_N=200, $U_N\,t/D$=640

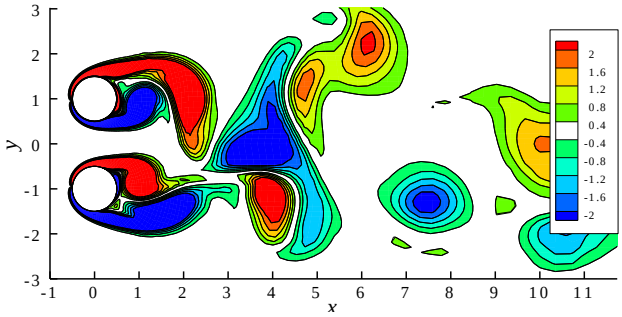

Fig. 5.19 Flow patterns for G/D=1, α=0° and Re_N=100 and 200

Fig. 5.20 shows the variation of the mean drag and RMS lift coefficients with the normal Reynolds number (Re_N) for α=0° and α=45°. The force coefficients for narrow and wide wakes are calculated separately except for Re_N = 100 and 200, where it is difficult to separate WW from NW in the time histories of the force coefficients as shown in Fig. 5.17 and 5.18. The mean drag coefficient decreases with increasing Reynolds number for both attack angles. The variation of the mean drag coefficient with the Reynolds number is similar to that of a single cylinder (Zhao *et al*., 2013). The RMS lift coefficients for both cylinders decreases significantly with increasing Reynolds number for both flow attack angles when the Reynolds number is greater than 200. The maximum RMS lift is found to be at Re_N = 200 in both cases. In the case of flow past a single cylinder, the RMS lift coefficient was also found to be maximum when the Reynolds number is about 200 (Zhao *et al*., 2013; Tong *et al*., 2014).

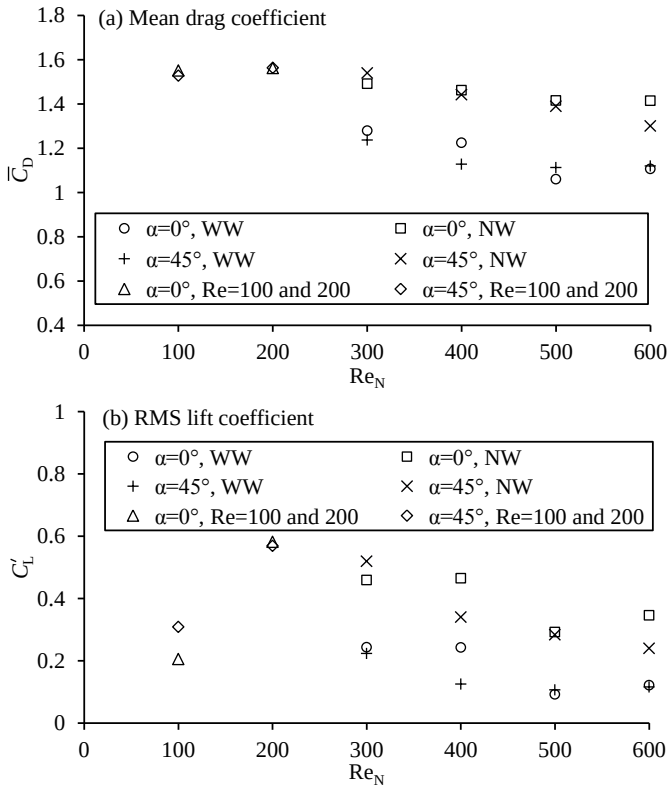

Fig. 5.20 Variation of the mean drag and RMS lift coefficients with the Reynolds number for *G*/*D*=1 (a) Mean drag coefficient; (b) RMS lift coefficient

To examine the effects of flow approaching angles more clearly, simulations for two more flow approaching angles (i.e. α=15° and 30°) are conducted at Re_N=500 and *G*/*D*=1. The time series of the force coefficients, together with those for α=0° and 45°, are shown in Fig. 5.21. It can be seen that there exist apparent differences between the forces of the two cylinders, which indicates the existence of a narrow wake and a wide wake for all the flow

approaching angles. Variations of the mean and RMS force coefficients with the flow approaching angles (α) at Re_N = 500 for both cylinders are shown in Fig. 5.22. Generally, the variations of the force coefficients with the flow approaching angle are weak in Fig. 5.22. The maximum difference between the RMS lift coefficient at the oblique attack case and that at the right attack case occurs at α=15°, which is about 20%. The effect of the flow approaching angle on the mean drag and lift coefficients are weaker than that on the RMS lift coefficient. Although the effect of the flow approaching angle on the RMS drag coefficient seems larger in percentage, it is less significant than that on the RMS lift coefficient because the RMS drag coefficient is much smaller than the RMS lift coefficient.

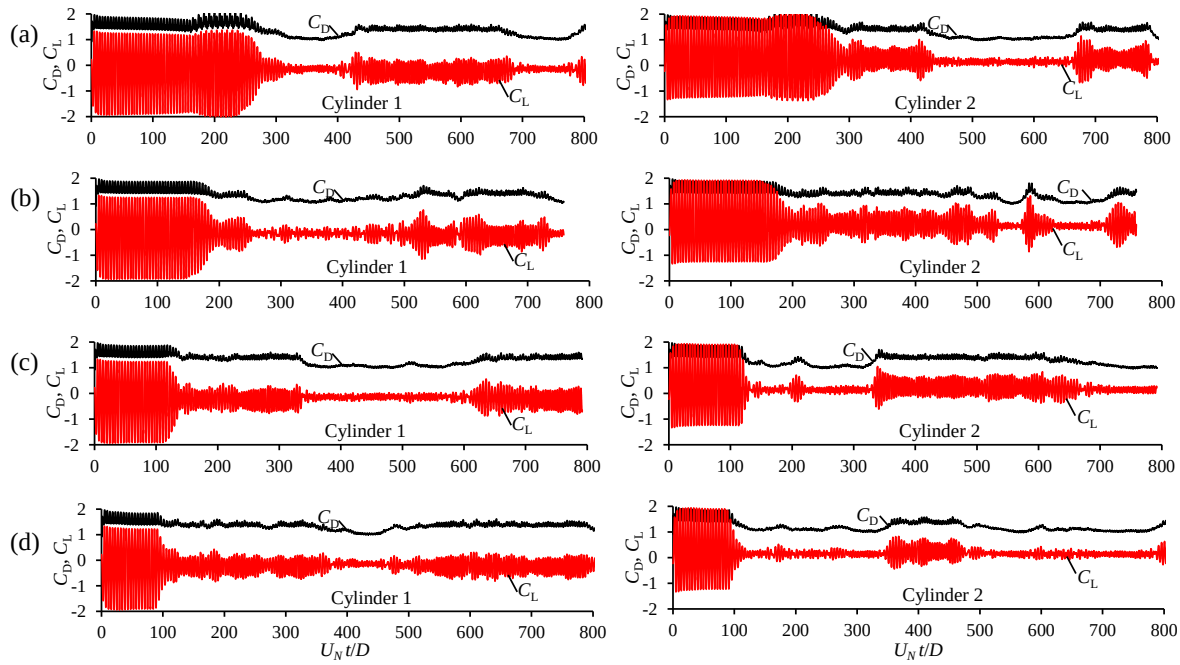

Fig. 5.21 Time histories of the force coefficients for Re_N=500 and gap of G/D=1. (a) α=0°; (b) α=15°; (c) α=30° and (d) α=45°.

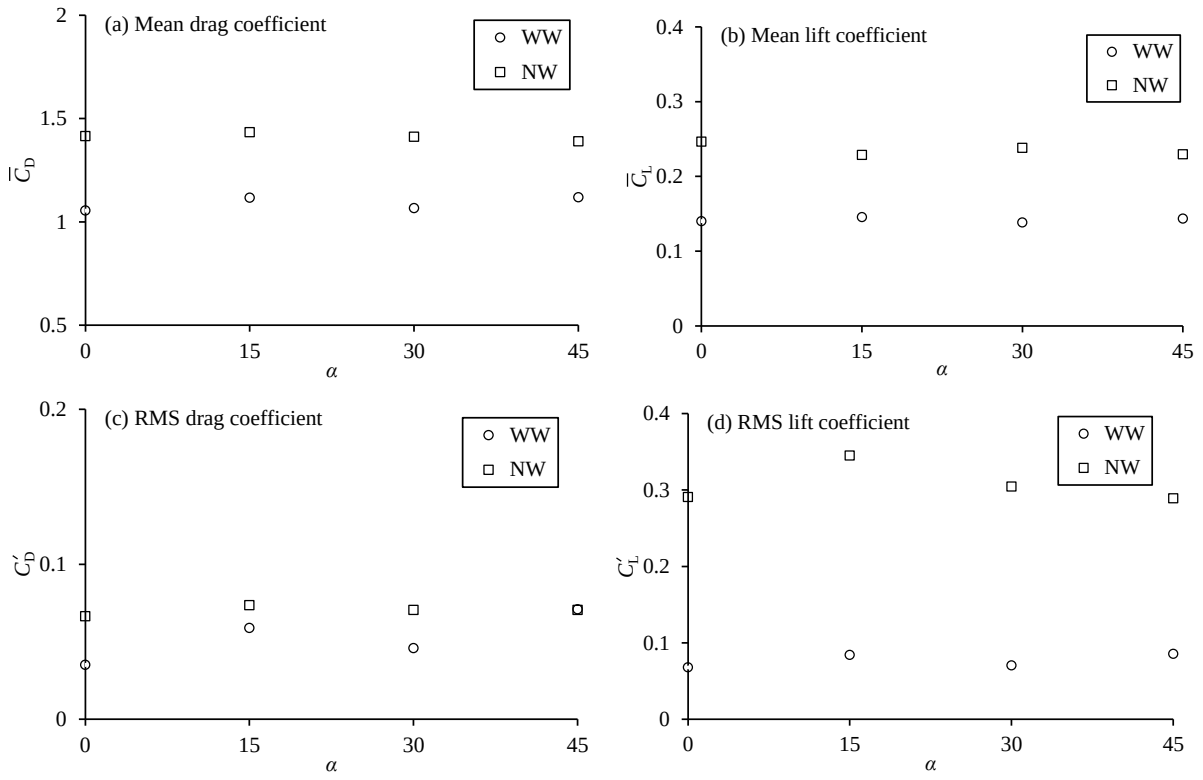

Fig. 5.22 Variation of force coefficients with different flow approaching angles (α) at Re_N = 500. (a) Mean drag coefficient, (b) Mean lift coefficient, (c) RMS drag coefficient and (d) RMS lift coefficient

5.4 CONCLUSIONS

Flow past two side-by-side circular cylinders has been investigated numerically by using the direct numerical simulation method. To identify the effects of the gap ratio on the flow, simulations are firstly conducted at four gap to diameter ratios of G/D= 0.5, 1, 3 and 5 and (Re_T=Re_N=500, α=0°), (Re_N=500, α=45°) and (Re_T=500, α=45°). For small gap ratios of G/D = 0.5 and 1, the biased flow were observed for both α=0° and 45°, leading to a wide and a narrow wake behind the cylinders. As reported in the experimental studies, the cylinder towards which the gap flow biases has a narrow wake and a higher drag coefficient than the other cylinder. For G/D=0.5, the gap flow is found to be biased towards one cylinder only until U_N t/D=800. For G/D=1, the gap flow changes its biased directions intermittently, forming the so-called flip-flopping flow regime. The flip-flopping of the gap flow pattern disappears when G/D = 3 and 5, for which, the vortex shedding from each cylinder is similar to that of a single cylinder, indicating the weakness of the interaction between the two wakes. All the vortex shedding patterns found at α=0° are also observed at α=45° at the same gap ratios.

The force coefficients for α=0° are compared with those for α=45° at the same Reynolds number. For a given normal Reynolds number of Re_N=500, the mean drag and lift coefficients at α=0° and 45° agree well with each other for all the gap ratios studied. The RMS drag and lift coefficients for the two flow attack angles agree well with each other when G/D=0.5 and 1 and differ by about 20% from each other when G/D=3 and 5. Simulations at Re_T=500, which is equivalent to Re_N=354 are also conducted. The results of the mean and RMS force coefficients at (Re_N, α) = (500, 45°) with those at α=0° are better than the results at (Re_T, α) = (354, 45°). This finding demonstrates that the Reynolds number based on the velocity component normal to the cylinder span should be used for the implementation of the independence principle for low Reynolds numbers in the turbulent flow regime.

The effect of the Reynolds number on the flow and force coefficients are studied by simulating the flow for Re_N=100 to 600 with an interval of 100, and G/D=1 and at two flow approaching angles of α = 0° and 45°. The flow is found to be 2D at Re_N=100 and weak three-dimensional at Re_N=200. For Re_N=100 and 200, it is difficult to identify stable biased flow because the biased direction of the gap flow change very frequently. The variations of the mean and RMS force coefficients with Reynolds number are similar to those for flow past a single cylinder. The mean drag coefficients for both WW and NW decrease with increasing Reynolds number and the maximum RMS lift coefficients occurs at Re_N=200. The numerical results of flow past two cylinders with a gap ratio of G/D=1 and flow approaching angles of 0°, 15°, 30° and 45° shows that the effects of the flow approaching angle on the mean drag and mean lift coefficients are much weaker than those on the RMS drat and lift coefficients.

CHAPTER 6

TREE-DIMENSIONAL FLOW PAST TWO CIRCULAR CYLINDERS IN TANDEM ARRANGEMENTS AT TWO DIFFERENT INCLINATION ANGLES

6.1 INTRODUCTION

Flow around two cylindrical structures has attracted attention from many researchers due to its importance in engineering applications either use on land or in the ocean. Two circular cylinders in tandem arrangements are commonly used to evaluate the interaction of multiple structures in a fluid flow where one cylinder is located upstream the other as shown in Fig. 6.1. They also lead to a remarkable complex flow pattern in a simple geometric configuration. The characteristics of the flow around the circular cylinders are dependent upon the gap ratio (G/D), the inclination angle of flow (α) and the Reynolds number (Re) which is defined as $Re = UD/v$, where U is the free-stream velocity and v is the kinematic viscosity of the fluid.

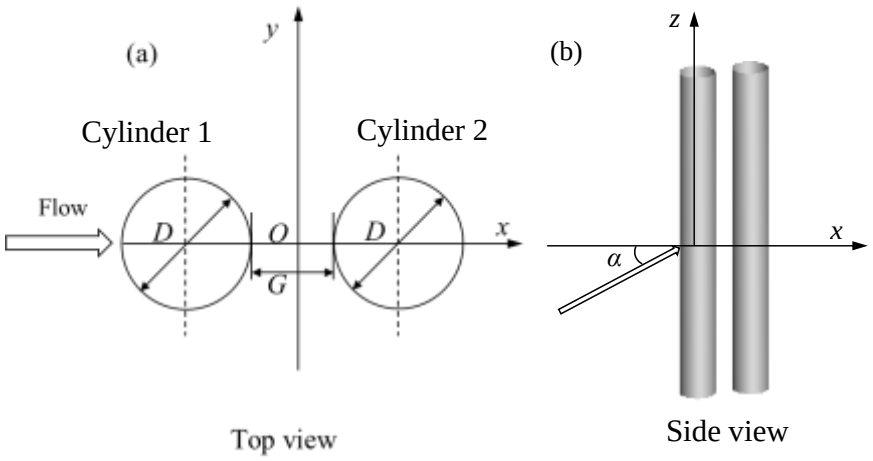

Fig. 6.1 Schematic diagram of flow past two tandem circular cylinders where cylinder 1 and 2 represent upstream and downstream cylinders respectively

The previous studies on flow past two cylinders in tandem configurations have found that the fluid flow can be classified into different flow regimes depending on the spacings between the cylinders (Zdravkovich, 1987; Ljungkrona and Sunden, 1993; Mittal *et al*., 1997; Meneghini *et al*., 2001; Lin *et al*. 2002; Alam *et al*. 2003). Extensive studies on flow over two tandem circular cylinders at different flow regimes have been carried out experimentally. Zdravkovich and Pridden (1977) reported the discontinuous jump of the base pressure of the

downstream cylinder at the critical spacing (L/D>3.5) between the two cylinders. The flow around two circular cylinders in a tandem arrangement in subcritical Reynolds numbers 3.3×10^3 <Re<12×10^3 at various spacing has been studied in the past by using smoke-wire technique (Ljungkrona and Sunden, 1993). It was reported that the change in the flow mode due to the change in the spacing between the cylinders has significant effect on the Strouhal number. Alam *et al*. (2003) carried out an experimental study on aerodynamics characteristics of two circular cylinders in a tandem arrangement at Re = 6.5×10^4 and reported the bistable flow at G/D=3.0 (critical spacing), the reattachment of shear layer occurred intermittently at G/D< 2.0. Xu and Zhou (2004) conducted experimental research of flow in the wake of two tandem cylinders based on hot-wire measurement and LIF flow visualization for Reynolds numbers between 800 and 4.2×10^4 and various spacing ratios (L/D = 1 – 15, L being the distance between the centre of two cylinders) and reported that the critical spacing ratio (L_{cr}/D) decreases with increasing Reynolds numbers (L_{cr}/D = 4.5 for Re = 1400, L_{cr}/D = 4 for Re = 8500 and L_{cr}/D = 3 for Re = 42000).

Numerical studies on flow past two circular cylinders in tandem arrangements have also been reported in literature. Meneghini *et al*. (2001) studied the shedding of vortices and flow interference between two circular cylinders in tandem and side-by-side arrangements for Reynolds numbers from 100 to 200 by using the two-dimensional fractional step finite element method and reported that their numerical results of the interference regimes agreed with the experimental results. Liu *et al*. (2014) simulated 2D flow past two circular cylinders in tandem arrangements at various spacing ratios ($0.1 \leq G/D \leq 6.0$) at a Reynolds number of 200 by solving the Navier-Stokes equations using the upwind finite element method and reported the hydrodynamic jump at G/D = 0.9 and 2.6 and agreed that more effort is needed to understand the 3D turbulent flow past the multiple bodies. Carmo and Meneghini (2006) employed the spectral finite element method to simulate 2D and 3D flow for various centre-to-centre spacing ratios from 1.5 to 8 at Reynolds numbers 160 – 320. It was found that the 3D vortical structures have significant effects on the fluid loads and 2D simulations are not able to accurately determine the interference regime in the vicinity of critical spacing. Papaioannou *et al.* (2006) studied flow around two tandem cylinders at centre-to-centre spacing ratios ranging from 1.1 to 5.0 and Reynolds numbers from 100 to 1000 based on the spectral/hp method and revealed the 3D effects on critical spacing at various Reynolds numbers. Carmo *et al*. (2010) studied flow past two circular cylinders in tandem arrangements by linear stability analysis and 3D direct numerical simulations at various

centre-to-centre spacing ratios from 1.2 to 10 and identified three different vortex shedding regimes (SG: symmetric in the gap, AG: alternating in the gap and WG: wake in the gap). Tong *et al*. (2015) performed 3D simulations on two identical circular cylinders at tandem, side-by-side and staggered arrangements at Reynolds number of 1000 and the spacing ratios (*L*/*D*) from 1.5 to 4.0. For a tandem arrangement, the small drag coefficients is reported due to complete or partial immerse of downstream cylinder in between the two shear layer from upstream cylinder.

Most of previous studies of flow past two tandem cylinders focused on the cases where the flow direction is perpendicular to the cylinders. In many engineering applications, the flow may approach the cylinder at an oblique attack angle. It is expected that the inclination angle of the flow has effects on the vortex shedding flow patterns (Gregory *et al*., 2009; Thapa *et al*., 2015). The focus of this study is to investigate the effect of the flow attack angle on the formation vortex shedding and the force coefficients for flow past two tandem cylinders by means of 3D direct numerical simulations at low subcritical Reynolds number (*Re* = 500) and spacing ratios ranges from 0.5 to 5.0.

6.2 NUMERICAL METHOD

The three-dimensional incompressible Navier-Stokes (NS) equations are solved for simulating the flow past two identical circular cylinders in a tandem arrangement as shown in Fig. 6.1. The length, the velocity and the pressure are non-dimensionalised by $x_i = x_i'/D$, $u_i = u_i'/U$ and $p = p'/\rho U^2$, respectively, where the primes stands for the dimensional values, x_1, x_2 and x_3 represent the coordinates *x*, *y* and *z*, respectively, u_i is the velocity component in the x_i-direction and ρ is the density of the fluid. The non-dimensional NS equations are written as

$$\frac{\partial u_i}{\partial t} + u_j \frac{\partial u_i}{\partial x_j} + \frac{\partial p}{\partial x_i} - \frac{1}{\mathrm{Re}} \frac{\partial^2 u_i}{\partial x_j^2} = 0, \tag{6.1}$$

$$\frac{\partial u_i}{\partial x_i} = 0 \tag{6.2}$$

The NS equations are solved by the Petrov-Galerkin finite element model (PG-FEM) developed by Zhao *et al*. (2009). The PG-FEM was successfully used to simulate flow past a

single cylinder at oblique attacks for Reynolds numbers in a wide range between 100 and 1000 (Zhao *et al*., 2013). A rectangular computational domain with the non-dimensional length of 50 in the flow direction, 9.6 in the spanwise direction of the cylinder and 40 in the cross-flow direction is used. The non-dimensional distance between the centre of two cylinders and the inlet boundary is 20. The initial values of the velocity and the pressure in the whole domain are set as zero. The non-dimensional velocity at the inlet boundary is given by

$$(u_1,\ u_2,\ u_3) = (1,\ 0,\ \tan\alpha) \tag{6.3}$$

A free-slip boundary condition is employed at the two side boundaries that are parallel to the *x*-*z* plane, namely, the velocity component and the pressure gradient perpendicular to the boundary are zero. When the flow approaches the cylinder at an inclined angle, fluid mass needs to be allowed to pass through the two end boundaries (the boundaries perpendicular to the cylinder axis). To allow the flow to pass the end boundaries, the periodic boundary condition is imposed by setting velocity and pressure gradients (in all three directions) on one of end boundary to be equal to their counterparts on another end boundary (Zhao *et al*., 2013). The periodic boundary condition at the two end boundaries allow the fluid flowing through the boundary. On the cylinder surface, no-slip condition is applied.

An example of the computational mesh for this study is shown in Fig. 6.2 which is for spacing ratio (*G*/*D*) of 0.5, where 96 elements are distributed along the circumference of each cylinder and 192 layers of hexahedral 8-node linear finite elements in the axial direction are distributed along the cylinder length (9.6). 64 CPUs are used to simulate for each case. The non-dimensional computational time step Δt is set to 0.004. All the simulations for this study were performed on the computers of the iVEC supercomputing facility in Western Australia.

The mesh density used in this study is the same as that used in Thapa *et al*. (2015), where flow past two side-by-side cylinders are studied. The detailed mesh dependency study has been performed by Thapa *et al*. (2015) in the case of single cylinder and two identical circular cylinders in side-by-side arrangement at *Re* = 500 and α=0º and will not be repeated here. The drag and lift coefficients on both cylinders are calculated as $C_D = \frac{F_x}{\rho DLU^2/2}$ and $C_L = \frac{F_y}{\rho DLU^2/2}$, where F_x and F_y are the drag and the lift forces in flow approaching direction and the cross-flow direction, respectively, which are calculated by the integration of the

pressure and shear stress along the whole surface of the cylinder, and L is the cylinder length. In the following discussion, the upstream and downstream cylinders are numbered as cylinders 1 and 2, respectively. The Strouhal number is defined as $St = \frac{fD}{U}$, where f is the frequency of oscillatory lift, which is obtained by performing the Fast Fourier Transform (FFT) analysis of the lift coefficient.

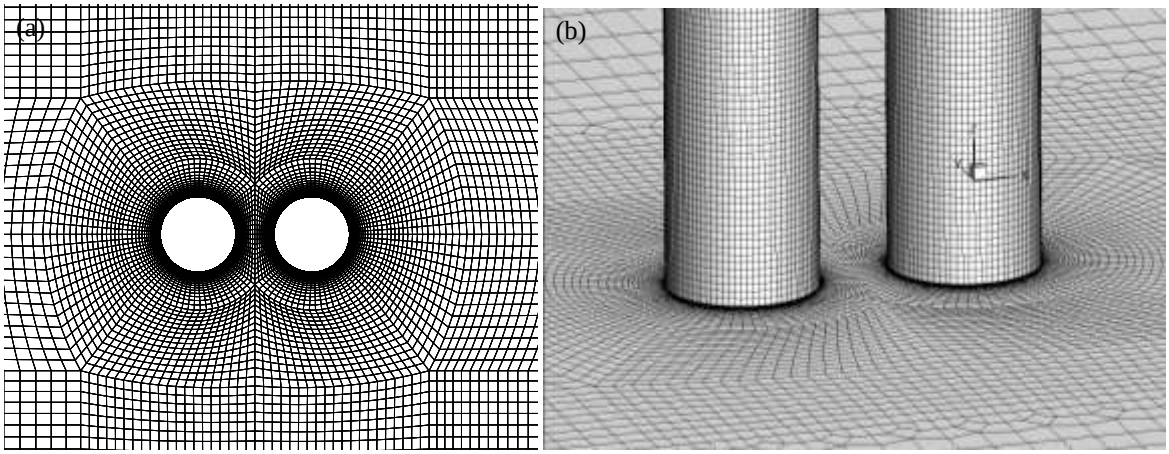

Fig. 6.2 Computational mesh near the cylinders; (a) 2D view and (b) 3D view

6.3 RESULTS AND DISCUSSIONS

The study is focused on the influence of the flow attacking angle at various spacing ratios at a low Reynolds number in the subcritical flow regime. The numerical simulation for this study is carried out for at least non-dimensional time (Ut/D) of 550 for all the cases to ensure the fully developed wake flow has been obtained. The flow attacking angles in this study are taken to be 0º and 45º for gap ratios 0.5, 1, 3 and 5. Also the gap ratios of 1.5, 2, 2.5 and 3.5 are simulated for right attack case only in order to compare the results with the data in previous studies (both experimental and numerical).

6.3.1 FORCE COEFFICIENTS

The time series of the force coefficients of two identical circular cylinders are shown in Fig. 6.3 and 6.4 for the spacing ratios G/D=0.5, 1, 3 and 5 and two different inclination angles in order to examine the effects of the inclination angle on the force coefficients. For the small spacing ratios (G/D = 0.5 and 1.0) which is classified as single bluff body region in the literature (Zdrakovich, 1987; Zhou and Yiu, 2006). The isolated circular cylinder at the same Reynolds number is also presented in Fig. 6.4 (e) for comparison purpose. The lift coefficient of each cylinder is smaller than the isolated single cylinder for the small gap ratio

(G/D = 0.5 and 1) at right and oblique attacks. The reduction of the lift coefficient was also reported by Liu *et al*. (2014). While the influence of the spacing ratio is significant, it appears the flow attack angle has little effects on the force coefficient. In the case of large spacing ratios (G/D = 3.0 and 5.0), cylinder 1 has smaller lift coefficient compared to cylinder 2 for both flow attacking angles. The oscillation amplitudes of the lift coefficient for G/D=3 and 5 are found greater than that of a single cylinder at the same Reynolds number as shown in Fig. 6.4 (a – e).

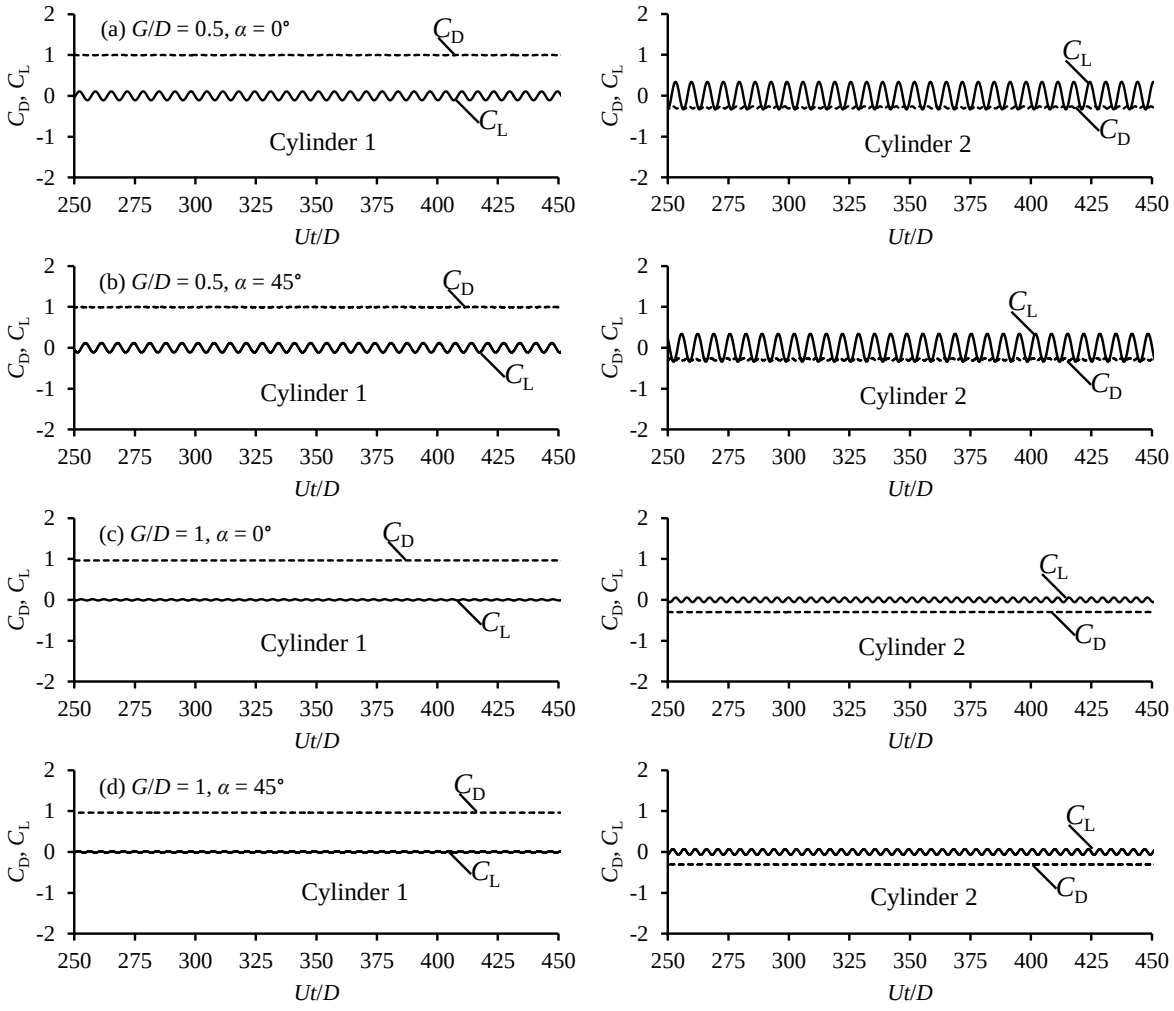

Fig. 6.3 Time histories of force coefficients at small spacing ratio (G/D= 0.5 and 1.0) for Re = 500

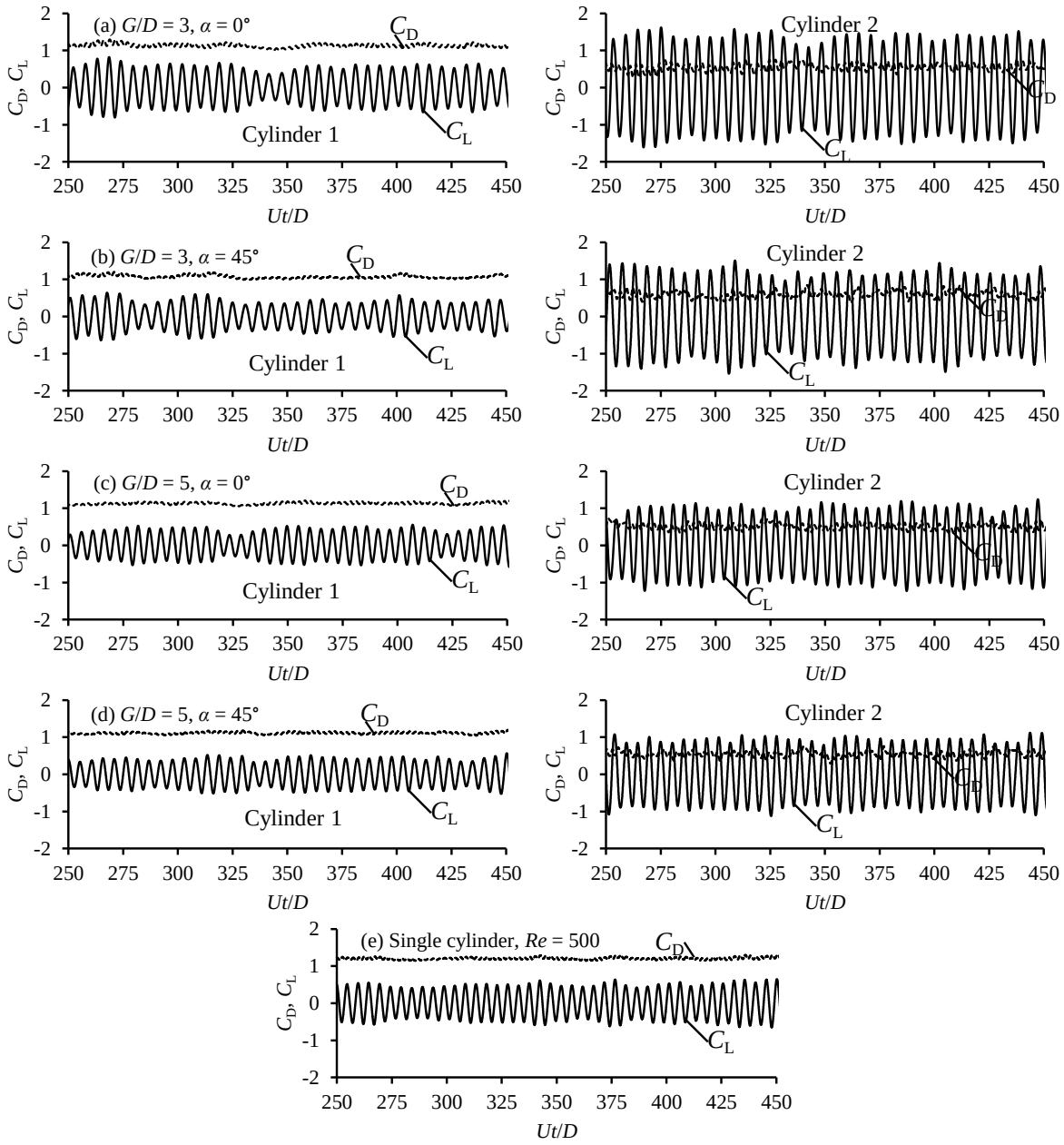

Fig. 6.4 Time histories of force coefficients at large spacing ratio (G/D= 3.0 and 5.0) for Re=500.

Fig. 6.5 (a) and (b) shows the comparison of the simulated mean drag coefficients on cylinders 1 and 2 with the experimental data and other numerical results. The slight decrease of the mean drag coefficients for cylinder 1 are noticed in Fig. 6.5 (a) whereas mean drag coefficient of cylinder 2 increases slightly as in Fig. 6.5 (b) with the increasing spacing ratio of until G/D = 2.5, where the mean drag coefficients of both cylinders increases suddenly, indicating the change in the wake flow pattern. The calculated 3D results agree well with previous experimental data and numerical results (both 2D and 3D). The calculated 3D results before the jump are found in between the 2D (Liu *et al.*, 2014) and experimental (Alam *et al.*, 2003b) results and after the jump are slightly higher than those 2D and

experimental results but almost identical to 3D results from Papaioannou *et al*. (2006). The mean drag coefficient of cylinder 2 is much smaller than that of cylinder 1, and compared to isolated cylinder at the same Reynolds number it is found to be decreased. Fig. 6.5 (c) is shown the comparison between the mean drag coefficients on both cylinders for two inclination angles. The influence of the inclination angles on the mean drag coefficients of cylinders 1 and 2 are very weak as shown in Fig. 6.5 (c).

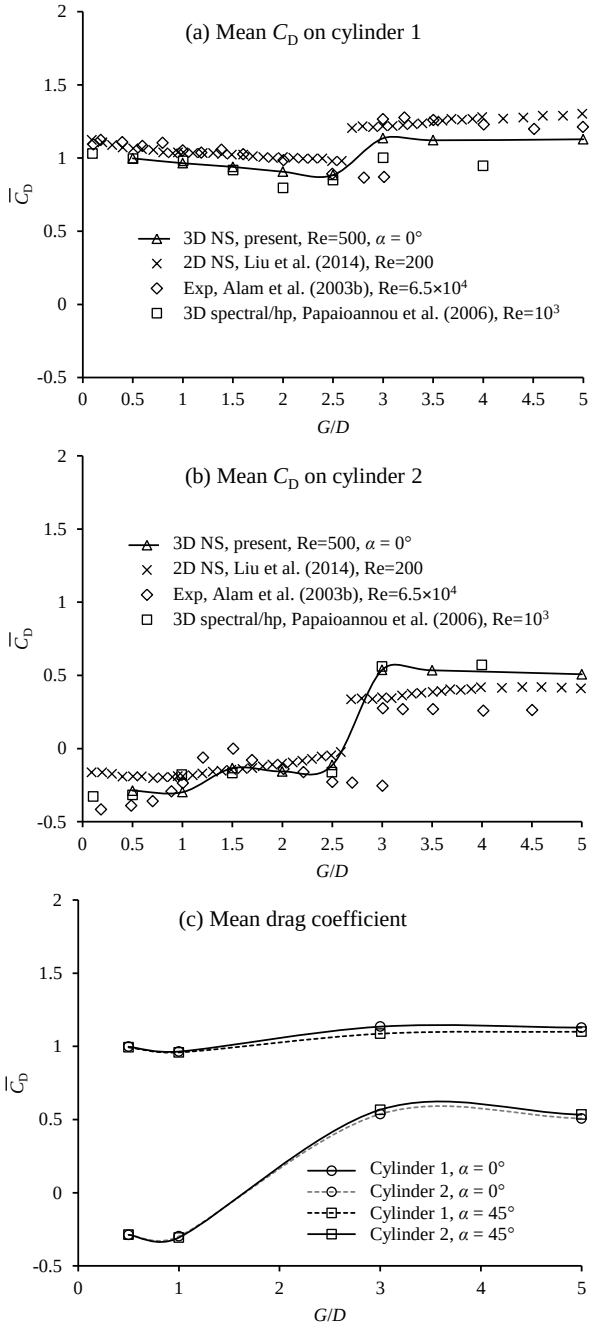

Fig. 6.5 Comparison of mean drag coefficient with numerical and experimental data at two flow attack angles

The variation of root-mean-square (RMS) lift coefficient with spacing ratio for both cylinders 1 and 2 at right attack angle case (α = 0°) are compared with other numerical and experimental results in Fig. 6.6. The RMS lift coefficient of cylinder 1 is very small until G/D = 2.5, where a sudden increase in the RMS lift coefficient is seen. The second cylinder experience larger RMS lift that compared to cylinder 1 as pictured in Fig. 6.6 (b), giving an additional small jump at G/D = 1.0. The larger RMS lift due to cylinder 2 is observed that compared to cylinder 1 and found to be agreed well with previous studies. Fig. 6.6 (c) compares the RMS lift coefficient from the two flow attack angles. The effect of the flow attack angle on the RMS lift coefficient is found to be very weak.

6.3.2 VORTEX SHEDDING FREQUENCY FROM TWO CIRCULAR CYLINDERS

Fast Fourier Transformation (FFT) of the lift coefficients of upstream and downstream cylinders is performed and the FFT spectra of the lift coefficient for both cylinders at right and oblique attacks are shown in Fig. 6.7. Due to the presence of single vortex street in the wake, the dominant frequencies of lift coefficients of two cylinders for the spacing ratio of 0.5 and 1 are found to be the same for both flow attack angles. The secondary peak can be seen at the spacing ratio of 3.0, which is much lower than the primary peak. The variation of the Strouhal number with the spacing ratio at two attacking angle together with 2D and 3D numerical results in Liu *et al*. (2014) and Papaioannou *et al*. (2006) respectively and experimental data in Alam *et al*. (2003b) are shown in Fig. 6.8. The Strouhal number is found to be decreased with increasing gap ratio until G/D = 2.5, where the Strouhal number jumps except at G/D = 1.0. The calculated Strouhal number for two cylinders are slightly smaller than single cylinder case for the same Reynolds number, whereas the Strouhal number for α=0º is found smaller than that for α=45º for both cylinders as shown in Fig. 6.8 (b). Both cylinders at α=0º attain almost identical Strouhal number compared to that with α=45º. However, Strouhal number for both cylinders at two different flow attack angles is still smaller than single cylinder for same Reynolds number of 500 and the present 3D results for Strouhal number at α = 0º and Re = 500 are in good agreement with previous experimental data and numerical results.

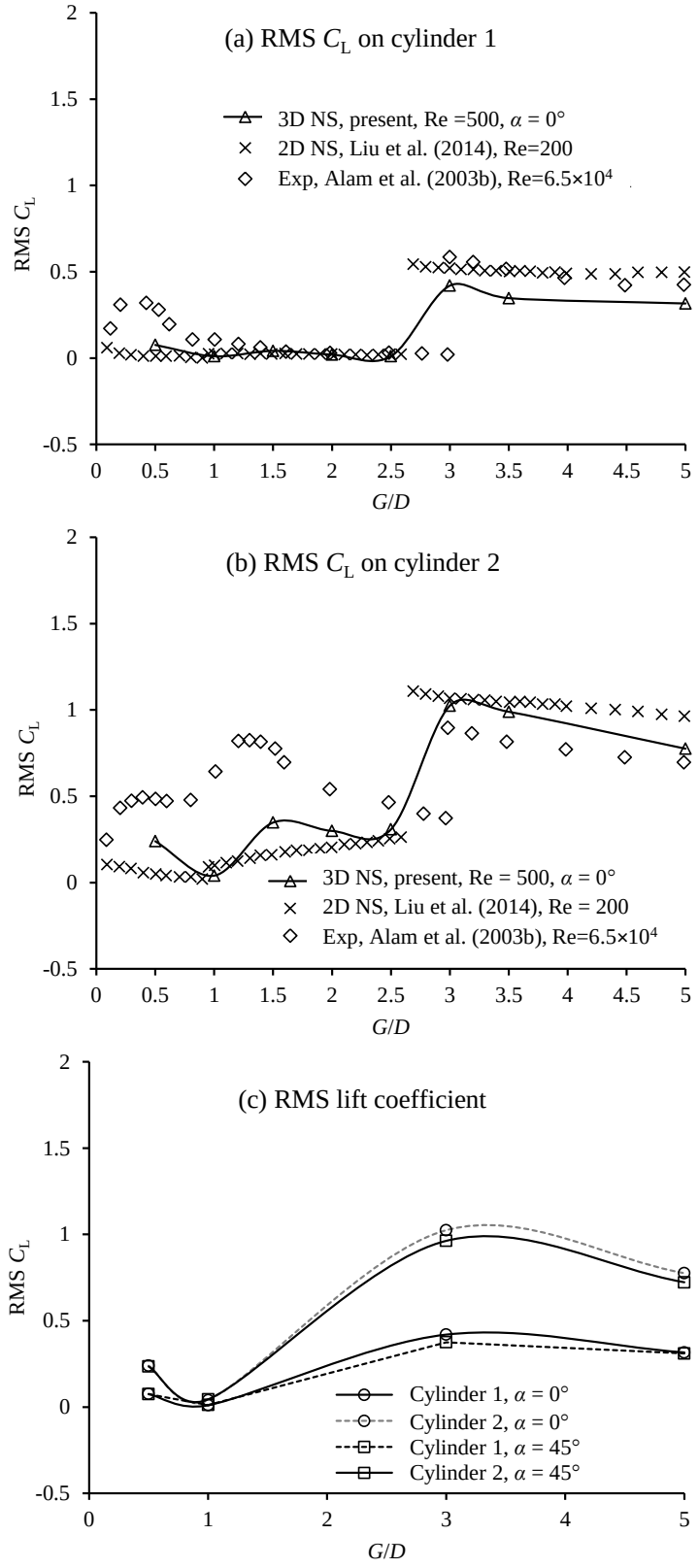

Fig. 6.6 Comparison of root mean square lift coefficient with numerical and experimental data at two flow attack angles

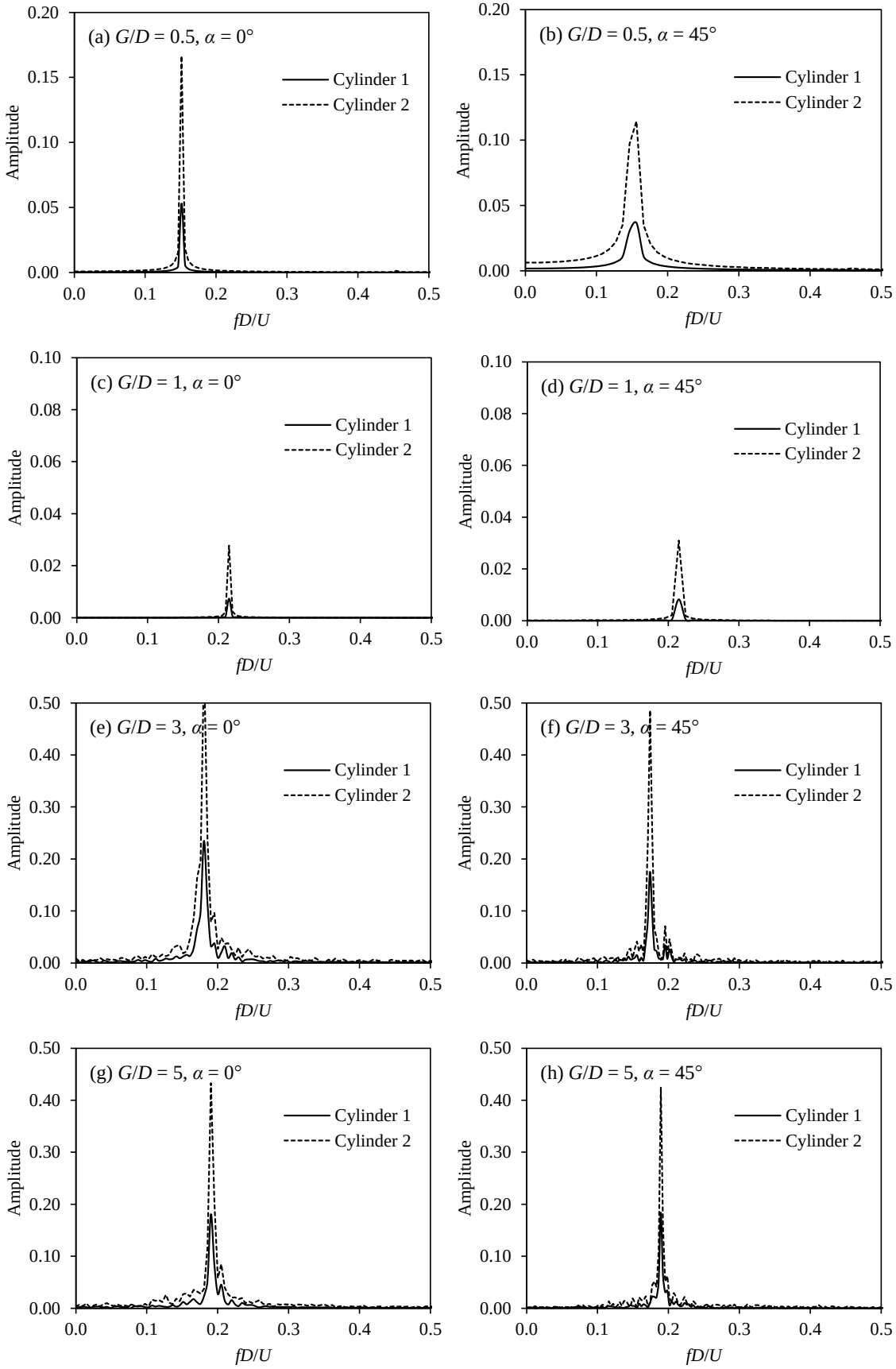

Fig. 6.7 Amplitude spectra of lift coefficient for upstream (cylinder 1) and downstream (cylinder 2) cylinders at right and oblique attack

6.3.3 FLOW PATTERN

The flow around two circular cylinders in tandem arrangements is found to be sensitive to spacing ratios and Reynolds number in the literature and it has been widely accepted that different flow regimes may occur at various spacing ratios (Zdravkovich, 1987; Xu and Zhou, 2004; Zhou and Yiu, 2006). For the convenience of study, the gap spacing ratios are divided here into two groups as small spacing (G/D = 0.5 and 1.0) and large spacing ratio (G/D = 3.0 and 5.0). The flow pattern around the cylinders will be discussed accordingly.

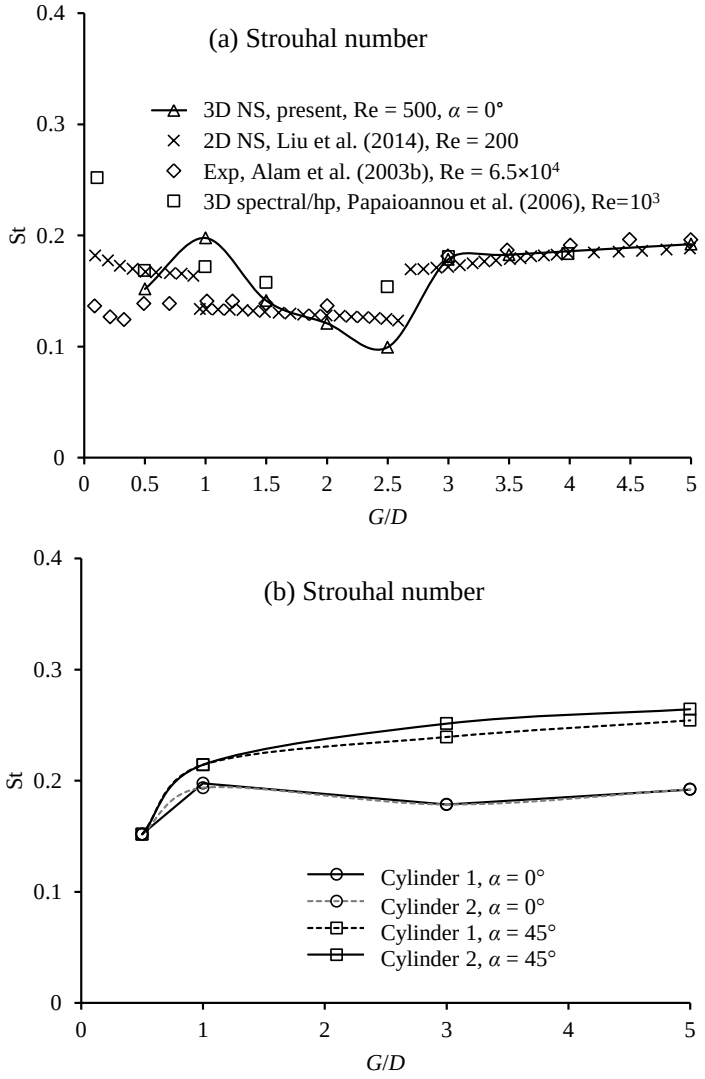

Fig. 6.8 Comparison of Strouhal number with numerical and experimental data at two flow attack angles

6.3.3.1 FLOW OVER SMALL SPACINGS

The iso-surface of second negative eigenvalue of e_2=-0.5 of the tensor $\mathbf{\Psi}^2 + \mathbf{\Omega}^2$ are used to represent the three-dimensional flow in the wake, where $\mathbf{\Psi}$ and $\mathbf{\Omega}$ are the symmetric and antisymmetric parts of velocity gradient tensor, respectively. For the purpose of identification of the location of vortex cores, $\mathbf{e}_2$ (second eigenvalue) is used to demonstrate the vortex structures for all the cases (Jeong and Hussain, 1995). Vorticity of iso-surface of e_2 = -0.5 for *Re* = 500, *G*/*D*=0.5 and 1 and two flow attack angles (α= 0º and 45º) are shown in Fig. 6.9. The flow is found to remain 2D for *G*/*D*=0.5 throughout the simulation for both flow attack angles as shown in Fig. 6.9 (a and b). When the spacing ratio is increased to 1.0, the very weak 3D flow appeared in the wake only for α= 0º, whereas for α= 45º the flow is still 2D throughout the simulation as in Fig. 6.9 (c and d). This phenomenon is observed for the first time to show the difference between the flow attacking angles in the sense of 3D simulation. For this small spacing ratio (*G*/*D*=0.5 and 1.0), the two cylinders act as one and cylinder 2 remains inside the vortex formation region of cylinder 1. The fluid flow in the gap between the cylinders remains almost steady when *G*/*D*=0.5 and 1.

The vortex shedding flow at the mid-section of the cylinders (on the xy-plane with *z*=4.8) are presented by the contours of the non-dimensional vorticity ω_z in Fig. 6.10 for *G*/*D*=0.5 and 1.0. The vorticity components in the *x*, *y* and *z* directions are calculated by $\omega_x = \frac{D}{U}(\frac{\partial w}{\partial y} - \frac{\partial v}{\partial z})$, $\omega_y = \frac{D}{U}(\frac{\partial u}{\partial z} - \frac{\partial w}{\partial x})$ and, $\omega_z = \frac{D}{U}(\frac{\partial v}{\partial x} - \frac{\partial u}{\partial y})$, respectively. When *G*/*D*=0.5, the vortex shedding appears only behind cylinder 2 and the vortex shedding from cylinder 1 is completly suppressed. For the gap ratio of 1.0 as shown in Fig. 6.10 (c), the shear layer from cylinder 1 seems to be very weak to wrap cylinder 2 for α=0º, leading to produce very weak 3D vortex shedding at the back of cylinder 2. But for oblique attack (α=45º) case, still the shear layer from cylinder 1 show the same property as in spacing ratio of 0.5.

(a) G/D = 0.5, α=0°, Ut/D=300

(b) G/D = 0.5, α=45°, Ut/D=300

(c) G/D = 1, α=0°, Ut/D=300

(d) G/D = 1, α=45°, Ut/D=300

Fig. 6.9 Vorticity iso-surface of e_2=-0.5 at small gap ratio (G/D= 0.5 and 1.0) for Re = 500 at two different attacking angles

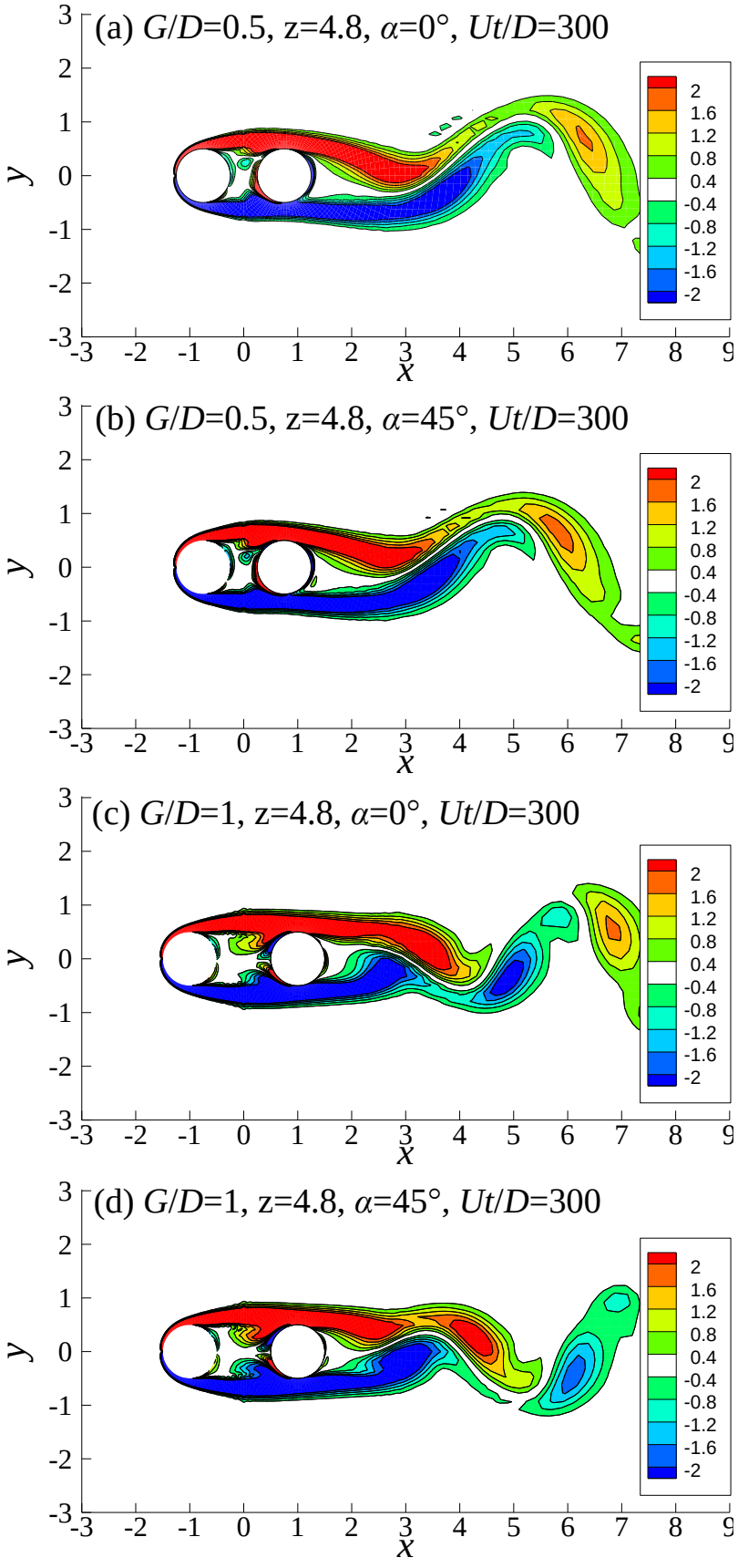

Fig. 6.10 Contour of axial vorticity at mid-section (z=4.8) for Re = 500

6.3.3.2 FLOW OVER LARGE SPACINGS

For the large spacing ratio (G/D = 3.0 and 5.0), the shear layers from cylinder 1 no longer wrap cylinder 2 due to the formation of vortex shedding behind cylinder 1 as shown in Fig. 6.11. The clear 3D vortex shedding can be seen in the wake for both flow attack angles. The vortex shedding between the gap started to occur at G/D=3.0 by rolling up the separated boundary layer from cylinder 1 and the formation of vortices in front of cylinder 2 and is reported as critical gap in the literature (Alam *et al*., 2003). The contours of axial vorticity at mid-section of cylinders are presented in Fig. 6.12 in order to clearly visualise the vortex shedding phenomena between two cylinders. The occurrence of lower pressure right behind the cylinder 1 leads to increase the mean drag force on the upstream cylinder as in Fig. 6.5. Due to the formation of vortex shedding from the both cylinders that are somehow similar to the flow over a single cylinder and hence identified in Fig. 6.8 with the Strouhal number at G/D=3.0 is 0.181 and is about 11% smaller than calculated single cylinder case at the same Reynolds number of 500 at α=0^o whereas at α=45^o, calculated strouhal number is found higher than single cylinder case which is about 18%. The formation of two individual vortex streets behind the cylinders can be observed at spacing ratio G/D = 5.0 as reported in Zdrakovich, (1986).

The formation of Karman vortex shedding from the both cylinders can be observed clearly and the location of cylinder 2 is far enough in order to form vortex shedding from cylinder 1 (Ishigai *et al*., 1972). The vortex shedding at G/D = 5.0 for both flow attack angles are found to be independently shed from cylinder 2 (Ohya *et al*., 1989) even though the existence of some influence from the cylinder 1 may occur in the wake and leading to the formation of almost same vortex shedding frequency as shown in Fig. 6.8 (b) for both flow attack angles and clearly noticed the larger frequency for the first time at oblique attack case compared to right attack angle case and is similar to G/D = 3.0. The calculated mean drag coefficient and RMS lift coefficient for both attacking angles are almost same and the values are similar to the previous studies at this gap spacing. The weak vortices are shed from cylinder 2 at this flow regime compared to small gap spacing due to quick dissipation of vortex shedding as reported in Zhou and Yiu (2006).

(a) G/D = 3, α=0°, Ut/D=300

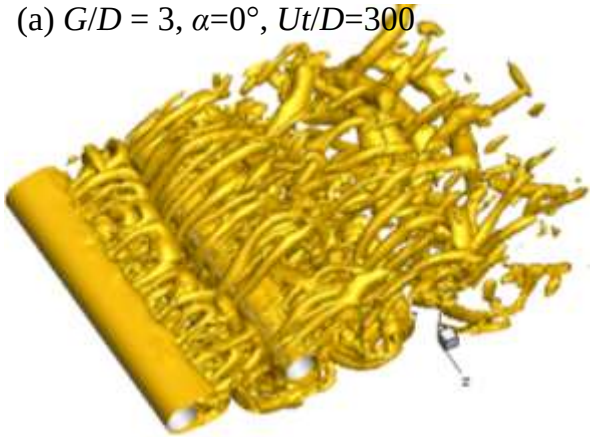

(b) G/D = 3, α=45°, Ut/D=300

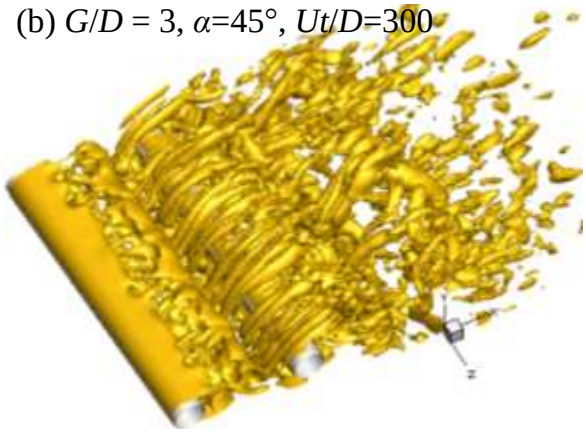

(c) G/D = 5, α=0°, Ut/D=300

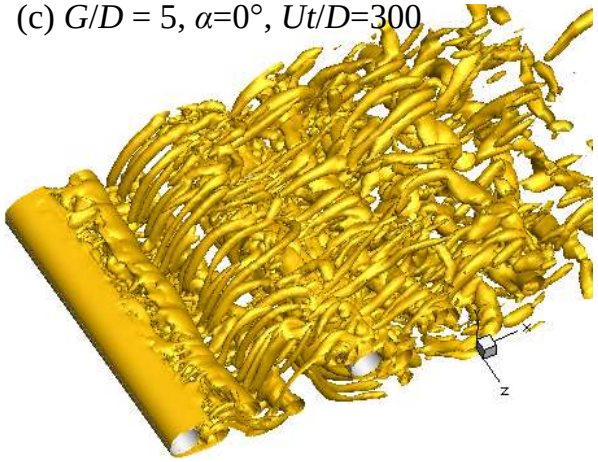

(d) G/D = 5, α=45°, Ut/D=300

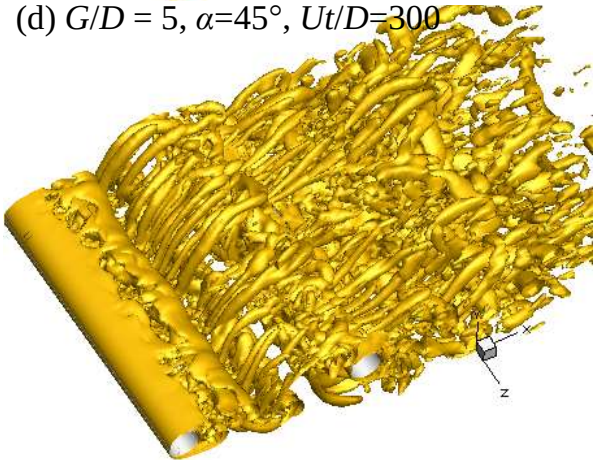

Fig. 6.11 Vorticity iso-surface of e_2=-0.5 for Re = 500 at two different attacking angles

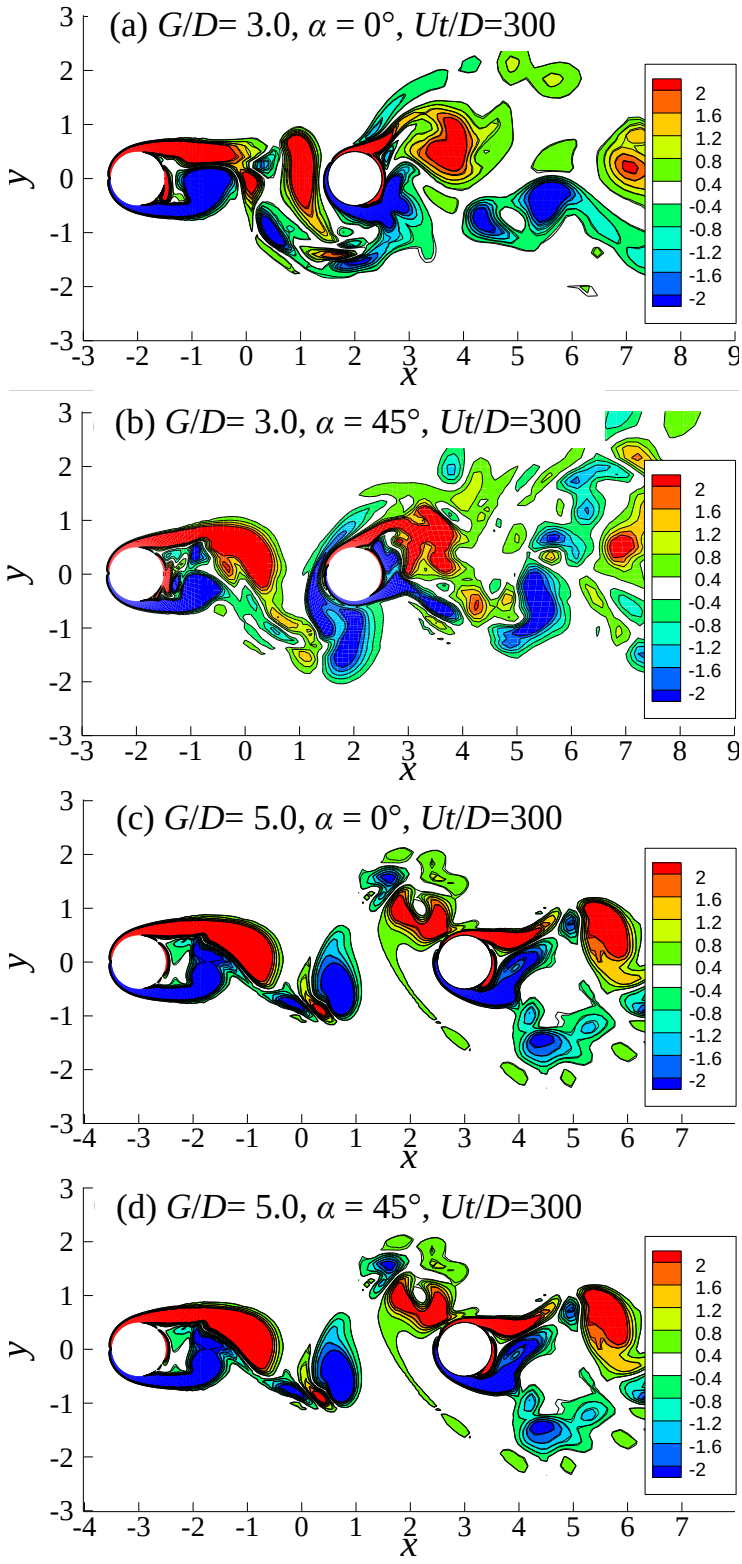

Fig. 6.12 Contour of axial vorticity at mid-section (z=4.8) for Re = 500

6.4 CONCLUSIONS

The numerical study of three-dimensional flow past two circular cylinders of identical diameters for *Re* = 500 and various span of gap spacings between the cylinders at two flow approaching angles are performed in order to find the influence of flow attacking angles at the studied gap spacings between the cylinders. The compared mean drag, RMS lift and Strouhal number with previous 2D and 3D study agreed well and are concluded as follows:

For the convenience of the study, the wake flows are divided into small (G/D = 0.5 and 1.0) and large (G/D = 3.0 and 5.0) gap spacings. For the small gap spacing (G/D = 0.5 and 1.0) the calculated force coefficients clearly show the 2D flow throughout the simulations for both flow attacking angles. However, very weak 3D flow appeared at gap spacing of 1.0 for α=0º only and identified by the instantaneous flow structure analysis whereas at α=45º the flow is found to be 2D throughout the simulation. The mean drag and RMS lift coefficient of each cylinder for both flow attacking angles are found smaller than the isolated single cylinder. The influence of flow approaching angles due to cylinder 1 and cylinder 2 have observed in comparison of Strouhal number where larger Strouhal number was observed for all the gap spacings except at G/D = 0.5. The clear 3D vortex shedding can be seen in the wake for both flow approaching angles at large gap spacings (G/D = 3.0 and 5.0). The vortex shedding between the gap spacing started to occur at G/D = 3.0 (critical gap spacing) by rolling up the separated boundary layer from cylinder 1 and the formation of vortices in front of cylinder 2 and the vortex shedding from cylinder 2 is found to be large but weak compared small gap spacing.

CHAPTER 7

THREE-DIMENSIONAL FLOW AROUND TWO CIRCULAR CYLINDERS OF DIFFERENT DIAMETERS IN A CLOSE PROXIMITY

Flow past two cylinders of different diameters in close proximity is simulated numerically for a constant diameter ratio of 0.45, a gap ratio of 0.0625 and a Reynolds number of 1000 (defined using the diameter of the main cylinder). The effect of the position angle α of the small cylinder relative to the large one on force coefficients and wake flow patterns are studied. Depending on the position angle α of the small cylinder, four wake flow modes are identified: the upstream interference mode for α=0°, 22.5° and 45°, the intermittent attached gap flow mode for α=67.5° and 90°, the attached gap flow mode for α=112.5° and 135° and the wake interference mode for α=157.5° and 180°. The RMS lift coefficients of both cylinders are reduced significantly compared with that of a single cylinder, regardless of the position angle of the small cylinder. Although the variation trends of the mean drag and lift coefficients with the position angle of the small cylinder obtained from the two-dimensional (2D) and three-dimensional (3D) simulations are similar, the 2D simulations overestimate the mean drag coefficient, the RMS drag and lift coefficients compared with those obtained from the 3D simulations.

7.1 INTRODUCTION

Piggyback pipelines that comprise of two pipelines of different diameters are often used in offshore oil and gas projects. Laying two pipelines together reduces not only the installation cost, but also the stabilization cost. In practice, the two pipelines are bundled together at certain intervals with a very small gap between them. Due to the lack of specific test data for piggyback pipelines, the common hydrodynamic design practice is to use the equivalent diameter assumption where the two pipelines are simplified into a single pipeline with an equivalent diameter of the sum of the diameters of the two pipelines (Zhao *et al*., 2005). It is unclear whether such a practice is too conservative or unsafe, because the influence of the gap between the two pipelines on the fluid dynamics and the forces of the piggyback pipelines could be non-linear.

Remarkably complex flow patterns have been discovered for flow past two identical cylinders either in side-by-side, tandem or staggered arrangement (Sumner, 2010). Previous

studies have shown that when two cylinders are in a tandem arrangement, they behave as a single elongated body if the gap between them is very small. The vortex shedding from the upstream cylinder occurs only when the gap is large enough, while a re-attachment flow regime is observed for intermediate gaps (Zdrakovich, 1987; Xu and Zhou, 2004). When two identical cylinders are in a side-by-side arrangement, the most prominent phenomenon is the biased jet flow from the gap and it was found that the biased direction of the flow changes intermittently when the gap is less than 1.2 times the cylinder diameter (Alam *et al*., 2003). When two cylinders are in a staggered arrangement, the flow approaching angle has a significant effect on the vortex shedding and the forces on the structures (Tong *et al*., 2015). Early numerical studies about flow past two identical cylinders were mainly based on 2D models and focused on low Reynolds numbers (Mittal *et al*., 1997; Meneghini *et al*., 2001). Recently, many 3D simulations have been conducted for flow past two cylinders in various arrangements and Reynolds number in the turbulent flow regime (Kondo and Matsukuma, 2005; Afgan *et al*., 2011; Thapa *et al*., 2015).

The studies on two cylinders of different diameters in fluid flow are rarer than those of two identical cylinders. Tsutsui *et al*. (1997) studied the interactive flow past two circular cylinders of different diameters at close proximity experimentally and numerically. In their experimental study, the separated shear layer from the main cylinder was found to re-attach and adhere to the rear surface of the main cylinder. The intermittent re-attachment and time-averaged fluid forces obtained numerically by Tsutsui *et al*. (1997) showed good agreement with the experimental results.

It has been found that a significant reduction of the fluid forces on a large cylinder can be achieved by properly placing a smaller cylinder close to it. Strykowski and Sreenivasan 1990 discovered experimentally the suppression of vortex shedding from a circular cylinder at low Reynolds numbers (Re = 40 – 100) by placing a small circular cylinder close to it. Dipankar *et al*. (2007) studied numerically the suppression of vortex shedding behind a circular cylinder by another control cylinder in the near wake region at low Reynolds numbers (Re = 63, 79 and 150). Dalton *et al*. (2001) studied the effect of installing a small control rod in the wake of a large cylinder on the vortex shedding flow through numerical simulations and flow visualizations, while Lee *et al*. (2004) investigated reduction of the lift force of a cylinder by an upstream control rod. In previous studies of flow past two cylinders of different diameters, the small cylinder was either placed upstream or downstream of the large cylinder, while less attention has been paid to the side-by-side and staggered cases. Zhao *et al*. (2007) studied

flow past two circular cylinders of different diameters using two-dimensional numerical simulations. It was found that the numerical results of the time-averaged force coefficients from the two-dimensional numerical model agree well with the experimental data. In contrast to the time-averaged drag force coefficients, it is well known that the 2D models overestimate the oscillation of the lift coefficient of cylinders. For example, the two-dimensional numerical results of the root mean square (RMS) lift coefficient in the subcritical flow regime in Zhao *et al*. 2007 is significantly greater than the measured data. It is therefore preferable to use three-dimensional simulations to investigate the interference between two cylinders in fluid flow.

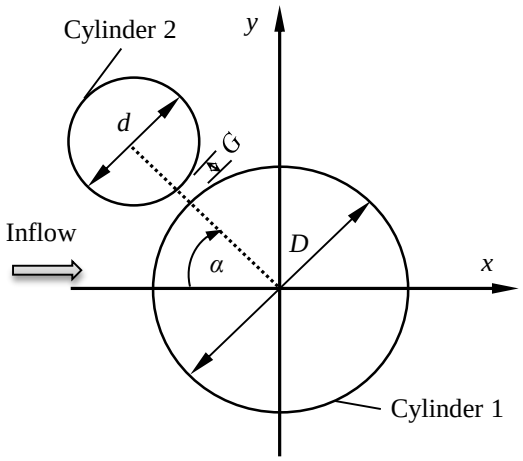

Fig. 7.1 Definition sketch of flow past two circular cylinders of different diameters

In this study, flow past two cylinders of different diameters in close proximity is investigated numerically by solving the three-dimensional Navier-Stokes (NS) equations. The position of the small cylinder is determined by the gap G between the two cylinders and the position angle α as shown in Fig. 7.1. The diameters of the large and the small cylinders are D and d, respectively. The diameter ratio between them is d/D=0.45. The study focuses on a very small gap between the two cylinders and the aim is to examine the effect of the position angle α of the small cylinder relative to the large cylinder on the wake flow pattern and the forces on the cylinders. The position angle ranges from 0° to 180° with an interval of 22.5°. The gap between the two cylinders is fixed at 0.0625D. The diameter and gap ratios are set the same as their counterparts used in the experiments by Tsutsui *et al*. 1997 in order to compare the numerical results with the experimental data. Since the vortex shedding characteristics from a circular cylinder are less dependent on the Reynolds number in the subcritical Reynolds number regime than in other regimes, the Reynolds number defined as $Re = UD/v$ with v being the kinematic viscosity of the fluid and U, the free stream velocity, is

fixed at 1000. The emphasis has been placed on the effects of the position angle of the small cylinder on the flow around the large cylinder.

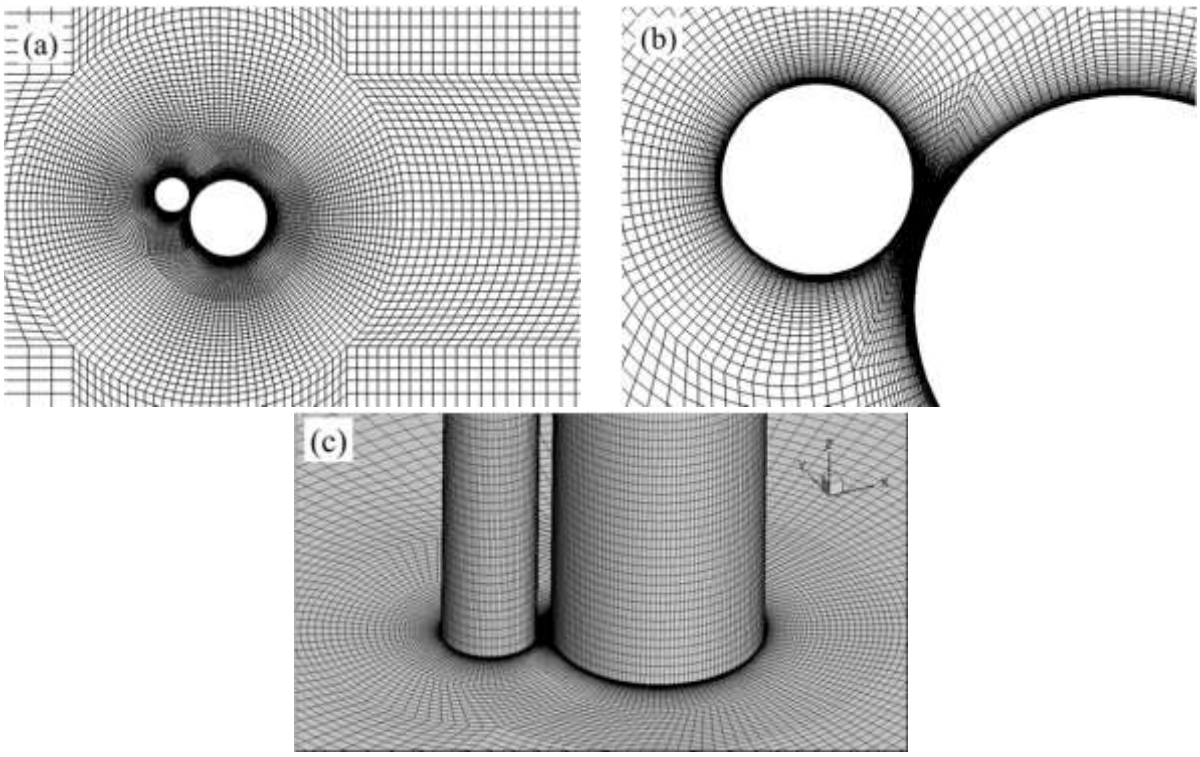

Fig. 7.2 Computational mesh near two circular cylinders at α = 22.5°; (a) 2D view around the cylinders; (b) Zoom in view near the gap and (c) 3D view around the cylinders

7.2 NUMERICAL METHOD

The two cylinders investigated in this study are shown in Fig. 7.1. The position of the small cylinder is determined by the gap between the cylinders G and the position angle α. The length, time, velocity and pressure are non-dimensionlised by $x_i = x_i'/D$, $t = Ut'/D$, $u_i = u_i'/U$ and $p = p'/\rho U^2$ respectively, where the primes stand for the dimensional values, x_1, x_2 and x_3 represent the coordinates x, y and z, respectively, t is the time, u_i is the velocity component in the x_i-direction, p is the pressure and ρ is the density of the fluid. The non-dimensional three-dimensional incompressible Navier-Stokes (NS) equations are written as

$$\frac{\partial u_i}{\partial t} + u_j \frac{\partial u_i}{\partial x_j} + \frac{\partial p}{\partial x_i} - \frac{1}{\mathrm{Re}} \frac{\partial^2 u_i}{\partial x_j^2} = 0, \tag{7.1}$$

$$\frac{\partial u_i}{\partial x_i} = 0, \tag{7.2}$$

The NS equations are solved by the Petrov-Galerkin finite element method developed by Zhao *et al*. (2009). The detail of the numerical method can be found in Zhao *et al*. (2009) and will not be repeated here. The dimensions of the rectangular non-dimensional computational domain are 60 in the *x*-direction (incoming flow direction), 40 in the *y*-direction and 9.6 in the *z*-direction (axial direction of the cylinders). Fig. 7.2 shows a typical computational mesh near the cylinders for α = 22.5°. The whole computational domain is divided into 192 layers of 8-node hexahedral tri-linear finite elements along the axial direction of the cylinders. On the circumferences of the large and the small cylinders, 130 and 96 elements are distributed, respectively. The total finite element numbers for all the cases are about 3.6 million. The non-dimensional computational time step Δt was set to 0.003. The initial values of the velocity and the pressure are set at zero in the whole domain. The non-dimensional velocity at the inlet boundary is given as

$$(u_1, u_2, u_3) = (1,0,0), \tag{7.3}$$

The free-slip boundary condition is employed at the two side boundaries that are parallel to the $x-z$ plane and the two end boundaries that are perpendicular to the cylinder axes. To employ the free-slip boundary condition, the velocity component and the pressure gradient perpendicular to the boundary are set to zero. On the cylinder surfaces, no-slip condition is applied.

The drag and lift coefficients on the large cylinder are calculated as $C_{D1} = 2F_{D1}/\rho DLU^2$ and $C_{L1} = 2F_{L1}/\rho DLU^2$ respectively, and those on the small cylinder are calculated by $C_{D2} = 2F_{D2}/\rho dLU^2$ and $C_{L2} = 2F_{L2}/\rho dLU^2$ respectively, where F_D and F_L are the drag and lift forces on a cylinder in the *x*- and *y*- direction, respectively, the subscripts 1 and 2 represent the large and small cylinders, respectively and *L* is the length of the cylinder. The drag and lift forces (F_D and F_L) of a cylinder are calculated by integrating the pressure and shear stress along the cylinder surface.

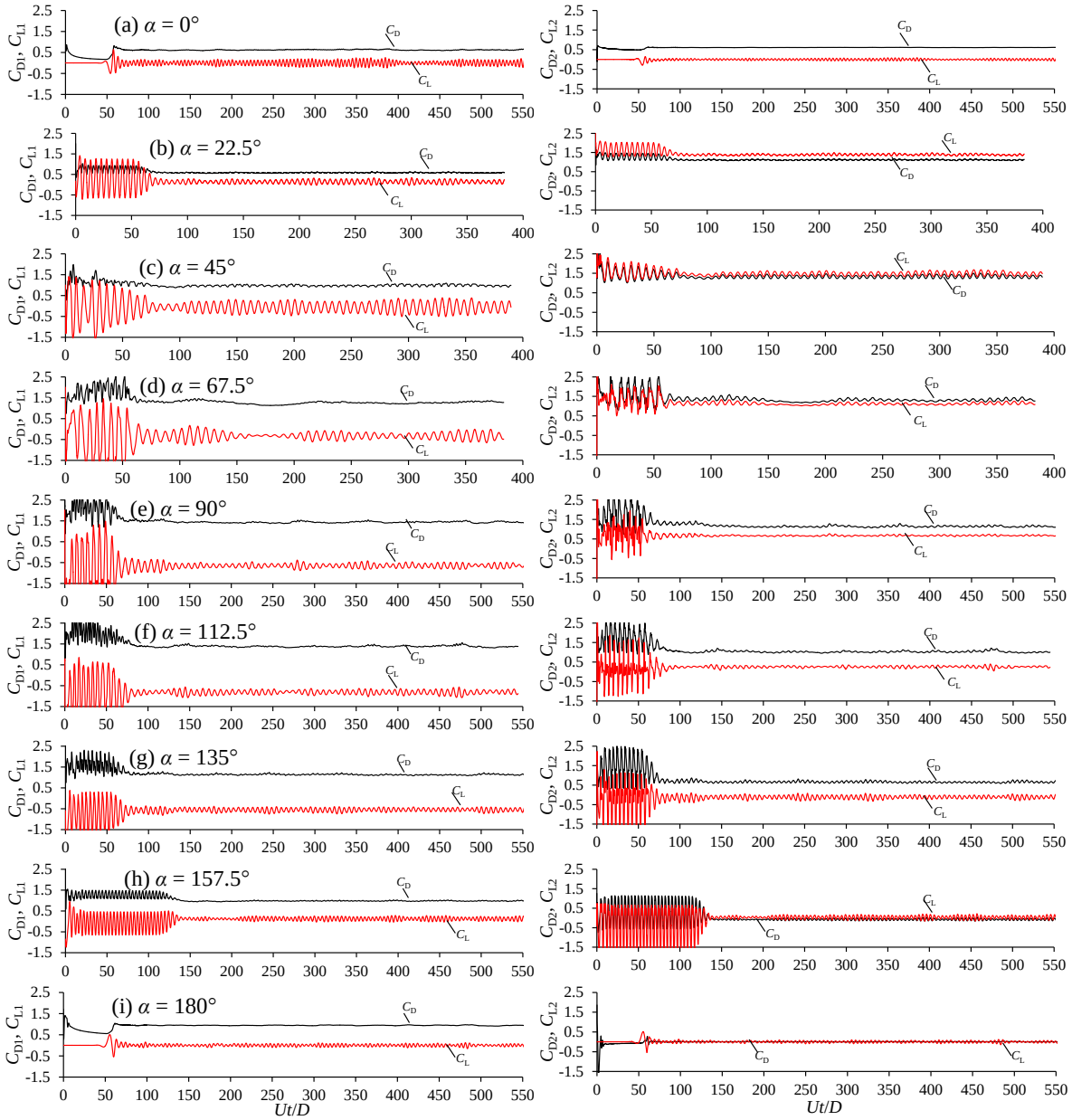

Fig. 7.3 Time histories of force coefficients for G/D= 0.0625. (a) α = 0°; (b) α = 22.5° ;(c) α = 45°; (d) α = 67.5°; (e) α = 90°; (f) α = 112.5°; (g) α = 135°; (h) α = 157.5°; (i) α = 180°

7.3 RESULTS AND DISCUSSIONS

While the gap ratio and diameter ratio are fixed at G/D=0.0625 and d/D=0.45, respectively, this study is focused on the influence of the position angle of the small cylinder relative to large (main) cylinder on the vortex shedding and the forces on the two cylinders. The Reynolds numbers based on the diameters of the large and small cylinders are 1000 and 450, respectively. The simulations are conducted for non-dimensional time of at least Ut/D = 350 to ensure that the fully developed wake flow has been obtained. The analysis is based on

the results after $Ut/D > 110$ when the fully developed vortex shedding has been obtained. The qualities of the meshes for the cases in this study are equivalent to that shown in Fig. 7.2.

Table 7.1 Results of the mesh dependency study

Mesh	L	N_{c1}	N_{c2}	Δz	Δr	$\overline{C}_{D1}$	$\overline{C}_{D2}$	$\overline{C}_{L1}$	$\overline{C}_{L2}$	S_{t1}
1	9.6	130	96	0.05	0.001	0.9846	0.2992	-0.0663	0.3308	0.1549
2	4.8	130	96	0.05	0.001	1.0033	0.3008	-0.0660	0.3314	0.1523
3	9.6	96	72	0.10	0.0018	1.0052	0.3015	-0.0600	0.3318	0.1530
4	9.6	96	72	0.05	0.0018	1.0020	0.3202	-0.0612	0.3312	0.1531
e12 (%)	–	–	–	–	–	1.90	0.55	0.45	0.18	1.68
e13 (%)	–	–	–	–	–	2.09	0.79	9.49	0.29	1.26
e14 (%)	–	–	–	–	–	1.77	7.03	7.68	0.11	1.17

7.3.1 MESH DEPENDENCY STUDY

The mesh dependency study was conducted to ensure that the meshes used in this study are dense enough to obtain accurate results. Simulations for α=45° are conducted using four different meshes (referred to be Meshes 1 – 4, respectively) listed in Table 7.1. In Table 7.1, N_{c1} and N_{c2} are the finite element numbers along the circumferential direction of cylinders 1 and 2, respectively, Δz is the mesh size in the axial direction of the cylinder and Δr is mesh size in the radial direction on the cylinder surfaces, and $\overline{C}_D$ and $\overline{C}_L$ are the mean (time averaged) drag and lift coefficients, respectively. Because the frequency of the lift coefficients of the two cylinders are found to be the same, only the Strouhal number of the large cylinder S_{t1} are shown in Table 7.1. The differences between the results form Mesh k and those from Mesh 1 are defined as e1k and they are listed in Table 7.1. It can be seen that the maximum changes in force coefficient and the Strouhal number as the result of reducing the cylinder length from 9.6 to 4.8 (Mesh 1 to Mesh 2) are 1.90% and 1.68%, respectively. Increasing the finite element sizes in the radial, axial and circumferential direction on the cylinder surface (comparing between Mesh 1 and Mesh 4) leads to a 9.49% change in $\overline{C}_{L1}$. Because the mean lift coefficient of the large cylinder $\overline{C}_{L1}$ is very small, 9.49% change in $\overline{C}_{L1}$ of corresponding to a very small value (0.0063). The difference between the mesh lift coefficients of cylinder 2 from meshes 1 and 4 is only 0.29%. The comparison between the results from the different meshes demonstrates that the finite element sizes in the radial, circumferential and axial directions of the cylinders for Mesh 1 has been sufficiently fine to

obtain accurate results. In the present study, the simulations for all the position angles (α) are conducted using meshes with the same density as Mesh 1.

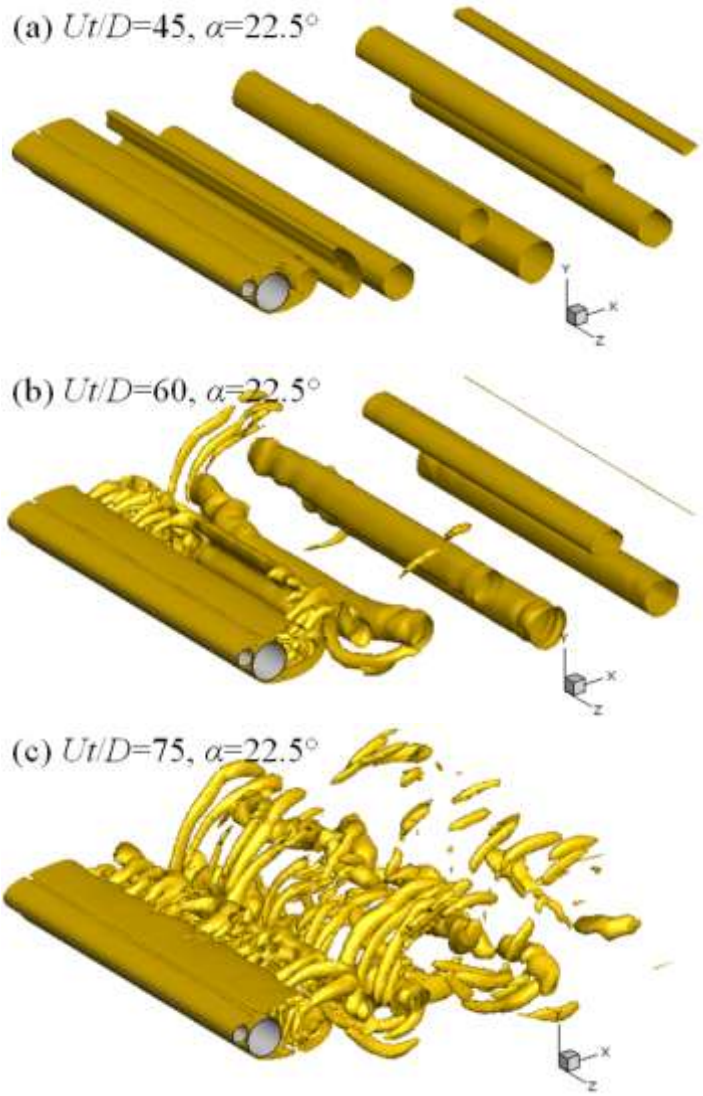

Fig. 7.4 Iso-surface of e_2= -0.5 at α = 22.5° for different non-dimensional time steps.

7.3.2 FORCE COEFFICIENTS

The time histories of the force coefficients of both cylinders are shown in Fig. 7.3 to examine the effect of α on the force coefficients. It is confirmed by the numerical flow visualization that two-dimensional (2D) vortex shedding is responsible for the large oscillation amplitudes of the force coefficients observed at the initial stage of the simulations (except for α = 0° and 180°). The amplitudes of the force coefficients are reduced significantly when the vortex shedding becomes fully three-dimensional (3D). Due to the symmetric configuration at α = 0° and 180°, the flow remains symmetric until Ut/D = 50. The drag and lift coefficients are reduced significantly after the flow transit from 2D to 3D

because part of the energy in the spanwise vortices, which is responsible for the oscillation of the force coefficients, is transferred to the streamwise vortices (Mansy *et al*., 1994) and the synchronization of the wake structure in the spanwise direction becomes weak. The sudden reduction of the force coefficients is not observed until Ut/D = 110 at α = 157.5°, implying that the two-dimensionality of the flow exists for a longer period than any of other position angles.

The correlation between the significant reduction of the oscillation amplitude of the force coefficients and the transition of the wake flow from 2D to 3D is further demonstrated by the wake flow structures during the transition period shown in Fig. 7.4. The 3D wake flow patterns are presented by the iso-surface of the second negative eigenvalue e_2 of the tensor $\mathbf{\Psi}^2+\mathbf{\Omega}^2$, where $\mathbf{\Psi}$ and $\mathbf{\Omega}$ are the symmetric and the anti-symmetric parts of the velocity-gradient tensor, respectively. The second eigenvalue e_2 can be used to accurately identify the location of the vortex cores (Jeong and Hussain, 1995). The two dimensional vortex shedding characterized by the alignment of vortices in the spanwise direction of the cylinders can be seen clearly at the early stage of simulation (Ut/D < 55) in Fig. 7.4 (a), whereas in Fig. 7.4 (b) the development of streamwise vortices from the two ends of the cylinders implies the formation of three-dimensional vortex shedding in the wake. The formation of vortex shedding patterns presented in Fig. 7.4 (b) is similar to the 2D to 3D flow transition of an isolated cylinder reported in Williamson, (1996). The energy transfer from the spanwise to the streamwise vortices and the slightly phase variation of the vortex shedding along the cylinder span due to the wobbly spanwise vortices lead to the reduction in the oscillation amplitudes of the force coefficients. The fully developed three-dimensional vortex shedding can be observed in Fig. 7.4 (c). The simulation results shown in Fig. 7.4 and Fig. 7.3 (b) clearly show that the reduction of oscillation amplitudes of force coefficients is induced by the flow transition from 2D to 3D. 2D numerical simulations are also performed in this study and the results of the force coefficient are compared with the 3D results later on. No significant reduction of the oscillation amplitudes of the force coefficients are observed in the 2D simulations. Since 3D numerical results are the focus of this study, the time histories of the force coefficients of the 2D simulations are not presented here.

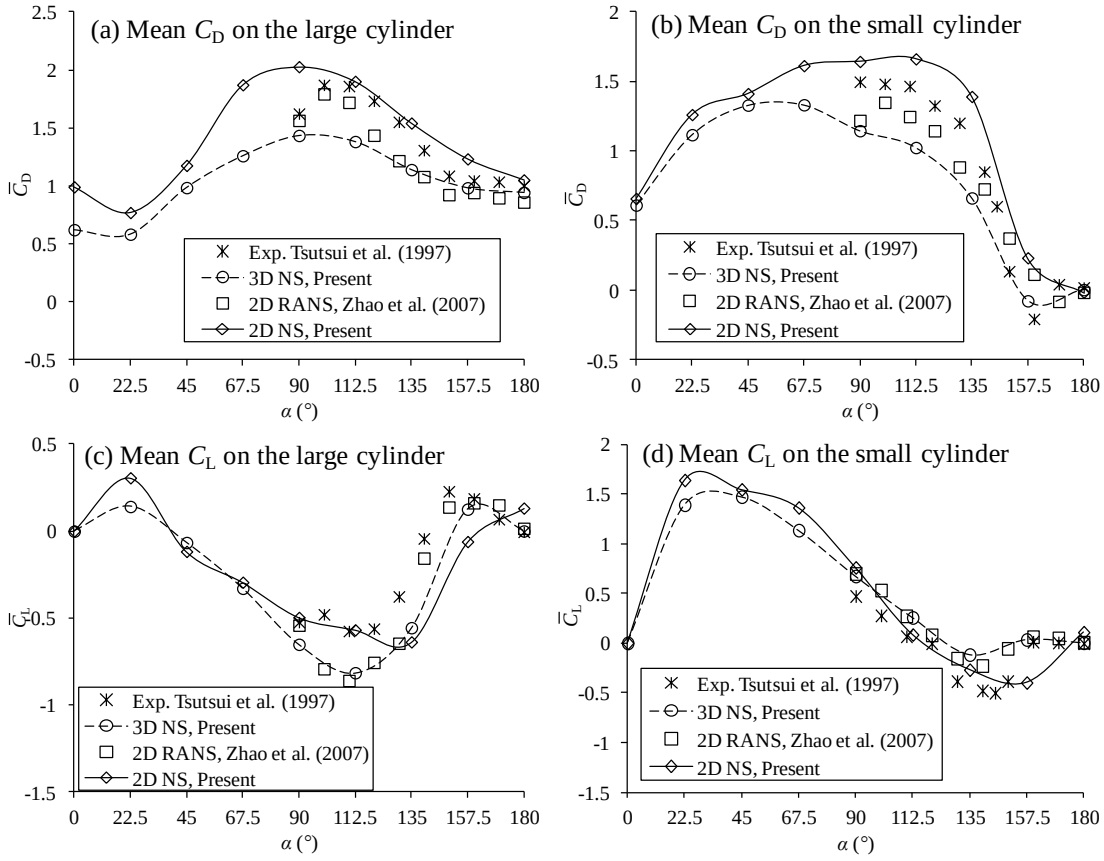

Fig. 7.5 Variations of the mean force coefficients with α

Fig. 7.5 shows the time-averaged force coefficients (defined as the mean force coefficient hereafter) of the two cylinders. The experimental data by Tsutsui *et al*. (1997), the numerical results based on 2D RANS and 2D NS equations are also included for comparison. The 2D NS results are obtained in this study using the 2D version of the numerical model. The experimental results by Tsutsui *et al*. (1997) and the 2D RANS results by Zhao *et al*. (2007) were obtained for a higher Reynolds number of 4.1×10^4, and they are only available for $\alpha \geq 90°$. It is expected that the mean flow feature and the effects of the position angle α on the force coefficients should be the same for Reynolds numbers in the subcritical flow regime ($300 < \mathrm{Re} < 10^5$). The mean drag coefficient of the large cylinder is increased significantly when the position of the small cylinder is at the side of the large cylinder. At α=90°, it is increased by about 56.5% compared with α=0°. It is decreased when the position of small cylinder lies either in front (0°< α < 45°) or behind the large cylinder (135°< α < 180°). The drag coefficient on the large cylinder is reduced because the small cylinder causes a reduction of the pressure on the front surface of the large cylinder when 0°< α < 45° and an increase of the base pressure of the large cylinder is observed when 135°< α < 180° (Zhao *et al*., 2007; Sakamoto *et al*., 1991).

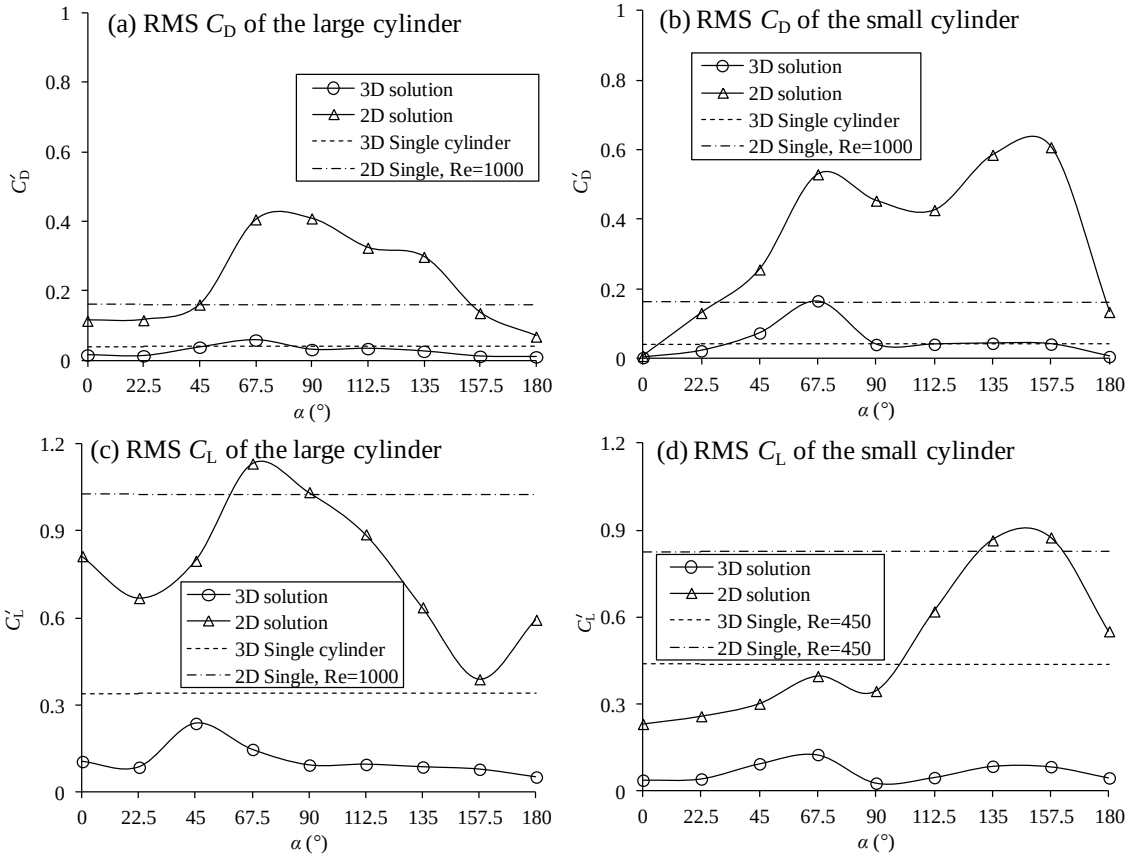

Fig. 7.6 Variations of RMS force coefficients with α for Re = 1000

The mean lift coefficient on the large cylinder is non-zero except for α = 0° and 180°. The variation of the mean drag coefficient of the small cylinder is similar to that of the large cylinder. The maximum mean lift coefficient on the small cylinder occurs at α = 22.5° and 45°, where the flow accelerates due to the presence of the large cylinder. From Fig. 7.5, it can be seen that the variation trends of the mean force coefficients with the position angle α calculated from different numerical models are similar to each other and close to the measured data. However, quantitatively, the differences between different models are obvious. The difference between the 2D and the 3D results is mainly due to the variation of the flow in the spanwise direction of the cylinder is not considered in the 2D model. The difference between the 3D results and the experimental data is mainly due to the difference in the Reynolds number.

Fig. 7.6 shows the variation of the root-mean-square (RMS) lift coefficient with the position angle α, together with the numerical results based on the 2D NS equations. Although the mean force coefficients based on the 2D NS equations seem to be similar to those based

on the 3D NS equations as shown in Fig. 7.5, the RMS force coefficients are significantly overestimated based by the 2D Model. Previous independent investigations also showed that the RMS lift coefficient for *Re* = 1000 obtained from 2D simulations is significantly greater than that from the 3D simulations (Tong *et al*., 2015). The 3D results of the RMS drag and lift coefficients of both cylinders occur when the small cylinder is located upstream shoulder of the large cylinder (α = 45° or 67.5°). The maximum RMS drag coefficients of the large and the small cylinders are 0.041 and 0.162, respectively, and they occur both at α = 67.5°. The maximum RMS lift coefficients of the large and the small cylinders are 0.237 and 0.093, and occur at α = 45° and 67.5°, respectively. The RMS drag coefficient on the large cylinder from the 2D numerical model follows a similar trend to that from the 3D model, but is significantly greater than the latter. In contrast to those obtained from the 3D model, the maximum drag and lift coefficients of the small cylinder from the 2D model occur at about α = 135° and 157.5° when the small cylinder is behind the large cylinder. From Fig. 7.6, it can be seen that the RMS drag and lift coefficients on both cylinders are reduced significantly compared with their counterparts of a single cylinder in the 3D numerical results, except for the RMS drag coefficient of the small cylinder at α = 67.5°, which is very close to that of a single cylinder.

7.3.3 VORTEX SHEDDING FREQUENCY

The vortex shedding frequencies around both cylinders are determined by conducting Fast Fourier Transform (FFT) of the lift coefficients and the FFT spectra are shown in Fig. 7.7. The dominant frequencies of the lift coefficient of the two cylinders are found to be the same because there is only one Vortex Street in the wake. Tsutsui *et al*. (1997) found two frequencies in the lift coefficients for position angles α between 90° and 130° and the two frequencies are very close to each other (less than about 15% difference). In Fig. 7.7 the secondary peak can also be seen for $67.5° \le \alpha \le 112.5°$. However, the amplitudes of these secondary peaks are much smaller than that of the primary peaks. In this study, the Strouhal number is determined based on the frequencies corresponding to the primary peak. The Strouhal number is defined based on the lift coefficient of the cylinders as $S_t = fD/U$, where f is the frequency of the oscillation of the lift coefficient.

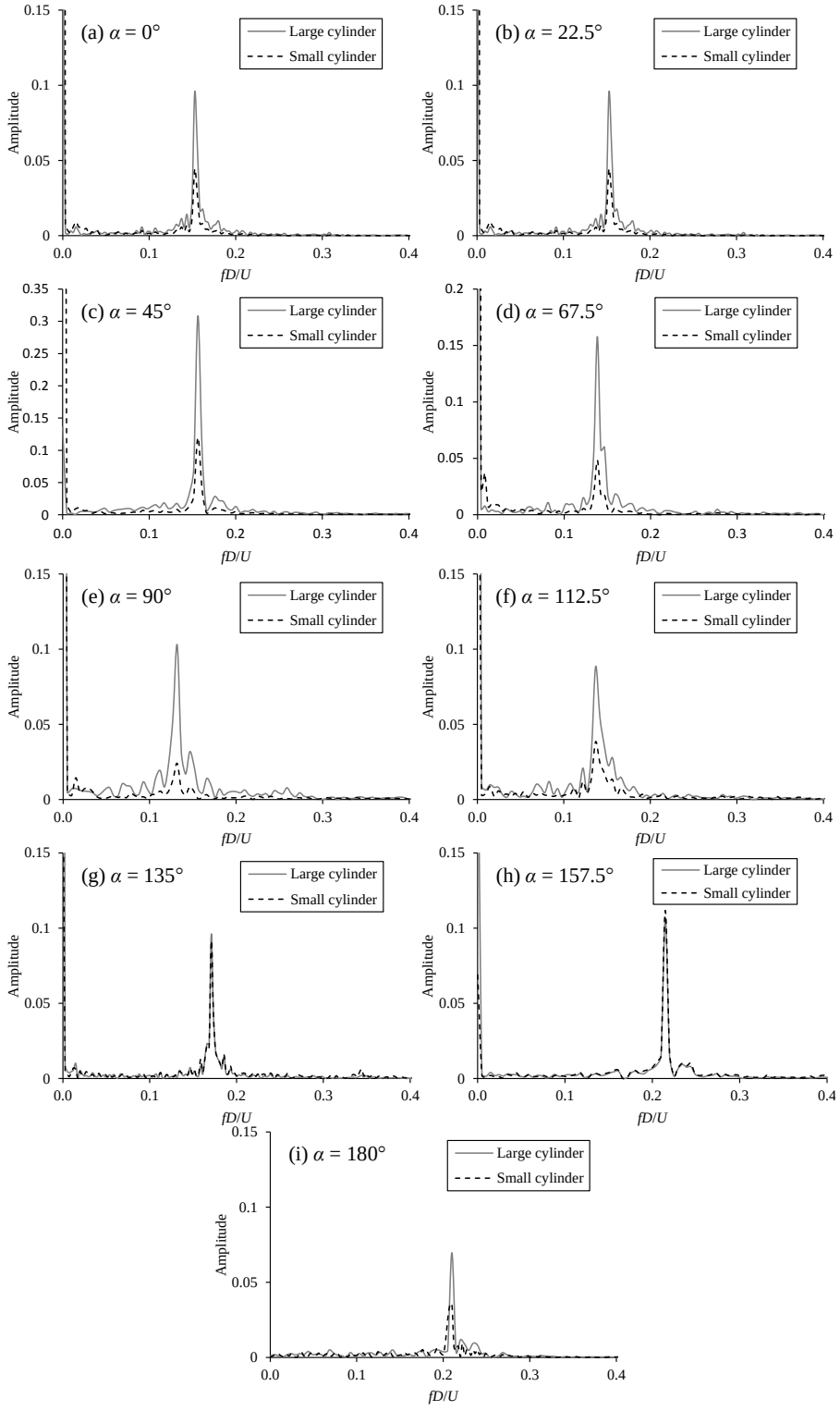

Fig. 7.7 Amplitude spectra of the lift coefficient for large and small cylinders: (a) α = 0°, (b) α = 22.5°, (c) α = 45°, (d) α = 67.5°, (e) α = 90°, (f) α = 112.5°, (g) α = 135°, (h) α = 157.5° and (i) α = 180°.

Fig. 7.8 shows the variation of the Strouhal number with the position angle α of the small cylinder, together with the experimental data in Tsutsui *et al.* (1997) and two-dimensional numerical results in Zhao *et al.* (2007). The two values for each angle α in the range of 90°-

130° correspond to the so-called reattachment state as in Tsutsui *et al*. (1997) and Zhao *et al*. (2007). The Strouhal number corresponding to the secondary peak in the power spectra of the lift coefficient is not included in Fig. 7.8 because it is much weaker than the primary peak.

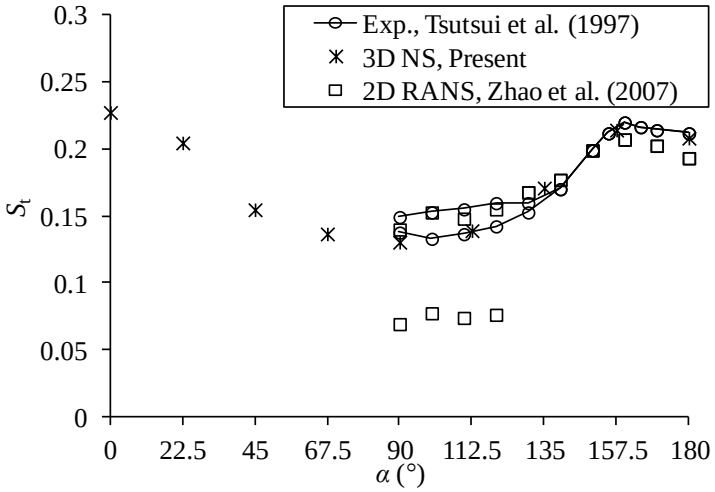

Fig. 7.8 Variation of the Strouhal number with α

The Strouhal number decreases with increasing α as the small cylinder is in the upstream positions ($0° \le \alpha \le 90°$) and increases with increasing α *as* the small cylinder is located at the downstream positions ($90° \le \alpha \le 180°$), as shown in Fig. 7.8. The minimum Strouhal number occurs when the small cylinder is positioned nearly about side-by-side ($67.5° < \alpha < 112.5°$) with the main cylinder. The reason for this is that, when the two cylinders are in side-by-side arrangement, increased dimension of the system in the cross-flow direction increases the vortex shedding period. The vortex shedding period is reduced also because the jet flow through the gap weakens the interaction of the vortices in the wake of the cylinder which will be discussed in detail in the next section. The maximum Strouhal number is observed when the small cylinder is located either in front ($\alpha = 0°$) or behind ($\alpha \ge 157.5°$) of the main cylinder. This is because the streamlined configuration reduces the dimension of the system in the cross-flow direction and makes the interaction between the shear layers from the two sides of the large cylinder easier. The calculated Strouhal numbers agree well with experimental results in Tsutsui *et al*. 1997.

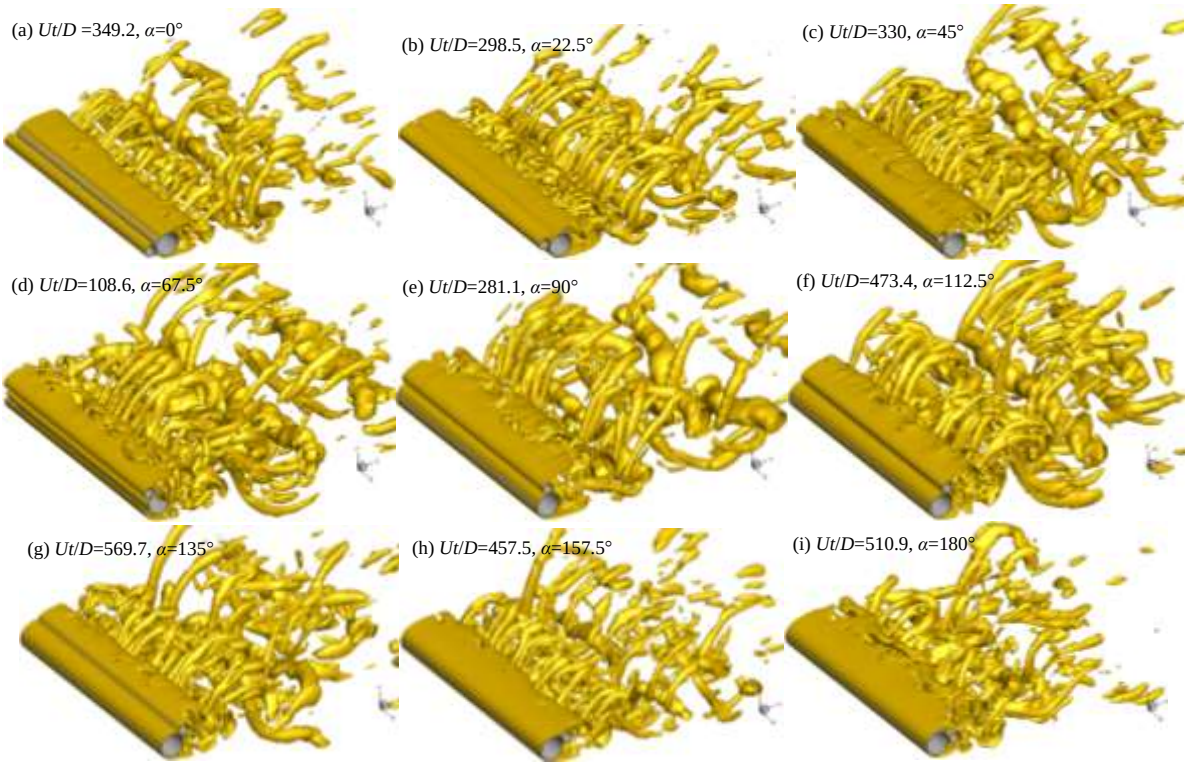

Fig. 7.9 Vortex structures at the instants when the lift coefficient reaches its maximum value represented by the iso-surfaces of e_2= -0.5

7.3.4 WAKE FLOW PATTERNS

Fig. 7.9 shows the iso-surface of e_2 at instants when the lift coefficient of the large cylinder reaches its maximum value for all the position angles. The distortion of the spanwise vortices and the development of the streamwise vortices can be clearly seen in Fig. 7.9. When Re = 1000, the wake structure of a single cylinder is in Mode B, which is featured by the generation of strong streamwise vortices and the dissipation of the spanwise vortices (Williamson, 1988). The wake flow patterns in Fig. 7.9 are very similar to the Mode B wake flow with strong streamwise vortices. At a few diameters downstream of the cylinders, the spanwise vortices are hardly identifiable using the e_2=-0.5 iso-surfaces.

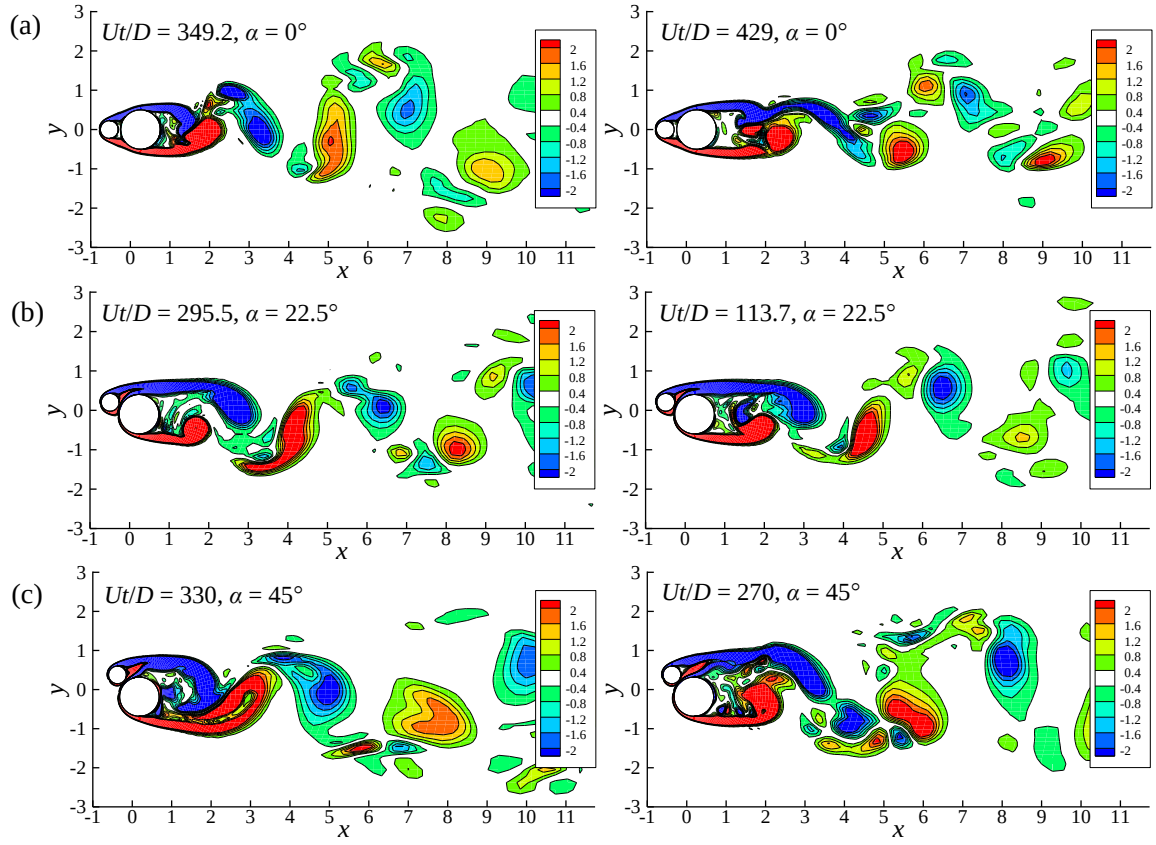

Fig. 7.10 Contours of axial vortices at the mid-section (z = 4.8) of the two cylinders: (a) α=0°, (b) α=22.5° and (c) α=45°

The cross-sectional flow features are visualized using the contours of the vorticities on planes perpendicular to the cylinders. The vorticity components in the x-, y- and z-directions are defined as $\omega_x = \partial w/\partial y - \partial v/\partial z$, $\omega_y = \partial u/\partial z - \partial w/\partial x$ and $\omega_z = \partial v/\partial x - \partial u/\partial y$ respectively. Fig. 7.10 shows the contours of the axial vorticity (ω_z) at the mid-section (z= 4.8) for small position angles of α = 0°, 22.5° and 45° at the instants when the lift coefficient on the large cylinder is at its maximum value. For α = 0°, no flow exists between the gap, and the vortex shedding from the large cylinder is similar to that of a single body. The oscillation of the lift coefficient due to the vortex shedding is weak because the upstream cylinder makes the whole structure more streamlined. As the angle α is increased from 0° to 45°, the velocity through the gap also increases. The jet flow from the gap merges into the shear layer from the top of the small cylinder. This enhances the shear layer from the top side of the large cylinder, and as the result, increases the oscillation amplitude of the lift coefficient of the large cylinder as shown in Fig. 7.6 compare with other position angles. The vortex shedding from the cylinders for $\alpha \le 45°$ is very similar to that of a single cylinder and the vortex shedding mode in Fig. 7.10 is called the upstream interference mode in this study.

The time histories of the drag and lift coefficients on both cylinders vary with time in a beating pattern at α = 67.5° (Fig. 7.3d). This beating phenomenon in forces is related to the changes of flow between one pattern and another alternatively, leading to the increase and decrease of the amplitude of the force coefficients. To explain this further, Fig. 7.11 shows the contours of the instantaneous spanwise vorticity at the mid-section of the cylinders at α = 67.5°. Fig. 7.11 (a – d) correspond to the instants when the amplitudes of the forces on both cylinders are large, while Fig. 7.11 (e – h) correspond to the instants when the amplitudes are small (see also the time histories of the force coefficients in Fig. 7.3 (d)). From Fig. 7.11, it can be seen how the jet flow through the gap affects the wake flow structure and hence the forces. The forces of the two cylinders oscillate almost regularly with time because of the vortex shedding generated by the interaction between the two shear layers from the top of the small cylinder and the bottom of the large cylinder. It has been found that the formation length of the wake vortices affects the velocity fluctuation in the wake and the force oscillation. The formation length is defined as "that point downstream of the body where the velocity fluctuation level has grown to a maximum, and thereafter decays downstream" (Bearman, 1965). An increase in the formation length leads to a decrease in the level of velocity fluctuation and a decrease in the base suction (Bearman, 1965; Griffin, 1995; Kim and Durbin, 1988). In Fig. 7.11 (a – d), the jet flow through the gap bends downward and attaches to the rear surface of the large cylinder. This allows the shear layer from the top of the small cylinder to form vortices near the cylinder. The biased gap flow toward the large cylinder weakens the oscillation of the forces on the large cylinder compared to that of a single isolated cylinder. The reduction of the force due to biased gap flow for flow past two side-by-side identical cylinders has been observed in Afgan *et al*. (2011), Ko *et al*. (1996). The gap flow detaches from the rear surface of the large cylinder intermittently. It can be seen in Fig. 7.11 (e – h) that the flow from the gap is nearly in the horizontal direction but slightly biases toward the small cylinder. This delays the interaction between the shear layers from the two sides of the system and further reduces the amplitude of the force coefficients of the cylinders.

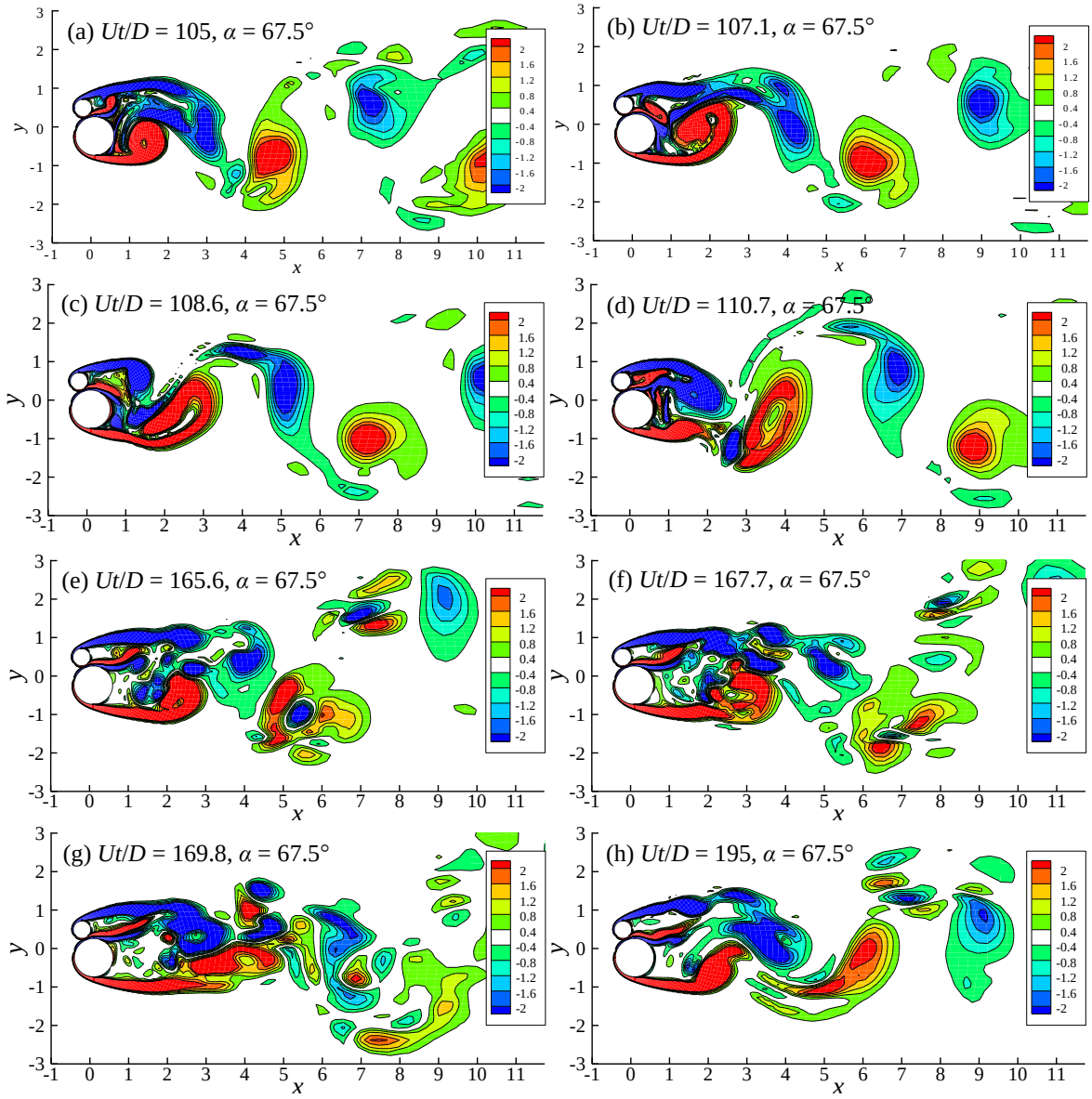

Fig. 7.11 Instantaneous contours of vorticity in the *z*-direction at the mid-section (z = 4.8) of the two cylinders for α = 67.5°

By conducting experimental investigation of flow through two cylinders at a nearly side-by-side arrangement with a diameter ratio of 0.5, Ko *et al*. (1996) found that the characteristics of the gap flow through two cylinders with a diameter ratio of 0.5 is very similar to that of two side-by-side cylinders of an equal diameter. Two flow modes were observed by Ko *et al*. (1996): the gap flow biases toward the large cylinder in Mode 1 and toward the small cylinder in Mode 2.

The two flow modes are also clearly observed in Fig. 7.11. When the gap flow is biased towards the large cylinder, it attaches to the rear surface of the large cylinder, forming a wall jet. Tsutsui *et al*. (1997) define this phenomenon as “reattachment”. However, when the gap

flow is biased towards the small cylinder, instead of attaching to the back surface of the small cylinder, the flow through the gap forms a free-jet that biases toward the small cylinder as shown in Fig. 7.11 (e – h). This is because the small cylinder cannot generate strong enough wake to suck the gap flow towards its back surface. The intermittent change of the flow pattern for α = 90° (Fig. 7.12) is similar to that for α = 67.5° (Fig. 7.11). The gap flow attaches to the rear surface of the large cylinder and in Fig. 7.12 (a – c) and detaches in Fig. 7.12 (d). The flow mode observed at α = 67.5° and 90° is defined as the intermittent attached gap flow mode.

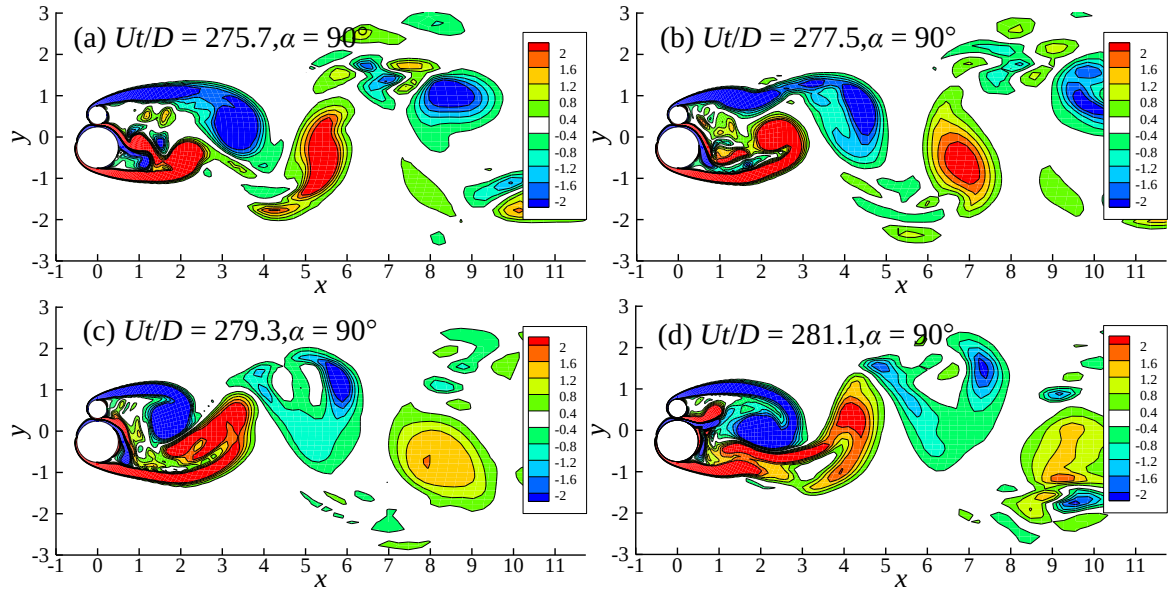

Fig. 7.12 Instantaneous contours of vorticity in the z-direction at mid-section (z = 4.8) of the two cylinders for α = 90°

When the position angle α is increased to 112.5° and 135°, the gap flow is always biased towards the large cylinder and attaches to the back surface of the large cylinder as shown in Fig. 7.13. The alignment of the two cylinders forces the gap jet flow to be in the diagonally downward direction and to attach to the back surface of the large cylinder. Free jet flow (separation of the gap flow from the back of the large cylinder) as observed when α = 67.5° and 90° is not observed. The wake flow for α = 112.5° and 135° is defined as the attached gap flow mode. When the gap flow attaches to the rear surface of the large cylinder, the separation point on the large cylinder becomes very close to its most downstream point, leading to a significant reduction in the oscillation amplitude of the lift coefficient.

When the position angle is 157.5° and 180°, the gap flow disappears and the small cylinder affects the interaction between the two shear layers from the two sides of the large cylinder as shown in Fig. 7.14. The vortex shedding in the wake of the cylinder is similar to that of a single cylinder. However, due to the existence of the small cylinder, the vortex formation length of the large cylinder is longer than that of a single cylinder, leading to a reduction of the amplitude of the lift force oscillation. Because the interaction between the top and bottom shear layers occurs behind the small cylinder, the vortex shedding does not lead to strong oscillation of the lift force of the small cylinder. The vortex shedding mode for α = 157.5° and 180° is called wake interference mode because the small cylinder affects the interference between the two shear layers from the large cylinder in the wake.

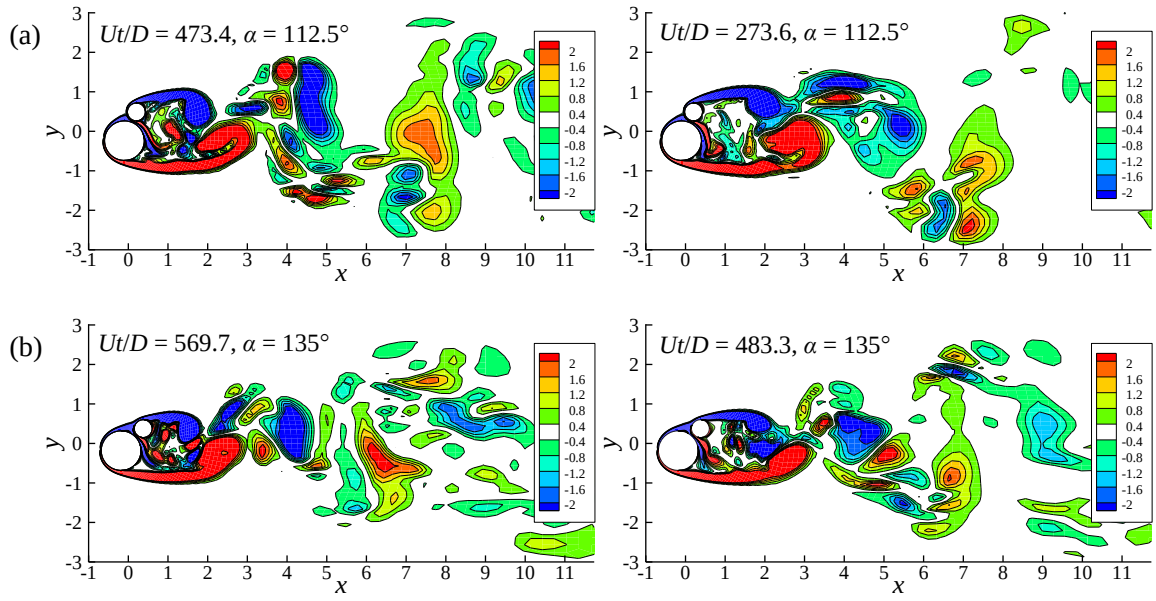

Fig. 7.13 Contours of axial vorticity at the mid-section (z = 4.8) of the two cylinders: (a) α = 112.5° and (b) α = 135°

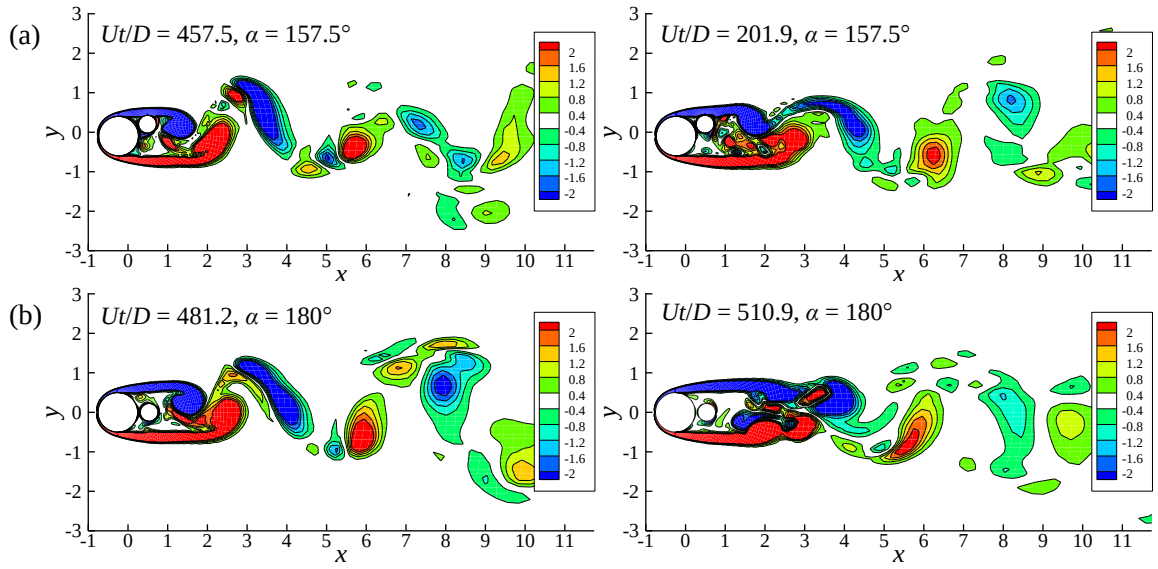

Fig. 7.14 Contours of axial vorticity for large position angles at the mid-section (z = 4.8) of the two cylinders: (a) α = 157.5° and (b) α = 180°

7.4 CONCLUSIONS

Three-dimensional numerical simulations of flow past two circular cylinders of different diameters in close proximity for *Re* = 1000 (based on the large cylinder's diameter) at a diameter ratio of 0.45 and a gap ratio of 0.0625 are conducted. The effect of the position angle of the small cylinder (α) relative to the large cylinder is studied for α ranging from 0° to 180° with an interval of 22.5°. The results are summarised as follows:

Depending on the position angle of the small cylinder, the wake flow can be divided into four modes: the upstream interference mode for α = 0°, 22.5° and 45°, the intermittent attached gap flow mode for α = 67.5° and 90°, the attached gap flow mode for α = 112.5° and 135° and the wake interference mode for α = 157.5° and 180°. The flow through the gap attaches and separates from the back surface of the large cylinder in the intermittent attached gap flow mode, and always attaches to the back surface of the large cylinder in the attached gap flow modes.

The calculated RMS force coefficients using the 3D model on both cylinders are found to be significantly smaller than that of a single cylinder. While the 2D numerical model predicts the similar mean force coefficients to those by the 3D model, it overestimates the RMS force coefficients significantly. The maximum RMS drag and lift coefficients from 3D simulation occur at either α = 45° or 67.5° for the large and small cylinders respectively. When the two cylinders are in a near side-by-side arrangement ($67.5° \le \alpha \le 112.5°$), the RMS lift

coefficients on both cylinders are reduced significantly, despite the increase in the mean drag coefficient. When $67.5° \le \alpha \le 112.5°$, the jet flow from the gap either attaches to the back surface of the large cylinder or is biased towards the small cylinder, forming a free jet flow. An attached gap flow to the rear surface of the large cylinder reduces the RMS lift coefficient by moving the flow separation position point towards downstream part of the cylinder surface, while a free jet flow reduces the RMS lift coefficient by weakening the interferences between the two shear layers from the two sides of the cylinder system.

CHAPTER 8

CONCLUSIONS AND FUTURE WORKS

8.1 CONCLUSIONS

Flow past inclined cylinders is studied extensively in this thesis to quantify the effect of the inclination angle of the cylinders on the vortex shedding flow and the forces of the cylinders by Direct Numerical Simulations (DNS). The simulations mainly focus on relatively low Reynolds numbers in the turbulent flow regime (Re<1000), considering the affordability of the computational time. The simulations are conducted in the end-effect free condition because the periodic boundary condition is used at the two end boundaries of the cylinder. Both a single isolated cylinder and two-cylinders in different arrangement are studied, including: one cylinder in uniform flow (Chapter 3), one cylinder close to a plane boundary (Chapter 4), two cylinders in side-by-side arrangement (Chapter 5), two cylinders in tandem arrangement (Chapter 6), two cylinders of different diameters (Chapter 7, only right attack angle is addressed in this case). While the research outcomes of each chapter have been listed in the conclusion section of the chapter and will not be repeated here, this chapter mainly lists the future work that will complete and improve the research in the topic of flow interaction with inclined cylinders.

8.2 FUTURE WORKS

While flow past cylinders at right attack angle has been investigated in numerous studies, the understanding of flow past inclined cylinders is far from complete. Following are the proposed future works that would improve our understanding of flow past inclined cylinders.

8.2.1 Flow past two cylinders of different diameters at oblique attacks

Chapter 7 of this thesis successfully describe the flow past two circular cylinders of different diameters at various positions of small cylinder relative to large cylinder on force coefficients and wake flow patterns in right attack case but practically in many engineering applications, when these structures experience the flow at different attacking angles (oblique attack angles) then there may have significant effects on vortex shedding and force characterisations on these structures while the flow is transiting from 2D to 3D in subcritical regime and is not investigated so far. Since the effects of attacking angles on cylindrical

structures can be significant it should not to be neglected and hence worth investigating as a future work.

8.2.2 Oscillatory flow past inclined cylinders

This thesis only studies steady flow past inclined cylinders. In practical offshore oil and gas engineering, cylindrical structures are subject to ocean waves, especially in the shallow water region. The wave motion is generally modelled by oscillatory flow when hydrodynamics of small scale cylindrical structures are studied. In addition to the Reynolds number, the Keulegan–Carpenter (also) number affects the flow and the effects of the KC number dominate that of the Reynolds number in the turbulent flow regime. Understanding the effects of the KC number on the applicability of the independence principle in oscillatory flow cases would improve the design of offshore cylindrical structures. However, this has not been addressed so far. The present numerical model can be implemented in the oscillatory flow cases.

8.2.3 Vortex induced vibrations of inclined cylinders

Because the vibration of cylinders in fluid flow is mainly due to the vortex shedding, it is commonly called vortex-induced vibration (VIV). The majority of existing studies of VIV of cylinders in fluid flow has been focused on the case where the flow direction is perpendicular to the cylinders. The Petrov-Galerkin Finite Element Model (PG-FEM) that was used in this thesis has been proved to be able to simulate VIV accurately (Zhao et al., 2014; Zhao, 2015). VIV of multiple inclined cylinders can be simulated using the numerical model to find out the influence of the interference between cylinders on the vibration.

8.2.4 Hydrodynamics around curved cylinders

Many cylindrical structures in offshore engineering are curved structures, such as mooring cables, catenary subsea risers, curved pipelines, etc. Flow around these structures is totally three-dimensional and very few numerical studies have been performed to simulate the hydrodynamics of these structures, mainly due to the limitation of the computer power. The fast development computing technology allows the researchers to conduct more and more complex numerical simulations. For example, iVEC supercomputer centre, where all the parallel calculations in this thesis have been performed, update the computing facilities very frequently to provide researchers with up to date computing power.

8.2.5 Flow past real pipelines in offshore engineering

In the thesis, flow past circular cylinders at relatively low Reynolds numbers was studied to find out the fundamental mechanisms of the effects of the flow approaching angle on the flow patterns and the forces on the cylinders. Future study should address the problems occurring the practical engineering.

The Reynolds number is very high in offshore pipeline engineering (up to 10^5 to 10^6). It is impossible to simulate the flow at such high Reynolds numbers using Direct Numerical Simulations unless the computer power is advanced significantly and this is unlikely to happen in the near future. Advanced turbulence models need to be used to simulate the flow at high Reynolds numbers.

In offshore engineering, pipelines are sometimes on the seabed surface or semi buried in the seabed sediment. The effects of the embedment of the pipelines in the seabed should be studied in the future work. The pipeline surfaces are generally rough in reality, the effects of the roughness on the flow and force need to studied in the future work.

References:

Afgan, I., Kahil, Y., Benhamadouche, S., Sagaut, P., 2011. Large eddy simulation of the flow around single and two side-by-side cylinders at subcritical Reynolds numbers. *Physics of Fluids* 23, 075101.

Akoz, M.S., Sahin, B., Akilli, H., 2010. Flow characteristic of the horizontal cylinder placed on the plane boundary. *Flow Measurement and Instrumentation* 21, 476–487.

Alam, M. M., Moriya, M., Sakamoto, H., 2003a. Aerodynamic characteristics of two side-by-side circular cylinders and application of wavelet analysis on the switching phenomenon. *Journal of Fluids and Structures* 18, 325-346.Alam, M.M., Moriya, M., Takai, K., Sakamoto, H., 2003b., Fluctuating fluid forces acting on two circular cylinders in a tandem arrangement at a subcritical Reynolds number. *Journal of Wind Engineering and Industrial Aerodynamics* 91, 139-54.

Barkley, D., Henderson, R. D., 1996. Three-dimensional Floquet stability analysis of the wake of a circular cylinder. *Journal of Fluid Mechanics* **322**, 215–241.

Bearman, P.W., 1965. Investigation of the flow behind a two-dimensional model with a blunt trailing edge and fitted with splitter plates. *Journal of Fluid Mechanics* 21, 241- 255.

Bearman, P. W., Wadcock, A. J., 1973. Interaction between a pair of circular cylinders normal to a stream. *Journal of Fluid Mechanics* 61, 499-511.

Bearman, P.W., Zdravkovich, M.M., 1978. Flow around a circular cylinder near plane boundary. *Journal of Fluid Mechanics* 89, 33-47.

Bimbato, A.M., Pereira, L.A.A., Hirata, M.H., 2013. Suppression of vortex shedding on a bluff body. *Journal of Wind Engineering and Industrial Aerodynamics* 121, 16-28.

Bloor, M. S., 1964. The transition to turbulence in the wake of a circular cylinder. *Journal of Fluid Mechanics* 19, 290-&.

Braza, M., Chassaing, P., Minh, H.H., 1986. Numerical study and physical analysis of the pressure and velocity fields in the near wake of a circular cylinder. *Journal of Fluid Mechanics* 165, 79-130.

Braza, M., Faghani, D., and Persillon, H., 2001. Successive stages and the role of natural vortex dislocations in three-dimensional wake transition. *Journal of Fluid Mechanics* **439**, 1–41.

Buresti, G., Lanciotti, A., 1992. Mean and fluctuating forces on a circular cylinder in cross flow near a plane surface. *Journal of Wind Engineering and Industrial Aerodynamics* 41, 639-650.

Camarri, S., Giannetti, F,. 2010. Effect of confinement on three-dimensional stability in the wake of a circular cylinder. *Journal of Fluid Mechanics* 642, 477-487.

Carmo, B.S., Meneghini, J.R., 2006. Numerical investigation of the flow around two circular cylinders in tandem. *Journal of Fluids and Structures* 22, 979-88.

Carmo, B.S., Meneghini, J.R., Sherwin, S.J., 2010.Secondary instabilities in the flow around two circular cylinders in tandem. *Journal of Fluid Mechanics* 644, 395-431.

Chen, L., Tu, J. Y., Yeoh, G. H., 2003. Numerical simulation of turbulent wake flows behind two side-by-side cylinders. *Journal of Fluids and Structures* 18, 387-403.

Cheng, B., Su, T.C., 2012. Investigation of flow past circular near planar boundary. *International Journal of Offshore and Polar Engineering* 22 (4), 276-281.

Chiba, K., Horikawa, A., 1987. Numerical solution for the flow of viscoelastic fluids around an inclined circular cylinder. II. The hydrodynamic force on a circular cylinder. *Rheol. Acta* **26**, 255–265.

Dalton, C., Xu, Y., Owen, J.C., 2001. The Suppression of lift on a circular cylinder due to vortex shedding at moderate Reynolds numbers. *Journal of Fluids and Structures* 15, 617–28.

Dipankar, A., Sengupta, T. K., Talla, S. B., 2007. Suppression of vortex shedding behind a circular cylinder by another control cylinder at low Reynolds numbers. *Journal of Fluid Mechanics* 573, 171-190.

Eisenlhr, H., Eckelmann, H., 1989. Vortex splitting and its consequences in the vortex street wake of cylinders at low Reynolds number. *Physics of Fluids* 1, 189-192.

Faltinsen, O. M., 1990. Sea loads on ships and offshore structures. *Cambridge University Press.*

Gioria, R. S., Meneghini, J. R., Aranha, J. A. P., Barbeiro, I. C., Carmo, B. S., 2011. Effect of the domain spanwise periodic length on the flow around a circular cylinder. *Journal of Fluids and Structures* 27, 792-797.

Gerrard, J. H., 1978. Wakes of cylindrical bluff bodies at low Reynolds number. *Philosophical transactions of the royal society a-Mathematical Physical and Engineering Sciences* 288, 351-382.

Griffin, O.M., 1995. A note on bluff body vortex formation. *Journal of Fluid Mechanics* 284, 217-224.

Grass, A.J., Raven, P.W.J., Stuart, R.J., Bray, J.A., 1984. The influence of boundary layer velocity gradients and bed proximity on vortex shedding from free spanning pipelines. *Journal of Energy resources Technology, Transactions of ASME* 106, 70-78.

Gregory, J. S., Matthew, J. F., kris, R., 2009. Wake instabilities with incidence angle variation. *Journal of Fluid Mechanics* 630, 43-69.

Hammache, M., Gharib, M., 1989. A novel method to promote parallel shedding in the wake of circular cylinders. *Physics of Fluids* A**1**, 1611–1614.

Hesam, S. M., Navid, N., 2011. Numerical simulation of flow over two side-by-side circular cylinders. *Journal of Hydrodynamics* 23, 792-805.

Ishigai, S., Nishikawa, E., Cho, K., 1972. Experimental study of structure of gas flow in tube banks with tube axes normal to flow. *Bulletin of the JSME* vol. 15, pp. 949-956.

Jensen, B.L., Sumer, B.M., Jensen, H.R., Fredsøe, J., 1990. Flow around and forces on a pipeline near a scoured bed in steady current. *Journal of Offshore Mechanical and Arctic Energy* 112, 206-213.

Jeong, J., Hussain, F., 1995. On the identification of a vortex. *Journal of Fluid Mechanics* 285, 69–74.

Jiang, R., Lin, J., 2012. Wall effects on flows past two tandem cylinders of different diameters. *Journal of Hydrodynamics* 24, 1-10.

Karniadakis, G.E., Triantafyllou, G.S., 1992. Three-dimensional dynamics and transition to turbulence in the wake of bluff objects. *Journal of Fluid Mechanics* 238, 1-30.

Kim, H. J., Durbin, P. A., 1988. Investigation of the flow between a pair of cylinders in the flopping regime. *Journal of Fluid Mechanics* 196, 431–448.

King, R., 1977. Vortex excited oscillations of yawed circular cylinders. ASME *Journal of Fluids Engineering* **99**, 495–502.

Ko, N.W.M., Wong, P.T.Y., Leung, R.C.K., 1996. Interaction of flow structures within bistable flow behind two circular cylinders of different diameters. *Experimental Thermal and Fluid Science* 12, 33-44.

Kondo, N., Matsukuma, D., 2005. Three-dimensional computation for flow around two circular cylinders in side-by-side arrangement by a third-order upwind finite element method. *International Journal of Computational Fluid Dynamics* 19, 37-43.

Kozakiewicz, A., Fredsøe, J., Sumer, B.M., 1995. Forces on pipelines in oblique attack: steady current and waves. *In Proceedings of the 5th International Offshore and Polar Engineering Conference*, The Hague, The Netherlands (International Society of Offshore and Polar Engineers) 2, 174–183.

Lam, K., Lin, Y.F., Zou, L., Liu, Y., 2010. Investigation of turbulent flow past a yawed wavy cylinder. *Journal of Fluids and Structures* 26, 1078-1097.

Lei, C., Cheng, L., Kavanagh, K., 1999. Re-examination of the effect of a plane boundary on force and vortex shedding of a circular cylinder. *Journal of Wind Engineering and Industrial Aerodynamics* 80, 263-286.

Lei, C., Cheng, L., Kavanagh, K., 2000. A finite difference solution of the shear flow over a circular cylinder. *Journal of Ocean Engineering* **27**, 271–90.

Lei, C., Cheng, L., Kavanagh, K., 2001. Spanwise length effects on three-dimensional modelling of flow over a circular cylinder. *Computer Methods in applied Mechanics and Engineering* 190, 2909-2923.

Lei, C., Cheng, L., Armfield, S.W., Kavanagh, K., 2000. Vortex shedding suppression for flow over a circular cylinder near a plane boundary. *Ocean Engineering* 27, 1109-1127.

Lee, S.J., Lee, S.I., Park, C.W., 2004. Reducing the drag on a circular cylinder by upstream installation of a small control rod. *Fluid Dynamic Research* 34, 233–250.

Lewis, C.G., Gharib, M., 1992. An exploration of the wake three dimensionalities caused by a local discontinuity in a cylinder diameter. *Physics of Fluids a-Fluid Dynamics* 4, 104-117.

Lin, J.C., Yang, Y., Rockwell, D., 2002. Flow past two cylinders in tandem: Instantaneous and averaged flow structure. *Journal of Fluids and Structures* 16, 1059-71.

Lin, W.J., Lin, C., Hsieh, S.C. Dey, S., 2009. Flow Characteristics around a Circular Cylinder Placed Horizontally above a Plane Boundary. *Journal of Engineering Mechanics* 135(7), 697-716.

Lin, J., Jiang, R., Cheng, Z., Ku, X., 2013. Poiseuille flow-induced vibrations of two cylinders in tandem. *Journal of Fluids and Structures* 40, 70-85.

Liu, M.-M., Lu, L., Teng, B., Zhao, M., Tang, G.-Q., 2014. Re-examination of laminar flow over twin circular cylinders in tandem arrangement. *Fluid Dynamics Research* 46, 025501.

Liu, Y., So, R. M. C., Lau, Y. L., Zhou, Y., 2001. Numerical studies of two side-by-side elastic cylinders in a cross-flow. *Journal of Fluids and Structures* 15, 1009-1030.

Ljungkrona, L., Sunden, B., 1993.Flow visualization and surface pressure measurement on 2 tubes in an in-line arrangement. *Experimental Thermal and Fluid Science* 6, 15-27.

Lucor, D., Karniadakis, G.E.M., 2003. Effects of oblique inflow in vortex-induced vibrations. *Flow, Turbulence and Combustion* 71, 375–389.

Mansy, H., Yang, P.M., Williams, D.R., 1994. Quantitative measurements of three-dimensional structures in the wake of a circular cylinder. *Journal of Fluid Mechanics* 270, 277-296.

Marshall, J.S., 2003. Wake dynamics of a yawed cylinder. ASME *Journal of Fluids Engineering* **125**, 97–103.

Meneghini, J.R., Saltara, F., Siqueira, C.L.R., Ferrari J.A., 2001. Numerical simulation of flow interference between two circular cylinders in tandem and side-by-side arrangements. *Journal of Fluids and Structures* 15, 327–350.

Miller, G.D., Williamson, C.H.K., 1994. Control of three-dimensional phase dynamics in a cylinder wake. *Experiments in Fluids* 18, 26-35.

Mittal, S., Kumar, V., Raghuvanshi, A., 1997. Unsteady incompressible flows past two cylinders in tandem and staggered arrangements. *International Journal for Numerical Methods in Fluids* 15, 1315–44.

Niemann, H.J., Hölscher, N., 1990. A review of recent experiments on the flow past circular cylinders. *Journal of Wind Engineering and Industrial Aerodynamics* 33, 197-209.

Norberg, C., 1994. An experimental investigation of the flow around a circular cylinder: influence of aspect ratio. *Journal of Fluid Mechanics* 258, 287–316.

Norberg, C., 2001. Flow around a circular cylinder: Aspects of fluctuating lift. *Journal of Fluids and Structures* 15, 459-469.

Ohya, Y., Okajima, A., Hayashi, M., 1989. Wake Interference and Vortex Shedding. *Encyclopedia of Fluid Mechanics* 8, 322-389.

Ong, M.C., Utnes, T., Holmedal, L.E., Myrhaug, D., Pettersen, B., 2010. Numerical simulation of flow around a circular cylinder close to a flat seabed at high Reynolds numbers using a k-ε model. Coastal Engineering 57, 931-947.

Ong, M.C., Utnes, T., Holmedal, L.E., Myrhaug, D., Pettersen, B., 2012. Near-bed flow mechanisms around a circular marine pipeline close to a flat seabed in the subcritical flow regime using a k-epsilon model. *Journal of Offshore Mechanics and Arctic Engineering-Transactions of the ASME* 134 (2), 021803.

Papaioannou, G.V., Yue, D.K.P., Triantafyllou, M.S., Karniadakis, G.E., 2006.Three-dimensionality effects in flow around two tandem cylinders. *Journal of Fluid Mechanics* 558, 387-413.

Prasad, A., Williamson, C. H. K., 1997. Three-dimensional effect in turbulent bluff-body wakes. *Journal of Fluid Mechanics* **343**, 235–265.

Prasad, A., Williamson, C. H. K., 1997. A method for the reduction of bluff body drag. Journal of Wind Engineering and Industrial Aerodynamics 71, 155-167.

Ramberg, S., 1983. The effects of yaw and finite length upon the vortex wakes of stationary and vibrating circular cylinders. *Journal of Fluid Mechanics* 128, 81–107.

Robichaux, J., Balachandar, S., Vanka, S. P., 1999. Three-dimensional floquet instability of the wake of square cylinder. *Physics of Fluids* 11, 560-578.

Roshko, A., 1954. On the development of turbulent wakes from vortex streets. *National Advisory Committee for Aeronautics (NACA) Report* 1191, 1-23.

Roshko, A., 1961. Experiments on the flow past a circular cylinder at a very high Reynolds numbers. *Journal of Fluid Mechanics* 10, 345-356.

Roshko, A., Steinolfson, A. and Chattoorgoon, V., 1975. Flow forces on a cylinder near a wall or near another cylinder. *In: Proceedings Of the 2nd US Conference Wind Engng Research* Fort Collins, paper IV-15.

Sakamoto, H., Tan, K., Haniu, H., 1991. An optimum suppression of fluid forces by controlling a shear layer separated from a square prism. *ASME Journal of Fluids Engineering* 113, 183–189.

Sarpkaya, T., Raines, T. S., Trytten, D. O., 1982. Waves forces on inclined smooth and rough circular cylinders. *Offshore Technology Conference* paper no. 4227.

Scarano, F., Poelma, C., 2009. Three-dimensional vorticity patterns of cylinder wakes. *Experiments on Fluids* 47, 69–83.

Schewe, G., 1983. On the force fluctuations acting on a circular cylinder in cross-flow from subcritical up to transcritical Reynolds numbers. *Journal of Fluid Mechanics* 133, 265-285.

Strykowski, P.J., Sreenivasan, K.R., 1990. On the formation and suppression of vortex shedding at low Reynolds numbers. *Journal of Fluid Mechanics* 218, 71–107.

Sumer, B. M. and Fredsøe, J., 2006. Hydrodynamics around cylindrical structures. *Hydrodynamics Around Cylindrical Structures* 26, 1-531.

Sumner, D., 2010. Two circular cylinders in cross-flow: A review. *Journalof Fluids and Structures* **26,** 849-899.

Sumner, D., Richards, M. D., Akosile, O. O., 2005. Two staggered circular cylinders of equal diameter in cross-flow. *Journal of Fluids and Structures* 20, 255-276.

Surry, J., Surry, D., 1967. The effect of inclination on the Strouhal number and other wake properties of circular cylinders at subcritical Reynolds numbers. Technical Report, UTIAS Technical note No. 116, Institute for Aerospace Studies.

Taneda, S., 1965. Experimental investigation of vortex streets. *Journal of the Physical society of Japan* 20, 1714-1721.

Taniguchi, S., Miyakoshi, K., 1990. Fluctuating fluid forces acting on a circular cylinder and interference with plane wall. *Experiments in Fluids* 9, 197-204.

Thakur, A., Liu, X., Marshall, J.S., 2004. Wake flow of single and multiple yawed cylinders. *ASME Journal of Fluids Engineering* 126, 861–870.

Thapa, J., Zhao, M., Cheng, L., Zhou, T., 2015. Three-dimensional simulations of flow past two circular cylinders in side-by-side arrangements at right and oblique attacks. *Journal of Fluids and Structures*, 55, 64-83.

Tong, F., Cheng, L., Zhao, M., Zhou, T., Chen, X., 2014. The vortex shedding around four circular cylinders in an in-line square configuration. Physics of Fluids 26, 024112.

Tong, F., Cheng, L., Zhao, M., 2015. Two- and three-dimensional numerical simulations of steady flow past two cylinders in staggered arrangements. *Journal of Fluid Mechanics*, 765, 114-149.

Tritton, D.J., 1959. Experiments on the flow past a circular cylinder at low Reynolds numbers. *Journal of Fluid Mechanics* 6, 547-567

Tsutsui, T., Igarashi, T., Kamemoto, K., 1997. Interactive flow around two circular cylinders of different diameters at close proximity: experiment and numerical analysis by vortex method. *J. Wind Eng. Ind. Aerodyn* 69, 279–291.

Tsutsui, T., and Igarashi, T., 2002. Drag reduction of a circular cylinder in an air-stream. *Journal of Wind Engineering and Industrial Aerodynamics* 90, 527-541.

Varshney, K., 2012. Vortex structures in the wake of inclined cylinders. *International Journal of Research and Reviews in Applied Sciences* 11, 477-485.

Vanatta, C.W., 1968. Experiment on vortex shedding from yawed circular cylinders. *AIAA Journal* 6, 931-933.

Wang, X.K., Tan, S.K., 2008. Comparison of flow patterns in the near wake of a circular cylinder and a square cylinder placed near a plane wall. *Ocean Engineering* 35 (5-6), 458-472.

Williamson, C. H. K., 1985. Evolution of a single wake behind a pair of bluff-bodies. *Journal of Fluid Mechanics* 159, 1-18.

Williamson, C. H. K., 1988. The existence of two stages in the transition to three-dimensionality of a cylinder wake. *Physics of Fluids* 31, 3165–3168.

Williamson, C. H. K., 1989. Oblique and parallel modes of vortex shedding in the wake of a circular cylinder at low Reynolds numbers. *Journal of Fluid Mechanics* **206**, 579–627.

Williamson, C. H. K., 1991. Three-dimensional aspects and transition of the wake of a circular cylinder. *Turbulent Shear Flows* 7, 173-194.

Williamson, C. H. K., 1992. The natural and forced formation of spot-like dislocations in the transition of a weak. *Journal of Fluid Mechanics* **243**, 393–441.

Williamson, C. H. K., 1996. Vortex dynamics in the cylinder wake. *Annual Review of Fluid Mechanics* **28**, 477–539.

Williamson, C. H. K., 1996. Three-dimensional wake transition. *Journal of Fluid Mechanics* **328**, 345–407.

Xu, G., Zhou, Y., 2004. Strouhal numbers in the wake of two inline cylinders. *Experiments in Fluids.* 37, 248-256.

Yang, P. M., Mansy, H., Williams, D. R., 1993. Oblique and parallel wave interaction in the near wake of a circular cylinder. *Physics of Fluids* 5, 1657-1660.

Yoon, D.H., Yang, K.S., Choi, C.B., 2012. Three-dimensional wake structures and aerodynamics coefficients for flow past an inclined square cylinder. *Journal of Wind Engineering and Industrial Aerodynamics* 101, 34-42.

Zang, Z., Gao, F., Cui, J., 2013. Physical modeling and swirling strength analysis of vortex shedding from near-bed piggyback pipelines. *Applied Ocean Research* 40, 50‑59.

Zdravkovich, M. M., Pridden, D. L., 1977. Interference between 2 circular cylinders – series of unexpected discontinuities. *Journal of Industrial Aerodynamics* 2, 255-270.

Zdravkovich, M. M., 1977. Review of flow interference between two circular cylinders in various arrangements. *Journal of Fluids Engineering* 99, 618-633.

Zdrakovich, M. M., 1986. Discussion; Effect of a vibrating upstream cylinder on a stationary downstream cylinder. *ASME Journal of Fluid Engineering* 108, 383-385.

Zdravkovich, M.M., Moriya, M., Sakamoto, H., 1986. Discussion on effect of vibrating upstream cylinder of two circular cylinders in tandem arrangement. *ASME Journal of Fluids Engineering* 108, 180-185.

Zdravkovich, M.M., 1987. The effects of interference between circular cylinders in cross flow. *Journal of Fluids and Structures* 1, 239-61.

Zdravkovich, M.M., 2003. Flow around circular cylinders. Volume 2: Applications, Oxford University Press,

Zhang, H., Fey U., Noack B. R., K¨onig M. and Eckelmann H., 1995. On the transition of the cylinder wake. *Physics of Fluids* **7**(4), 779–794.

Zhang, J., Dalton, C., 1998. A three-dimensional simulation of a steady approach flow past a circular cylinder at low Reynolds number. *International Journal for Numerical Methods in Fluids* 26, 1003-1022.

Zhao, M., Cheng, L., Teng, B., Liang, D., 2005. Numerical simulation of viscous flow past two circular cylinders of different diameters. *Applied Ocean Research* **27**, 39–55.

Zhao, M., Cheng, L., Teng, B., Dong, G., 2007b. Hydrodynamic forces on dual cylinders of different diameters in steady currents. *Journal of Fluid and Structures* 23, 59-83.

Zhao, M., Cheng, L., Teng, B., 2007a. Numerical modelling of flow and hydrodynamic forces around a piggyback pipeline near the seabed. *Journal of Waterway Port coastal and Ocean Engineering-ASCE* 133, 286-295.

Zhao, M., Cheng, L., Zhou, T., 2009. Direct numerical simulation of three-dimensional flow past a yawed circular cylinder of infinite length. *Journal of Fluids and Structures* **25**, 831–847.

Zhao, M., Cheng, L., Zhou, T., 2011. Three-dimensional numerical simulation of oscillatory flow around a circular cylinder at right and oblique attacks. *Ocean Engineering* **38**, 2056–2069.

Zhao, M., 2012. Influence of the position angle of the small pipeline on vortex shedding flow around a sub-sea piggyback pipeline. *Costal Engineering Journal* 54.

Zhao, M., Thapa, J., Cheng, L., Zhou, T., 2013. Three-dimensional transition of vortex shedding flow around a circular cylinder at right and oblique attacks. *Physics of Fluids* 25, 014105.

Zhao, M., Cheng, L., An, H., Lu, L., 2014. Three-dimensional numerical simulations of vortex-induced vibration of an elastically mounted rigid circular cylinder in steady current. *Journal of Fluids and Structures* 50, 292-311.

Zhao, M., 2015. Numerical simulation of vortex-induced vibration of a circular cylinder in a spanwise shear flow. *Physics of Fluids* 27, 063101.

Zhou, Y., Wang, Z. J., So, R. M. C., Xu, S. J., Jin, W., 2001. Free vibrations of two side-by-side cylinders in a cross-flow. *Journal of Fluid Mechanics* 443, 197-229.

Zhou, Y., Zhang, H. J., Yiu, M. W., 2002. The turbulent wake of two side-by-side circular cylinders. *Journal of Fluid Mechanics* 458, 303-332.

Zhou, Y., Yiu, M. W., 2006. Flow structure, momentum and heat transport in a two-tandem cylinder wake. *Journal of Fluid Mechanics* 548, 17-48.

Zhou, T., Razali, S. F. M., Zhou, Y., Chua, L. P., Cheng, L., 2009. Dependence of the wake on inclination of a stationary cylinder. *Experiment in Fluids* **46**, 1125–1138.

Zhou, T., Wang, H., Razali, S. F. M., Zhou, Y., Cheng, L., 2010. Three-dimensional vorticity measurements in the wake of a yawed circular cylinder. *Physics of Fluids* 22, 015108.